

Dissertation zur Erlangung des Doktorgrades
der Fakultät für Chemie und Pharmazie
der Ludwig-Maximilians-Universität München



Cellular responses to nucleic acid-protein crosslinks

Shubo Zhao

aus

Shenyang, Liaoning, China

2023

Erklärung

Diese Dissertation wurde im Sinne von § 7 der Promotionsordnung vom 28. November 2011 von Herrn Prof. Dr. Julian Stingele betreut.

Eidesstattliche Versicherung

Diese Dissertation wurde eigenständig und ohne unerlaubte Hilfe erarbeitet.

München,*10.01.2023*.....

.....
Shubo Zhao

Dissertation eingereicht am 16.01.2023

1. Gutachter: Prof. Dr. Julian Stingele
2. Gutachter: Prof. Dr. Roland Beckmann

Mündliche Prüfung am 14.02.2023

Table of contents

List of publications	1
Contribution report	2
List of abbreviations	3
Summary	5
1 Introduction	7
1.1 DNA damage and repair.....	7
1.1.1 DNA damage.....	8
1.1.2 Mechanisms of DNA repair.....	12
1.2 DNA-protein crosslinks (DPCs)	23
1.2.1 Types of DPCs	24
1.2.2 DPC resolution	26
1.3 Ubiquitylation in DNA damage repair.....	44
1.3.1 Ubiquitylation.....	44
1.3.2 Ubiquitylation in nucleotide excision repair.....	47
1.3.3 Ubiquitylation in double-strand break repair	50
1.3.4 Ubiquitylation in DNA damage tolerance (DDT)	51
1.3.5 Ubiquitylation in Fanconi anemia pathway	54
1.3.6 Deubiquitylation.....	55
1.4 RNA-protein interaction	58
1.4.1 RNA categories	59
1.4.2 Methodology to study RNA-protein interaction	62
1.5 Ribosome and translation.....	65
1.5.1 The composition of the ribosome	66
1.5.2 The translation cycle	67
1.6 Translation-associated quality control and cellular responses.....	70

1.6.1 Ribosome-associated protein quality control (RQC).....	71
1.6.2 Translation-coupled mRNA quality control	74
1.6.3 Ribosome-associated stress responses.....	77
2 Aims of these studies	81
3 Summary of publications	83
3.1 A ubiquitin switch controls autocatalytic inactivation of the DNA-protein crosslink repair protease SPRTN	83
3.2 Translation-coupled sensing and degradation of RNA-protein crosslinks....	84
4 Discussion.....	85
4.1 Ubiquitin switch regulates SPRTN stability.....	85
4.2 Recruitment of SPRTN to chromatin upon DPCs	88
4.3 Regulation of SPRTN's enzymatic activity.....	91
4.4 RNA-protein crosslink resolution	93
4.4.1 Translation-coupled ubiquitylation and resolution of RPCs	93
4.4.2 Additional factors involved in RPC resolution?	95
4.5 Physiological and pathological roles of RPCs	97
4.5.1 RPCs and ribosomopathies.....	97
4.5.2 RPCs and aging	99
Reference.....	101
Acknowledgments	162
Publication.....	165

List of publications

This dissertation has been prepared from October 2018 to December 2022, under the supervision of Professor Dr. Julian Stinglele at the Gene Center of the Ludwig-Maximilian University in Munich. This cumulative thesis is based on the following publication and manuscript:

Publication 1

Shubo Zhao, Anja Kieser, Hao-Yi Li, Hannah K Reinking, Pedro Weickert, Simon Euteneuer, Denitsa Yaneva, Aleida C Acampora, Maximilian J Götz, Regina Feederle, Julian Stinglele. A ubiquitin switch controls autocatalytic inactivation of the DNA-protein cross-link repair protease SPRTN. *Nucleic Acids Res.* 2021 Jan 25; 49 (2): 902-915.

Manuscript 1

Shubo Zhao[#], Jacqueline Cordes[#], Karolina M. Caban, Maximilian J. Götz, Timur Mackens-Kiani, Anthony J. Veltri, Niladri K. Sinha, Pedro Weickert, Graeme Hewitt, Thomas Fröhlich, Roland Beckmann, Allen R. Buskirk, Rachel Green, Julian Stinglele. Translation-coupled sensing and degradation of RNA-protein crosslinks.

[#]These authors contributed equally to this work

Contribution report

1 Publication | Zhao et al. (2021)

This publication reveals the regulation mechanism of SPRTN mediated by ubiquitin switch during DPC repair. I performed the *in vivo* experiments to identify that USP7 is the deubiquitylating enzyme of SPRTN and demonstrated the interaction between USP7 and SPRTN. Furthermore, I conducted immunoprecipitation and cycloheximide chase assays which proved that mono-ubiquitylation of SPRTN regulates its degradation by autocleavage and proteasome. In addition, I generated *USP7* gene knock-out cell lines and revealed they are more sensitive to formaldehyde. I also compared the contribution of other potential DUBs to the sensitivity of formaldehyde and the association with SPRTN. I prepared Figures 1A-D, 3, 4, 5, S4, S5. Finally, I contributed to the writing of the manuscript.

Manuscript 1 | Zhao and Cordes et al. (2022)

This study demonstrates that RNA-protein crosslink (RPC) formation serves as a central aspect of aldehyde-induced toxicity. Crosslinked proteins trigger translation stress and can be resolved by translation-coupled ubiquitylation followed by proteasomal degradation. I established and optimized the conditions to induce RPCs which were used throughout the project. I performed sensitivity assays together with Jacqueline Cordes showing that formation of RPCs is toxic to cells. Moreover, I generated gene knock-out cells and demonstrated the activation of RSR, ISR and RQC pathways upon RPCs induction. Furthermore, I prepared polyA pull-down samples for MS measurements together with Jacqueline Cordes. These data were analysed by Maximilian J. Götz, which revealed that a subset of mRNA-crosslinked proteins is degraded by the ubiquitin-proteasome system. These results were confirmed by western blotting by myself and Jacqueline Cordes. I contributed to the preparation of Figures 1c, 2a-b, 3b, 4c, 5a-b, d-e, g-h and Extended Data Figures 1b, d-e, 2a, 6a, c, e, f. I prepared Figures 1e, 2c-i, 3f, 5c, f and Extended Data Figures 1a, f, 2b, d-g, 3, 4e-l, 5a-b, 6b. Finally, I contributed to the writing of the manuscript.

List of abbreviations

4-SU	4-thiouridine
5-aza-dC	5-aza-2'-deoxycytidine
5-dRP	5-deoxyribose-phosphate
6-SG	6-thioguanosine
8-oxoG	8-oxo-7,8-dihydroguanine
AP site	Apurinic/aprimidinic site
BER	Base excision repair
BR	Basic region
CLIP	Crosslinking and immunoprecipitation
CPDs	Cyclobutane pyrimidine dimers
CPT	Camptothecin
CRL	Cullin-ring type e3 ligase
DBA	Diamond-blackfan anemia
DDR	DNA damage response
DDT	DNA damage tolerance
DNA-PKcs	DNA-dependent protein kinase, catalytic subunit
DPC	DNA-protein crosslink
DPCL	DNA-platinum-protein complex
DSB	Double-strand break
DSBR	Double-strand break repair
DUB	Deubiquitylating enzyme
EJC	Exon junction complex
FA	Fanconi anemia
GG-NER	Global genome nucleotide excision repair
HR	Homologous recombination
HSC	Hematopoietic stem cell
ICL	Interstrand crosslink
IDL	Insertion-deletion loop
IP	Immunoprecipitation
IR	Ionizing radiation
ISR	Integrated stress response
LSU	Large subunit
MMR	Mismatch repair
MS	Mass spectrometry
ncRNA	Noncoding RNA
NER	Nucleotide excision repair
NGD	No-go decay
NHEJ	Non-homologous end joining

List of abbreviation

NLS	Nuclear localization signal
NMD	Nonsense-mediated decay
NSD	Non-stop decay
ORF	Open reading frame
PAR-CL	Photoactivatable ribonucleoside-enhanced crosslinking
PCNA	Proliferating cell nuclear antigen
PIC	Preinitiation complex
PIP	PCNA-interacting peptide
Pol II	RNA polymerase II
Pol β	Polymerase β
PTM	Post-translational modification
RAP	RNA affinity purification
RBD	RNA-binding domains
RBP	RNA-binding protein
RBR	RING-between-RING
RING	Really interesting new gene
RISC	RNA-induced silencing complex
ROS	Reactive oxygen species
RPC	RNA-protein crosslink
RQC	Ribosome-associated protein quality control
RRM	RNA recognition motif
RRS	Recovery of RNA synthesis
RSR	Ribotoxic stress response
SHP	p97-interacting motif
SSB	Single-strand break
SSBR	Single-strand break repair
SSU	Small subunit
TC	Ternary complex
TC-NER	Transcription-coupled nucleotide excision repair
TFIIH	Transcription initiation factor II H
TLS	Translesion synthesis
Ub	Ubiquitin
UBD	Ubiquitin binding domain
UBZ	The ubiquitin-binding zinc finger
UTR	Untranslated region
UV	Ultraviolet
WT	Wild-type
ZBD	Zinc-binding domain

Summary

Nucleic acids are involved in various fundamental biological processes, ranging from storing genetic information to directing protein synthesis. Therefore, ensuring that DNA and RNA are reproduced, transcribed, and translated accurately is critically important for the perpetuation of life. However, these nucleic acid polymers are easily damaged by endogenous and exogenous agents, leading to genome instability, protein synthesis collapse, and eventually to human disease development and carcinogenesis. Over the past decades, DNA damage repair and tolerance mechanisms have been well studied. Recently, DNA-protein crosslinks (DPCs) received attention as a novel type of DNA damage arising from endogenously produced reactive metabolites, such as formaldehyde, and various chemotherapeutic agents including topoisomerase poisons.

DPC repair involves the degradation of the protein adduct by the metalloprotease SPRTN, which is activated by specific DNA structures. A substantial fraction of SPRTN is constitutively mono-ubiquitylated in cells. Moreover, the recruitment of SPRTN to chromatin upon DPC induction is accompanied by rapid deubiquitylation. However, the function of SPRTN mono-ubiquitylation is poorly understood. Here, we report that the ubiquitylation of SPRTN plays a crucial role in regulating SPRTN's enzymatic activity and stability. We demonstrate that mono-ubiquitylation is induced in an E3 ligase-independent manner and does not control chromatin access of the enzyme. Our results reveal that mono-ubiquitylation inactivates SPRTN by triggering autocatalytic cleavage in *trans* and priming poly-ubiquitylation for proteasomal degradation in *cis*. Finally, we discover that the deubiquitylating enzyme USP7 is the factor responsible for deubiquitylating SPRTN upon DPC induction. Our data suggest that USP7 antagonizes the ubiquitylation of SPRTN to reduce autocleavage which in turn increases SPRTN's lifetime on DNA damage sites, therefore, enabling efficient DPC proteolysis. Consistently, loss of USP7 results in accumulation of DPCs and hypersensitivity upon exposure of cells to formaldehyde.

Given the reactivity of formaldehyde and the abundance of RNA, we hypothesize crosslinks between RNA and proteins (RPCs) form frequently as well, and cells must have evolved quality control systems to sense and resolve RPCs.

Summary

RPCs are usually utilized as approaches to query RNA-protein interactions and resulted in the successful identification of many novel RNA binding proteins (RBPs) and the sequence of their target RNAs. However, whether RPCs form endogenously, and how they affect cellular physiology and are relevant to pathology has not been systematically explored. In this study, we employ the photoactivatable ribonucleoside enhanced crosslinking (PAR-CL) method to generate RPCs. We demonstrate that the formation of RPCs leads to cell death and growth defects. A non-lethal RPC dose affects cellular translation, which is recovered over time. Moreover, further experiments reveal that PAR-CL induces several ribosome-associated stress responses and quality control pathways due to collided ribosomes, which contribute to resistance or sensitization of cells to RPC formation. The results are similar to formaldehyde treatment, suggesting that RPC is a major quality control problem induced by formaldehyde. Finally, data obtained using a polyA pull-down assay suggest that a subset of proteins crosslinked to mRNA undergo translation-dependent poly-ubiquitylation, which appears to contribute to their resolution by the proteasome.

1 Introduction

1.1 DNA damage and repair

DNA is the most fundamental component of every living organism's genetic information, which is a long chain made up of four types of nucleotides. The nucleotide comprises a phosphate group, a 5-carbon sugar, and a nitrogen base. Phosphate-diester bonds link two adjacent nucleotides to form a backbone comprised of sugar and phosphate molecules along the DNA molecule (Crick et al., 1954). In the DNA double helix, the complementary purines and pyrimidines form hydrogen bonds that connect the two single strands (Minchin and Lodge, 2019). However, endogenous and exogenous agents constantly challenge the integrity of DNA (Nickoloff et al., 2021). Around 70,000 DNA lesions arise in cells every day, ranging from single nucleotide modification, DNA single or double-strand break, covalent crosslinks between adjacent bases and DNA-protein crosslinks (DPCs) (Fugger et al., 2021; Weickert and Stinglele, 2022) (Figure 1). If cells cannot repair these substantial DNA damages, they will cause genome instability, carcinogenesis, certain human diseases, and aging (Chatterjee and Walker, 2017; Tubbs and Nussenzweig, 2017). Therefore, ensuring the fidelity of the genetic code is critically important for the perpetuation of life (Chatterjee and Walker, 2017). Fortunately, cells evolved a variety of DNA repair pathways to overcome different types of DNA damages for protection of genomic integrity (Nickoloff et al., 2021).

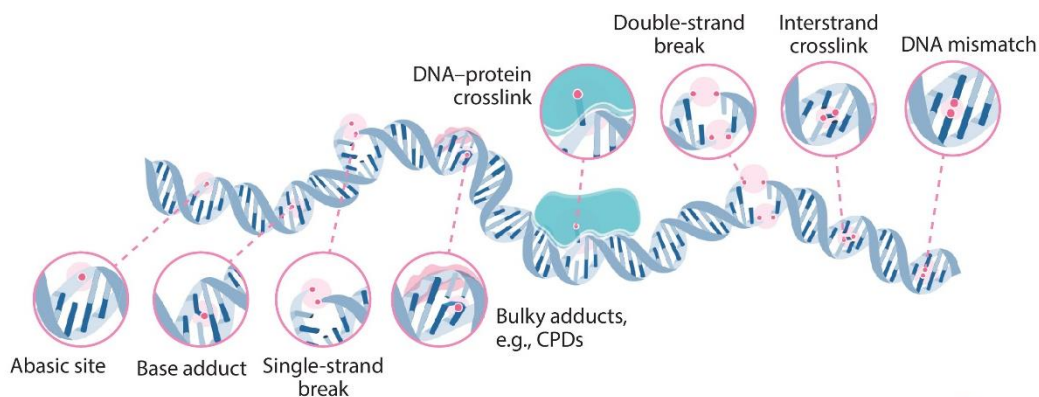


Figure1: Schematic overview of diverse DNA lesions caused by endogenous and exogenous agents. These types of DNA damages include abasic sites, small and bulky base adducts, single and double DNA strand breaks, interstrand crosslinks, DNA base pair mismatches and DNA-protein crosslinks (which are bulkier than CPDs). Figure from (Weickert and Stinglele, 2022).

1.1.1 DNA damage

1.1.1.1 Mismatch of bases

The entire genome of cells is duplicated remarkably faithful and passed on to daughter cells during DNA replication. High-fidelity DNA polymerases play crucial roles in this process (Ganai and Johansson, 2016; Loeb and Monnat, 2008). These DNA polymerases involved in DNA replication bear 3'-5' exonuclease-based proofreading activity, which assists them in removing misincorporated nucleotides from newly synthesized DNA (Bebenek and Ziuzia-Graczyk, 2018; Bebenek and Kunkel, 2004; Hopfield, 1974). Nonetheless, some misincorporated nucleotides can still escape proofreading, resulting in base substitution, insertion or deletion mismatches (Hsieh and Yamane, 2008; Kloor et al., 2014). If these mismatched bases are not repaired in time, the error will persist during the next round of replication, driving genomic mutagenesis.

1.1.1.2 Hydrolytic DNA damage

Hydrolytic deamination of DNA bases

Removing an amine group from a molecule is a process called deamination. Adenine (A), guanine (G), and cytosine (C) can lose their exocyclic amine during deamination in a pH- and temperature-dependent manner (Lindahl, 1993; Shen et al., 1994). Hydrolytic deamination of A, G, C, and 5-methyl cytosine (5 mC) convert the bases to hypoxanthine, xanthine, uracil (U), and thymine (T) which base pair with C, C/T, A, and A respectively (Chatterjee and Walker, 2017; Davies et al., 2012; Shapiro and Yamaguchi, 1972). These base changes can be inherited by daughter cells and lead to permanent mutations in the genome. For example, cytosine deamination can introduce a U-G mismatch which further produces C-G→T-A substitution (Gates, 2009; Lindahl, 1993).

Abasic sites

Every day, thousands of abasic sites are generated in each cell, which refer to the loss of a nucleobase, leaving an apurinic/aprimidinic site (AP site) (Lindahl, 1993). A common source of AP sites is depurination, wherein the N-glycosidic bond between purine and deoxyribose is hydrolysed without interrupting the phosphate

backbone (Chatterjee and Walker, 2017; Lindahl and Barnes, 2000). Loss of cytosine and thymine bases also occurs, but this depyrimidination happens much slower (Lindahl and Karlstrom, 1973). In addition to spontaneous hydrolysis mediated by water, the abasic site is also an intermediate in the base excision repair (BER) pathway derived from DNA glycosylase cleavage (Wilson and Barsky, 2001). Both endogenous and exogenous stressors, such as reactive oxygen species (ROS), alkylating agents, high temperature and ionizing radiation (IR) can cause AP site formation (Nakamura et al., 2000; Talpaert-Borlè, 1987; Wang et al., 2009). As one of the most abundant types of DNA insult, abasic sites can trigger genomic mutations, DNA strand breaks, and polymerase stalling (Boiteux and Guillet, 2004; Loeb and Preston, 1986).

1.1.1.3 Chemical modification of bases

Humans are continuously exposed to a wide range of environmental chemicals and endogenously produced free radicals or electrophiles, mediating covalent bond formation between DNA bases and chemical add-ons (Balbo et al., 2014; Miller, 1978; Rajalakshmi et al., 2015). These DNA adducts can lead to abnormal replication and permanent mutation of genetic information, which further alter cell division control and ultimately result in tumor development (Loeb and Harris, 2008; Rajalakshmi et al., 2015).

Small base adducts

Small base adducts arise from nucleobase modifications including alkylation and oxidation. DNA alkylation refers to transfer of an alkyl group to a DNA nitrogen base. Almost all of the heteroatoms in DNA can be potentially alkylated and generate alkylation products such as O-6-methylguanine (O6-MeG), N-3-methyladenine (N3-MeA), N-7-methylguanine (N7-MeG), etc. (Gates, 2009; Grady and Ulrich, 2007). DNA alkylation happens spontaneously or results from exposure to endogenous chemicals, such as nitrosamines, as well as from exogenous agents, including tobacco smoke, temozolomide, and dacarbazine (Drabløs et al., 2004; Kondo et al., 2010; Shuker and Margison, 1997; Szyfter et al., 1996). In addition, DNA oxidation is another common type of base modification that refers to adding oxygen atoms to purine and pyrimidine bases. (Cooke et al., 2003; Poetsch, 2020). A prominent example of DNA oxidation is 8-oxo-7,8-dihydroguanine (8-oxoG) which constantly

appears inside the cells resulting from exposure to endogenous or exogenous ROS, generated from cellular respiration, peroxisomal metabolism, ionizing radiation, etc. (Henle and Linn, 1997; Lindahl, 1993; Poetsch, 2020). DNA bases subjected to alkylation or oxidation will not strongly distort DNA structure but carry the risk of inducing abasic site formation, genetic mutations or even stalling of DNA synthesis. For example, O⁶-MeG leads to mispairing with thymine rather than cytosine, retaining a G-C→A-T point mutation. Moreover, 8-oxoG base pairs with adenine instead of cytosine, causing a G-C→T-A transition (Kamiya et al., 1992; Loechler et al., 1984.; Shrivastav et al., 2010).

Bulky base adducts

In addition to simple chemical groups, some bulky chemical groups can also be covalently attached to a nitrogenous base of DNA when cells are exposed to genotoxic aromatic compounds, including polycyclic aromatic hydrocarbons (PAHs), aromatic amines, toxins, etc. (Geacintov, 1986; Mah et al., 1989; Phillips, 2005; Smela et al., 2001). A typical example is benzo(a)pyrene, which appears in tobacco smoke, grilled meats, etc. Upon activation of cytochromes P450, it is converted to benzo(a)pyrene diol epoxide (BPDE), a reactive alkylation agent that can bind to guanine covalently (Geacintov, 1986; Meehan et al., 1997). Notably, many of these reactive electrophiles are carcinogens, suggesting a connection between DNA adduct formation and tumorigenesis (Pfeifer et al., 2002; Phillips, 2005; Yun et al., 2020). Another prominent type of bulky adduct is Ultraviolet (UV)-radiation-induced pyrimidine dimers, wherein a covalent linkage occurs between two adjacent cytosine or thymine residues on the same side of DNA (Chatterjee and Walker, 2017). A frequently generated photoproduct is cyclobutane pyrimidine dimers (CPDs), a cyclobutyl loop formed between two neighboring pyrimidine bases. Additionally, cisplatin, an effective chemotherapeutic drug, is reported to form covalent bonds with DNA which further generate 1,2-GG or 1,2-AG intrastrand crosslink DNA adducts (Eastman, 1987; Rocha et al., 2018). These adducts can lead to permanent mutations or DNA helix conformation changes which further halt DNA polymerases and disrupt DNA replication (Choi and Pfeifer, 2005; Davies, 1995).

1.1.1.4 DNA strand breaks

DNA forms a double-strand helix structure with a backbone made of deoxyribose and phosphate groups (Crick et al., 1954). DNA is constantly subjected to endogenous and exogenous threats that induce discontinuities in the phosphate-diester bonds, leading to breaks in one or both DNA strands (Mehta and Haber, 2014). Single-strand breaks (SSBs) can arise from oxidative attack by ROS or occur as an intermediate during BER (Dempfle and DeMott, 2002; Hegde et al., 2008). In addition, erroneous activation of topoisomerase 1 (TOP1) during transcription or replication can lead to SSBs (Caldecott, 2008; Wang, 2002). Double-strand breaks (DSBs) happen much less frequently than SSBs, but are one of the most cytotoxic types of DNA lesion (Mehta and Haber, 2014). DSBs can originate from exogenous agents such as IR, wherein high-energy particles or photons attack DNA's phosphate-sugar backbone. Moreover, IR can also generate free radicals through water radiolysis, which creates SSBs, and further cause DSBs, if in close proximity to each other (Cannan and Pederson, 2016; Yamaguchi et al., 2005). Additionally, certain anticancer chemotherapeutic drugs, mechanical stress on the chromosomes, abortive topoisomerase 2 activity (TOP2), etc. can also lead to nicks on both sides of complementary DNA strands. These insults impact the DNA's integrity and cause genomic instability and carcinogenesis (Cannan and Pederson, 2016; Khanna and Jackson, 2001).

1.1.1.5 Interstrand crosslinks (ICLs)

DNA interstrand crosslink (ICLs) refers to a covalent linkage between two DNA bases from opposing strands (Huang and Li, 2013). It is caused by various agents ranging from artificially or naturally synthesized agents such as nitrogen mustard, cisplatin, mitomycin C (MMC), and psoralen to endogenous agents including acetaldehyde and malondialdehyde. These "crosslinkers" bear two separate reactive groups that react with independent nucleobases forming a covalent linkage (Noll et al., 2006). ICLs are highly toxic because they block the separation of DNA strands, during essential cellular processes such as replication and transcription (Enoiu et al., 2012). Remarkably, due to the cytotoxicity of ICLs and the higher proliferation ability of cancer cells, those ICL-inducing agents are widely used in

chemotherapy, especially for cancers with defects in DNA repair pathways (Cass et al., 2003; Deans and West, 2011).

1.1.2 Mechanisms of DNA repair

As discussed above, DNA is permanently threatened by multiple endogenous and exogenous genotoxic agents (De Bont and van Larebeke, 2004). The resulting lesions alter the double helix structure and introduce permanent mutation in the genome, leading to deleterious consequences such as cell death or carcinogenesis. (Torgovnick and Schumacher, 2015). Cells have evolved specific repair pathways to maintain genetic integrity by resolving or tolerating diverse DNA insults. Defects in DNA repair mechanisms result in premature aging, tumor development, and are responsible for many inherited human syndromes (Maynard et al., 2015; Torgovnick and Schumacher, 2015).

1.1.2.1 Direct repair

Direct repair is the most straightforward repair mechanism that directly reverses a modified base to a normal one without DNA backbone breakage or new DNA synthesis (Fu et al., 2012; Nay and O'Connor, 2013). The base dealkylation process involves two prominent protein families: methylguanine DNA methyltransferase (MGMT) and AlkB homologs (ALKBH). MGMT catalyses the demethylation of O⁶-MeG by directly transferring the methyl group on the O-methyl base adduct to its cysteine catalytic residue, followed by degradation through the ubiquitin-proteasome system (Ellison et al., 1989; Peng and Pei, 2021). The hydroxylation of N-1-methyladenine (N1-MeA) or N-3-methylcytosine (N3-MeC) is carried out by ALKB, an alpha-ketoglutarate- and Fe(II)-dependent dioxygenase which oxidizes the methyl groups on the N-methyl bases and releases them as formaldehyde (Begley and Samson, 2003; Gutierrez and O'Connor, 2021). Notably, alkylation at N-3-adenine or N-7-guanine sites cannot be remediated directly but are repaired by excision repair pathways (Wyatt and Pittman, 2006; Ye et al., 1998) (Figure 2).

Introduction

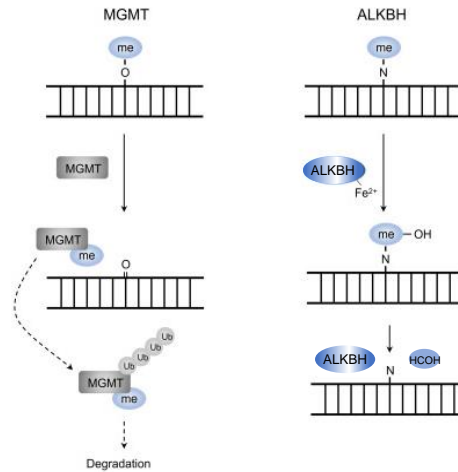


Figure 2: Schematic depiction of direct repair mechanism for alkylated DNA. Left panel: direct demethylation of an O-alkyl DNA lesion by MGMT. Right panel: direct demethylation of an N-alkyl DNA lesion by ALKBH. Figure adapted from (Peng and Pei, 2021).

1.1.2.2 Excision repair

Excision repair mechanisms are more complicated compared to direct repair and involve multiple enzymatic reactions. In excision repair, a damaged fragment of DNA is eliminated, followed by new DNA synthesis and gap healing, utilizing the intact strand as a template (Sancar, 1996). These lesions comprise modified single bases, helix-distorting lesions, and incorrect base pairs, which are removed by base excision repair (BER), nucleotide excision repair (NER), and mismatch repair (MMR), respectively. These excision repair mechanisms all involve similar procedures: damage identification, lesion resection, DNA synthesis, and gap filling (Fu et al., 2012) (Figure 3).

Base excision repair (BER)

BER is engaged in repairing damaged single nucleotide bases with non-bulky adducts originating from chemical modifications such as oxidation, alkylation, and deamination or base loss generated from depurination (Liu et al., 2007). BER starts with base excision by a damage-specific DNA glycosylase which removes the damaged base to generate an AP site, followed by phosphodiester bond cleavage by AP-endonuclease 1 (APE1), ultimately yielding 3-hydroxyl (3'-OH) groups and 5-phosphate (5'-P) groups or 5-deoxyribose-phosphate (5'-dRP) residues (Hegde et al., 2008). To date, 8 out of 11 identified glycosylases are demonstrated to be

Introduction

monofunctional, which only have a glycosylase activity. The other three are bifunctional, bearing both glycosylase and AP lyase activity (Alseth et al., 2005; Ide and Kotera, 2004).

Short-patch BER and long-patch BER are two sub-pathways of base excision repair which involve the synthesis of a single nucleotide or a longer nucleotide fragment, respectively. However, the choice between short- and long-patch BER is currently not fully understood. In the short-patch BER, DNA polymerase β (Pol β) is recruited to remove the 5'-dRP via β -elimination reaction, resulting in 5'-P termini followed by insertion of the correct nucleotide prior to DNA ligase I or III (LIG1/3)-mediated nick sealing (Krokan and Bjørås, 2013). Bifunctional glycosylases contain glycosylase activity as well as β or β , δ -elimination lyase activity, which produce a

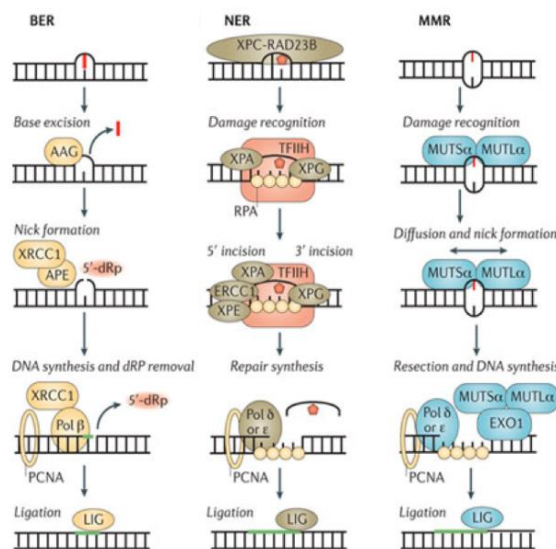


Figure3: Schematic depiction of the cellular mechanisms of excision repair. Left Panel: base excision repair, which involves DNA glycosylase (AAG as an example)-mediated AP site formation followed by AP lyase backbone excision, base(s) insertion and backbone ligation; Middle panel: example of GG-NER, wherein the DNA distortion is recognized by XPC-RAD23B-CETN2 complex, followed by the subunits of TFIIH binding, uncoiling, cleaving off the damage sites, after which the gap is filled by DNA synthesis and ligation. Right panel: mismatch repair, wherein MutS α detects the misincorporated base prior to removal of the mismatched base by MutL α and EXO1, followed by new DNA synthesis and ligation to substitute the erroneous base. Figure from (Fu et al., 2012).

3'-OH group and a 5'-P group with the help of APE or polynucleotide kinase/phosphatase (PNKP), followed by single base insertion by Pol β (Krokan and Bjørås, 2013; Sung and Demple, 2006). Long-patch BER occurs when 5'-dRP group in the gap is resistant to Pol β lyase activity, for example due to oxidized, reduced

or adenylated 5'-dRP. It is the dominant mechanism during S phase but occurs also in non-proliferating cells (Beard et al., 2019; Krokan and Bjørås, 2013). The repair culminates in a canonical DNA synthesis in which proliferating cell nuclear antigen (PCNA) loads Pol β (in non-proliferating cells) or Pol δ/ϵ (in proliferating cells) on the damaged strand and synthesizes a 2-12 nucleotides flap to replace DNA adjacent to the lesion. This process is initiated by Flap structure-specific endonuclease 1 (FEN1) incision and LIG1-mediated ligation (Svilar et al., 2011).

Additionally, the engagement of poly (ADP-ribose) polymerase 1 (PARP1) and X-ray repair cross-complementing protein 1 (XRCC1) are also observed in some types of BER. Here PARP1 is considered as the first responder that binds to lesion-containing DNA and modifies itself and other proteins to recruit other repair factors, therefore, accelerating BER. XRCC1, as a scaffold protein, interacts with PARP1 and Pol β to stabilize the recruitment of Pol β and ensure the completion of BER (Beard et al., 2019; Fu et al., 2012; Hanssen-Bauer et al., 2011; Krokan and Bjørås, 2013).

Nucleotide excision repair (NER)

NER repairs bulky lesions caused by alkylating chemicals and UV, which generate DNA distortions. Unlike BER, which targets a single modified base, NER identifies damage through the physical constitution of DNA. NER can be classified into two major branches: global genome NER (GG-NER) and transcription-coupled NER (TC-NER). The deficiency of NER results in several detrimental disorders: Xeroderma Pigmentosum (XP), Cockayne syndrome (CS) and trichothiodystrophy (TTD) (Cleaver et al., 2009).

GG-NER is initiated by the XPC-RAD23B-CETN2 complex that detects and binds to disrupted DNA structures (Kusakabe et al., 2019; Sugawara et al., 1998). Lesions that result in mild helix distortions (such as CPDs) are poor substrates for this sensor. Therefore they need the CPD-specific sensor DDB1-DDB2 heterodimer to bind the damaged site and kink the DNA, assisting the binding of XPC (Kobaisi et al., 2019; Scrima et al., 2008). Furthermore, DDB1 is also reported as a scaffold to recruit ubiquitin ligase CUL4A to ubiquitylate DDB2 and XPC, promoting DDB2 proteasomal degradation and enhancing XPC's DNA binding activity (Ribeiro-Silva et al., 2020; Sugawara et al., 2005). After detecting the lesions, the transcription initiation factor IIH (TFIIH) complex, encompassing around ten protein subunits, probes the lesions and launches subsequent unwinding, excision, and sealing

procedures. First, ATPase/helicase XPD and XPB engage in DNA uncoiling from 5' and 3', respectively, creating a 20-30 nt bubble DNA substrate followed by XPA binding to the 5' edge of the bubble and XPG located on the 3' side. In parallel, replication protein A (RPA) interacts with a damage-free DNA strand to protect nuclease cleavage (Kokic et al., 2019; Krasikova et al., 2010; Spivak, 2015). Afterwards, the endonuclease enzyme complex ERCC1-XPF, which binds to XPA, mediates lesion cleavage from the 5' side and the removal of the XPC-RAD23B complex. Subsequently, clamp loader RFC, sliding clamp PCNA, and DNA polymerases (Pol $\epsilon/\delta/\kappa$) start DNA synthesis coinciding with XPG-dependent 3' incision. The final step of NER is sealing XPG-generated nick by utilizing DNA ligases. LIG1 is involved in replicating cells, while LIG3 α participates in nonreplicating cells (Krasikova et al., 2021; Yu et al., 2014).

TC-NER happens when RNA polymerase II (Pol II) is stalled during transcription, starting with the recruitment of CSB to RNAP Pol II complex, and further recruits CSA and other NER factors, but not XPC (Spivak, 2015). UV-stimulated scaffold protein A (UVSSA) is the primary factor that CSA recruits to facilitate the association of the TFIIH complex. Other factors involved in TC-NER include a ubiquitin E3 ligase complex CRL4^{CSA} (CSA-DDB1-CUL4-RBX1) which conjugates ubiquitin on CSB and mediates its degradation while ubiquitin-specific-processing protease 7 (USP7) antagonizes CSB degradation (Melis et al., 2013). Remarkably, recent studies noticed that during TC-NER, RPB1, a subunit of Pol II, is ubiquitinated by cullin-ring type E3 ligases (CRLs) on the site of lysine 1268 (K1268), which acts as a switch to turn on TC-NER (Nakazawa et al., 2020; Tufegdžić Vidaković et al., 2020). The following steps involve lesion removal and DNA resynthesis, as in GG-NER.

Mismatch repair (MMR)

Apart from nucleobase modification, misincorporation of nucleotides can also occur during DNA replication, further leading to mispairing of complementary DNA strands. These errors, including base-base mismatches and insertion-deletion loops (IDLs), are substrates for MMR (Montelone, 2015). MMR is an evolutionarily conserved biological process to stabilize genome integrity, enhancing DNA replication fidelity by around 100 times. Generally, MMR occurs in four steps: mismatch detection, daughter strand incision, new DNA synthesis, and backbone ligation (Chatterjee and Walker, 2017; Iyer and Pluciennik, 2021). Firstly, mispaired

bases or small IDLs and large IDLs are recognized by MutS α (MSH2-MSH6 heterodimer) and MutS β (MSH2-MSH3 heterodimer), respectively (Jiricny, 2013; Kunkel and Erie, 2005). After which, MutL α (MLH1-PMS2 heterodimer) is recruited to MutS α/β complex, forming a tetrameric slide clamp complex (Pluciennik et al., 2010; Qiu et al., 2015). Next, the mismatch-carrying strand should be incised by endonuclease MutH in *E. coli*. However, since no MutH homology protein exists in eukaryotic cells, MutL α is thought to activate the excision. PMS2, a subunit of MutL α , possesses potential endonuclease activity that is activated in a PCNA-dependent manner (PCNA is localized to MutS α/β and MutL α complex during MMR). Studies suggest that PCNA discriminates between DNA template and daughter strand by recognising pre-existing DNA nicks on daughter strands (Kadyrov et al., 2006; Pluciennik et al., 2010; Putnam, 2021; Zhang et al., 2005). A more study also suggested that misincorporated ribonucleotides signals strand-discrimination via the nicks generated from RNase H2-initiated ribonucleotide excision repair (Ghodgaonkar et al., 2013). After excision, exonuclease 1 (EXO1) carries out 5'-3' hydrolytic activity to remove mismatched bases from the nascent DNA. After that, correct DNA is resynthesized by Pol δ , and the nick is sealed by LIG1 (Kadyrov et al., 2007).

1.1.2.3 Single-strand break repair (SSBR)

SSBs form as a result of oxidative attack and abortive TOP1 activity (Hegde et al., 2008; Mei et al., 2020). Leaving SSBs unrepaired increases the risk of replication or transcription collapse and human disease development, such as spinocerebellar ataxia with axonal neuropathy 1 and ataxia-oculomotor apraxia 1 (El-Khamisy et al., 2005; Reynolds et al., 2009). SSBR is considered as a specialized BER pathway since they overlap extensively between repair factors (Abbotts and Wilson, 2017). When the SSB is generated directly from the oxidative attack-induced sugar disintegration, PARP1 rapidly binds to damaged deoxyribose. It triggers Poly (ADP-ribose) ation (PARylation) on itself and other target proteins. PARP1 binding further accumulates more repair factors, such as XRCC1, APE1, PNKP, APTX (aprataxin) and DNA polymerases through protein-protein interaction or PARylation. After which, PARylation is disassembled by Poly (ADP-ribose) glycohydrolase (PARG) (Davidovic et al., 2001). Moreover, the various termini residues of the damage site

need to be converted to 3'-OH and 5'-P before initiating gap filling and healing. This end processing step is carried out by different enzymes such as PNKP, APE1, Pol β , and APTX, depending on the types of broken termini. In the next step, the left-behind gap is either inserted with one nucleotide (short patch) by Pol β followed by LIG3-mediated ligation or is repaired with a replacement of a 2-12 nt flap (long patch) by Pol β , Pol δ and/or Pol ϵ , aided by FEN1 and PCNA. After which, the gap sealing is carried out by LIG1 (Caldecott, 2008; Chatterjee and Walker, 2017). For the erroneously activated TOP1 triggered SSB, wherein TOP1 generates a nick with 3'-TOP1 adduct and 5'-OH. The end-processing is carried out by tyrosyl-DNA phosphodiesterase 1 (TDP1), producing 3'-P ends hydrolysed by PNKP coincides with 5'-OH termini phosphorylation. The restored 3'-OH and 5'-P ends are further repaired through short- or long-patch SSB (Mei et al., 2020).

1.1.2.4 Double-strand break repair (DSBR)

DSBs arise much less frequently than SSBs because of the double phosphate backbones of complementary strands (Mehta and Haber, 2014). However, exogenous agents such as radiation and chemotherapeutic drugs or endogenous processes, for instance, meiosis and immunoglobulin class-switch, can break both strands simultaneously (Khanna and Jackson, 2001). Unrepaired DSBs lead to genome instability, including mutagenesis or chromosome rearrangements ultimately resulting in cell death, tumorigenesis, and detrimental disorders development (Jackson and Bartek, 2009). Cells employ two main mechanisms to cope with these cytotoxic insults: homologous recombination (HR) and non-homologous end joining (NHEJ).

Homologous recombination (HR)

HR is strictly restricted to the S and G2 cell cycle phases since it requires homologous DNA sequences as a template to carry out high-fidelity repair of DSBs (Huertas, 2010). First, the MRN (MRE11-RAD50-NBS1) complex detects and binds to the damage site, followed by a 5'-3' nucleolytic resection mediated by MRE11, which harbors both endonuclease and 3'-5' exonuclease activities with the help of another endonuclease, CtBP-interacting protein (CtIP). The resulting 3' overhangs can be further extended by 5'-3' exonuclease EXO1 or single-strand endonuclease DNA2 and helicase BLM (Bloom syndrome protein) (Cannan and Pederson, 2016;

F. Zhao et al., 2020). Next, RPA binds to the naked ssDNA to protect against nuclease degradation and is subsequently replaced by RAD51, which is recruited via the PALB2-BRCA1-BRCA2 complex (Holloman, 2011; Xia et al., 2006). RAD51, as a recombinase, can initiate searching for the complementary homologous DNA sequence prior to broken strand invasion and annealing. Once RAD51 finds the homolog, it promotes the 3'-OH residue extending fulfilled by Pol δ with intact homologous DNA as a template and rejoining the 5' end of impaired chromosome aided by DNA ligase (McVey et al., 2016). After which, the formed double holiday junction is resolved by “dissolution” or “resolution” mediated by BLM-TOP 3 α -RMI1-RMI2 (BTR) complex and the MUS81-EME1-SLX1-SLX4 (SLX-MUS) complex or GEN1 endonuclease, respectively (Matos and West, 2014) (Figure4).

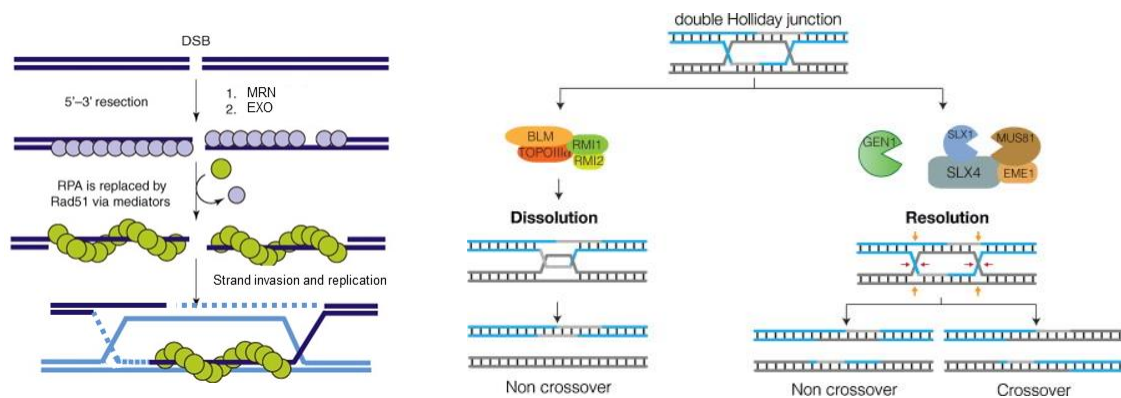


Figure 4: Schematic depiction of the cellular mechanisms of homologous recombination. Left panel: DSB detection and 5'-3' resection mediated by MRN complex and EXO1, followed by RPA binding to ssDNA and replaced by RAD51, which initiates strand invasion. After which, the damaged DNA is synthesized by DNA polymerase and rejoined by DNA ligase, forming a double-holiday junction. Right panel: the mechanical resolution of the double-holiday junction. The BTR complex is engaged in “dissolution” mechanism, which generates non-crossover recombinants. SLX-MUS complex, formed by MUS81-EME1 and SLX1-SLX4 or GEN1, is involved in “resolution” mechanism which produces non-crossover or crossover recombinants. Figure adapted from (Matos and West, 2014; Mimitou and Symington, 2009).

Non-homologous end joining (NHEJ)

In contrast to HR, NHEJ can happen at any cell cycle phase since it directly ligates the two break ends without a homologous template. Consequently, NHEJ often introduces some errors or loss of genetic information (Khanna and Jackson, 2001). NHEJ is initiated by the abundant heterodimeric protein complex Ku70/Ku80, which has high affinity for the broken DNA ends. Ku70/Ku80 forms a ring structure fitting in major and minor grooves of DNA and serving as a scaffold to facilitate the

Introduction

recruitment of other NHEJ components, including DNA-PKcs (DNA-dependent protein kinase, catalytic subunit), XRCC4, XRCC4-like factor (XLF). (Chatterjee and Walker, 2017; Walker et al., 2001; B. Zhao et al., 2020). If the damaged ends are 'clean', XRCC4 and XLF bridge them together, followed by LIG4-mediated ligation; otherwise, DNA-PKcs together with endonuclease Artemis initiate end processing first, after which the broken ends are ligated by LIG4 (Cannan and Pederson, 2016) (Figure 5). Alternatively, cells can also undergo alternative NHEJ (aNHEJ), which can occur in classical NHEJ (cNHEJ)-proficient or deficient cells, but it is much more erroneous than cNHEJ (Deriano and Roth, 2013). In aNHEJ, PARP1 competes with Ku70/Ku80 heterodimer for DNA end binding, which further recruits MRN/CtIP to carry out end resection. Exposed ssDNA of the two dsDNA ends are then able to anneal using local microhomologies, XRCC1, Pol θ , and LIG3/1 initiate gap filling (Cannan and Pederson, 2016; Haince et al., 2008; Sallmyr and Tomkinson, 2018) (Figure 5). Notably, 53BP1 (p53-binding protein 1) plays an essential role in limiting aNHEJ and HR, while promoting cNHEJ. 53BP1 is phosphorylated by ATM and subsequently recruits RIF1 to protect DSB ends from resection (Bothmer et al., 2010; Gelot et al., 2015).

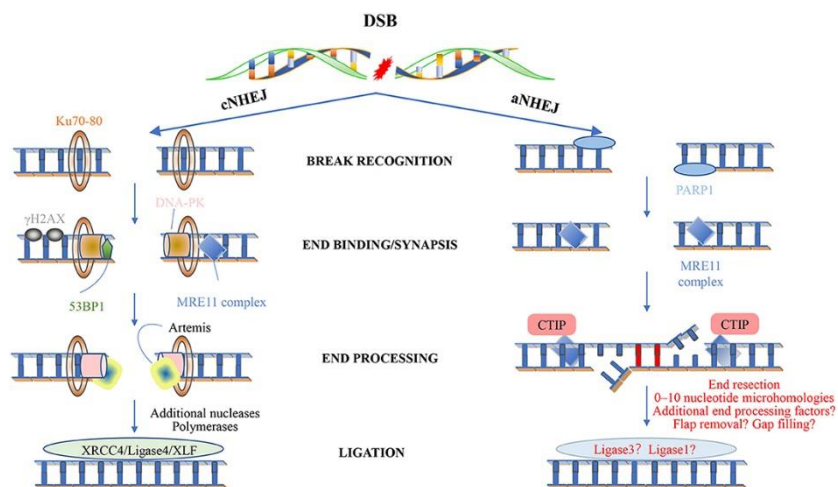


Figure 5: Schematic depiction of the cellular mechanisms of non-homologous end joining. Left panel: repair principles of classical NHEJ, wherein the damage ends are recognized by Ku70/Ku80 heterodimers followed by DNA-PKcs-mediated end processing prior to end rejoining. Right panel: the repair process of alternative NHEJ. aNHEJ involves the DSB end resection carried out by MRN/CtIP complex and gap filling completed by Pol θ and LIG1/3. Figure from (Li et al., 2022).

1.1.2.5 Translesion synthesis (TLS)

Strictly defined, TLS is a damage tolerance pathway rather than a DNA repair mechanism since it allows replication forks to bypass different types of DNA damage without repair. TLS is carried out by highly conserved DNA polymerases, which are mainly DNA polymerases belonging to the B family (including Pol ζ) and Y family (including Pol η , Pol ι , Pol κ , and REV1) (Chatterjee and Walker, 2017; Lehmann, 2006; Ma et al., 2020). TLS occurs when DNA damage repair pathways are not efficient enough. A prominent example is UV-light generated CPDs, which, if NER cannot resolve them in time, will lead to persistence in S-phase and replication fork stalling (Cortez, 2019). When the replisome encounters a DNA lesion, the helicase CMG bypasses the distortion and keeps unwinding DNA while replicative polymerases (Pol α , δ , ϵ) stall, leading to the accumulation of ssDNA (Maiorano et al., 2021). TLS polymerases have flexible active sites, which assist them in accommodating damaged bases to synthesize across diverse lesions. These polymerases can utilize the damaged DNA as a template and randomly insert nucleotides opposite to impaired DNA. However, they are less faithful than replicative DNA polymerases due to the lack of 3'-5' exonuclease proofreading activity (Sale, 2013). TLS is initiated by mono-ubiquitylation of PCNA, mediated by E2 conjugation enzyme RAD6 and E3 ligase RAD18 (Hoege et al., 2002). Y family polymerases are recruited by mono-ubiquitylated PCNA through PCNA-interaction peptide (PIP) of Pol η , ι , and κ or the BRCT (BRCA1 C-terminal) domain of REV1 and their ubiquitin-binding domain (Kannouche et al., 2004). The subsequent procedure can be divided into two steps. First, Pol η , ι , κ or REV1 (inserter enzyme) replaces standard replicative polymerases after loading on DNA insults and incorporates one nucleotide in the complementary side of damaged DNA (Korzhev and Hadden, 2016). Next, the inserter TLS enzyme is replaced by an extender TLS enzyme, usually Pol ζ or Pol κ , followed by DNA lesions bypass and DNA extension (Chatterjee and Walker, 2017). Notably, UV-induced TT-CPD is bypassed error-free by Pol η alone (Masutani et al., 1999). In addition, mono-ubiquitylated PCNA can be further poly-ubiquitylated by the MMS2-UBC13-HLTF/SHPRH complex, which triggers error-free DNA synthesis utilizing newly synthesized sister chromatid as the template involving strand invasion and template switch (Branzei, 2011; Ripley et al.,

2020). In summary, TLS can prevent cells from having un-replicated chromosomes but might at the cost of introducing mutations by low-fidelity polymerases

1.1.2.6 Interstrand crosslink (ICL) repair

ICLs are lesions in which crosslinking occurs between two nucleobases of opposite strands. ICLs are particularly toxic because they interfere with DNA-double helix separation during replication, leading to replication collapse (Moldovan and D'Andrea, 2009). These insults are detected and repaired by the Fanconi anemia (FA) pathway, which is named after the human syndrome of the same name. FA is characterized by sub-fertility, bone marrow failure, and an increased risk of leukemia and solid tumor development (Fanconi, 1967; Kee and D'Andrea, 2012). Mutations in several different protein-coding genes caused the inheritable disorder. Losing the expression of these so called FANC proteins results in cellular sensitivity towards ICL-inducing agents, such as cisplatin and mitomycin C. Consequently, the sensitivity to ICL-inducing agents is also used to diagnose FA (Deans and West, 2011).

FANC proteins are essential factors for the repair of ICLs (Kaddar and Carreau, 2012). There are 22 identified FANC proteins that can be clustered into four groups based on the repair step they participate in (Semlow and Walter, 2021). A well-studied ICL repair model is the replication fork convergence-triggered FA pathway, which is coupled to DNA CMG helicase eviction (Ceccaldi et al., 2016; Niedernhofer et al., 2005; Semlow and Walter, 2021). In this case, FANCM, the only component of group 1 FANCs, detects the stalled replication fork by forming a complex together with MHF1, MHF2, and FAAP24 first (Basbous and Constantinou, 2019). Next, this heterotetrameric complex recruits group 2 FANCs forming the FA core complex, which is comprised of a ubiquitin E2 ubiquitin-conjugating enzyme FANCT and a large E3 ligase complex containing FANCA, B, C, E, F, G, L, FAAP20, and FAAP100 (Machida et al., 2006; Rickman et al., 2015; Semlow and Walter, 2021). FA core complex further mono-ubiquitylates group 3 FANCs, FANCI and FANCD2 (ID2 complex), which is crucial for the following unhooking and recombination steps mediated by group 4 FANCs (Ishiai et al., 2008; Smogorzewska et al., 2007). ID2 complex ubiquitylation recruits FANCP (SLX4), a scaffold protein, which interacts with a structure-specific endonuclease FANCP (SLX4)-ERCC1 to unhook the ICL,

leaving behind a single-strand break in one of the strands (Klein Douwel et al., 2014). The opposite strand is subsequently used as a template for new DNA synthesis assisted by TLS polymerases Pol ζ , a heterodimer formed by REV3 and REV7 (FANCV) and REV1, which can bypass the ICL hook (Kim and D'Andrea, 2012). Finally, the ICL hook is excised by the NER pathway, followed by HR to complete the repair (Wood, 2010). HR is carried out by the remaining FANCs, including FANCD1 (BRCA2), FANCO (RAD51C), FANCR (RAD51), FANCU (XRCC2), FANCN (PALB2), FANCS (BRCA1), FANCW (RFWD3), and FANCI (BRIP1) (Miele et al., 2015; Semlow and Walter, 2021) (Figure 6).

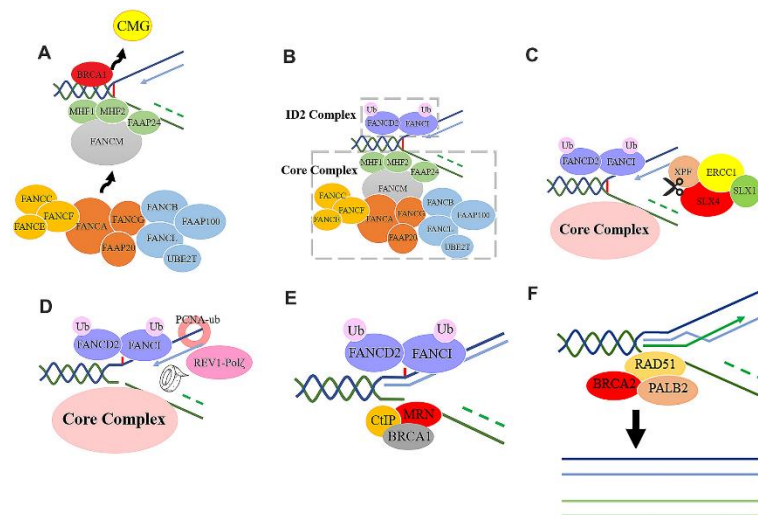


Figure 6: Schematic depiction of the roles of the Fanconi anemia proteins in the repair of DNA ICLs. **A.** Stalled replication fork triggers CMG complex unloading followed by FANCM and its associators localization to the damage site, which further recruits FA core complex; **B.** ID2 complex is mono-ubiquitylated by FA core complex; **C.** DNA endonucleases are recruited to DNA lesions and execute incision; **D.** TLS polymerases Pol ζ and REV1 initiate DNA synthesis to bypass the ICL hook; **E. F.** The remaining DSB is repaired via HR pathway, utilizing TLS synthesized double-strand DNA as a template. Figure from (Dan et al., 2021).

1.2 DNA-protein crosslinks (DPCs)

DPCs are unique DNA lesions which are composed of proteins covalently bound to DNA. They are caused by the permanent trapping of enzymatic reaction intermediates and are also generated by endogenous toxic metabolites and exogenous crosslinking agents, including several chemotherapeutic agents (Nakano et al., 2017; Stinglele et al., 2017). Unrepaired DPCs are detrimental to cells because they interfere with essential chromatin transactions such as

replication and transcription, which leads to genome instability, premature aging, and tumorigenesis (Lessel et al., 2014; Maskey et al., 2017). DPCs were initially considered to be simply a subtype of bulky DNA damages that can be repaired by canonical DNA repair pathways, including NER and HR. Emerging evidence suggests that resolving DPCs requires multiple pathways to degrade protein components, followed by tolerance to or removal of the remaining DNA-peptide crosslinks (Ashour and Mosammaparast, 2021; Weickert and Stinglele, 2022).

1.2.1 Types of DPCs

DPCs are derived from various sources and can involve different proteins associated with DNA. Based on the nature of crosslinked proteins and DPC formation principles, DPCs are classified as enzymatic or non-enzymatic (Figure 7).

1.2.1.1 Enzymatic DPCs

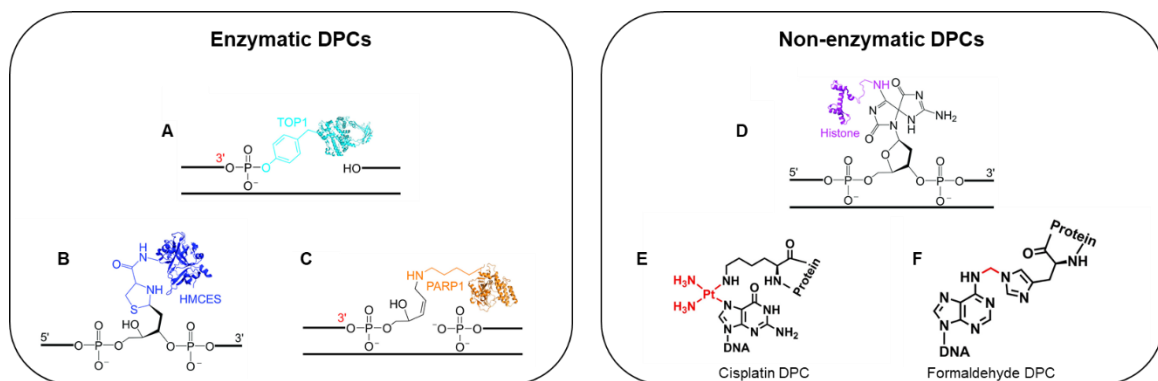


Figure 7: Illustration of chemical structures of diverse DPCs. **A.** TOP1 crosslinks to the 3' end of an SSB through a phosphotyrosyl linkage; **B.** HMCES crosslinks to an AP site on single-strand DNA through a thiazolidine linkage; **C.** PARP1 crosslinks to an AP site at the 3' end of an SSB via a reduced Schiff base linkage; **D.** Covalent linkage formed between the N-terminal histone amine and oxidized 8-oxoG; **E.** Chemical structure of DPCs induced by cisplatin; **F.** Chemical structure of DPCs induced by formaldehyde. Figure adapted from (Groehler IV et al., 2017; Wei et al., 2021).

Enzymatic DPCs arise through enzymatic reactions which involve the formation of a transient covalent bond between DNA and the enzyme. However, under certain circumstances, such as in the presence of small-molecule inhibitors or DNA damage, these transient intermediates become stabilized, permanently trapping the covalent DNA-protein complex (Stinglele et al., 2015; Zhang et al., 2020). Such enzymes include DNA topoisomerases (TOPs), DNA polymerases, DNA methyltransferases

(DNMTs), apurinic or apyrimidinic (AP) lyases, and DNA glycosylases (Kiianitsa and Maizels, 2013). The most well-established examples of enzymatic DPCs are TOPs cleavage complexes (TOPccs). TOPs physiologically relieve torsional stress within DNA by cutting the phosphate backbone of either one or both strands, followed by covalent bond formation between a catalytic tyrosine residue and the break end. Therefore, TOPccs are always accompanied by SSBs or DSBs. Usually, TOPs are released from DNA after relieving torsional stress followed by strand religation. However, these transient covalent cleavage intermediates are easily trapped. For instance, DNA distortion and small molecules like camptothecin (CPT) and etoposide, lead to permanent trapping of TOPs and stable DPCs generation. (Pommier and Marchand, 2012; Stinglele and Jentsch, 2015). Moreover, enzymatic DPCs can also arise from crosslinking of DNMT to methylated 5-aza-2'-deoxycytidine (5-aza-dC), a cytosine analogue that acts as a pseudosubstrate for DNMT1. The covalent linkage is formed between DNMT1 and 5-aza-dC by preventing the final β elimination step of DNMT1's catalytic cycle which is required to release the enzyme (Gnyszka et al., 2013; Santi et al., 1984). In addition, recent studies reported that DPC formation could also shield deleterious DNA lesions during replication. A prominent example are DPCs formed by HMCES (5-Hydroxymethylcytosine binding, ES-cell-specific), which forms a thiazolidine linkage with an AP sites in single-strand DNA to protect ssDNA from breakage (Mohani et al., 2019).

1.2.1.2 Nonenzymatic DPCs

Unlike enzymatic DPCs, wherein the covalent linkage occurs between a particular enzyme and a DNA substrate, nonenzymatic DPCs can involve many proteins in the vicinity of DNA when cells are exposed to reactive compounds like aldehydes, metal ions, and several types of radiation (Stinglele and Jentsch, 2015). Notably, nonenzymatic DPCs usually involve proteins crosslinked to intact DNA strands, distinct from enzymatic DPCs, which are either accompanied by DNA strand breaks or incomplete nucleotides (Zhang et al., 2020). For example, formaldehyde is a highly potent crosslinker widely used as a reagent in studies investigating DNA-protein interactions. Formaldehyde-induced DPC formation occurs in several steps. First, formaldehyde reacts with an exposed amino acid forming a methylol adduct

and then converses to a Schiff base via dehydration. After that, the Schiff base reacts with DNA nucleobase, another nucleophile, to produce a methylene-bridged DPC (Hoffman et al., 2015; Lu et al., 2010; Solomon et al., 1988). Remarkably, formaldehyde is present in the environment and released endogenously through DNA, RNA, or histone demethylation and lipid peroxidation (Ruggiano and Ramadan, 2021a). Besides that, acetaldehyde, a highly reactive compound, is produced from ethanol oxidation and causes DPC via the identical mechanism as formaldehyde (Ide et al., 2015; Stingele et al., 2015).

Furthermore, nonenzymatic DPCs can also be generated by exogenous physical and chemical agents, such as IR and cisplatin. The mechanisms of IR-produced DPCs remains poorly understood, but investigators found that IR-triggered DPC formation is increased under hypoxic conditions, suggesting a potential clinical value of DPC induction in treating hypoxic tumors (Frankenberg-Schwager, 1990; Nakano et al., 2017; Zhang et al., 1995). Additionally, it is widely accepted that the anticancer effects of cisplatin, part of a much-used class of platinum-based chemotherapeutic drugs, come from DNA adduct formation. Of note, some studies demonstrated that cisplatin also forms DNA-platinum-protein complexes (DPCLs), which play an essential role in cytotoxicity, suggesting DPCL formation might also contribute to the therapeutic activity of cisplatin (Chvállová et al., 2007; Eastman, 1987; Woźniak and Walter, 2000).

To conclude, DPCs are toxic to cells since they result in replication and transcription collapse, so their induction can be used as an approach to treat cancer. At the same time, DPC generation can also be beneficial for cells by protecting genomic DNA from detrimental lesions. Thus, studying the principles of DPCs formation and resolution will be instrumental to understand homeostasis maintenance mechanisms and to develop novel chemotherapeutic applications (Kühbacher and Duxin, 2020; Mohni et al., 2019).

1.2.2 DPC resolution

As mentioned above, DPC comprises three components: the DNA, the crosslinked protein, and the covalent linkage between DNA and protein, which can be attacked as repair targets (Stingele et al., 2017). Due to the diversity of the potential components of DPCs, multiple pathways evolved to work together to resolve these

DNA lesions (Ruggiano and Ramadan, 2021a). Based on the target of each repair pathway, DPC repair can be classified into three categories: nuclease-dependent DPC repair, direct crosslink hydrolysis, and proteolysis-dependent DPC repair (Stingele et al., 2017; Zhang et al., 2020).

1.2.2.1 DNA repair pathways in DPC resolution

Previous studies suggested that the canonical DNA repair pathways, NER and HR, are involved in DPC repair. The first evidence came in early genetic studies of *E. coli* by analysing the sensitivity of DNA repair enzyme-deficient *E. coli* strains to DPC-inducing agents, including formaldehyde and 5-aza-dC. Investigators found that *recA* mutant, which is exclusively abortive in HR, was sensitive to both formaldehyde and 5-aza-dC. However, a *uvrA* mutant, which is defective in NER, exhibited sensitivity only to formaldehyde, suggesting that the different natures of the DPCs induced by formaldehyde and 5-aza-dC entail different ways of repair (Nakano et al., 2007; Salem et al., 2009). Formaldehyde crosslinks various proteins randomly, of which sizes range from 9-33 kDa in bacteria, while 5-aza-dC specifically crosslinks DNA methyltransferases, around 53 kDa. Moreover, *in vitro* experiments demonstrated that NER cannot excise DPCs comprised of a 16 kDa protein but can make an excision on the DNA containing shorter polypeptides. Hence, the researchers assumed that NER has limitations in removing bulky DPCs, up to 12-14 kDa, whereas oversized DPCs are processed exclusively by HR (Ide et al., 2015; Minko et al., 2005; Nakano et al., 2007). Subsequent genetic studies in yeast similarly confirmed the involvement of NER and HR in formaldehyde-triggered DPC repair, claiming that NER dominantly repairs DPCs caused by acute high dose exposure of formaldehyde, and HR aids repair of DPCs induced by chronic low doses of formaldehyde (de Graaf et al., 2009).

In mammalian cells, *in vitro* studies showed that cell-free extracts efficiently eliminated DPCs containing a 4 or 12 amino acids-long polypeptide but were unable to make incisions for those containing T4 endonuclease V (16 kDa) or HhaI, a prokaryotic DNA methyltransferase (37 kDa). NER-deficient cell-free extracts failed to excise DPCs. Processing the crosslinked proteins by proteolytic digestion like proteinase K or chymotrypsin yields a preferential substrate for NER (Baker et al., 2007; Reardon and Sancar, 2006). *In vivo* experiments notably demonstrated that

HR deficient cells were highly sensitive to formaldehyde and 5-aza-dC, whereas NER mutants were mildly sensitive, indicating a less critical contribution of NER than HR in DPC removal (Nakano et al., 2009).

Given that HR-deficient cells are highly sensitive to formaldehyde and 5-aza-dC, accompanied by the formation of RAD51 or γ H2AX nuclear foci (indicative of DSB formation) and increased rates of sister chromatin exchange upon the treatment of DPC inducing agents, it is clear that HR plays a pivotal role in the tolerance to DPCs. Moreover, the involvement of HR in the removal of DPCs likely depends on the formation of DSBs near DPC sites (Nakano et al., 2009; Shaham et al., 1997). MRN is an essential nuclease complex initiating the DNA end resection process during HR, comprising MRE11, the nuclease, RAD50, the ATPase, and NBS1, the regulatory factor. Typically MRN complex executes its end-processing function via endo- and exonuclease activities (Paull, 2018). It has no preferential protein adduct to target, therefore, it can nucleolytically remove diverse protein adducts at the 5' or the 3' end of DSBs, exposing a clean DNA terminus for the following canonical DSBs repair mechanisms (Ashour and Mosammaparast, 2021). For instance, TOP2cc is caused by topoisomerase 2 being covalently bound to DNA, where a double-strand break is created and two TOP2 crosslinked to both 5'-termini of the double-strand break via 5'-phosphotyrosyl bonds followed by DNA religation (Riccio et al., 2020). Hence, permanent existing TOP2 adducts must be eliminated prior to DSB repair. Multiple studies reported that the MRN complex might facilitate the removal of TOP2 covalent adducts from DNA. Both *in vitro* and *in vivo* evidence reveal that MRE11-deficiency leads to failure of TOP2cc elimination, which is suppressed by introducing TDP2 (tyrosyl phosphodiester linkage hydrolase) overexpression, suggesting MRE11 contributes crucially to genome stability maintenance through excision of TOP2cc (Deshpande et al., 2016; Hoa et al., 2016; Lee et al., 2012).

This repair strategy is evolutionary conserved from phages to prokaryotes and eukaryotes. Consistent observations have been achieved in T4 bacteriophages, wherein the repair of m-AMSA (an antitumor agent) induced TOPccs was dependent on gp46/47 (MR complex) (Stohr and Kreuzer, 2001; Woodworth and Kreuzer, 1996). Similarly, in *E. coli*, the protein-bound DNA ends are nucleolytically processed by the SbcCD (MR) complex accompanied by pure DSB insertion (Connelly et al., 2003). Also, the Mre11-Rad50-Xrs2 (homologs of MRN in

mammalian cells) complex (MRX) in budding yeast plays an essential role in resistance to TOPs-targeting agents (Malik and Nitiss, 2004). In addition, DSBs with SPO11 covalently attached to 5' termini ends are formed during meiotic recombination in budding yeast. The endonucleolytic activity of MRX is employed to remove protein adducts resulting in SPO11 release, and DPC-free DSB ends containing a 3' overhang, which is subsequently subjected to HR (Neale et al., 2005).

To summarize, the NER-dependent DPC repair mechanism is limited by the size of protein adducts. Indeed, DPCs containing larger proteins (>10 KDa) seemed to reduce the efficiency of DPC removal by NER nucleases. Previous data also suggested that pre-cleavage of crosslinked proteins by specialized DPC proteases or the proteasome is essential for accessing the NER repair machinery to the damage sites (Stingele et al., 2017; Zhang et al., 2020). Additionally, the HR repair pathway can target bulky DPCs, but the MRN complex nuclease activity is restricted to DNA ends, suggesting that DPCs involving proteins associated with intact DNA cannot be recognized by MRN complex-mediated HR (Käshammer et al., 2019; Zhang et al., 2020). This shows that the involvement of NER and HR in DPC resolution is highly coordinated in cells (Nakano et al., 2007).

1.2.2.2 Tyrosyl-DNA phosphodiesterase-dependent hydrolysis

As mentioned above, different components of DPC can be a target for repair, including the covalent bond between protein and DNA. However, due to the diversity of these chemical linkages, cells cannot evolve a specific enzyme to reverse every type of covalent bond. Notably, some enzymatic DPCs occur highly frequently. Consequently, the cells employ specific enzymes to cope with these lesions. The most well-studied examples are TOPccs, which are formed to release DNA torsional stresses during transcription, replication, and proper chromosomal segregation. Tyrosyl-DNA phosphodiesterases (TDPs) are reported to directly hydrolyse the phosphotyrosyl bonds formed between the DNA termini and TOPs (Pommier et al., 2014). Of note, TOPccs need to be pre-digested before hydrolysis to allow TDPs to the lesions (Stingele et al., 2017).

TDP1 hydrolyses TOP1cc

TOP1cc refers to the covalent intermediate between TOP1 and DNA arising during the process of DNA relaxation, wherein TOP1 cleaves a single strand and becomes

covalently attached to the 3'-P end with its active site tyrosine residue, leaving the 5'-OH end free to rotate to relieve torsional stress followed by DNA reannealing and TOP1 release (Champoux, 2001; Stewart et al., 1998). Abortive activity of TOP1 leads to TOP1 being permanently attached to DNA breaks, forming the enzymatic DPC.

TDP1 was firstly detected to be involved in hydrolysing phosphotyrosyl bonds at the 3' end of DNA in yeast (Pouliot et al., 1999). Afterward, substantial evidence verified that TDP1 is an evolutionally conserved enzyme in all eukaryotic cells, and TDP1 deficiency results in the accumulation of TOP1-DNA covalent complexes and sensitivity toward TOP1 inhibitors in yeast and human (Interthal et al., 2005; Pouliot et al., 2001).

Intriguingly, *in vitro* studies investigated that substrates containing full-length TOP1 were resistant to TDP1 cleavage while containing 53 or 108 amino acids of TOP1 were efficiently cleaved by TDP1 suggesting that the TOP1-adduct requires proteolytic processing before TDP1 hydrolysis (Interthal and Champoux, 2011). Sequential experiments reported that the proteasome plays a crucial role in degrading TOP1 in a SUMOylation-ubiquitylation-dependent manner. Proteasomal degradation of crosslinked TOP1 is initiated by SUMOylation of TOP1 mediated by SUMO E3 ligase PIAS4 (Siz1 in yeast), followed by SUMO-triggered poly-ubiquitylation induced by ubiquitin E3 ligase RNF4 (Slx5-Slx8 in yeast) (Lin et al., 2008; Steinacher et al., 2013; Sun et al., 2020a).

According to biochemical studies, TDP1 executes its function by forming a transient covalent intermediate followed by release from DNA through a nucleophilic attack, leaving an SSB with 3'-P and 5'-OH end, which must be further processed by PNKP to generate 3'-OH and 5'-P DNA end, followed by break repair using the BER pathway (Interthal et al., 2001; Khim et al., 2012) (Figure 8).

Introduction

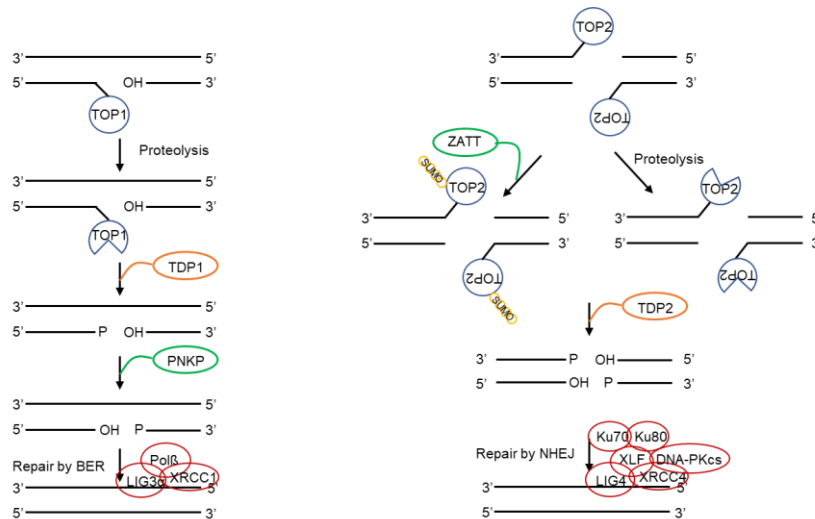


Figure 8: Schematic depiction of cellular mechanisms for the repair of TOPccs by hydrolysis through TDPs. Left panel: repair of TOP1cc, digest by proteasome is followed by TDP1 attacking the 3' phosphotyrosyl bonds. After that, the SSB is processed by PNKP and repaired by BER. Right panel: repair of TOP2cc, digest by the proteasome or SUMOylate by ZATT, followed by TDP2 attacking the 5' phosphotyrosyl bonds. The exposed 3'-OH and 5'-P DNA ends are repaired by NHEJ. Figure based on illustrations in (Khim et al., 2012; Zagnoli-Vieira and Caldecott, 2020).

In addition, genomic mutation of TDP1 results in spinocerebellar ataxia with axonal neuropathy, an autosomal recessive neurodegenerative disease (Takashima et al., 2002). The patients bear a substitution of histidine 493 with an arginine residue in TDP1, which decreases TDP1's catalytic activity causing defective TOP1-DPC repair and leading to TDP1 itself becoming trapped on DNA (El-Khamisy et al., 2005; Interthal et al., 2005). While TDP1-deficient mice do not exhibit a similar pathological phenotype to human beings, the molecular basis needs to be studied further (Hirano et al., 2007; Katyal et al., 2007).

TDP2 hydrolyses TOP2cc

The transient TOP2-DNA intermediate is generated during TOP2 resolving topologically entwined DNA and is known as TOP2 cleavage complex (TOP2cc) (Nitiss, 2009). Many clinical chemotherapeutic TOP2 inhibitors impede the TOP2 catalytic cycle, leading to stabilization of the TOP2cc and accumulation of this type of cytotoxic DPC (Ricci et al., 2020). Since TOP2 generates DSBs, the TOP2ccs are continuously formed on both 5'-P ends of DNA breaks with 5'-phosphotyrosyl covalent bonds.

In vitro data demonstrated that TDP2, an exclusive 5'-tyrosyl DNA phosphodiesterase, directly hydrolyses the 5'-phosphotyrosyl linkage between

TOP2 and DNA breaks (Ledesma et al., 2009). Further studies investigated that TDP2-deleted cells are hypersensitive to TOP2 poisons, including doxorubicin, amsacrine (m-AMSA), and etoposide, indicating that TDP2 is a significant factor in resolving TOP2cc and maintenance of genome stability (Gómez-Herreros et al., 2013; Ledesma et al., 2009; Zeng et al., 2011). Notably, unlike TDP1, which forms a covalent-linked intermediate with its DNA substrate during hydrolysis, TDP2's catalytic activity requires Mg^{2+}/Mn^{2+} and functions without covalent complex formation (Adhikari et al., 2012; Gao et al., 2012; Sun et al., 2020b). After processing, the 3'-OH and 5'-P DNA ends are restored, which allows direct ligation mainly by the NHEJ machinery (Gómez-Herreros et al., 2013).

Previous research suggested that similar to TOP1cc resolution, TOP2cc also requires pre-proteolysis mediated by ubiquitin/26S proteasome pathway (Mao et al., 2001). Subsequent studies further confirmed this finding and investigated that the initiation of TOP2cc degradation shared a conserved way with TOP1cc, in which PIAS4 catalyses SUMOylation of TOP2 and followed by RNF4 mediated ubiquitylation (Sun et al., 2020a). However, emerging evidence revealed that the SUMO E3 ligase ZATT (ZNF451) facilitates TDP2 interacting with SUMOylated TOP2 and immediate release of TOP2 from DNA substrate in a proteasome-independent manner (Schellenberg et al., 2017) (figure 8). Additionally, the inactivation of proteasome does not entirely abolish TOP2cc removal, implying proteasome degradation is not an exclusive way for TOP2cc to be accessible for TDP2 (Kühbacher and Duxin, 2020; Tsuda et al., 2020).

1.2.2.3 Proteolysis-dependent DPC repair

An involvement of the proteasome in DPC elimination has been proposed already quite some time ago (Quievryn and Zhitkovich, 2000). Furthermore, subsequent research demonstrated that the ubiquitin-proteasome systems targets TOP1ccs and TOP2ccs to release the access sites for TDPs (Debethune, 2002; Desai et al., 1997; Lin et al., 2008; Mao et al., 2001; Vaz et al., 2017). Recently, the investigation of proteases, including SPRTN/Wss1, ACRC/GCNA, FAM111A, and DDI1, suggested that the protein component of DPCs is processed into small polypeptides by these enzymes and followed by DNA repair processes (Bhargava et al., 2020; Dokshin et al., 2020; Kojima et al., 2020; Serbyn et al., 2020; Stingele et al., 2016, 2014). Given

that the NER-dependent DPC repair pathway is limited to resolving small protein adducts (approx 8-16 KDa), pre-processing bulky DPCs may play an essential role in efficient DPC resolution (Vaz et al., 2017).

DPC proteolysis by the proteasome

The 26S proteasome is the most well-studied proteolytic machinery in cells of which substrates are modified by poly-ubiquitin (Collins and Goldberg, 2017). The original evidence implicating the 26S proteasome in DPC removal came out more than two decades ago. Scientists observed that topoisomerases are ubiquitylated upon the treatment with TOPs poisons, and inhibition of proteasome delayed TOPccs degradation. Furthermore, the inactivation of proteasome sensitized cells toward DPC-inducing agents, like CPT and low-dose formaldehyde, suggesting that the proteasome is required for DPC repair (Desai et al., 2001, 1997; Lin et al., 2008; Mao et al., 2001; Ortega-Atienza et al., 2015). Subsequent research demonstrated that TOPccs are ubiquitylated in a SUMOylation-dependent manner, and this modification ultimately drives the proteasome-mediated degradation of the protein component of DPCs (Sun et al., 2020a). Simultaneously, HMCES which is crosslinked to protect ssDNA, can also be modified by ubiquitin and be resolved by the proteasome (Mohni et al., 2019).

In contrast to the above findings, investigators who utilized *the Xenopus* egg extract system to follow the M.HpaII DPC repair *in vitro* discovered that inhibition of the proteasome did not significantly affect DPC repair. Notably, the addition of a deubiquitylating enzyme (DUB) inhibitor, which blocks the ubiquitin cycling leading to depletion of free ubiquitin, dramatically inhibited M.HpaII destruction, which is restored by adding free ubiquitin, indicating the availability of ubiquitin but not proteasome activity is required for DPC repair (Duxin et al., 2014). Moreover, depletion of ATP-dependent proteases in *E.coli*, which function similarly to the proteasome in eukaryotic cells, did not trigger hypersensitivity upon exposure to formaldehyde and azacytidine (Nakano et al., 2007).

These controversial conclusions could be explained by the fact that the proteasome inhibitors used in the studies, as mentioned above, might inhibit not only proteasome activity but also reduce the availability of nuclear ubiquitin that was required in other signalling pathways (Takeshita et al., 2009). It was also argued that these experiments rather showed increased ubiquitylation of the total TOPs pool than TOPccs modification. Also, the high-dose CPT used in previous works

might lead to TOPccs elimination beyond physiological repair capacity, thereby inhibiting other potential repair pathways (Ruggiano and Ramadan, 2021a). It is difficult to conclude that DPCs are removed by proteasome directly or that the phenotype is caused by the synergistic effect of proteasome inhibitors, which depletes the nuclear ubiquitin pool or leads to exceeding levels of DPCs (Ruggiano and Ramadan, 2021a; Vaz et al., 2017).

To sum up, although recent studies found that both enzymatic and nonenzymatic DPCs are modified by ubiquitin, and DPC proteolysis is a ubiquitin-dependent process, the precise roles of the proteasome in regulating DPC processing are still under investigation (Borgermann et al., 2019; Larsen et al., 2019; Mohni et al., 2019; Ruggiano et al., 2021; Sun et al., 2020a).

DPC proteolysis by protease SPRTN/Wss1

Apart from proteasome-directed DPC degradation, researchers identified a more specific pathway to target crosslinked protein adducts in recent years involving different proteases. Weak suppressor of Smt3 (Wss1) is the first metalloprotease discovered with a link to DPC repair. Depletion of Wss1 and TDP1 hyper-sensitizes yeast to CPT and results in the accumulation of TOP1ccs. Also, Wss1-deficient yeast strains are sensitive to the DPC-inducing agent, formaldehyde. In addition, *in vitro* assays revealed that Wss1 can process various DNA-binding proteins, such as histone H1 and TOP1, in a DNA-dependent manner. Conclusively, these data indicated the crucial role of Wss1 in DPC resolution (Stingele et al., 2014). Notably, a concomitant study using *Xenopus* egg extract as a model to follow DPC repair showed that DPCs are processed by a replication-coupled enzyme, suggesting a replication-dependent, proteasome-independent DPC repair mechanism. However, this enzyme in metazoans remained unknown at that time (Duxin et al., 2014). In 2016, this specialized enzyme in mammalian cells was found to be SPRTN by different groups independently (Lopez-Mosqueda et al., 2016; Stingele et al., 2016; Vaz et al., 2016).

SPRTN was first characterized as a regulator of TLS, which is recruited to DNA damage sites via the interaction with PCNA and p97. However, the precise role of SPRTN in TLS remains debatable. Conflicting results showed the dependence of SPRTN in the recruitment or release of TLS polymerase from DNA damage sites (Centore et al., 2012; Ghosal et al., 2012; Kim et al., 2013; Mosbech et al., 2012). Later studies investigated that SPRTN is involved in repairing formaldehyde-

induced nonenzymatic DPCs and enzymatic DPCs triggered by TOPs inhibitors. Loss of SPRTN results in lethality after treatment with various DPC-inducing agents but did not cause sensitization to ICL induction or replication inhibition. These *in vivo* data also revealed accumulation of nonspecific DPCs and TOPccs as well as deceleration of DPCs removal due to SPRTN deficiency. Furthermore, *in vitro* biochemistry assays demonstrated a DNA-dependent protease activity of SPRTN, which proteolyzed diverse DNA binding proteins like histones and TOPs (Lopez-Mosqueda et al., 2016; Maskey et al., 2017; Stingele et al., 2016; Vaz et al., 2016). The above evidence indicates the involvement of SPRTN in general DPCs elimination.

Even though lacking substrate preference is beneficial for SPRTN to target variable crosslinked protein adducts, it is also potentially dangerous for cells to proteolyze proteins surrounding the chromatin. Therefore, cells require regulation strategies to control the localization and limit the proteolytic activity of this nonspecific protease (Ruggiano and Ramadan, 2021b).

SPRTN was initially found to be activated by ssDNA and dsDNA (Lopez-Mosqueda et al., 2016; Mórocz et al., 2017; Stingele et al., 2016; Vaz et al., 2016). Later structural studies further discovered two DNA binding domains of SPRTN which are the zinc-binding domain (ZBD) and basic region (BR) that bind to ssDNA and dsDNA, respectively (Li et al., 2019; Reinking et al., 2020). Concomitantly, *in vitro* biochemistry assays proved that SPRTN was activated by ss/dsDNA junction or DNA bubbles, which challenged the previous paradigm that SPRTN is activated non-specifically (Figure 9). This feature of SPRTN allows it to act on proteins specifically around activating DNA structures, for example during replication or transcription, and prevent cleavage of soluble nuclear proteins and intact DNA-binding proteins such as histones (Reinking et al., 2020; Ruggiano and Ramadan, 2021a).

Furthermore, SPRTN harbours several protein-protein-interaction motifs, including the PCNA-interacting peptide (PIP box), the ubiquitin-binding zinc finger (UBZ), and the ATPase p97-interacting motif (SHP box) (Stingele et al., 2015) (Figure 9). Strikingly, although DPC is usually accompanied by ubiquitylation, this modification seems not essential for SPRTN-mediated proteolysis since SPRTN could degrade DPCs that are not ubiquitylated (Larsen et al., 2019), suggesting other interactions are present between SPRTN and DPCs.

Introduction

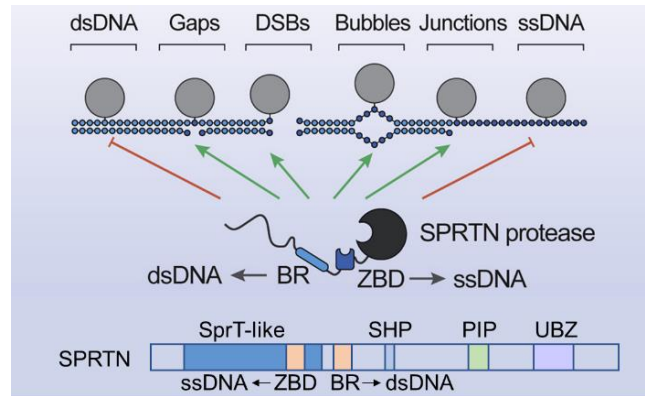


Figure 9: Schematic of the DNA features activating SPRTN and SPRTN's domain structure. Upper panel: SPRTN is activated by dsDNA with unpaired DNA bases, including gaps, ends, bubbles, junctions, etc. but not dsDNA and strict ssDNA. Lower panel: an overview of SPRTN's structure, which contains a SprT-like protease domain, followed by two DNA-binding domains, ZBD and BR. The C-terminus bears a p97-interacting motif (SHP), PCNA-interacting peptide (PIP) and ubiquitin-binding zinc finger (UBZ). Figure adapted from (Reinking et al., 2020).

SPRNTN's localization to DNA damage sites was believed to be modulated by interaction with ubiquitylated PCNA via PIP and UBZ motifs (Centore et al., 2012; Juhasz et al., 2012). Therefore, a similar recruitment mechanism was thought to be in place and supported by the evidence that wild-type (WT) SPRNTN but neither PIP nor UBZ mutant restored the SPRNTN silencing-induced deficiency of DPC-repair upon formaldehyde treatment (Mórocz et al., 2017). However, the direct roles of PCNA in DPC repair remained unclear. In addition, SPRNTN bears a p97 interaction motif, p97 being a ubiquitin and SUMO-dependent segregase that drives protein unfolding for proteasome degradation or disassembly (Franz et al., 2016; van den Boom and Meyer, 2018). A recent study identified a mechanism wherein the PARP inhibitor-induced tightly trapped PARP1 was extracted from chromatin by p97 in a SUMO-targeted ubiquitylation-dependent manner (Krastev et al., 2022). Notably, this pathway existed similarly in DPCs repair, wherein the SUMOylation-dependent ubiquitylation modified crosslinked proteins are degraded by the proteasome (Liu et al., 2021; Sun et al., 2020a). Therefore, it is conceivable that p97 is involved in unfolding DPCs to facilitate DPC removal. In 2020, Fielden et al. identified that Testis expressed 264 (TEX264) is a novel factor involved in TOP1ccs repair. TEX264 binds to unmodified and SUMOylated TOP1 and facilitates recruitment of p97 and SPRNTN to DPCs for proteolysis prior to TDP1-mediated

covalent bonds hydrolysis (Fielden et al., 2020). However, p97's precise role in removal of other DPCs remains to be established.

In addition, previous studies suggested that SPRTN bears several types of post-translational modification, including phosphorylation, ubiquitylation, and acetylation regulating its localization and activation (Halder et al., 2019; Huang et al., 2020; Stinglele et al., 2016). Among them, the ubiquitylation of SPRTN has been studied the most. For a long time, people have observed that in cells, a substantial fraction of SPRTN exists in a mono-ubiquitylated form protected by the UBZ domain (Centore et al., 2012; Juhasz et al., 2012; Machida et al., 2012). Exposure to formaldehyde leads to deubiquitylation of SPRTN, which was considered a chromatin recruitment mechanism (Stinglele et al., 2016). However, the precise function of SPRTN's ubiquitin switch in DPC repair remains poorly understood due to the lack of information on the DUB. Researchers attempted to identify the mono-ubiquitylation sites of SPRTN, while substitutions of potentially modified lysines retained the modification, suggesting the modified residues are quite promiscuous (Stinglele et al., 2016). Notably, both *in vitro* and *in vivo* data suggested SPRTN is capable of autocleavage *in trans*, which is accepted as a mechanism of evicting SPRTN from sites of DNA damage in cells to prevent unwanted protein degradation (Mórocz et al., 2017; Stinglele et al., 2016; Vaz et al., 2016). Strikingly, this autocleavage of SPRTN appears when cells are exposed to low dose formaldehyde, whereas high dose formaldehyde triggers deubiquitylation of SPRTN rather than autocleavage, implying a possible correlation between SPRTN autocleavage and ubiquitylation (Stinglele et al., 2016). Furthermore, two studies reported that SPRTN undergoes phosphorylation and acetylation, which is either initiated by CHK1 to regulate SPRTN's localization to chromatin during replication stress prevention or is added by PCAF and GCN5 to facilitate SPRTN's recruitment to damaged chromatin sites, respectively (Halder et al., 2019; Huang et al., 2020). It is unclear how these two modifications regulate SPRTN's chromatin relocation as they often inhibit DNA binding ability (Wei et al., 2021).

DPC proteolysis by other proteases

Recently, additional proteases have emerged as potential DPC repair factors, including DNA damage-inducible protein 1 (Ddi1) in yeast, Germ cell nuclear acidic protein (GCNA), and Family with sequence similarity 111 member A (FAM111A) in higher eukaryotes. These enzymes, including SPRTN/Wss1, share highly similar

Introduction

structure organization, like their protease domain, DNA-binding domain, and PIP box or ubiquitin-/SUMO-binding domain, inferring to the similarities in regulation of their activity (Figure 10). Nevertheless, these proteases might repair different types of DPCs or in different cell cycle phases or distinct developmental stages (Ruggiano and Ramadan, 2021a; Wei et al., 2021).

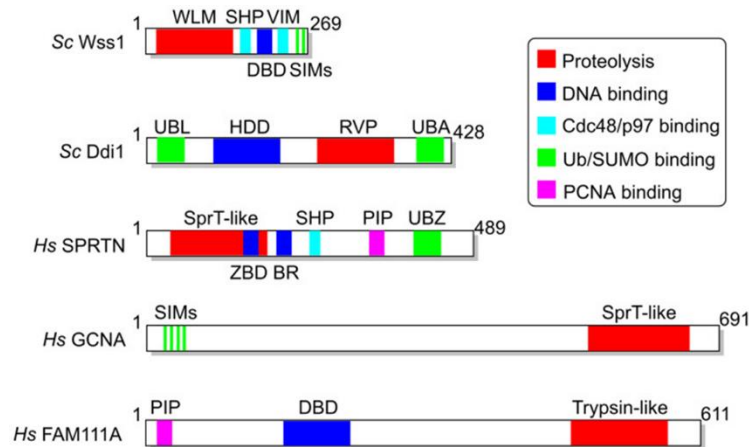


Figure 10: Schematic overview of the domain structures of DPC proteases. Protease domains are colored in red, DNA binding domains are in dark blue (DBD/HDD/ZBD/BR), Cdc48/p97-binding motives are in light blue (SHP/VIM), ubiquitin or SUMO-binding domains are in green (UBL/UBA/UBZ or SIM), PCNA-interacting peptides are in purple (PIP). Figure from (Wei et al., 2021).

Wss1-deficient yeast strains are not sensitive to CPT, suggesting there might be other I repair pathways together parallel to Wss1 to cope with TOP1ccs (Kühbacher and Duxin, 2020; Stingle et al., 2014). Recently, Ddi1 was reported as a yeast protease that removes various enzymatic and nonenzymatic DPCs independently of proteasome and Wss1 (Serbyn et al., 2020). Ddi1 contains a helical domain (predicted DNA-binding domain), a retroviral-like protease domain (RVP), a ubiquitin binding-like domain (UBL), and a ubiquitin-associated domain (UBA) (Wei et al., 2021). In higher eukaryotes, it was previously demonstrated that Ddi1's aspartic protease activity is involved in regulation of the proteasome pathway; DDI-1 in worms and its homologs in human cells, DDI2, activate the transcription factor SKN-1A or NRF1 by proteolytic cleavage to upregulate proteasome gene expression for compensation upon proteasome dysfunction (Koizumi et al., 2016; Lehrbach and Ruvkun, 2016). Further experiments showed that Ddi1 is a ubiquitin-dependent protease and preferentially targets poly-ubiquitylated substrates when the proteasome is overwhelmed (Dirac-Svejstrup et al., 2020; Yip et al., 2020). The

first insight into Ddi1's involvement in DPC elimination was indicated by a genetic interaction between Ddi1 and Wss1. Investigators observed that double depletion of Ddi1 and Wss1 sensitizes yeast cells to various DPC-inducing agents, including CPT, etoposide, and formaldehyde. Notably, CPT-induced hypersensitivity in Ddi1 and Wss1 deficient yeast is rescued by TOP1 depletion, suggesting TOP1 is the target of Ddi1 and Wss1 (Serbyn et al., 2020; Svoboda et al., 2019). Moreover, the protease and helical domains of Ddi1 are indispensable for the survival of Ddi1- and Wss1-mutant yeast upon the treatment of formaldehyde and CPT and are partially essential for etoposide resistance (Serbyn et al., 2020). However, it was not possible to demonstrate the protease activity of Ddi1 on DNA-bound substrates *in vitro*, even in the presence of ssDNA, dsDNA, and mono- or poly-ubiquitin chains, implying that additional co-factors are required (Serbyn et al., 2020). In addition, Ddi1 was reported to evict RBP1, a subunit of the RNA polymerase II, from chromatin via its proteolytic activity during replication stress. Nonetheless, it remained unclear whether Ddi1 targeted RBP1 as a crosslinked adduct or a stalling roadblock (Ruggiano and Ramadan, 2021a; Serbyn et al., 2020). Collectively, direct biochemical evidence that Ddi1 acts as a protease in DPC repair remains insufficient.

GCNA, also known as acidic repeat-containing protein (ACRC), was identified as an SprT-like metalloprotease domain-containing protease, which bears an intrinsically disordered region (IDR) and SUMO interacting motives (SIMs) (Carmell et al., 2016). It was commonly used as a germ cell marker, until recently GCNA was discovered to play an essential role in protecting genome integrity. Researchers found that GCNA deficiency results in genomic instability across species, including *D. melanogaster*, *C. elegans*, zebrafish, and human germ cell tumors (Bhargava et al., 2020). Furthermore, in human tumor cells, people investigated that upon treatment of cells with formaldehyde and 5-aza-dC, GCNA colocalized with chromatin and DNMT1 in a SUMO/SIMs-dependent manner (Borgermann et al., 2019). In line with the result that GCNA interacts with SUMOylated DPCs, GCNA is also associated with TOP2 during mitosis in worms (Dokshin et al., 2020). More specifically, the loss of GCNA leads to hypersensitization of the germline to DPC-inducing agents, including formaldehyde and etoposide. Also, GCNA-deficient *D. melanogaster* ovaries/embryos and zebrafish embryos accumulate more DPCs, and loss of GCNA generates more SPO11-associated DSBs in flies, formed via a topoisomerase-like mechanism. This evidence suggests that GCNA protects

genome stability by facilitating DPC elimination (Bhargava et al., 2020; Borgermann et al., 2019; Dokshin et al., 2020; Keeney et al., 1997). GCNA is enriched in the G2/M phase, whereas SPRTN is predominantly expressed during S and G2 phases. Moreover, the localization of GCNA and SPRTN in *C. elegans* was complemented among cell cycle phases. Loss of both GCNA and SPRTN results in an additive effect on aberrant chromosome numbers in worm germ cells compared to single protein deficiency, indicating the independent involvement of these two proteins in genomic stability maintenance (Bhargava et al., 2020; Dokshin et al., 2020; Mosbech et al., 2012). Notably, mouse GCNA lacks the protease domain, but *Gcna*-null mutant exhibited sterility in male mice, suggesting GCNA has a crucial function distinct from DPC proteolysis. It was recently found that GCNA is a histone chaperone to support DNA replication and maintenance of murine spermatogonial stem cells (Carmell et al., 2016; Dokshin et al., 2020; Ribeiro and Crossan, 2022). Collectively, the direct function of GCNA's protease activity in DPC removal has not been evaluated biochemically yet, and further experimentation will be imperative to conduct.

FAM111A is a putative serine protease that bears a trypsin-like protease domain, a DNA-binding domain, and a PIP motif (Alabert et al., 2014; Kojima et al., 2020). FAM111A was initially characterized as a PCNA-associated protein facilitating PCNA loading on replication sites and an SV40 large T antigen interactor involved in host range restriction, but the function of its trypsin-like protease domain remained unclear (Alabert et al., 2014; Fine et al., 2012). Recently, researchers described that FAM111A deficiency sensitizes cells to PARP inhibitors and CPT, which generates PARP1-DNA complexes and TOP1ccs, respectively. Further experiments demonstrated that loss of FAM111A leads to CPT-mediated TOP1ccs accumulation and increases replication fork stalling triggered by Niraparib and CPT, implicating FAM111A involved in the digestion of protein obstacles encountered by replication forks. In addition, similar to SPRTN self-cleavage, autocleavage of FAM111A is also observed *in vitro* and *in vivo*, depending on the DNA-binding domain and catalytic site (Kojima et al., 2020). Kenny-Caffey syndrome and osteocraniostenosis patients with *FAM111A* mutations display hypoparathyroidism and skeletal development failure symptoms (Unger et al., 2013). Biochemical assays indicated these FAM111A mutants from patients were hyperactive, which generated more FAM111A truncations, implying the connection between increased

autocleavage activity of FAM111A and cytotoxicity derived in patients (Hoffmann et al., 2020; Kojima et al., 2020; Nie et al., 2021). Furthermore, emerging research indicated that HMCES is a potential substrate of FAM111A and revealed the dual role (promote or impair) of FAM111A in replication regulation (Rios-Szwed et al., 2020). Taken together, FAM111A might potentially be able to proteolyze DPCs. However, its regulation mechanism and direct evidence of the involvement of its protease activity in DPC resolution remain to be determined.

1.2.2.4 Replication-coupled DPC proteolysis

DPCs are large roadblocks that impede DNA replication. Previous studies observed that proliferating cells are more sensitive to formaldehyde and CPT than non-proliferating cells suggesting that the cytotoxicity of DPCs can result from DNA replication block (Hsiang et al., 1989; Vaz et al., 2016). Consistent with these findings, loss of DPC repair protease Wss1 in yeast leads to cell cycle arrest in the G2 phase upon formaldehyde treatment, while overexpression of SPRTN in human cells promoted DNA replication fork progression upon exposure of cells to formaldehyde and CPT, indicating this enzyme aids DNA replication completion (Stingele et al., 2014; Vaz et al., 2016). Furthermore, DPCs are rapidly removed during the S-phase, which is reduced upon SPRTN deficiency, indicating that the repair of DPCs is DNA replication-dependent (Vaz et al., 2016). More direct evidence was provided using in *Xenopus* egg extract. The investigators indicated the involvement of multiple steps in DPC repair, including helicase bypass, DPC proteolysis, and DNA synthesis resume, which are stimulated by DNA replication (Duxin et al., 2014). This proteolytic mechanism to remove DPCs was subsequently determined to involve two redundant mechanisms: DPC proteolysis by SPRTN and proteasomal degradation (Larsen et al., 2019). Further studies identified more factors that are involved in replication-coupled DPC repair.

DPC repair is initiated by the replisome encountering a DPC that triggers stalling of CMG, the replicative helicase complex composed of CDC45, MCM2–7, and GINS, which translocates along the leading strand in 3'-5' direction (Fu et al., 2011). Previous research suggested that CMG bypass of protein adducts crosslinked to leading strand DNA requires DPC proteolysis (Duxin et al., 2014). However, more recent evidence demonstrated that CMG could bypass the lesions

directly with the aid of RTEL1 (regulator of telomere elongation helicase 1), a 5'-3' helicase on the lagging strand (Sparks et al., 2019). Notably, CMG bypass is usually accompanied by DPC ubiquitylation mediated by TRAIP ubiquitin E3 ligase, which facilitates ubiquitylation of DPC for proteasomal degradation but does not affect CMG bypass (Larsen et al., 2019; Sparks et al., 2019). Strikingly, *in vitro* assay showed TRAIP deficient *Xenopus* egg extract still ubiquitylates DPC on ssDNA, suggesting the presence of another E3 ligase in the context of ssDNA-protein crosslink (Larsen et al., 2019). This additional E3 ligase was later identified as RFWD3, which physically interacts with RPA and is activated by ssDNA resulting from RTEL1 stretching. When the proteins are covalently bound to lagging strand DNA, CMG bypass damage sites rapidly, leaving behind ssDNA generated from lagging strand DNA polymerase stalling. This additional DPC ubiquitylation by RFWD3 is beneficial for DNA damage bypass (Duxin et al., 2014; Fu et al., 2011; Gallina et al., 2021). Once bypassed by CMG, the DPC lesion impedes replicative polymerases and triggers DPC degradation mediated by SPRTN (non-ubiquitylated DPC) or proteasome (ubiquitylated DPC) (Larsen et al., 2019) (Figure 11).

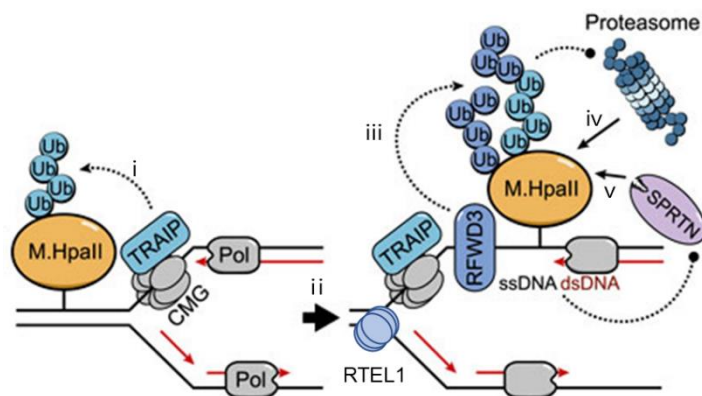


Figure 11: Schematic illustration of replication-coupled DPC repair in *X. laevis* egg extracts. A DPC on the leading strand stalls DNA helicase CMG, causing ubiquitylation of DPC by CMG-associated E3 ligase TRAIP. After that, DNA helicase RTEL1 travels opposite CMG, aids CMG in bypassing DPCs and stretching ssDNA, leading to RFWD3-mediated DPC ubiquitylation, which further leads to proteolysis by the proteasome and SPRTN. Figure adapted from (Leng and Duxin, 2022).

These results suggest that DNA replication acts as a sensing mechanism that recognizes DPCs and triggers DPC bypass, removal, and replication resumption.

1.2.2.5 Bypass and removal of DNA-peptide crosslinks

DPC protease-mediated proteolysis reduces the sizes of crosslinked proteins but cannot evict the lesion completely, which still blocks DNA replication and transcription. Therefore, these peptide remnants require a further process to remove or bypass the DNA-peptide crosslinks (Wei et al., 2021). The DNA-peptide crosslinks can be recognized as bulky DNA adducts which undergo canonical DNA damage repair pathways, such as NER, TDP1/TDP2 hydrolysis and TLS bypass during replication (Ruggiano and Ramadan, 2021a).

Due to the diverse structure of DPCs, distinct enzymes are employed to resolve the remained peptides. For instance, it is commonly accepted that when proteins are attached to intact DNA phosphate backbones, TLS polymerases aid the replication fork to bypass these lesions along with NER, which removes the adducts to restore DNA helical structure (Baker et al., 2007; Minko et al., 2008, 2002; Naldiga et al., 2019; Reardon and Sancar, 2006; Wickramaratne et al., 2016). TOP1 peptides, covalently bound to the 3' end of DNA, are hydrolysed by TDP1. However, emerging evidence suggests AP endonuclease 2 (APE2) also bears 3' to 5' exonuclease activity which contributes to the 3'-phosphotyrosine linkage incision and degradation of damaged DNA to expose a 3'-OH group. (Álvarez-Quilón et al., 2020; Li et al., 2019). Moreover, *in vitro* data suggests that ERCC1-XPF participates in 3'-phosphotyrosine adduct removal in an RPA-dependent manner generating 3'-OH and 5'-OH termini (Takahata et al., 2015). The downstream repair pathways could be short- or long-patch BER (Mei et al., 2020; Takahata et al., 2015). Although the repair pathways targeting peptides crosslinked to the 5' end of DNA are not well understood, long-patch BER has been implicated as a potential mechanism (Wei et al., 2021) (Figure 12).

Introduction

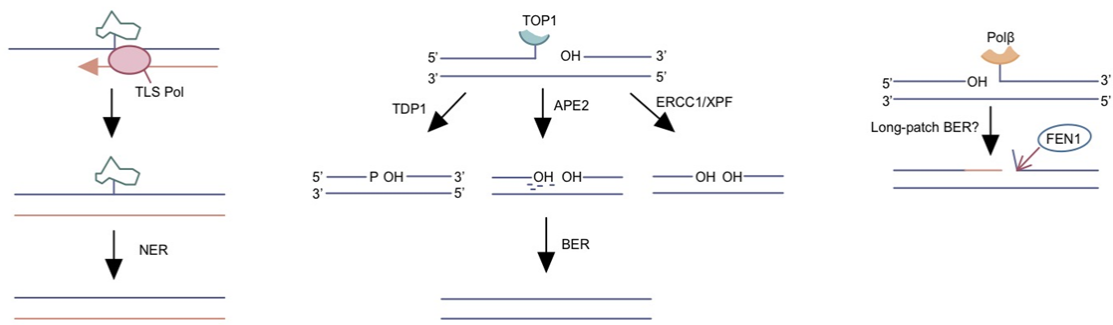


Figure 12: Schematic illustration of removal of different types of DPCs. Left panel: peptide crosslinked to intact DNA is bypassed by TLS polymerase during replication, followed by NER pathway. Middle panel: the DNA-TOP1 peptide crosslink is removed by TDP1, APE2, or ERCC1-XPF followed by BER pathway. Right panel: the Pol β peptide crosslinked to 5' end of DNA is likely repaired by long-patch BER pathway wherein FEN1 removes the damaged DNA and crosslinked protein residue. Figure based on illustrations in (Kühbacher and Duxin, 2020; Wei et al., 2021).

1.3 Ubiquitylation in DNA damage repair

Many DNA repair factors undergo post-translational modifications (PTMs), such as phosphorylation, PARylation, ubiquitylation, SUMOylation, which modulate enzymatic activities, protein stability and localization, and facilitate proper protein-protein interactions (Bai et al., 2020). Compared to other modifications, ubiquitylation involves a complicated enzymatic cascade reaction, and is also reversible (Song and Luo, 2019). Ubiquitin-mediated modification is an essential regulatory mechanism in DNA damage repair, controlling NER, DSBR, TLS, and FA pathways (Che et al., 2021; Rechkunova et al., 2019; Tan and Deans, 2021; Yu et al., 2020).

1.3.1 Ubiquitylation

Ubiquitin (Ub) is a protein comprised of 76 amino acids (8.6 kDa) which are highly conserved across all eukaryotes and expressed ubiquitously in most tissues of eukaryotic organisms (Haglund and Dikic, 2005). It is the protein unit added in a process known as ubiquitylation, wherein Ub is covalently added to amino acid residues of substrates. Ubiquitylation comprises three sequential steps mediated by Ub-activating enzymes (E1s), Ub-conjugating enzymes (E2s), and Ub ligases (E3s) (Hershko and Ciechanover, 1998) (Figure13). Briefly, a thioester bond is formed

between the cysteine group of E1s and the C-terminal glycine residue of ubiquitin in an ATP-dependent process accompanied by release of AMP and two phosphate groups. The activated Ub is next transferred to the active cysteine residue of E2s through a transesterification reaction, followed by Ub transmission from E2s to target proteins catalysed by E3s (Guo and Tadi, 2022). This enzymatic cascade reaction results in an isopeptide bond formation between Ub and lysine residues of the substrates, which is the most common covalent linkage of ubiquitylation. The non-canonical linkages include Ub being attached to cysteine residues through a thioester bond, serine, threonine, tyrosine residues through a hydroxyester bond, or protein's N-termini via a peptide bond (McDowell and Philpott, 2013).

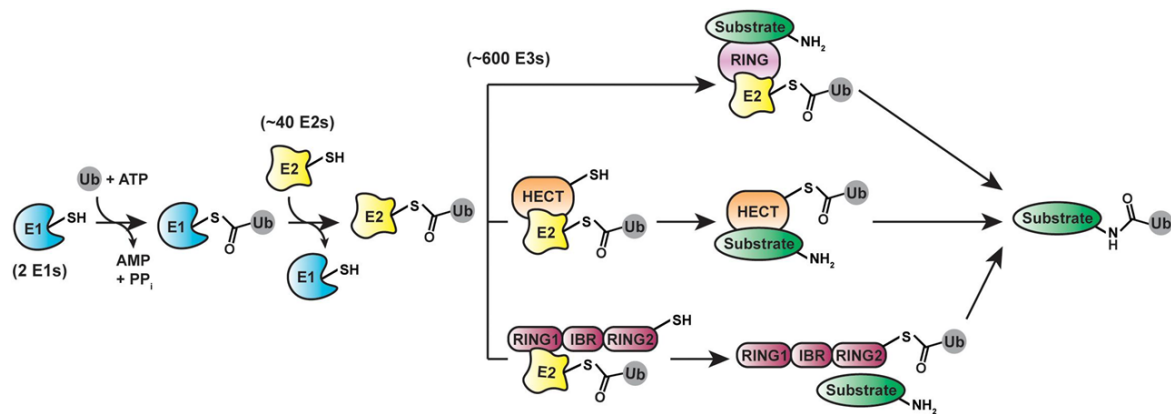


Figure 13: Schematic illustration of the cellular process during ubiquitylation. Ubiquitin is initially activated by E1, followed by Ub transmission to E2. After that, Ub is transferred to the substrate catalysed by E3. There are three distinct classes of ubiquitin ligases: RING, which bridges E2 and substrate together, mediating a direct transmission (top panel), HECT (middle panel) or RBR (bottom panel), which covalently binds to Ub and then transfers Ub to the substrate. Figure from (Deol et al., 2019).

The human genome contains only two ubiquitin-activating enzymes, UBA1 and UBA6, and a greater number of E2s (at least 40 in humans) (Groettrup et al., 2008; Wu et al., 2003). Compared with E1s and E2s, E3s are the most abundant ubiquitin-associated enzymes in cells that contain multiple families of enzymes or multiprotein complexes (more than 600 in humans), suggesting that each type of E2 can associate with several E3s (Hershko and Ciechanover, 1998; Song and Luo, 2019).

These diverse E3s can bind and modify specific protein substrates in numerous cellular contexts. Based on their structural domains and mechanisms of transferring

Introduction

Ub, E3s are classified into three families: really interesting new gene (RING), homologous to the E6AP carboxyl terminus (HECT), and RING-between-RING (RBR) (Morreale and Walden, 2016; Zheng and Shabek, 2017). These three families of E3s transfer Ub to substrates differently, wherein the RING E3 ligases serve as a scaffold bridging E2-ubiquitin and the substrate together, mediating a direct conjugation. This family is the most abundant type of E3s, which bear either a zinc-binding domain or a U-box domain that recruits ubiquitin-charged E2 (Deshaies and Joazeiro, 2009; Morreale and Walden, 2016). HECT-type E3s process Ub transmission through a two-step reaction: first, they form a covalent bond with Ub, after which they transfer Ub to the substrates. HECT E3 ligases harbor two lobes: a larger N-terminal lobe (N-lobe) which interacts with the Ub-charged E2 and a smaller C-terminal lobe (C-lobe) which carries the catalytic cysteine for accepting the Ub (Morreale and Walden, 2016; Weber et al., 2019). Additionally, the last group of E3s, RBR has features of both RING and HECT E3 ligases, containing an E2-interacting RING domain and a second domain termed RING2 that includes an active cysteine required for the formation of the E3-Ub complex from which the ubiquitin is conjugated to substrates (Morreale and Walden, 2016; Walden and Rittinger, 2018).

Ubiquitylation was initially identified as a mechanism for targeting substrates for proteasomal degradation (Glickman and Ciechanover, 2002). In the last decades, more types of Ub-mediated modifications have been established, which may occur as the addition of one ubiquitin molecule to a single substrate protein residue (mono-ubiquitylation), a single ubiquitin on multiple modified sites (multi-monoubiquitylation), or as the extension of mono-ubiquitylation by sequential rounds of ubiquitylation (poly-ubiquitylation) (Komander and Rape, 2012; Song and Luo, 2019). The variety of possible Ub modifications results in diverse cellular functions. It has been well-established that mono- and multi-monoubiquitylation lead to changes in intracellular localization or activity of a protein, or the formation of protein complexes which further affect various cellular processes, such as endocytosis, membrane trafficking, and nucleosomal rearrangement (Hoeller et al., 2006; Pavri et al., 2006; Sasaki et al., 2011; Su et al., 2013; Wang et al., 2013). Poly-ubiquitylation refers to the formation of a ubiquitin chain which results from the extension of monoubiquitin by linking a glycine residue of free ubiquitin with one of its seven lysine residues (K6, K11, K27, K29, K33, K48, K63) or an N-terminus of

substrate-associated ubiquitin (Komander and Rape, 2012). Poly-ubiquitin chains are named by the residue of basal Ub, which are targeted by additional Ub. For instance, poly-ubiquitin chains linked via lysine 48 and lysine 63 are called K48- and K63-chains, respectively, and amino-terminal methionine-linked poly-ubiquitin chain is called M1 linkage (Song and Luo, 2019). K48-mediated poly-ubiquitylation is the most typical modification which often results in proteasomal degradation of the modified proteins (Chau et al., 1989; Finley, 2009). K63-chains are not associated with protein disruption but are shown to play essential roles in endocytic trafficking, inflammation, translation, and DNA repair (Pickart and Fushman, 2004). Moreover, M1 linkage is involved in cell death, immune signalling, and protein quality control (Dittmar and Winklhofer, 2020). Other linkage types have been detected in cells, but the cellular functions of these atypical poly-ubiquitin chains are still poorly understood. Emerging research suggests that K6 participates in mitophagy, K11 is involved in DNA damage response, K27 has roles in the inflammatory response and DNA damage response, K29 regulates proteotoxic stress response and HR DNA repair pathways, and K33 is implicated in protein trafficking. Notably, in cells, different Ub-chain linkage can act synergistically because proteins can undergo mixed or branched poly-ubiquitylation modification (Liao et al., 2022).

1.3.2 Ubiquitylation in nucleotide excision repair

NER is subdivided into GG-NER and TC-NER, which targeted DNA damage throughout the genome or exclusively within transcribed DNA, respectively (Hanawalt, 2002). Nearly 30 proteins are involved in the NER pathway, and several NER factors undergo poly-ubiquitylation to facilitate the regulation of DNA repair by modulating protein-protein interaction and the stability of proteins (Li et al., 2011; Rechkunova et al., 2019).

In GG-NER, DNA distortions are initially recognized by XPC, sometimes with the help of the heterodimer DDB1-DDB2 when the distortions are mild (Hwang et al., 1999; Tang and Chu, 2002). These two factors were initially discovered as the substrates of the DDB-CUL4A-RBX1 E3 ubiquitin ligase complex (CRL4A^{DDB2}), wherein CUL4A and RBX1 form the E3 ligase catalytic core complex, and DDB1 serves as an adaptor for binding the substrate protein, DDB2. DDB2 is poly-ubiquitylated by CRL4A^{DDB2}, coinciding with the recruitment of XPC mediated by

DDB2 and CRL4A^{DDB2}-triggered XPC poly-ubiquitylation (Fischer et al., 2011; Fitch et al., 2003; Sugasawa et al., 2005). Poly-ubiquitylated DDB2 dissociates from the DNA lesions leading to its proteolysis by the proteasome, whereas poly-ubiquitylation of XPC enhances its affinity for DNA damage rather than degradation (Sugasawa et al., 2005). However, the precise biological functions of these modifications remain controversial. The original model suggested that degradation of DDB2 hands the damage over to XPC, therefore creating space for the recruitment and assembly of downstream NER complexes (Chitale and Richly, 2017; Li et al., 2011). However, a later study demonstrated that upon exposure to UVC, XPC protected DDB2 from ubiquitylation and degradation, allowing DDB2 to persist on the DNA and initiate repair events, ensuring sufficient cellular DNA repair capacity (Matsumoto et al., 2015). Moreover, poly-ubiquitylated XPC and DDB2 are substrates of the p97 segregase complex (comprised of p97 and its co-factors UFD1-NPL4 and UBDX760), leading to their subsequent proteasomal degradation. Depleting p97 showed increased residence time of XPC and DDB2 on damaged DNA, which eventually reduced NER efficiency and lead to genotoxicity, highlighting the importance of the timely extraction of damage recognition factors from chromatin after executing their functions (Puumalainen et al., 2014). The type of poly-ubiquitin chains synthesized by CRL4A^{DDB2} on DDB2 is assumed to be K48-linked since it regulates the proteolytic degradation of DDB2 (Rechkunova et al., 2019). XPC undergoing p97-induced segregation also hints towards it having K48-linked poly-ubiquitin chains. However, the modified lysine residue of XPC and the E2/E3 pair catalysing its modification to facilitate p97-mediated segregation remain unknown (Chitale and Richly, 2017). In addition, polySUMO2 chains are conjugated to XPC, which are further modified by K63-linked ubiquitin chains formed by the E2 UBC13-MMS2, and the E3 RNF111. This nonproteolytic modification promotes the eviction of XPC from DNA lesions after NER initiation, which is required for stabilizing the recruitment of endonucleases XPG and ERCC1/XPF to ensure efficient progression of the NER reaction (Poulsen et al., 2013; van Cuijk et al., 2015).

In TC-NER, Pol II functions as the DNA damage sensor, which stalls on the lesion, resulting in the subsequent recruitment of TC-NER factors, including CSA, CSB, and UVSSA, to initiate the repair process (Brueckner et al., 2007; van der Weegen et al., 2020). Similar to DDB2, CSA can also form an E3 complex with DDB1-CUL4-RBX1 (Groisman et al., 2003). This CRL4^{CSA} ubiquitin ligase complex

is structurally identical to the CRL4^{DDB2} complex, which is involved in GG-NER (Fischer et al., 2011). However, unlike DDB2, which serves as both substrate and component of the E3 complex, CSA is not ubiquitylated but facilitates the association between the ubiquitin molecular machinery and the substrate protein, CSB (Rechkunova et al., 2019). Poly-ubiquitylated CSB is extracted from damaged chromatin by the p97 segregase and its cofactors UFD1 and UBXN7, handing over CSB to proteasomal degradation. Inhibition of proteolytic degradation increases retention of CSB on the damaged sites. While this enhances recovery of RNA synthesis (RRS), it negatively impacts cell viability after UV irradiation, suggesting that timely clearance of CSB is crucial for efficient assembly of downstream NER factors (Groisman et al., 2006; J. He et al., 2016). RNA Pol II is also ubiquitylated and undergoes proteolysis in response to UV irradiation (Bregman et al., 1996; Luo et al., 2001). However, the regulation mechanism remains controversial since several distinct E3 ligases are identified involving in DNA damage-induced poly-ubiquitylation of Pol II, including the CRL4^{CSA} complex, NEDD4, Elongin A complex, BRCA1/BARD1 (BRCA1-associated RING domain protein 1) heterodimer, and von Hippel-Lindau protein (VHL) (Anindya et al., 2007; Harreman et al., 2009; Kleiman et al., 2005; Kuznetsova et al., 2003; Nakazawa et al., 2020; Starita et al., 2005). It was initially believed that proteolysis of the stalled Pol II allows NER factors such as TFIIH complex, access to the lesion, promoting repair complex assembly. In contrast, some studies argue that degradation of Pol II is not required in TC-NER but acts as a last-resort mechanism to allow access of slower repair mechanisms, such as GG-NER (Wilson et al., 2013). Recently two groups independently found that RPB1, the catalytic subunit of Pol II, is ubiquitylated specifically on K1268 by CRL4^{CSA}. This modification coordinates the recruitment of TFIIH and ubiquitylated UVSSA, which is essential for surviving DNA damage and transcription (Nakazawa et al., 2020; Tufegdžić Vidaković et al., 2020). *In vivo* experiments revealed that RPB1 K1268R mutant in *Xpa* knock-out mice led to Cockayne syndrome-like phenotypes, suggesting that the single ubiquitylation of RPB1 is essential in TC-NER and the development of Cockayne syndrome (Nakazawa et al., 2020). Subsequent research demonstrated that ELOF1 is a core TC-NER factor that binds and directs CRL4^{CSA} towards RNA Pol II and facilitates ubiquitylation of RPB1 on the site of K1268 (van der Weegen et al., 2021).

1.3.3 Ubiquitylation in double-strand break repair

PTMs, including ubiquitylation of histones, play an essential role in DNA damage repair regulation which is in place to orchestrate cell cycle, DNA replication, and transcription. Ubiquitylated histones not only alter chromatin structure at the sites neighbouring DSBs but also function as an integrative signalling platform for repair machinery recruitment which further affects the choice between HR and NHEJ (Aquila and Atanassov, 2020; Mattioli and Penengo, 2021; Schwertman et al., 2016).

ATM is a serine/threonine-protein kinase recruited and activated by DSBs, which mediates phosphorylation of H2AX to initiate DSBs responses. (Burma et al., 2001; Rogakou et al., 1998). Mediator of DNA damage checkpoint protein 1 (MDC1) binds γ H2AX (phosphorylated H2AX) via its BRCT domains, followed by ATM-mediated MDC1 phosphorylation and RNF8 recruitment through the forkhead-associated (FHA) domain of this RING-type E3 ligase (Kolas et al., 2007; Mailand et al., 2007; Stucki et al., 2005). At the DSBs, RNF8 catalyses K63-polyubiquitylation on linker histone H1 and L3MBTL2 (lethal(3)malignant brain tumor-like protein2), which is tethered by MDC1 to the vicinity of the DNA damage sites, facilitating the recruitment of RNF168 (Nowsheen et al., 2018; Thorslund et al., 2015). RNF168 then ubiquitylates H2A/H2AX at K13 and K15 to promote the stable retention of the pivotal DNA repair factors, BRCA1 and 53BP1, at chromatin areas neighbouring DSBs. These factors then compete with each other at committing the cells to HR or NHEJ, respectively (Bohgaki et al., 2013; Mattioli et al., 2012; Nowsheen et al., 2018).

The RNF168-catalysed H2AK15 mono-ubiquitylation, and di-methylation of histone H4 lysine 20 (H4K20me₂), are recognized by 53BP1 (Botuyan et al., 2006; Fradet-Turcotte et al., 2013). In the G1 phase of the cell cycle, the recruitment of 53BP1 counteracts HR by promoting the formation of 53BP1-RIF1-REV7 and 53BP1-PTIP-Artemis complexes, which thereby prevents the recruitment of BRCA1 to DSBs, and inhibits end resection while promoting NHEJ (Callen et al., 2013; Chapman et al., 2013; Di Virgilio et al., 2013; Escribano-Díaz et al., 2013; Wang et al., 2014; Zimmermann et al., 2013). Furthermore, cullin-RING E3 ligase complex CRL3^{KEAP1} ubiquitylates PALB2 in the G1 phase, which associates with BRCA2 and prevents its interaction with BRCA1, suppressing HR. (Orthwein et al., 2015).

Additionally, the E3 ubiquitin ligase, APC/C^{Cdh1}, comprised of anaphase-promoting complex/cyclosome (APC/C) and its cofactor Cdh1 assist HR restraint by inducing degradation of CtIP after mitotic exit and in the late S/G2 phase (Lafranchi and Boer, R de, 2014).

The recruitment of BRCA1 was initially found to depend on RAP80, which recognizes RNF8-mediated K63 ubiquitin chains on chromatin and recruits BRCA1-BARD1 heterodimer via interaction with BRCA1's BRCT domain (Hu et al., 2011; Sobhian et al., 2007; Yu et al., 2020). Recently it has been reported that BARD1 recognizes H2AK15 mono-ubiquitylation via a tandem BRCT-domain-associated ubiquitin-dependent recruitment motif (BUDR), followed by recruitment of BRCA1 to DSBs, suggesting two pathways exist to direct BRCA1 localization (Becker et al., 2021; Sherker et al., 2021). In the S/G2 phase, 53BP1 is phosphorylated and facilitates transient recruitment of RIF1 to DSB sites prohibiting HR. BRCA1-directed, PP4C/PP4R2-dependent dephosphorylation of 53BP1 leads to the eviction of 53BP1-induced DNA end resection barriers and RIF1 removal, allowing BRCA1 binding and the subsequent resection and invasion steps of HR (Isono et al., 2017). The RING domain of BRCA1 facilitates chromatin localization of CtIP by ubiquitylation (Yu et al., 2006). A subsequent study revealed that BRCA1-CtIP interaction is dispensable for DNA-end resection but accelerates the process (Cruz-García et al., 2014). Besides K13 and K15 modifications, H2A also undergoes K125/127/129 ubiquitylation, caused by the BRCA1/BARD1 E3 ligase complex. H2A-ubiquitylation recruits SMARCD1, which removes histone marks recognized by 53BP1, leading to 53BP1 repositioning and driving the completion of DNA-end resection (Densham et al., 2016; Kalb et al., 2014; Tong et al., 2020).

1.3.4 Ubiquitylation in DNA damage tolerance (DDT)

Cells have evolved a range of repair mechanisms to cope with DNA damage. However, when DNA lesions escape from repair and are encountered by replicative DNA polymerases, DNA replication is impeded. Three distinct DDT pathways are employed to handle or bypass unrepaired DNA lesions during the S/G2 phase, further protecting cells from DNA breaks and reducing the risk of replication fork collapse. These three DDT branches are characterized as error-prone translesion synthesis (TLS), error-free template switching (TS) and fork reversal (FR) pathways

Introduction

(Ler and Carty, 2022) (Figure 14). PCNA plays a crucial role in DTT serving as a platform to recruit replication factors and proteins involved in replication-coupled and post-replicative repair (Ashour and Mosammamarast, 2021; Moldovan et al., 2007). PCNA bears several PTMs, among which ubiquitylation is the key player driving the choice among TLS, TS and FR (Andersen et al., 2008).

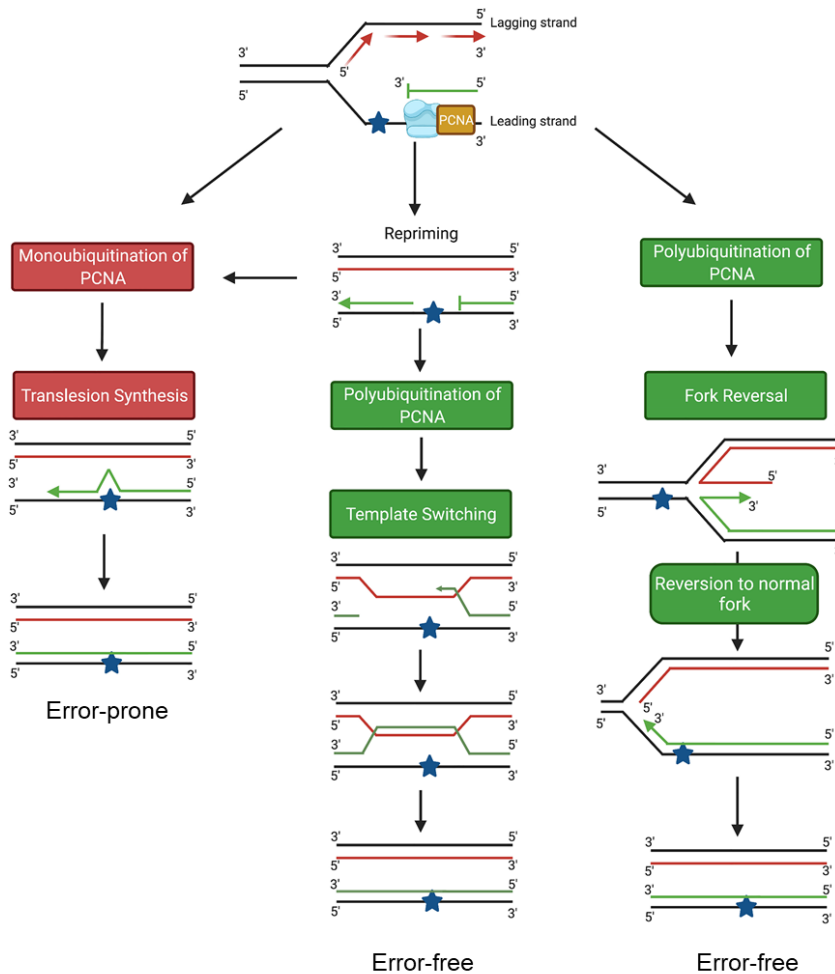


Figure 14: Schematic depiction of DNA damage tolerance pathway choice determined by PCNA modification. Left panel: TLS pathway mediated by mono-ubiquitylation of PCNA wherein the lesion is bypassed by TLS polymerases. Middle panel: TS pathway mediated by poly-ubiquitylation of PCNA, which involves strand invasion, repair synthesis and DNA recombination. Right panel: FR pathway mediated by poly-ubiquitylation of PCNA, wherein the replication fork is regressed, followed by fork reversion. Figure adapted from (Ler and Carty, 2022).

In response to replication stress, PCNA undergoes mono-ubiquitylation at K164 mediated by sequential ubiquitylation enzymes: UBA1 (E1), RAD6 (E2), and RAD18 (E3) (Hoege et al., 2002). RPA recruits the RAD6-RAD18 E2-E3 ubiquitin ligase complex via its direct interaction with RAD18, as replication stress promotes

a conformational change of RPA, increasing its affinity with RAD18 for efficiently mono-ubiquitylating PCNA on DNA (Hedglin et al., 2019). Notably, mono-ubiquitylation of PCNA K164 residue is also detected in a RAD18-independent manner suggesting the existence of other ubiquitin ligases, which were later revealed to be RNF8 and CRL4^{Cdt2} (Cullin4-RING ligase (CRL4)-DDB1-Cdt2). However, they are not as dominant as RAD18 (Simpson et al., 2006; Terai et al., 2010; Zhang et al., 2008). Mono-ubiquitylated PCNA switches its interaction with high-fidelity replicative polymerases Pol δ or Pol ϵ to low-fidelity TLS polymerases including Pol η , Pol ι , Pol κ , Pol λ , Pol ζ , or REV1, which help replication forks to bypass lesions by synthesizing DNA using their large active site. The recruitment of TLS polymerases to sites of DNA damage through direct interaction with mono-ubiquitylated PCNA occurs via their ubiquitin-binding motifs and PIP box, BRCT domain, and/or polymerase-associated domain (PAD) (Leung et al., 2018). TLS involves a sequential action implemented by two TLS polymerases: one inserts a nucleotide across the lesion first, and the second extends the nascent DNA strand. However, how the interplay between TLS polymerases and replicative polymerases occurs at the replication fork remains controversial (Leung et al., 2018; Maiorano et al., 2021).

In addition, the K164 mono-ubiquitylation of PCNA can be further extended by the Mms2-Ubc13-Rad5 complex (in yeast), forming K63-linked poly-ubiquitin chains. The formation of PCNA poly-ubiquitylation activates TS or FR, the error-free branches of the lesion bypass pathway (Branzei et al., 2004; Parker and Ulrich, 2009). In mammalian cells, in addition to Ubc13-Mms2, two Rad5 orthologs exist: helicase-like transcription factor (HLTF) and SNF2 histone linker PHD RING helicase (SHPRH). They were identified as components of E3 complexes which facilitate PCNA poly-ubiquitylation (Unk et al., 2008, 2006). Surprisingly, PCNA still undergoes poly-ubiquitylation in mouse embryonic fibroblast cells (MEFs) lacking both SHPRH and HLTF, and the cells are not hypersensitive to DNA-damaging agents, indicating the existence of yet another E3 ligase (Krijger et al., 2011). Zinc finger, RAN-binding domain-containing 3 (ZRANB3)/annealing helicase 2 (AH2) harbours an NPL4 zinc finger (NZF) motif, a variant of a ubiquitin-binding domain that recognizes K63-linked ubiquitin chains specifically. Furthermore, it bears a canonical PIP box and AlkB2 PCNA-interaction motif (APIM), thus stabilizing itself at the fork via interacting with poly-ubiquitylated PCNA (Ciccia et al., 2012; Weston

et al., 2012; Yuan et al., 2012). ZRANB3 has multiple roles in DDT. It can stimulate fork regression via its annealing helicase activity to mediate global fork slowing and promote replication fork restart. ZRANB3 can also act as a strand-specific endonuclease to dissociate replication fork D-loop intermediate in turn to limit inappropriate recombination events (Ciccina et al., 2012; Cipolla et al., 2016; Leung et al., 2018; Vujanovic et al., 2017). This fork reversal mechanism is dominant in human cells, whereas TS is more common in yeast. During TS, the stalled replication is reprimed, followed by strand invasion and gap filling utilizing the newly synthesized sister chromatid as the template, forming the sister chromatid junction (SCJ), which is resolved by Sgs1/Top3/Rmi complex (BLM-TOP3 α -RMI-RMI2 in mammalian cells) (Bi, 2015; Branzei and Szakal, 2016; Pilzecker et al., 2019).

1.3.5 Ubiquitylation in Fanconi anemia pathway

Fanconi anemia is a rare genetic disease caused by mutations of FA genes (22 genes are known currently). It results in impaired DNA damage repair and is accompanied by chromosomal instability. Proteins encoded by FA genes, along with other FA-associated proteins, comprise a biochemical signal pathway, known as the FA pathway, which is responsible for the detection, repair, and tolerance of endogenous DNA lesions, most prominently ICLs (Deans and West, 2011; Nalepa and Clapp, 2018).

The FA pathway is thought to occur in the following steps: 1. collision and unload of replication machinery in a p97-mediated manner; 2. FANCM-FAAP24-MHF1-MHF2 complex assembly and recruitment of FA core complex; 3. mono-ubiquitylation of the ID2 complex by the FA core complex and subsequent activation of nucleases; 4. recruitment and activation of HR factors to re-establish replication fork and 5. deubiquitylation of ID2 leading to its release from DNA (Niraj et al., 2019). A central event in this pathway is the mono-ubiquitylation of the ID2 complex components FANCD2 and FANCI on two specific lysine residues (K561 and K523, respectively), which leads to their retention on chromatin and activation of ICL repair during replication (Garcia-Higuera et al., 2001; Smogorzewska et al., 2007; Taniguchi et al., 2002; Wang et al., 2004).

The mono-ubiquitylation of the ID2 complex is carried out by three main ubiquitylation enzymes, UBA1 (E1), FANCT (also called UBE2T, E2) and FANCL

(E3) (Machida et al., 2006; Meetei et al., 2003). The E3 RING ubiquitin ligase FANCL clamps the ID2 complex at DNA lesion to signal recruitment of cellular nucleases for ICL removal (Klein Douwel et al., 2014; Knipscheer et al., 2009; Smogorzewska et al., 2007). This modification also triggers the activation of DNA recombination to restart and/or complete replication (Kais et al., 2016). Furthermore, most FA patients carry FA protein mutations that results in a lack of FANCD2 mono-ubiquitylation whereas the proteins are still expressed. The absence of ID2 ubiquitylation hypersensitizes cells to ICL-inducing agents, indicating the crucial role of ID2 ubiquitylation in the FA pathway (Shimamura et al., 2002; Tan and Deans, 2021).

The detailed molecular function of this modification remained ambiguous, until structural and biochemical studies recently revealed that FANCD2 forms a homodimer that cannot bind DNA, while the association with FANCI enables the heterodimer to interact with DNA. The mono-ubiquitylated ID2 complex transforms into a locked clamp that encircles DNA to initiate subsequent repair reactions (Alcón et al., 2020; Wang et al., 2020). Moreover, people investigated that mono-ubiquitylation of the ID2 complex does not promote any new protein-protein interactions *in vitro*. However, lacking ubiquitin, the proteins only associate with DNA for short periods (Tan et al., 2020). Further research demonstrated that mono-ubiquitylation of FANCD2 but not FANCI promotes the ID2 complex binding to dsDNA, while ubiquitylation of FANCI largely protects the ID2 complex from deubiquitylation mediated by USP1-UAF1 (Rennie et al., 2020). Emerging evidence showed that the ubiquitylation of either FANCD2 or FANCI promotes the ubiquitylation of another subunit (Lemonidis et al., 2022). Conclusively, these data suggest that ubiquitylation of FANCI and FANCD2 have distinct functions but converge to promote and maintain ID2-DNA interaction to initiate DNA repair (Alcón et al., 2020; Lemonidis et al., 2022; Rennie et al., 2020; Tan et al., 2020; Wang et al., 2020).

1.3.6 Deubiquitylation

Protein ubiquitylation is a reversible and dynamic post-translational modification that can be balanced by the opposing activities of ubiquitin E3 ligase and deubiquitylating enzymes (DUBs) (D'Andrea and Pellman, 1998). DUBs are a large

group of proteases that remove ubiquitin from proteins to regulate protein stability, protein-protein interaction, activity or localization by antagonizing ubiquitylation mediated by E3 ligases (Turcu et al., 2009). DUB-mediated deubiquitylation plays a vital role in genomic integrity, disease development and therapeutics (M. He et al., 2016). For example, ubiquitin-specific protease 1 (USP1) deubiquitylates PCNA and FANCD2 to limit the error-prone TLS-induced unwanted mutagenesis and inactivate ID2 complex after completion of ICL repair, respectively (Huang et al., 2006; Kim and Kim, 2016). Moreover, emerging evidence indicates that germline and somatic mutation of DUB genes or altered expression are correlated with human diseases, such as ectopic USP28 expression-induced colorectal cancer and malignancies caused by high-level ubiquitin carboxy-terminal hydrolase (Diefenbacher et al., 2014; Fang et al., 2010).

1.3.6.1 Deubiquitylating enzymes

Currently, nearly 100 DUBs are known in humans, which can be categorized into seven distinct protein families based on their sequence and domain conservation: ubiquitin-specific proteases (USPs), ubiquitin C-terminal hydrolases (UCHs), Machado-Josephin domain proteases (MJDs), ovarian tumor proteases (OTU), motif interacting with ubiquitin (MIU)-containing novel deubiquitylases (MINDYs), ZUP1 and Jab1/Mov34/Mpr1 Pad1 N-terminal+ (MPN+) (JAMM) domain proteases (Clague et al., 2019).

DUBs can be further classified into two main classes according to their catalytic site: cysteine proteases and metalloproteases, which have different enzymatic mechanisms. The majority of DUBs are cysteine peptidases, except the JAMM family, which is activated in a zinc-dependent manner, thus characterized as zinc metallopeptidase (Harrigan et al., 2018; Verma et al., 2016). Cysteine protease DUBs bear a catalytic triad comprised of Cys-His-Asp/Asn residues (C-H-D/N). The deubiquitylating process starts with the binding of the substrate via a nucleophilic attack and covalent bond formation between the activated cysteine of the DUB and the oxyanion hole of ubiquitin-modified protein, followed by amide bond breakage and amine product release. The histidine of the DUB's catalytic triad activates the oxygen of a water molecule, which attacks ubiquitin-associated carbonyl leading to the conjugation of oxhydriyl. After that, the covalent adduct (carboxylic acid-

conjugated Ub) is removed from the cysteine residue to restore the DUB's active site (Clark, 2016; Hanpude et al., 2015). Metalloprotease DUBs specifically target poly-ubiquitin chains, especially K63 and K48 poly-ubiquitin linkage. JAMM DUB family-mediated catalysis requires activated water molecules and a conserved glutamate. The catalytic site of the metalloprotease DUB contains an aspartic acid, a serine, and two histidine residues. In the process of hydrolysis, a zinc ion is coordinated by His-Asp residues and a water molecule. Nucleophilic attack of the water molecule on the carbonyl carbon of the isopeptide bond donates the hydrogen ion to glutamic acid. A proton from glutamic acid is then transfers to amide nitrogen leading to cleavage of the distal ubiquitin from protein substrate (Ambroggio et al., 2003; Gopinath et al., 2016; Shrestha et al., 2014)

1.3.6.2 USP7 in DNA repair

USP is the largest family of DUBs consisting of 58 described members involved in regulating diverse cellular processes, such as cell cycle and DNA damage repair (Cruz et al., 2021). USP7, also known as Herpesvirus-associated ubiquitin-specific protease (HAUSP), is a deubiquitylase, most commonly known as a critical regulator of the p53-MDM2 pathway (Li et al., 2002). It recently emerged as a key player in genome stability pathways and cancer progression. Therefore, it is also considered a novel promising drug target for cancer therapy (Valles et al., 2020; Wang et al., 2019).

USP7 has diverse substrates involved in several DNA damage repair pathways, such as DSB repair, NER and TLS. For instance, USP7 promotes stability of MDC1, an initiator of DSB repair pathway that facilitates the accumulation of RNF8 and RNF168 on damage sites and subsequently triggers the recruitment of 53BP1 or BRCA1 to promote the repair of DSBs (Stewart et al., 2003). Loss of USP7 leads to failed engagement of the MRN-MDC1 complex and an inability to recruit the downstream factors 53BP1 and BRCA1 to DNA lesions (Su et al., 2018). Furthermore, USP7 can deubiquitylate and stabilize RNF168 and RNF169 to promote and limit the accumulation of 53BP1/BRCA1 at DSBs, respectively, suggesting it has an essential role in balancing DSB repair activation (An et al., n.d.; Zhu et al., 2015). In addition, both XPC and CSB are targets of USP7, which participate in GG-NER and TC-NER, respectively. Poly-ubiquitylation of XPC is

functionally essential for enhancing its recruitment to damaged DNA, followed by p97-mediated extraction and RNF111-mediated degradation. USP7 physically interacts with and deubiquitylates XPC both *in vitro* and *in vivo*, stabilizing XPC and preventing it from premature proteolysis (He et al., 2014). In TC-NER, CSB undergoes ubiquitylation carried out by the CUL4A^{CSA} E3 ligase complex, which is subsequently extracted from chromatin by the p97 segregase and committed to the proteasome for proteolysis for downstream repair processing (J. He et al., 2016). Previous research found that an interaction between UVSSA and USP7 is important to recruit the DUB to chromatin and to subsequently increase the stability of CSB (Schwertman et al., 2012; Zhang et al., 2012). Further experiments revealed that USP7 acts as a CSB but not UVSSA deubiquitylating enzyme to maintain CSB levels after UVC-induced DNA damage (Zhu et al., 2020). Taken together, these findings suggest that even though CSB degradation plays an essential role in the recovery of transcription, USP7 helps to delay this process ensure complete repair (Valles et al., 2020). Additionally, USP7 also enhances RAD18 stability by associating with RAD18 directly and disassembling poly-ubiquitin chains from RAD18. Depletion of USP7 results in decreased RAD18 protein levels, reduced PCNA mono- and poly-ubiquitylation and impediment of DNA synthesis after UVC irradiation (Zlatanou et al., 2016). Moreover, both *in vitro* and *in vivo* results demonstrate that USP7 physically binds and deubiquitylates Pol η to increase its cellular stability. In addition, ectopic expression of USP7 facilitates UV-induced mono-ubiquitylation of PCNA by stabilizing Pol η (Qian et al., 2015). To sum up, these results suggest a crucial role of USP7 in regulating the DNA damage bypass pathway by fine-tuning ubiquitylation of the PCNA sliding clamp.

1.4 RNA-protein interaction

Ribonucleic acid (RNA) is assembled as a chain of nucleotides that contain a ribose sugar, a nitrogenous base of guanine (G), uracil (U), adenine (A), or cytosine(C), and a phosphate group. Unlike DNA which appears as paired double-stranded chain, RNA is found in nature mostly as a single strand; exceptions are the genomes of double-stranded RNA viruses and transcripts endogenously formed from repetitive DNA (Wang and Farhana, 2022; Weber et al., 2006). RNA plays essential roles in various biological processes, such as controlling gene expression, catalysing

biological reactions, and regulating protein synthesis. Most nascent RNA is associated with and controlled by several protein partners to carry out its cellular functions (Cusack, 1999). Both RNA and its associated proteins (also known as RNA-binding proteins, RBPs) can undergo conformational changes to form stable complexes during RNA processing (Gopinath, 2009). These RNA-protein complexes are considered regulatory units for post-transcriptional gene regulation, including mRNA transport, mRNA translation modulation and RNA splicing regulation (Oliveira et al., 2017). RBPs can recognize specific RNA structures and modifications that guide RNA-protein interactions to carry out RNA-processing events (Lewis et al., 2017).

Identification of RBPs and determination of their RNA binding sites or motifs are paramount for understanding their function in the regulation of different cellular fundamental processes (Weissinger et al., 2021). So far, researchers have developed multiple approaches to capture the RNA interactome and have characterized over two-thousand RBPs, the majority of which bear well-determined RNA-binding domains (RBDs), such as RNA recognition motif (RRM), double-stranded RNA (dsRNA) binding domain and zinc fingers while hundreds of newly discovered RBPs generally lack canonical RBDs (Hentze et al., 2018; Lunde et al., 2007). There are many different methods to study RNA-protein interactions by enrichment and purification of RNA-protein complexes, such as crosslinking and immunoprecipitation (CLIP), protein-crosslinked RNA extraction (XRNAX), identification of direct RNA interacting proteins (iDRiP), Phenol Toluol extraction (PTex). Following purification, mass spectrometry (MS) analysis or RNA high-throughput sequencing are used to identify the involved protein and RNA components (Minajigi et al., 2015; Trendel et al., 2019; Ule et al., 2003; Urdaneta et al., 2019).

1.4.1 RNA categories

In eukaryotic cells, there are three main types of RNA: messenger RNA (mRNA), ribosomal RNA (rRNA), and transfer RNA (tRNA), which participate in the process of protein synthesis (Wang and Farhana, 2022). In addition to these three categories of RNA, there are also several varieties of noncoding RNA (ncRNA), including small nuclear RNA (snRNA), microRNA (miRNAs), and small interfering RNA (siRNA),

Introduction

that participate in RNA splicing, gene regulation, and RNA interference (Dana et al., 2017; O'Brien et al., 2018; Valadkhan and Gunawardane, 2013).

mRNA accounts for 1-5% of the total cellular RNA in cells. It is a single-stranded linear polynucleotide complementary to one of the DNA double strands of a gene. mRNA is transcribed by RNA polymerase II and it carries the genetic information transported from the nucleus to the cytoplasm, where proteins are synthesized. (Wang and Farhana, 2022). The newly transcribed RNA transcript (also known as pre-mRNA) contains noncoding and coding regions known as introns and exons, respectively, requiring maturation before being exported to the cytoplasm and utilized as a template for translation (Bentley, 2014). The pre-mRNA processing events include 5'-end capping (7-methylguanosine (m7G) addition to mRNA's 5' end), cleavage and removal of introns, and 3'-end polyadenylation (addition of a sequence of adenine nucleotides, the poly(A) tail, to the 3' termini) (Shatkin and Manley, 2000; Zorio, 2004). mRNA maturation protects the mRNA from degradation, aids mRNA transport, and contributes to translation initiation (Pal, 2020; Wang and Farhana, 2022). The matured mRNA is recognized by the translation machinery via the 5' cap in the cytoplasm. It serves as a track for the ribosomes to move along and decode each triplet of nucleotides on the mRNA as corresponding to an amino acid with the help of tRNA, which leads to the production of specific polypeptide chains. In summary, mRNA acts as a bridge between the genetic information in DNA and the amino acid sequence of proteins (Alberts et al., 2002).

tRNA is the smallest of the three main types of RNA, consisting of about 76-90 nucleotides. It is a ribonucleic acid that carries matching amino acids to ribosomes based on mRNA nucleotide sequence. It transfers amino acids to the growing protein polypeptide chains. Thus, it serves as an adapter in the translation process, which physically links the mRNA and the amino acid sequence of proteins (Sharp et al., 1985). tRNA is transcribed by RNA polymerase III, and similar to mRNA, it undergoes processing during maturation, which includes multiple steps: cleavage of 5' and 3' ends, the addition of the terminal CCA residues to the 3' end, specific nucleotide modifications and removal of introns (Betat et al., 2014). tRNA has a cloverleaf-like structure due to the complementary pairing in various positions. The structure features a 3' acceptor arm (forming an ester linkage with an amino acid), a D-arm (stabilizing the tRNA tertiary structure), an anticodon arm (forming a hydrogen bond with complemented mRNA), a T Ψ C arm (T-arm, recognized by the

Introduction

ribosome during translation), and a variable arm (recognized by aminoacyl-tRNA synthetase) (Figure 15) (Berg and Brandl, n.d.; Giegé and Frugier, 2013; Krahn et al., 2020).

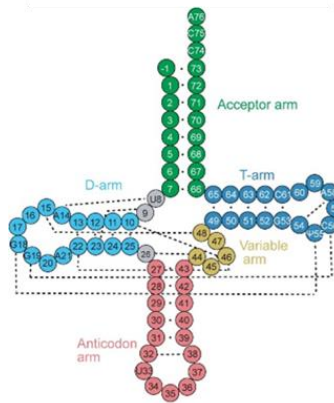


Figure 15: Secondary structural representation of a tRNA molecule coloured based on specific regions: acceptor arm (green), D-arm (light blue), anticodon arm (pink), variable arm (yellow) and T-arm (dark blue). Figure from (Krahn et al., 2020).

rRNA accounts for around 80% of the total cellular RNA in yeast and 50% in proliferating mammalian cells. (Moore and Steitz, 2002; Moss and Stefanovsky, 2002). rRNA transcription occurs in the nucleus and is performed by RNA polymerase I and III. In eukaryotes, Pol I and Pol III first transcribe two long precursor molecules, 45S and 5S pre-rRNA, respectively. After rRNA processing, 45S pre-mRNA is then processed into 28S, 5.8S, and 18S rRNAs, and 5S pre-rRNA is into 5S matured rRNA (Aubert et al., 2018; Granneman, 2004). rRNAs are both structural and functional components of ribosomes, together with ribosomal proteins forming the translation machinery to generate polypeptide chains (Moore and Steitz, 2002).

The RNAs mentioned above are involved in protein synthesis. Another group of regulatory RNA has functions in gene editing, gene regulation, gene expression, etc. These transcripts are commonly termed ‘noncoding RNAs’ and can be categorized into two classes based on their length: long ncRNAs (lncRNA, >200 nt) and small ncRNAs (sncRNA) (Brosnan and Voinnet, 2009). A prominent example of lncRNA is X-inactive specific transcript (Xist), a significant effector during the X chromosome inactivation process. Xist deficiency leads to disruption of inactivation of the corresponding X chromosome, while duplication of the Xist gene on another

chromosome induces inactivation of that chromosome (Penny et al., 1996). Examples of sncRNAs include snRNA, miRNA and siRNA. snRNAs are small, with an average length of around 150 nt nuclear-localized ncRNAs that are transcribed by either Pol II or Pol III (Henry et al., 1998). They are responsible for the splicing of introns of pre-mRNA by forming spliceosomes with small nuclear ribonucleoproteins (snRNP) (Lamond, 1993). miRNAs are single-stranded RNA molecules of very short length (approximately 22 nt). Pol II transcribes canonical miRNAs from introns of pre-mRNAs, followed by maturation carried out by endonucleases, such as Drosha and Dicer (Bartel, 2018). Studies have demonstrated that miRNAs interacting with an untranslated region (UTR) on mRNAs induce mRNA degradation and suppress translation. In contrast, miRNAs binding to promoter regions can activate gene expression (Dharap et al., 2013; Humphreys et al., 2005; Zhang et al., 2018). siRNAs are a class of double-stranded ncRNAs that bear similar sizes to miRNA (21-23 nt). siRNAs are produced from long dsRNAs and small hairpin RNAs by the Dicer enzyme (Bernstein et al., 2001; Dana et al., 2017). They inhibit gene expression by degrading mRNA. In brief, the siRNAs are incorporated into the RNA-induced silencing complex (RISC), after which the duplex is separated, and one strand is removed from the complex. The other strand guides RISC to the complementary site on mRNA, followed by a cleavage carried out by the catalytic RISC protein, Argonaute (O'Keefe, 2021). Due to their ability to interfere with gene expression, siRNAs are widely used as tools to study single gene function, and they are also considered as potential therapeutic agents for disease (Cejka et al., 2006; Gavrillov and Saltzman, 2012).

1.4.2 Methodology to study RNA-protein interaction

Methods for studying RNA-protein interactions can be classified into two categories based on the molecule of interest they start with. There are RNA-centric and protein-centric methods, which begin with the purification of a given RNA or class of RNAs and the purification of a particular protein or protein species, respectively. MS usually follows RNA-centric methods to identify the associated proteins, while protein-centric processes are followed by sequencing the RBPs-binding RNAs across the transcriptome (McHugh et al., 2014; Ramanathan et al., 2019). However, these approaches are limited to characterizing interactions of one particular protein

or RNA species. Recently, several unbiased, comprehensive protocols have been established that isolate protein-crosslinked RNA irrespective of RNA type but rather extract them based on their physicochemical differences (Queiroz et al., 2018; Trendel et al., 2019; Urdaneta et al., 2019).

Capturing the RNA-protein interactome requires strong interactions between RNA and protein at the intracellular level. RNA-protein complexes are rapidly captured by crosslinking, which prevents the rearrangement or disintegration of the complexes (Majumder and Palanisamy, 2021). Short wavelength UV light is the dominant method for crosslinking RNA-protein complexes, inducing covalent bond formation between two aromatic rings present in RNA and interacting proteins (Poria and Ray, 2017) (Figure 16). UV irradiation crosslinks RNA and protein at their contact point, thus displaying a direct RNA-protein interaction. However, the efficiency of this method is relatively low (Majumder and Palanisamy, 2021). Another variant approach was developed that significantly increased crosslinking efficiency: photoactivatable ribonucleoside-enhanced crosslinking (PAR-CL), here a nucleotide analogue (such as 4-thiouridine (4-SU) or 6-thioguanosine (6-SG)) is incorporated into nascent RNA transcripts, followed by long-wavelength UV irradiation inducing efficient crosslinking of photoreactive nucleoside-labelled cellular RNAs to interacting RBPs (Hafner et al., 2010; Meisenheimer and Koch, 1997) (Figure 16). The drawback to this approach is that it can only be applied in specific cell lines due to the limitation of photoactivatable nucleosides incorporation efficiency (Ule et al., 2018). Other crosslinking methods include chemical crosslinking carried out by chemical crosslinkers, such as formaldehyde, diepoxybutane, 2-iminothiolane, and DTT (Bäumert et al., 1978; Kim and Kim, 2019; Wower et al., 1981; Zaman et al., 2015). Formaldehyde is a widely used crosslinker for chromatin immunoprecipitation (ChIP) and ribonucleoprotein immunoprecipitation (RIP) assays (Matsunaga et al., 2001; Niranjanakumari et al., 2002) (Figure 16). It is a reversible crosslinking agent, which is beneficial for the subsequent reverse transcription-PCR (RT-PCR) reaction to detect bound RNAs. However, formaldehyde also crosslinks protein with protein, thus it is not easy to distinguish the direct RNA-protein complexes from the protein–protein-RNA complexes (Majumder and Palanisamy, 2021; Ramanathan et al., 2019).

Introduction

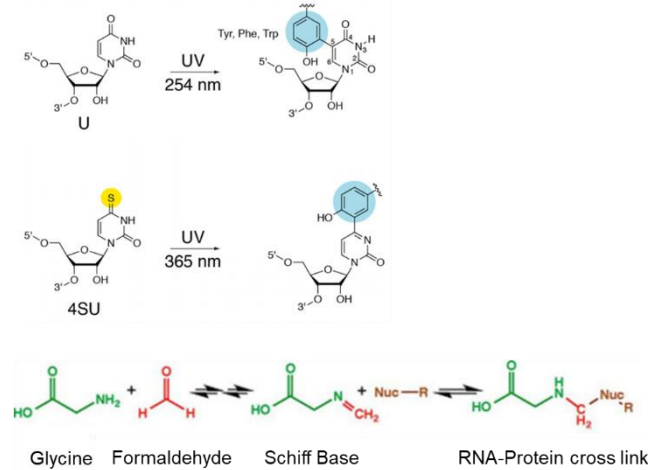


Figure 16: The schematic depiction of UV or formaldehyde-mediated crosslinking reactions of RNA and protein. Upper panel: UVC (254 nm) crosslinks uridine and aromatic amino acids, Tyrosine (Tyr), Phenylalanine (Phe) and Tryptophan (Trp). Middle panel: UVA (365 nm) crosslinks 4-thiouridine and aromatic amino acids. Bottom panel: formaldehyde-mediated crosslink between an amino acid (Glycine as an example) and an RNA nitrogen base. Figure from (Hoffman et al., 2015; McHugh et al., 2014).

One general approach to enrich mRNA is utilizing oligo(dT) to capture RNAs with a poly(A) tail, followed by proteomic identification of poly(A)RNA-binding proteome (Castello et al., 2012). However, this method is limited to isolating polyadenylated RNA and loses most non-polyadenylated ncRNA, including tRNA, rRNA, snRNA, etc. (Trendel et al., 2019). Another typical RNA affinity purification (RAP) method is MS2 *in vivo* biotin-tagged RAP (MS2-BioTRAP), which utilizes the interaction between the MS2 hairpin loop and MS2 coat protein to tether RNA-protein interaction. In brief, the repeats of MS2 aptamer are appended to RNA, and the tagged RNA is isolated by coupling the MS2 protein to a resin (Marchese et al., 2016). Pulling down protein components of RNA-protein complexes is usually subjected to immunoprecipitation (IP), which takes advantage of the specific association between a protein of interest and its antibody (Majumder and Palanisamy, 2021). In general, RNA-centric methods are not as extensively used as protein-centric methods because they require a large amount of material to reach detectable levels of proteins (Bantscheff et al., 2007). The unbiased purification of RNA-protein complexes has also been developed based on the physicochemical properties of crosslinked RNPs. In this case, extraction with organic solvents is used to purify crosslinked RNPs (Queiroz et al., 2018; Trendel et al., 2019; Urdaneta et al., 2019).

Proximity labelling can also be used to identify RNA-protein interactions which does not rely on crosslinking. For instance, an RNA of interest is tagged with a BoxB aptamer which recruits RNA-protein interaction detection (RaPID, λ N-HA-BirA*) fusion protein (BirA is a biotin ligase), thereby biotinylating proteins bound to the adjacent RNA motif of interest. The biotinylated proteins are captured by streptavidin beads followed by protein identification by MS (Ramanathan et al., 2018).

Alternatively, fusion of the enzyme ADAR or poly(U) polymerase to an RBP of interest results in deamination of nearby adenosines or adds poly(U) tails to bound RNAs, respectively. The specific RBP-binding RNA is detected by sequencing of the RNA. The deamination of adenosine results in inosine substitution, which is read as a guanosine when analysed by RNA sequencing, generating a A-G transition (McMahon et al., 2016). Poly(U) polymerase-attached poly-uracil chains at the 3' end of interacting RNAs are considered as tags during RNA sequencing (Lapointe et al., 2015).

In general, the above-mentioned non-crosslink purification is beneficial for its low cost in both time and materials consuming. Still, it may lead to re-association or formation of non-specific RNA-protein interactions in solution (McHugh et al., 2014).

1.5 Ribosome and translation

In 1958, Francis Crick first proposed the concept of the “Central dogma of molecular biology,” which states that DNA contains genetic information converted into a functional protein product (Crick, 1958). Briefly, the genetic information stored in DNA is first transcribed into RNA which then serves as a template for protein synthesis. Proteins are produced during a process called translation where ribosomes travel along the mRNA, decode it and produce polypeptide chains according to the mRNA sequence. Subsequently, the polypeptide chains are folded into their native three-dimensional structure, after which the proteins become biologically active. The translation process is relatively conserved throughout species, including three main steps: initiation, elongation, and termination (Ganoza et al., 2002). Proteins are involved in nearly all cellular activities by functioning as enzymes, antibodies, structural components, messengers, and transport or storage proteins. Regulation of protein synthesis plays a vital role in homeostasis maintenance, and aberrant regulation of translation can result in numerous diseases.

Thus, understanding the molecular mechanism of translational control is critical (Hershey et al., 2012).

1.5.1 The composition of the ribosome

In eukaryotic cells, the ribosome (80S) comprises two subunits: large subunit (LSU) and small subunit (SSU), designated as 60S subunit and 40S subunit, respectively (Figure 17). The 80S ribosome of human cells has a molecular weight of about 4.3 MDa. Its 60S subunit consists of 28S, 5S, and 5.8S rRNAs and 47 proteins, while the 40S subunit contains a single 18S rRNA chain and 33 proteins (Khatter et al., 2015). The biogenesis and maturation of the two subunits occurs separately. Following maturation, the subunits can assemble on an mRNA molecule to form a translation-competent 80S ribosome. This process is catalysed by more than 200 ribosome assembly factors (Klinge and Woolford, 2019; Singh et al., 2021). After assembly, the ribosomes start to read the mRNA in 5'-3' direction and catalyse the formation of poly amino acid chains by transferring the amino acids from their attached aminoacyl-tRNAs to the end of the growing polypeptide chain.

The ribosome has three positions to accommodate tRNA: the A site, P site, and E site, which refer to aminoacyl-tRNA (aa-tRNA), peptidyl-tRNA, and deacylated tRNA binding sites, respectively (Garipey and Dickinson, 2006) (Figure 17). During translation, the aminoacyl-tRNA firstly occupies the A site (located in the decoding center in the SSU) via the complementary interaction between its anticodon and codon on mRNA (Frank, 2003; Sergiev et al., 1998). Subsequently, the tRNA configuration changes from canonical state (A/A- and P/P-tRNA) to pre-translocation hybrid state (A/P- and P/E-tRNA). This coincides with peptide bond formation catalysed in the peptidyl transferase center (PTC) residing in the LSU. Thus, the nascent peptide chain is extended by one amino acid (Dorner et al., 2006; Polacek and Mankin, 2005). Following this, in the translocation step, the de-acylated tRNA moves to the E-site and the peptidyl-tRNA moves to the P-site, restoring a canonical P/P- and E/E-tRNA state. From this state, the E site tRNA is subsequently released from the ribosome and a new tRNA can be recruited in the A site, beginning the cycle anew (Kirillov et al., 1983). In summary, tRNAs travel through A-P-E sites in the ribosome as they deliver amino acids in the process of translation. When a stop codon appears at the A site, the release factor proteins (RFs) recognize the

Introduction

stop codon and facilitate the hydrolysis of the completed polypeptide chains from the P site tRNA (Youngman et al., 2007).

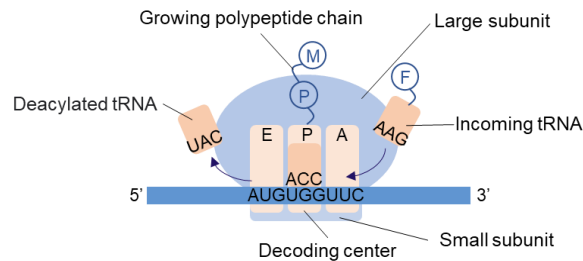


Figure 17: Schematic illustration of the ribosome structure, which consists of two subunits, a large subunit and a small subunit. The assembled ribosome bears three tRNA binding sites, the A/P/E site, which binds the entering aminoacyl-tRNA, holds the peptidyl-tRNA and carries the deacylated tRNA, respectively. During translation, tRNAs translocate from the A to the P to the E site. Figure based on the illustrations in (Frank, 2003).

1.5.2 The translation cycle

The translation process is conserved across all species and occurs in three main stages, initiation, elongation and termination. Each stage has consists of multiple processes carried out by a series of factors (Kapp and Lorsch, 2004; Roux and Topisirovic, 2012).

Initiation is a complex process that involves the initiator methionine tRNA (tRNA^{Met}) binding to the P site of the SSU, while 40S and 60S subunits are assembled into an 80S ribosome at the start codon on mRNA, which is almost exclusively methionine (Met) (Aitken and Lorsch, 2012; Chukka et al., 2021; Hinnebusch and Lorsch, 2012; Jackson et al., 2010; Pestova et al., 2001; Querido et al., 2020). In detail, the tRNA^{Met} forms a ternary complex (TC) with GTP-associated eukaryotic initiation factor (eIF) 2 followed by TC binding to ribosome SSU aided by eIF3, eIF5, and eIF1, leading to the formation of 43S preinitiation complex (PIC) comprising an SSU, eIF1, eIF1A, eIF3, TC and eIF5. The 43S PIC is then recruited to the 5' end of mRNA via the interaction with the cap-binding complex eIF4F (consisting of eIF4G, eIF4E, eIF4A), eIF4B and poly(A)-binding protein (PABP) resulting in 48S PIC formation. eIF4E binds to the 5' end of mRNA, whereas PABP recognizes the 3' polyA tail of mRNA, causing circularization of mRNA (Querido et al., 2020; Wells et al., 1998). Subsequently, the 48S PIC scans along

Introduction

the mRNA from 5' to 3' until reaching the start codon. Following the initiation codon recognition, eIF5B, a GTPase, hydrolyses the GTP of TC, leading to the release of eIF2-GDP from the SSU. Eventually, the LSU joins the complex to form 80S ribosomes coinciding with the dissociation of other eIFs catalysed by eIF5B. The released eIF2-GDP complex is recycled to eIF2-GTP by the guanine nucleotide exchange factor (GEF) activity of eIF2B for the new round of initiation (Figure 18) (Jackson et al., 2010; Jennings et al., 2013; Schmidt et al., 2016).

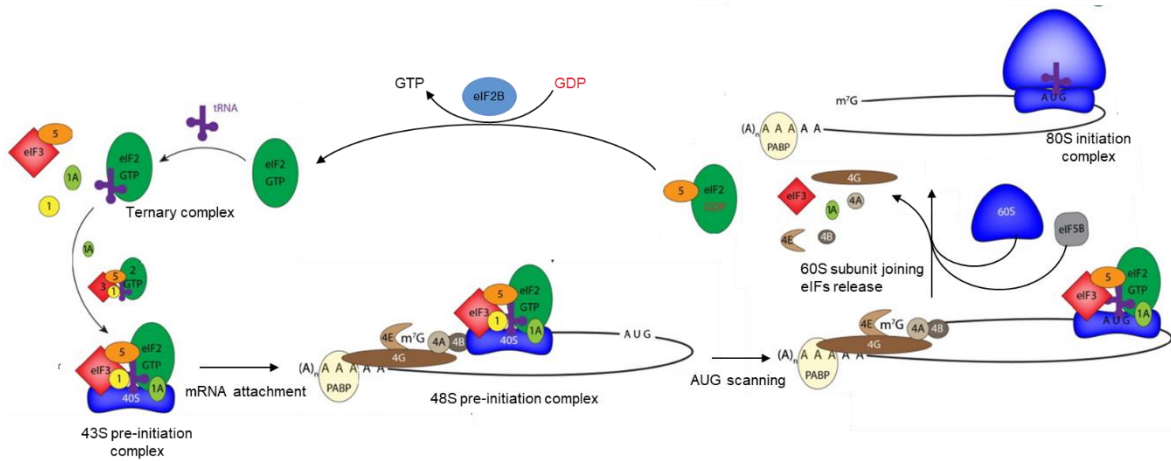


Figure 18: Schematic illustration of translation initiation in eukaryotes. In brief, tRNA^{Met} binds to GTP-associated eIF2, forming a ternary complex, followed by 43S pre-initiation complex assembly comprising the ternary complex, eIF1, eIF3, eIF5 and small ribosomal subunit. After that, the 43S pre-initiation complex attaches to the mRNA forming 48S PIC with eIF4E and PABP, scanning for an AUG start codon. Finally, the ribosomal large subunit and eIF5B join to the small subunit to form the 80S initiation complex coinciding with the dissociation of eIF2-GDP and other eIFs. The released eIF2-GDP is recycled via nucleotide exchange catalyzed by eIF2B. Figure adapted from (Schmidt et al., 2016).

After forming a complete ribosome with a tRNA^{Met} located at the P site, the ribosome starts to move along the mRNA, accompanied by growing of the polypeptide chain (Figure 19). The initiator tRNA occupies the P site in the ribosome leaving behind an empty A site ready to receive an additional aa-tRNA carrying a new amino acid to be added behind the previous one, beginning the formation of a peptide chain (Dever et al., 2018). Translation elongation is a process in a three-step circulation: decoding, peptide bond formation, and tRNA translocation. Elongation begins with the delivery of the second aa-tRNA to the A-site, which is carried out by eukaryotic translation elongation factor (eEF)1A that associates with GTP and forms a TC together with aa-tRNA. Following the interaction between anticodon on aa-tRNA and codon on mRNA at the A site, eEF1A catalyses GTP

Introduction

hydrolysis and is released from the aa-tRNA, leading to aa-tRNA accommodation in the A site. Like eIF2-GDP, the eEF1A-GDP can also be recycled to eEF1A-GTP by the GEF, eEF1B (Andersen et al., 2001; Mateyak and Kinzy, 2010). The subsequent step is peptidyl transfer and peptide bond formation, during which the synthesized peptide is transferred from the peptidyl-tRNA to the newly coming aa-tRNA, which is catalysed in the PTC of the ribosome leading to the formation of a new extended peptidyl-tRNA (Polacek and Mankin, 2005). Finally, the deaminoacyl-tRNA and peptidyl-tRNA is translocated to the E and P site, respectively. eEF2 promotes this process in a GTP hydrolysis-dependent manner (Spahn et al., 2004; Taylor et al., 2007).

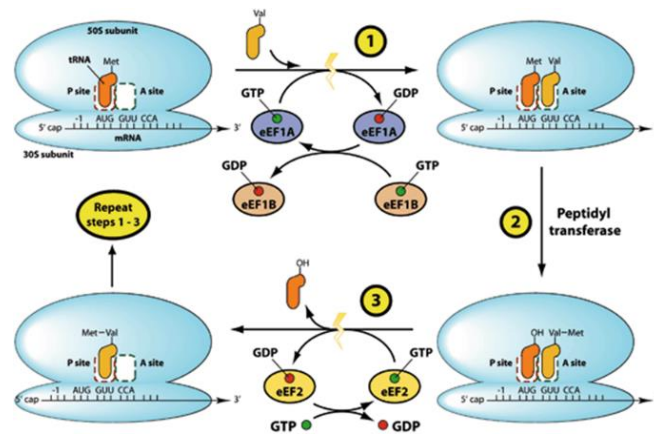


Figure 19: Schematic illustration of translation elongation in eukaryotes. An additional aa-tRNA is positioned in the A site coinciding with hydrolysis of eEF1A-associated GTP. After that, the peptidyl bond is formed, transferring the previous polypeptide chain to the new tRNA in the A site, followed by ribosome moving forward by one codon and the release of the deaminoacyl-tRNA mediated by eEF2. Figure from (Scaggiante et al., 2014).

The final translation stage is termination, which depends on two eukaryotic release factors (eRFs) and the ribosome itself. When a stop codon enters the A site of the ribosome, termination is initiated, which terminates protein synthesis and leads to the ribosome leaving the mRNA (Hershey et al., 2012) (Figure 20). The process involves termination codon recognition and hydrolysis of the ester bond of the peptidyl-tRNA to release the nascent polypeptide as well as ribosome splitting. eRF1 recognizes all three termination codons (UAA, UAG, and UGA) and is also responsible for peptidyl-tRNA hydrolysis. eRF3 is a ribosome-dependent GTPase that assists eRF1 in releasing the completed polypeptide. Briefly, eRF1-eRF3-GTP binds to the A site of the ribosome, followed by GTP hydrolysis and eRF3 release.

Introduction

Subsequently, an ATPase, ABCE1 (ATP binding cassette subfamily E member 1), directs eRF1 in an active position. After which, the catalytic GGQ motif of eRF1 is positioned to catalyse the cleavage of peptidyl tRNA bond leading to polypeptide release. In parallel, ATP hydrolysis results in conformational rearrangement of ABCE1, which was proposed to supply the mechanical force driving ribosomal subunit separation (Dever and Green, 2012; Pisarev et al., 2010). Following ribosome splitting, the mRNA, tRNA, and ribosomal subunits are released for another round of translation.

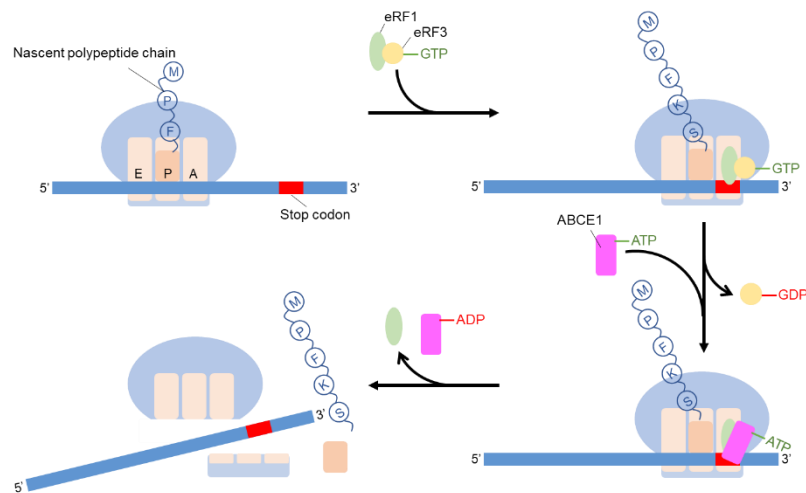


Figure 20: Schematic illustration of translation termination in eukaryotes. eRF1 forms a ternary complex with eRF3-GTP and binds to the stop codon. eRF3 hydrolyzes GTP, releasing itself from the ribosome. After that, ABCE1-ATP binds and leads eRF1 to position and catalyze the cleavage of the ester bond of the peptidyl-tRNA, resulting in the peptide dropping off the ribosome coinciding with ABCE1-associated ATP hydrolysis and the separation of the ribosomal subunits. Figure based on the illustrations in (Sitron and Brandman, 2020).

1.6 Translation-associated quality control and cellular responses

Translation is a vital process that produces functional proteins for maintaining homeostasis. However, this process can fail for several reasons, including problematic mRNAs (premature polyadenylation, robust secondary structures, oxidized RNA), amino acid starvation, and tandem rare codons. As a consequence, ribosomes stall leading to queuing or stacking of ribosomes on the mRNA and eventually resulting in ribosome collision and production of incomplete polypeptides and aggregation. These aberrant proteotoxic products are linked to neurodegenerative disorders, cell stress, cell cycle restriction, and aging (Darnell et al., 2011; Eshraghi et al., 2021; Ikeuchi et al., 2019a; Stein et al., 2022; Stoneley et

al., 2022; Wu et al., 2020). Therefore, rapidly eliminating these problematic transcripts and aberrant proteins is crucial to prevent the accumulation of toxic products. In the last decades, the molecular principles of degrading problematic mRNAs and truncated nascent proteins, as well as ribosome stalling-induced cellular stress responses and ribosome rescue, have been revealed by various research groups (D'Orazio and Green, 2021; Yip and Shao, 2021). Strikingly, all these mechanisms are initiated by ribosome stalling suggesting that the ribosome acts as a sensor for abnormal translation.

1.6.1 Ribosome-associated protein quality control (RQC)

Interrupted translation produces partially synthesized proteins that are harmful to cells. In response, cells evolved a surveillance mechanism to degrade these inappropriate proteins and rescue stalling ribosomes via RQC. In short, this pathway comprises three main steps: recognition of stalling ribosome, ribosome dissociation, and degradation of aberrant nascent peptide chains (Sitron and Brandman, 2020) (Figure 21).

At least two unique molecular features distinguish stalled ribosomes from functional translational ribosomes: an empty decoding center (A site) and interior collided ribosome interfaces (Yip and Shao, 2021). Cells have developed distinct mechanisms that detect and rescue stalled ribosomes, depending on where stalling occurs on the mRNA. Truncated mRNA, stop-codon readthrough, or endonucleolytic mRNA cleavage at the internally collided ribosomes results in mRNA 3'-end ribosome stalling with an empty A site. This requires the PELO-HBS1L complex to recognize stalled ribosomes by directly binding the ribosomes that lack mRNA in the A site followed by a downstream surveillance pathway. Whereas two different proteins are responsible for the detection of ribosomes stalled on internal sections of mRNAs: ZNF598 and RACK1, which is a RING E3 ligase and a ribosome-associated protein, respectively (Park et al., 2021; Pisareva et al., 2011; Sitron and Brandman, 2020; Sundaramoorthy et al., 2017). Structural and biochemical studies demonstrated that ZNF598 recognizes and binds to collided ribosomes, catalysing mono-ubiquitylation of ribosome SSU protein RPS10, RPS20, and RPS3. RACK1 is believed to stabilize the collided disome species to initiate RQC and promote the ubiquitylation of RPS10 mediated by ZNF598 (Ikeuchi et al.,

2019b; Juskiewicz et al., 2018; Simms et al., 2017b; Sundaramoorthy et al., 2017). In addition, endothelial differentiation-related factor 1 (EDF1) associates with collided ribosomes in a ZNF598-independent manner which subsequently recruits the GIGYF2-4EHP complex to inhibit translation initiation on the problematic mRNAs in order to minimize further collisions (Juskiewicz et al., 2020a; Sinha et al., 2020). Thereafter, the stabilized ribosome collision interfaces and the ubiquitylation of ribosomal proteins lead to the recruitment of downstream ribosome splitting factors.

After detecting stalled ribosomes, two distinct pathways are employed for disassembly. HBS1L and PELO are paralogs to the eRF1-eRF3, which position themselves in the ribosome similarly but distinctly. Briefly, the PELO-HBS1L complex recognizes the empty A site on the ribosome by extending a β -loop into the mRNA entry channel. Following this, GTP hydrolysis by HBS1L and conformational change release HBS1L from the ribosome, leading to the binding of ATPase ABCE1 to the ribosome recruited by PELO. Finally, ABCE1 dissociates stalled ribosomes into the 40S and 60S subunits in an ATP-dependent but largely poorly understood mechanism. Notably, the downstream pathways of PELO and eRF1 differ since PELO lacks eRF1's catalytic GGQ motif and therefore does not hydrolyse the ester bond of the peptidyl-tRNA, leaving the nascent chain attached to the 60S subunit (Gouridis et al., 2019; Pisareva et al., 2011; Shao et al., 2016; Shoemaker et al., 2010; Sitron and Brandman, 2020). Furthermore, most stalled ribosomes contain a tRNA in the A-site and are not optimal substrates for the PELO-HBS1L complex, demanding an alternative mechanism to split ribosomes. The ZNF598-mediated marking of collided ribosome by ubiquitylation is recognized by the RQC-trigger (RQT) complex that facilitates the splitting of stalled ribosomes. The RQT complex includes three activating signal cointegrator 1 complex (ASCC) subunits, ASCC1-3 and thyroid receptor-interacting protein 4 (TRIP4/ASC-1). The DNA helicase ASCC3 bears ATPase activity which is needed to split the leading stalled ribosome. ASCC2 is also involved in ribosome disassembly, whereas ASCC1 may not function in RQC. However, whether ASCC2's ubiquitin-binding ability is required for RQC remains controversial. The rest of the ASCC-associating factors are likely not essential in RQC-related ASCC function (Hashimoto et al., 2020; Juskiewicz et al., 2020b; Matsuo et al., 2020). Following ASCC/RQT complex-mediated disassembly of leading ribosome the ubiquitylated 40S ribosomal proteins of the trailing

ribosomes can be deubiquitylated and translation is resumed (Garshott et al., 2020; Juskiewicz et al., 2020b; Meyer et al., 2020). In yeast, when the ASCC3 ortholog Slh1 is not present, ribosomes are subject to endonucleolytic cleavage by the nuclease Cue2, which cleaves upstream of the stalled ribosome, converting the trailing ribosome into an ideal substrate for Dom34-Hbs1 complex (yeast homolog of human PELO-HBS1L complex). However, these conclusions need to be further verified in mammalian cells (D'Orazio et al., 2019; Guydosh and Green, 2017; Juskiewicz et al., 2020b)

Ribosome dissociation results in formation of free 40S subunit and a peptidyl-tRNA-associated 60S ribosome subunit. The 40S is recycled for new rounds of translation initiation while the nascent proteins, usually truncated or non-native, attached to the stalled 60S ribosomes undergo proteasome-mediated degradation (Brandman and Hegde, 2016). The nuclear export mediator factor (NEMF) and listerin (LTN1) are the critical factors in eliminating these aberrant intermediates. NEMF has strong binding affinity to ribosomes and selectively recognizes the 60S-tRNA interface over 80S or empty 60S. This specific binding ability prevents 40S rejoining and promotes recruitment of the E3 ubiquitin ligase LTN1 to 60S for nascent chain ubiquitylation (Shao et al., 2015; Shen et al., 2015; Sitron and Brandman, 2020; Yip and Shao, 2021). Once LTN1 is recruited to the 60S, its RWD domain interacts with large subunit ribosomal proteins, positioning the catalytic RING domain outside the ribosomal exit tunnel, and recruiting E2 enzymes to catalyse K48-linked poly-Ub chain formation on the substrates, triggering their proteasomal degradation (Bengtson and Joazeiro, 2010; Shao et al., 2013). Notably, several studies in yeast discovered that Rqc2 (the yeast homolog of NEMF) catalyses the addition of alanine and possibly threonine residues (CAT tails) to the C-terminal nascent peptides in a non-templated manner, which is proposed to extract lysines buried under the ribosome exit tunnel for ubiquitylation or produce more spaces for listerin to target structured polypeptides (Shen et al., 2015; Sitron and Brandman, 2019). TCF25 is also functional in RQC, which might promote K48 ubiquitin linkage formation or recruit the downstream factor p97. However, the mechanism is elusive and the results obtained in yeast and mammalian cells are conflicting (Kuroha et al., 2018; Osuna et al., 2017; Shao et al., 2015). Afterward, the ubiquitylated nascent proteins need to be delivered to the proteasome for degradation. This process was initially believed to be conducted by p97 and its

cofactors UFDL1 and NPLOC4 (UN complex). The UN complex binds to poly-ubiquitylated protein, enabling p97 to unfold the substrates and send them to the proteasome (Brandman et al., 2012; Verma et al., 2013). Recent studies revealed that p97 is insufficient to pull out the nascent protein from the ribosome. Another factor, ANKZF1 in mammals or Vms1 in yeast, a functional homolog of eRF1, was reported to act as a tRNA endonuclease towards the tRNA's 3'-CCA leading to nascent polypeptide release from the 60S. These data suggest that p97 is relevant in unfolding aberrant substrates rather than extracting them from ribosomes (Su et al., 2019; Verma et al., 2018; Zurita Rendón et al., 2018).

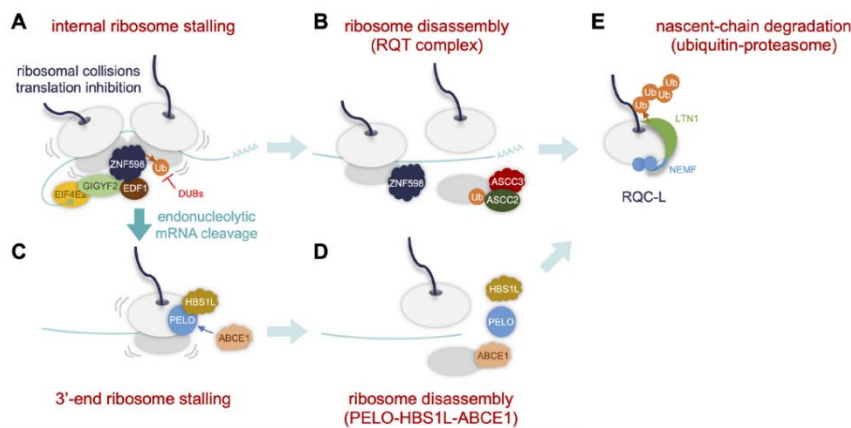


Figure 21: Schematic overview of RQC pathways. **A.** ribosome collisions occur when ribosome stall during translation, which further triggers ZNF598-mediated ubiquitylation of ribosomal proteins to recruit ribosome splitting factors and recruitment of EDF1 to suppress problematic mRNA being translated; **B.** ASCCs/RQT complex-triggered stalled ribosomes splitting; **C** and **D.** Ribosomes stall with empty A sites or internal ribosome stalling-triggered endonucleolytic mRNA cleavage resulting in 3'-end ribosome stalling which is recognized by PELO-HBS1L complex, followed by ABCE1-triggered ribosome separation; **E.** 60S-associated nascent polypeptide chains undergo LTN1-dependent poly-ubiquitylation followed by proteasomal degradation. Figure adapted from (Park et al., 2021).

1.6.2 Translation-coupled mRNA quality control

Ribosomes may stall for diverse reasons, some of the most common being faulty mRNAs, such as excessive mRNA secondary structure, mRNA truncation, premature poly(A) sequence and premature stop codons. (Chandrasekaran et al., 2019; Simms et al., 2017a). Cells evolved various translation-dependent mRNA surveillance mechanisms to degrade aberrant transcripts (Inada, 2013; Roy and Jacobson, 2013; Shoemaker and Green, 2012). The major mRNA quality control pathways are nonsense-mediated decay (NMD), non-stop decay (NSD), and no-go

decay (NGD), which sense different types of defective mRNAs and facilitate their degradation (D'Orazio and Green, 2021).

The NMD pathway recognizes and eliminates mRNAs that contain premature stop codons, which usually result from errors during co-transcriptional RNA splicing (D'Orazio and Green, 2021). An exon junction complex (EJC) forms on a pre-mRNA strand deposited approximately 20-24 nt upstream of the junction of two exons which were joined together during RNA splicing in the nucleus (Le Hir et al., 2000). Authentic termination codons are typically located in the final exon of spliced mRNAs and thus downstream of EJCs. During canonical translation termination, the EJCs are displaced by the ribosome, followed by ribosome splitting and protein release. However, premature stop codons result in early ribosome release, leaving remaining EJCs on the mRNA. This abnormal termination leads to UPF1, an RNA helicase, and a complex comprised of serine/threonine kinases SMG1-SMG8-SMG9 joining the eRF1-eRF3 translation termination complex to form the SMG1-UPF1-eRFs (SURF) complex in coordination with UPF2 and UPF3, triggering SMG1-mediated UPF1 phosphorylation. Phosphorylated UPF1 induces translational repression and recruits nucleases to accomplish mRNA decay (Kashima et al., 2006; Kurosaki et al., 2019; Nicholson et al., 2010; Serdar et al., 2016; Shoemaker and Green, 2012). Endonuclease SMG6 is recruited and catalyzes mRNA cleavage between the EJC site and premature termination codons. The 3'-cleavage product is degraded by XRN1, a 5'-3' exonuclease, while the 5'-cleavage product is most likely cleared by the exosome. Activated UPF1 can also recruit the SMG5-SMG7 heterodimer, which further recruits decapping and/or deadenylation machinery to promote exonucleolytic degradation of unprotected mRNA carried out by XRN1 from 5' direction and by the exosome from 3' direction (Eberle et al., 2009; Huntzinger et al., 2008; Kervestin and Jacobson, 2012; Kurosaki et al., 2019; Lejeune et al., 2003; Schmid and Jensen, 2008; Unterholzner and Izaurralde, 2004).

The NSD is a cellular mechanism that detects and degrades aberrant mRNAs lacking proper stop codons to prevent these transcripts from being translated. These defective mRNAs can derive from erroneous transcription termination, premature polyadenylation, or point mutations that damage the termination codons (Frischmeyer et al., 2002; Klauer and van Hoof, 2012). Decoding these aberrant transcripts leads to ribosome stalling at the 3' end of the mRNA template, leaving

the A site empty, serving as an ideal substrate for the PELO-HBS1L complex (Chandrasekaran et al., 2019; Guydosh and Green, 2017; Koutmou et al., 2015; Lu and Deutsch, 2008; Saito et al., 2013; Tsuboi et al., 2012). Following ribosome splitting, the released mRNAs are degraded by the exosome from the 3' direction (Frischmeyer et al., 2002; van Hoof et al., 2002). In yeast, Ski7, a member of the eRF3 family, is proposed to recognize the ribosome stalled at the 3' end of a nonstop mRNA poly(A) tail, recruiting the exosome-SKI complex composed of Ski2, Ski3, and Ski8 to degrade the faulty mRNAs (Araki et al., 2001; Benard et al., 1999; van Hoof et al., 2002). However, mammalian cells do not express Ski7; therefore, the PELO-HBS1L complex was suggested as a potential regulator capable of binding to the 3' end of a faulty mRNA and associating with the exosome-SKI complex to eliminate nonstop mRNA (Saito et al., 2013). In addition, Ski7 deficiency in yeast leads to dissociation of poly-A tail binding protein PABP, allowing 5' mRNA decapping followed by a 5'-3' decay pathway mediated by Xrn1 (Inada and Aiba, 2005).

NGD is triggered when ribosomes stall internally on mRNAs due to various reasons, including rare codons, strong secondary structures and specific features of nascent peptides (Doma and Parker, 2007; Karamyshev and Karamysheva, 2018; Letzring et al., 2010). Ribosome stalling during translation elongation usually triggers ribosome collisions, a common trigger of RQC. Thus, NGD and RQC usually happen simultaneously (Ikeuchi et al., 2019b). NGD was recently found to be a mRNA surveillance pathway and was initially observed in yeast, but has not yet been well established in mammalian cells (Wu and Brewer, 2012). Rescuing ribosomes trapped on mRNAs within the open reading frame (ORF) is quite complicated since the internal ribosome stalling results in A site occupied by a proper codon; therefore it is not easily recognizable for the Dom34-Hbs1 complex as a substrate. Previous studies suggested that in yeast, the NGD pathway involves endonucleolytic mRNA cleavage, thereby producing 5' and 3' intermediates, which are eliminated by exosome and exonuclease Xrn1, respectively (Doma and Parker, 2006). A subsequent genetic screen in yeast identified an essential endonuclease, Cue2, that might participate in NGD in a Hel2 (yeast homolog of human ZNF598)-dependent manner. The cleavage mediated by Cue2 is believed to occur between two stalled ribosomes, leading to the generation of fragmented mRNAs (D'Orazio et al., 2019). The 5' fragment bears a stalled ribosome with an empty A site which is

dissociated via the Dom34-Hbs1 complex, and the released mRNA is degraded by exosome similarly to the NSD pathway. Meanwhile, RQT complex releases the stalled ribosome from the 3' mRNA fragment, which is then eliminated by Xrn1 from its 5' end (Best et al., 2022; Doma and Parker, 2006; Inada, 2017; Tsuboi et al., 2012).

1.6.3 Ribosome-associated stress responses

Cellular stress responses refer to molecular adaption or defence reactions that occur when cells are exposed to environmental stimuli, such as extreme temperature, toxic compounds, viral infection and ultraviolet light irradiation, leading to damage to nucleic acids, proteins, and lipids. Cells respond to such stressors by triggering a variety of mechanisms, ranging from activation of survival pathways for stress tolerance to promoting programmed cell death, like apoptosis, which eventually eliminates damaged cells (De and Mühlemann, 2022; Fulda et al., 2010; Kültz, 2005). Environmental stresses perturb systemic cellular homeostasis. For example, chemical damage to mRNAs affects their structural properties, leading to ribosome stalling and aberrant translation (Galluzzi et al., 2018; Li et al., 2006; Rubio et al., 2021; Yan et al., 2019; Yan and Zaher, 2019). Ribosome collisions have been proposed as a universal consequence of ribosome stalling, which trigger mRNA surveillance pathways and ZNF598-dependent RQC. Emerging results suggest that ribosome collisions serve as a beacon for the recruitment of ribosome-associated factors to initiate cellular stress responses, including the ribotoxic stress response (RSR) and the integrated stress response (ISR), to fine-tune cellular homeostasis and modulate cell fate (Morris et al., 2021; Vind et al., 2020b; Wu et al., 2020; Yan and Zaher, 2019).

1.6.3.1 The ribotoxic stress response (RSR)

RSR is a conserved cellular stress response pathway which was initially found to be triggered by damage of the 3'-end of 28S rRNA and inhibition of protein synthesis. During RSR, stress-activated protein kinases (SAPKs), including JNK (c-JUN N-terminal kinase) and p38, members of the MAPK (mitogen-activated protein kinase)

family, are activated to promote cellular recovery (Iordanov et al., 1998, 1997; Shifrin and Anderson, 1999).

Three kinases were reported to be involved in recognition of the problem and activation of RSR, namely PKR (double-stranded RNA-dependent protein kinase), HCK (hematopoietic cell kinase), and ZAK α (leucine-zipper and sterile- α motif kinase). However, the evidence for PKR and HCK's roles in RSR is poor (Goh et al., 2000; Vind et al., 2020a; Zhou et al., 2014, 2005, 2003). In contrast, ZAK α is a well-characterized RSR component that initiates downstream MAPK cascade signalling upon exposure to translation inhibitors (anisomycin and cycloheximide), ribotoxins (ricin, Shiga toxin, and α -sarcin) and UV irradiation. However, the activation mechanism remained uncertain until recently (Jandhyala et al., 2008; Vind et al., 2020b; Wang et al., 2005). The ZAK gene in human cells encodes two alternatively spliced transcripts that produce two protein isoforms, ZAK α and ZAK β , with distinct C termini. Recent studies demonstrated that ZAK α , the longer isoform carrying an additional sterile alpha motif compared to ZAK β , can directly associate with elongating ribosomes by inserting its flexible C terminus into the ribosomal inter-subunit space mediated by the interaction of surface charges. ZAK α is activated and decreases its ribosomal affinity when ribosomes stall (Vind et al., 2020b; Wu et al., 2020). Previous evidence has revealed that in response to environmental stresses, activation of JNK and p38 are related to cell cycle modulation and apoptosis promotion (Darling and Cook, 2014; Duch et al., 2012). Consistently, a growth-based genome-wide CRISPR screen and biochemical experiments demonstrated that loss of ZAK α results in cellular resistance to higher doses of anisomycin, whereas p38 phosphorylation contributes to cell survival upon exposure of cells to lower doses of anisomycin (Wu et al., 2020). Notably, constitutive activation of ZAK α is associated with human limb development defects leading to split-hand/foot malformations, and ZAK α deficiency in the worm compromises its lifespan, implicating the physiological importance of RSR in organisms (Spielmann et al., 2016; Vind et al., 2020b). Taken together, these findings indicate that ribosome stalling-elicited RSR mediates cell-fate decisions in different contexts via facilitating both pro-survival and pro-apoptotic pathways (Park et al., 2021; Vind et al., 2020a; Wu et al., 2020).

1.6.3.2 The integrated stress response (ISR)

ISR is a typical adaptive stress response that cells evolved in response to diverse environmental stimuli and pathological conditions, such as proteostasis defects, amino acid deprivation, viral infection and redox imbalances. (Costa-Mattioli and Walter, 2020; Pakos-Zebrucka et al., 2016). The ultimate consequence of ISR is the shut-down of global protein synthesis and the simultaneous up-regulation of the synthesis of a few selected proteins, including the transcription factor ATF4, to promote homeostasis restoration (Lu et al., 2004).

The global translation inhibition is initiated by eIF2 α phosphorylation. eIF2 α together with eIF2 β and eIF2 γ forms a heterotrimer called eIF2, which is associated with GTP and forms TC with tRNA^{iMet} during translation initiation. After that, the final product, eIF2-GDP needs to be recycled to eIF2-GTP by eIF2B for the next round of translation initiation (Boye and Grallert, 2020; Preiss and W Hentze, 2003; Wek, 2018). ISR triggers eIF2 α phosphorylation at Ser51, which induces a conformational rearrangement of eIF2 α , increasing its affinity with eIF2B, while interfering with the GDP conversion activity of eIF2B. Consequently, phosphorylated eIF2 α acts as a competitor of unphosphorylated eIF2 α , sequestering eIF2B and resulting in global translation initiation reduction (Bogorad et al., 2017; Gordiyenko et al., 2019; Kashiwagi et al., 2019; Kenner et al., 2019; Krishnamoorthy et al., 2001; Schoof et al., 2021).

Human *ATF4* mRNA bears three upstream open reading frames (uORFs) located 5'to the coding DNA sequence (CDS). In unstressed cells, ribosomes initiate scanning at uORF1 followed by re-initiating at the downstream uORF2, which overlaps out-of-frame with the *ATF4* CDS, therefore precluding translation of *ATF4*. Under stressed conditions, phosphorylation of eIF2 α results in limited TC availability. Thus, scanning ribosomes skip uORF2 and re-initiate at the *ATF4* CDS (Harding et al., 2000; Pakos-Zebrucka et al., 2016; Vattem and Wek, 2004). ATF4 is a transcriptional activator that up-regulates the transcription of stress response genes, such as C/EBP-homologous protein (CHOP), ATF3, and Tribbles homolog 3 (TRIB3), etc. (Han et al., 2013; Siu et al., 2002). Moreover, ATF4 also selectively represses expression of some genes (Ameri and Harris, 2008). Additionally, various stress conditions facilitate transcriptional regulation of *ATF4* mediated by different transcription factors (Pakos-Zebrucka et al., 2016). This combination of

transcriptional and translational control of ATF4 ensures induction or suppression of downstream regulators to maintain the balance between stress adaptation and cell death (Dey et al., 2010). Therefore, phosphorylation of eIF2 α plays a dual role in ISR: short-lived ISR promotes pro-survival signalling pathways via inhibiting global protein synthesis while up-regulating critical stress-combating genes, aiming at restoring homeostasis; prolonged ISR or failed pro-adaptive response lead to programmed cell death (Dey et al., 2010; Harding et al., 2003; Lu et al., 2004; Pakos-Zebrucka et al., 2016; Rozpędek et al., 2016; Rutkowski et al., 2006)

Currently, four kinases are reported to participate in phosphorylating eIF2 α in distinct cellular contexts, namely PKR, PKR-like ER kinase (PERK), general control non-derepressible 2 (GCN2), and heme-regulated eIF2 α kinase (HRI), which sense viral infection, endoplasmic reticulum (ER) stress and hypoxia, amino acid deficiency, and heme deprivation or mitochondrial dysfunction, respectively (Fessler et al., 2020; Guo et al., 2020; Tian et al., 2021). Modest inhibition of translation by anisomycin leads to ribosome collision and GCN2-dependent eIF2 α phosphorylation (Wu et al., 2020). In contrast, a high concentration of anisomycin that causes uniform stalling of ribosomes on mRNA does not activate ISR, suggesting GCN2 serves as a sensor of ribosomal collision and activates ISR in case of aberrant translation (Wu et al., 2020). Previous studies indicated that the accumulation of uncharged tRNAs activates GCN2 during amino acid starvation. GCN2 contains a histidyl-tRNA synthetase (HisRS)-like domain that binds multiple deacylated tRNAs, resulting in a conformational change and GCN2 activation (Dong et al., 2000; Wek et al., 1995). However, GCN2 is also activated by various stressors that do not trigger a global increase in uncharged tRNAs. Further genetic screening and *in vitro* biochemical experiments revealed that GCN2 directly binds to the ribosomal P-stalk, a part of the ribosome adjacent to the A site, inducing conformational changes in the HisRS-like and kinase domains of GCN2 and ISR activation (Inglis et al., 2019). Given that the ribosomal P-stalk is usually occupied by the translation elongation factors and stimulates their GTPase activity during translation, the hypothesis arises that active translation leads to GCN2 repression, whereas translational stress enables GCN2 to associate with the ribosome and initiate ISR (Harding et al., 2019; Inglis et al., 2019; Vind et al., 2020a).

2 Aims of these studies

Ensuring the integrity of DNA and RNA is highly essential for organisms to not only maintain the genetic information, but also to ensure its usage for functional protein production. However, nucleic acid chains are permanently subjected to chemical insults from endogenous and exogenous sources such as ROS, UV light, and alkylating agents. Damaged DNA and RNA have toxic consequences leading to permanent alteration of genomic information and faulty protein synthesis, which can cause premature aging and disease. Canonical DNA-repair pathways have been extensively studied for many decades, but DNA-protein crosslinks (DPCs) have only recently emerged as a novel source of genome instability that interferes with transcription and replication. DPC-specific repair mechanisms were unknown until a proteolytic enzyme, SPRTN, was discovered that maintains genome stability by degrading the protein components of DPCs. Subsequent studies showed that SPRTN lacks substrate preference which is useful to target diverse protein adducts, but demands tight control to avoid unwanted proteolysis of surrounding chromatin proteins. In addition, it was reported that SPRTN is deubiquitylated upon DPC induction. However, the role of this modification in regulating DPC repair remains unclear.

The first part of this thesis aims to investigate the function of SPRTN ubiquitylation and deubiquitylation in regulating DPC repair. To address this question, we initially aimed to identify the involved deubiquitylating enzyme (DUB) by conducting an *in vitro* DUB library screen. The second aim of this project is to test if this ubiquitin switch regulates the recruitment of SPRTN to chromatin and/or affects its protease activity in cells lacking the involved DUB. Moreover, the function of SPRTN modification will be investigated by overexpressing SPRTN-ubiquitin fusion variants mimicking SPRTN ubiquitylation.

Moreover, given the central role of RNA in many fundamental biological processes and the reactivity of RNA, we suspect that RNA-protein crosslinks (RPCs) frequently form in cells. However, currently, almost nothing is known on the cellular consequences of RPC formation, as well as the mechanisms of their resolution. Therefore, the second part of this study attempts to reveal the cellular

Aims of these studies

consequences and responses to RPC formation and to identify factors contributing to RPC resolution. Therefore, we aim to develop a tool to specifically induce cellular RPCs to determine the toxicity of RPC formation and the associated cellular responses by measuring cell viability and signalling events after RPC induction. Finally, to study the principles of RPC resolution, we will combine polyA pull-down experiments with mass spectrometry-based proteomics to monitor the fate of RPCs.

3 Summary of publications

3.1 A ubiquitin switch controls autocatalytic inactivation of the DNA-protein crosslink repair protease SPRTN

Shubo Zhao, Anja Kieser, Hao-Yi Li, Hannah K Reinking, Pedro Weickert, Simon Euteneuer, Denitsa Yaneva, Aleida C Acampora, Maximilian J Götz, Regina Feederle, Julian Stingele.

Nucleic Acids Research. 2021 Jan 25; 49 (2): 902-915.

DNA-protein crosslinks (DPCs) are unique lesions that physically block important chromatin transactions such as replication and transcription due to their bulkiness. DPC repair involves the degradation of the protein adduct by the metalloprotease SPRTN, regulated by the recognition of specific DNA structures instead of specific amino acid sequences. This lack of substrate preference is helpful in targeting diverse protein adducts, however, it demands tight control in return.

This publication reveals the crucial role of SPRTN ubiquitylation in regulating its enzymatic activity and stability during DPC repair. We demonstrated that mono-ubiquitylation inactivates SPRTN by triggering autocatalytic cleavage *in trans* and priming poly-ubiquitylation for proteasomal degradation *in cis*. An *in vitro* DUB screen discovered that the deubiquitylating enzyme USP7 is the factor responsible for deubiquitylating SPRTN upon DPC induction. Loss of USP7 results in increased accumulation of DPCs and hypersensitivity when cells are exposed to formaldehyde.

To conclude, this work suggests that USP7 antagonizes the inactivation of SPRTN by deubiquitylation, therefore, increasing the protease's stability on damaged DNA and enabling efficient DPC proteolysis. It defines the mechanistic details of a ubiquitin switch controlling the potentially harmful proteolytic activity of SPRTN.

3.2 Translation-coupled sensing and degradation of RNA-protein crosslinks

Shubo Zhao[#], Jacqueline Cordes[#], Karolina M. Caban, Maximilian J. Götz, Timur Mackens-Kiani, Anthony J. Veltri, Niladri K. Sinha, Pedro Weickert, Graeme Hewitt, Thomas Fröhlich, Roland Beckmann, Allen R. Buskirk, Rachel Green, Julian Stinglele.

[#]These authors contributed equally to this work

Reactive aldehydes are cytotoxic compounds that can arise under normal physiological conditions and challenge genome stability by generating DNA-DNA interstrand crosslinks (ICLs) and DNA-protein crosslinks (DPCs). Defects in ICLs or DPCs repair lead to severe human syndromes such as bone marrow failure and premature ageing, indicating that endogenous aldehydes constantly threaten cells. However, it remains largely unclear whether aldehydes trigger RNA-proteins crosslinks (RPCs) formation, how they affect cellular physiology, and whether cellular mechanisms exist to resolve RPCs.

This study suggests that ribosomes play an essential role in sensing and initiating the degradation of RPCs. We repurposed photoactivatable nucleoside-enhanced crosslinking (PAR-CL) as a tool to mimic RNA damage triggered by aldehydes and demonstrated that RPC formation causes translational stalling and ribosome collisions which activate the ribotoxic stress response (RSR) and the integrated stress response (ISR) contributing to cell death. Furthermore, we showed that certain crosslinked mRNA-binding proteins are modified by poly-ubiquitin chains in a translation-coupled manner and subsequently degraded by proteasome.

Taken together, our findings reveal that PAR-CL is an effective tool to study cellular consequences of reactive aldehydes-induced RNA damage without inducing DNA damage and in addition to ICLs and DPCs, RPCs contribute to the toxicity of aldehydes.

4 Discussion

This dissertation reveals mechanistic details on the regulation of SPRTN during DPC repair and explores the cellular responses to RPC formation. The first part of the thesis lays out the mechanism of a ubiquitin switch controlling the inactivation of SPRTN. It provides evidence that mono-ubiquitylation of SPRTN triggers proteasomal degradation and autocatalytic cleavage, which in contrast to previous assumptions implicating this modification in regulation of chromatin access. The second part of the work is concerned with the cellular consequences of RPC formation. Here we reveal that translating ribosomes are required to sense these lesions and that RNA damage is in part responsible for the toxicity caused by abundant endogenous aldehydes such as formaldehyde.

4.1 Ubiquitin switch regulates SPRTN stability

Mono-ubiquitylation is a post-translational modification that can either prime poly-ubiquitylation for proteasomal degradation or have regulatory functions (Hicke, 2001; Ronai, 2016). During genome maintenance, many vital factors undergo mono-ubiquitylation to facilitate downstream processes. For instance, in ICL repair, FANCI and FANCD2 proteins are mono-ubiquitylated by FA core complex on specific lysine residues, which stabilizes the association between ID2 complex and dsDNA (Rennie et al., 2020). Another prominent example is ubiquitylation of PCNA, a DNA clamp that interacts with replicative DNA polymerases. Replication fork stalling leads to PCNA mono-ubiquitylation catalysed by RAD18, enabling recruitment of TLS polymerases, which can synthesize across small DNA adducts (Watanabe et al., 2004). Furthermore, during TC-NER, stalled RNA polymerase II undergoes mono-ubiquitylation by CUL4^{CSA}, which triggers poly-ubiquitylation and proteasomal degradation, serving as the last resort to provide space for alternative repair mechanisms and transcription restart (Nakazawa et al., 2020; Tufegdžić Vidaković et al., 2020). Notably, all these proteins are ubiquitylated on specific sites during DNA repair. In contrast, SPRTN is constitutively mono-ubiquitylated, and this modification is mediated and shielded by its C-terminal ubiquitin-binding zinc finger,

UBZ domain. Previous studies and this work showed that mono-ubiquitylation of SPRTN is promiscuous. However, a rapid deubiquitylation of SPRTN was observed in the presence of formaldehyde, a crosslinker commonly used to induce DPC, suggesting a prominent role of deubiquitylation in regulating SPRTN during DPC repair (Stingele et al., 2016; Zhao et al., 2021).

During the preparation of this thesis, two other DUBs were implicated in SPRTN deubiquitylation, VCPIP1 and USP11, whose loss was reported to result in defective formaldehyde-induced deubiquitylation of SPRTN and sensitization of cells to DPC induction (Huang et al., 2020; Perry et al., 2021). However, in our *in vitro* DUB library screening and biochemical experiments, we found that USP7 functioned as a specific deubiquitylating enzyme of SPRTN. This thesis further revealed that catalytic-inactive USP7 but not VCPIP1 or USP11 specifically bind to mono-ubiquitylated SPRTN. In sum, this suggests that USP7 is the primary regulator of SPRTN mono-ubiquitylation. However, these controversial results require further studies to discover the underlying mechanisms and to test if this ubiquitin switch of SPRTN is a universal regulation when cells are challenged by DPCs. Notably, previous studies suggested that the ubiquitin switch may regulate the access of SPRTN to chromatin, because the recruitment of SPRTN to chromatin is always accompanied by rapid deubiquitylation (Stingele et al., 2016). However, research from other groups and us demonstrated that loss of deubiquitylation resulted in both unmodified and modified SPRTN being enriched on chromatin upon FA treatment, indicating that deubiquitylation happens downstream or in parallel to chromatin localization (Perry et al., 2021; Zhao et al., 2021). Collectively, these data suggest that this reversible modification of SPRTN must have other functions during DPC repair and highlight the importance of understanding the regulatory mechanisms of DUBs for SPRTN deubiquitylation.

Mono-ubiquitylation can prime poly-ubiquitylation for proteasomal degradation (Braten et al., 2016). Using cycloheximide chase experiments, we showed that mono-ubiquitylated SPRTN has a shorter half-life than unmodified SPRTN, which is blocked by proteasomal inhibition. In parallel, we also detected that proteasomal inhibition stabilizes higher molecular weight species of WT SPRTN but not of a UBZ mutant variant, suggesting that mono-ubiquitylation leads to proteasomal degradation of SPRTN by priming poly-ubiquitylation. We further generated SPRTN-ubiquitin fusion variants to mimic mono-ubiquitylated SPRTN, which

resulted in destabilization compared to WT SPRTN. Moreover, overexpression of the ubiquitin fusion but not catalytically inactive version (E112Q) led to increased accumulation of shorter SPRTN fragments, which are thought to originate from SPRTN autocleavage. In further support of this idea, recombinant ubiquitin-fused SPRTN displayed higher autocleavage activity compared to WT SPRTN *in vitro*. These results raise the hypothesis that mono-ubiquitylation of SPRTN enhances its autocleavage capacity, which is further supported by the fact that mutation of the UBZ domain reduces autocleavage.

Furthermore, overexpression of WT USP7 but not catalytic-inactive USP7 antagonized both SPRTN modification and autocleavage. In agreement, data suggesting that USP11 functions as a DUB of SPRTN (Perry et al., 2021), demonstrated that loss of USP11 or USP7 leads to an increased level of SPRTN autocleavage, whereas overexpression of USP11 dramatically suppressed this phenotype. To sum up, these data imply that when DPCs challenge cells, SPRTN is deubiquitylated by one or more DUBs to limit inactivation of the enzyme by autocleavage and proteasomal degradation.

However, how mono-ubiquitylation enhances SPRTN's autocleavage remains unclear. SPRTN was previously reported to dimerize on DNA (Li *et al.*, 2019). Therefore, it is possible that mono-ubiquitylation of SPRTN enhances dimerization through the interaction of ubiquitin and UBZ domain. Dimerization might trigger conformational changes in SPRTN exposing its active site and, thereby, promoting autocleavage. We observed that SPRTN-ubiquitin fusion variant is more active than WT SPRTN in terms of cleaving catalytically inactive SPRTN. Similarly, fusion of ubiquitin to catalytically inactive SPRTN increases its cleavage by WT SPRTN (preliminary data, not shown). These results suggest that ubiquitin-modified SPRTN is a better enzyme and a better substrate during autocleavage *in trans*. Strikingly, the interaction between two SPRTN molecules was not affected by fusing a ubiquitin to the C terminal tail of SPRTN, indicating that the interaction between ubiquitin and UBZ is not absolutely required for SPRTN dimerization but may rather be important for activating the enzyme. However, this assumption requires further verification by structural analysis and biochemical experiments. Furthermore, we also observed an increase of autocatalytic SPRTN fragments upon fusing ubiquitin to the a SPRTN UBZ mutant variant. This suggests that the interaction between ubiquitin and UBZ is not essential for SPRTN inactivation, implying that an additional ubiquitin-binding

domain exists in SPRTN. This idea is supported by our results showing that inactive USP7 stabilized mono-ubiquitylated species of the UBZ mutant. To conclude, how two SPRTN molecules interact with each other and the role of a putative additional ubiquitin-binding domain of SPRTN require further exploration.

Previous studies demonstrated that SPRTN undergoes autocleavage in a DNA-dependent manner, suggesting that this process occurs specifically at sites of DNA damage. Accordingly, we hypothesize that when cells face DPCs, SPRTN is recruited to DNA damage sites followed by deubiquitylation mediated by at least three DUBs, which inhibits autocleavage, thereby increasing DPC repair activity. Our study on the ubiquitin switch of SPRTN reveals the mechanistic details of the regulatory mechanism, which restrains the potential toxic protease through automatic inactivation.

4.2 Recruitment of SPRTN to chromatin upon DPCs

SPR TN functions as a protease that targets the protein components of DPCs, which requires its recruitment to the lesions. Previous research from our laboratory and other groups revealed that SPR TN bears two DNA binding domains, a basic region (BR) and a Zn²⁺ binding domain (ZBD), which bind to dsDNA and ssDNA, respectively (Li et al., 2019; Reinking et al., 2020). However, how SPR TN recognizes damage sites and gets recruited mainly remained unknown.

SPR TN was initially characterized as a regulatory factor involved in tolerance of UV-induced DNA damage, for which it interacts with ubiquitylated PCNA through UBZ and PIP domains (Centore et al., 2012; Juhasz et al., 2012). However, previous studies demonstrated that upon DPC induction, SPR TN variants with alterations of key residues within PIP or UBZ are still recruited to chromatin, suggesting that the interaction with PCNA is not required for SPR TN to access chromatin. In addition to PIP and UBZ domains, SPR TN bears a SHP-box mediating the interaction with p97 (Davis et al., 2012; Mosbech et al., 2012). p97 was previously reported as a segregase which extracts proteins from their environments, such as complexes, membranes and chromatin (Rape et al., 2001; van den Boom and Meyer, 2018). p97 was recently shown as essential for extracting inhibitor-trapped PARP1 from chromatin (Krastev et al., 2022). Additionally, investigators also demonstrated that SPR TN is recruited to TOP1ccs by interacting with p97 and its cofactor TEX264,

which associates with DNA replication forks (Fielden et al., 2020). These findings indicate that associating with p97 might be involved in localizing SPRTN to chromatin. However, this idea conflicts with the observations that SPRTN SHP mutant variants are still enriched on chromatin upon formaldehyde treatment, suggesting that p97 is dispensable (Stingele et al., 2016). However, it may be that p97 specifically recruits SPRTN to TOP1ccs, while recruitment to other types of DPCs is independent of p97.

Research also suggested that SPRTN associates with the replisome through interaction with key components of the replication machinery, such as PCNA, or the MCM complex (Vaz et al., 2016). This conclusion is further supported by the fact that SPRTN is present on nascent DNA and travels with replication fork, as determined by iPOND experiments. Moreover, SPRTN is also found on chromatin in the absence of DNA damage (Halder et al., 2019; Maskey et al., 2017; Vaz et al., 2016). These findings might explain how SPRTN travels with the replisome and degrade endogenous DPCs, but this is not sufficient to interpret the increased SPRTN levels on chromatin after DPC induction unless DPC formation induces more new replication origin firing, which has not been validated yet (Lopez-Mosqueda et al., 2016; Stingele et al., 2016).

Recent studies demonstrated that DPC-inducing agents trigger widespread SUMO-targeted ubiquitylation on DPCs via the PIAS4-RNF4 pathway, which triggers DPC degradation by the proteasome. Thus, SPRTN's UBZ domain may also engage with specific ubiquitylation signals on the DPC itself. In agreement, SPRTN Δ UBZ mutant strongly reduced its ability to precipitate ubiquitin and SUMO conjugates (Krastev et al., 2022; Liu et al., 2021; Ruggiano et al., 2021; Sun et al., 2020a). This assumption corresponds to our previous hypothesis that the interaction between SPRTN and ubiquitin signals on DPCs exposes monoubiquitin on SPRTN, thereby allowing USP7 to remove the modification (Zhao et al., 2021). However, in contrast to this interpretation, an assay performed in *Xenopus* egg extracts revealed proficient SPRTN-mediated DPC cleavage even when the ubiquitylation of DPCs was prevented (Larsen et al., 2019). These observations suggest that not all DPCs are modified by ubiquitin, and that they can undergo other PTMs or interact with additional proteins to recruit SPRTN to the lesion. Another alternative explanation is that some other proteins in the proximity of DPCs are modified by ubiquitin and subsequently recruit SPRTN to the damage sites. Moreover, people utilized global

Discussion

SUMO or ubiquitin E1 inhibitors to investigate the role of each modification in SPRTN relocalization and DPC removal (Borgermann et al., 2019; Ruggiano et al., 2021). However, it is not possible to distinguish whether these modifications occur on the DPC or on proteins in its vicinity. Abrogating TOP1 SUMOylation by mutating four key lysines residues showed only a minor effect on TOP1ccs repair in $\Delta tdp1$ and $\Delta wss1$ yeast strains (Serbyn et al., 2021). However, to date, no *in vivo* assay has been conducted in mammalian cells to investigate if impairing DPC modifications defects SPRTN recruitment or DPC repair. Therefore, further cellular studies are required to define the precise role of modifications of the DPC itself or surrounding proteins in the recruitment of SPRTN to chromatin.

In addition to ubiquitylation, the role of phosphorylation and acetylation of SPRTN in regulating chromatin localization have been studied. Halder et al. demonstrated that replication fork stalling triggers phosphorylation of serines 373, 374 and 383 on SPRTN by CHK1. SPRTN phosphorylation in turn leads to cleavage of CHK1 evicting it from replicative chromatin and releasing N-terminal kinase-activated CHK1 fragments. Interestingly, the phosphorylation of SPRTN regulated its localization to chromatin. Ectopic expression of CHK1 led to hyper-accumulation of SPRTN on chromatin, and overexpression of phosphorylation-mimetic but not phosphorylation-defective SPRTN variants resulted in the restoration of DNA replication defects in SPRTN-depleted cells, indicating the essential role of SPRTN phosphorylation in chromatin localization and securing DNA replication (Halder et al., 2019). In addition, Huang et al. revealed that VCPIP1 deubiquitylates SPRTN upon DPC induction, which is followed by PCAF/GCN5-mediated SPRTN acetylation on lysine 230 (K230), which promotes SPRTN relocation to the DNA damage sites. Arginine substitution of K230 abrogated recruitment of SPRTN to chromatin, while a glutamine (mimicking hyperacetylated SPRTN) substitution increased the chromatin association of SPRTN in unstressed cells, suggesting that acetylation of SPRTN regulates its chromatin access. However, it is unclear if these two modifications of SPRTN (phosphorylation and acetylation) directly regulate SPRTN relocalization or control chromatin binding by influencing SPRTN auto-inactivation. Therefore, the connection between modifications of SPRTN and its stability or autocleavage should be tested in the future.

Taken together, SPRTN can bind to DNA damage sites via its DNA binding domains, but the precise mechanism of how SPRTN is recruited to chromatin

remains largely unknown: is SPRTN recruited by PTMs on the DPC itself or on surrounding proteins? Future studies need to address these questions and determine if a general mechanism appears to direct SPRTN localization, and if not, how are the signals coordinated to guide SPRTN to lesions in different scenarios?

4.3 Regulation of SPRTN's enzymatic activity

Previous studies found that complete loss of SPRTN causes early embryonic lethality, and SPRTN hypomorphic mice with insufficient SPRTN levels present with senescence and progeria phenotype, indicating that SPRTN is essential for viability (Maskey et al., 2014). Patient mutations in the *SPRTN* gene result in a premature stop codon leading to loss of the C-terminal of SPRTN (SPRTN- Δ C) or a tyrosine to a cysteine exchange at position 117 (SPRTN-Y117C), which leads to the development of Ruijs-Aalfs syndrome (RJALS). This human genetic disorder is characterized by abnormal facial and skeletal features and development of hepatocellular carcinoma (Lessel et al., 2014; Ruijs et al., 2003). It has been proposed that unrepaired endogenous DPCs cause the pathology of Ruijs-Aalfs syndrome patients (Stingele et al., 2017).

Given that the Y117C substitution reduced SPRTN autocleavage as well as substrate cleavage and failed to rescue hypersensitivity to DPC-inducing reagents but had no effect on DNA binding ability, it is assumed that the active site of this variant might be unable to form correctly because of the proximity of Y117 to the catalytic center (E112) (Lessel et al., 2014; Lopez-Mosqueda et al., 2016; Stingele et al., 2016; Vaz et al., 2016). Compared to the Y117C variant, SPRTN- Δ C is mislocalized to the cytoplasm due to loss of the nuclear localization signal (NLS). Although SPRTN- Δ C bears an intact protease domain and retains autocleavage activity, it can only partially resolve DPCs (Lopez-Mosqueda et al., 2016; Stingele et al., 2016; Vaz et al., 2016). Preliminary data from our group found that the addition of NLS to SPRTN restores its localization to the nucleus but does not fully rescue DPC cleavage, corresponding to previous observations on TOP2cc degradation and indicating that the C-terminus of SPRTN is indispensable for SPRTN activation regardless of cellular localization (Lopez-Mosqueda et al., 2016). SPRTN harbours three protein-protein interaction motifs for binding PCNA, p97, and ubiquitin in its C-terminal tail. However, SPRTN UBZ mutant but not SHP and PIP are impaired in

Discussion

DPC proteolysis in frog egg extracts (Larsen et al., 2019). Consistently, preliminary data from our group showed that only the SPRTN UBZ mutant variant abolished DPC cleavage in cells. Moreover, the addition of free ubiquitin facilitates both SPRTN autocleavage and substrate cleavage, indicating the importance of interaction between ubiquitin and SPRTN UBZ domain in regulating SPRTN enzymatic activity (Lopez-Mosqueda et al., 2016).

Intriguingly, patients lacking the entire C-terminal domain of SPRTN are viable, whereas completely losing SPRTN expression is lethal, which is in agreement with previous findings that SPRTN- Δ C remains partial protease activity (Lessel et al., 2014; Lopez-Mosqueda et al., 2016; Stinglele et al., 2016; Vaz et al., 2016). However, it remains unclear why the RJALS syndrome variant SPRTN- Δ C retains a large degree of function despite mislocalizing to the cytoplasm and lacking the ability to bind ubiquitin. First of all, preliminary data from our group demonstrated that adding an Exportin-1 inhibitor restored SPRTN- Δ C localization to the nucleus, suggesting that SPRTN's localization is a dynamic process. Secondly, our data showing that SPRTN- Δ C can undergo mono-ubiquitylation indicates that a second ubiquitin-binding domain may exist in SPRTN- Δ C (Zhao et al., 2021). Finally, we observed a reduction in formaldehyde-induced cellular autocleavage of SPRTN- Δ C compared to WT, perhaps resulting in longer lifetime of SPRTN- Δ C at sites of DNA damage. Taken together, we hypothesize that SPRTN- Δ C can resolve DPCs, albeit less efficient than the WT enzyme. In addition, SPRTN- Δ C might also raise problems due to the lack of negative regulation, which may contribute to the phenotypes observed in Ruijs-Aalfs syndrome patients.

To sum up, the DNA-dependent DPC protease activity of SPRTN is quite well understood. Further studies need to explore the potential additional ubiquitin-binding motif of SPRTN to investigate the precise role of SPRTN mono-ubiquitylation in DPC proteolysis. Our data demonstrated that ubiquitin-fusion enhanced autocleavage of SPRTN but not substrate cleavage, which could indicate that excessive auto-inactivation of SPRTN prohibits DPC cleavage. Therefore, altering SPRTN autocleavage sites (to prohibit autocleavage) will be critical for distinguishing SPRTN's activity in auto-inactivation and substrate degradation. Moreover, the principles of SPRTN recruitment to DPCs remain largely unknown. Even though some factors were implicated (Fielden et al., 2020; Kröning et al., 2022), no general consensus has emerged on the mechanism of SPRTN

recruitment. Whether a universal pathway exists that senses DPC lesions and activates SPRTN remains unclear. Recently, PIAS4-RNF4-mediated SUMO-targeted ubiquitylation has been observed to be involved in the removal of various DPCs, including M.Hpall, DNMT1, TOP1, TOP2-DPCs and trapped PARP1, suggesting it might be a conserved signal that directs DPCs proteolysis (Sun, et al., 2020; Liu et al., 2021; Krastev et al., 2022). If so, how are the diverse DNA-crosslinked proteins or proteins surrounding DPC recognized by the PIAS4 SUMO E3 ligase? Replisomes encountering the DNA insults can be excluded, because DPCs still undergo SUMO-targeted ubiquitylation independent of replication. Also, SUMO inhibition in *Xenopus* egg extracts did not affect replication-coupled DPC proteolysis, leading to the assumption that transcription might be involved in sensing DPCs (Liu et al., 2021). Moreover, it is hard to state if SUMO-targeted ubiquitylation on DPCs signals the proteolysis by SPRTN, since SPRTN-mediated DPC cleavage has not been detected *in vivo* yet. Hence, a reliable *in vivo* method is demanded to determine which proteins are crosslinked and to show their repair kinetics.

4.4 RNA-protein crosslink resolution

The cellular and biochemical data obtained in this study suggest that RPCs are a quality control problem that potentially originates from endogenous formaldehyde. RPCs lead to ribosome stalling and ribosome collisions, which further result in the activation of ribosome collision-associated signalling pathways, including RSR, ISR and RQC. The results of cellular viability assays indicate that RSR and ISR trigger cell death upon RPC formation, while ZNF598, initiator of RQC, protects cells against RPCs. However, the phenotype observed in ZNF598-deficient cells is relatively mild, suggesting that RQC is not the major mechanism to counteract RPCs. Therefore, this work suggests that cells must have evolved other pathways to resolve RPCs.

4.4.1 Translation-coupled ubiquitylation and resolution of RPCs

Our polyA pull-down experiments demonstrated that mRNA-crosslinked proteins undergo poly-ubiquitylation, indicating a functional role of this modification in RPC resolution. To better understand the contribution of ubiquitylation to the resolution

Discussion

of RPCs, we established an approach that combines polyA pull-down with ubiquitin E1 inhibitor and MS measurements to follow the resolution kinetics of crosslinked proteins in the presence or absence of ubiquitylation. Studying different species of mRNA-crosslinked proteins specifically, YBX1, YBX3, HDLBP, SND1, and SERBP1 gave us insight into different potential RPC resolution pathways. We observed that the addition of ubiquitin E1 inhibitor blocks the resolution of HDLBP- and SND1- but not YBX1- and YBX3-mRNA crosslinks, suggesting that there are at least two different pathways to resolve RPCs: ubiquitin-dependent and ubiquitin-independent. Notably, the turnover of SERBP1-mRNA crosslinks seems to be unaffected by the Ub-E1 inhibitor based on MS analysis which is in contrast to western blotting results. We hypothesized that mRNA-crosslinked SERBP1 are poly-ubiquitylated but that this modification has no effect on its turnover (therefore, some poly-ubiquitylated SERBP1 would collapse into the SERBP1 band in the presence of ubiquitin E1 inhibitor in western blotting experiments, while the total amounts are not affected, as measured by MS).

Moreover, poly-ubiquitylated proteins are typically the substrates of proteasomal proteolysis or lysosomal autophagy, which are two vital pathways for protein degradation in eukaryotic cells (Komander and Rape, 2012). The 26S proteasome is the major proteolytic machinery that recognizes poly-ubiquitin chains, especially K48 chains, on substrates and sequentially unfolds, deubiquitylates and degrades poly-ubiquitin-modified proteins (Bard et al., 2018). Autophagy is a cellular process that was originally considered to be a non-selective mechanism to eliminate bulky dysfunctional cytosolic material in response to starvation, wherein the double membrane autophagosome sequesters the damaged proteins or organelles followed by lysosome fusion and substrate degradation (Klionsky, 2007). Emerging evidence suggests the existence of selective autophagy, which degrades various cellular organelles or substances, including misfolded protein aggregates, mitochondria and ribosomes. In many types of selective autophagy, substrates undergo poly-ubiquitylation, wherein the poly-ubiquitin chains serve as a signal for autophagy receptors (Chen et al., 2019; Khaminets et al., 2016; Stolz et al., 2014). The addition of proteasome inhibitor (MG132) but not autophagy inhibitor (Bafilomycin A1) stabilized the levels of mRNA-crosslinked SND1 and HDLBP, implying that the degradation of these RPCs is specifically dependent on proteasome.

Strikingly, inhibiting translation by high dose anisomycin (ANS, leads to global ribosome stalling) diminishes poly-ubiquitylation of crosslinked proteins to a large extent, indicating that this modification is translation-dependent. Moreover, the clearance of mRNA-crosslinked SND1, HDLBP, YBX1 and YBX3 but not SERBP1 was abolished by inhibiting translation with high dose ANS. Combining these results we proposed that translating ribosomes can serve as a sensor to detect mRNA-crosslinked proteins and trigger their ubiquitylation followed by proteasomal degradation as well as existence of a ubiquitin- and proteasome-independent turnover mechanism. We think the resolution of YBX1- or YBX3-mRNA-crosslinks which is ubiquitin- and proteasome-independent could be caused by mRNA degradation. In this setting, mRNA cleavage may also occur in a translation-dependent manner. The fate of SERBP1 mRPCs remains unclear.

The model presented in our manuscript suggests that ribosomes trigger ubiquitylation and proteasomal degradation of the protein adducts ahead and stall with crosslinked peptide remnants in the A site. To test this model, T-C conversion rates could be measured immediately or 30 minutes after induction of RPCs. If the model is correct, the accumulation of T-C conversion in the A-sites would be more increase over time, suggesting that ribosome stall with crosslinked amino acids in the A site over time. Moreover, the addition of high-dose ANS, Ub-E1 inhibitor or MG132 which abrogate RPCs clearance would be expected to diminish the accumulation of T-C conversions in the A-site. The fate of mRNAs containing crosslinked peptide remnants and why cells employ distinct mechanisms for different types of crosslinked proteins are exciting future research questions.

4.4.2 Additional factors involved in RPC resolution?

In this study we discovered that RPC formation is toxic and triggers translation inhibition which further induces cellular stress responses and quality control pathways regulating cellular viability. Nevertheless, we did not investigate a specific factor involved in RPC resolution apart from the proteasome. Our data demonstrated that mRNA-crosslinked proteins undergo translation-dependent poly-ubiquitylation, which is essential for resolving a large proportion of RPCs. Therefore, determining the precise involved ubiquitin E3 enzymes that facilitate this ubiquitylation will be critical to understand the mechanism of how RPCs are resolved

by the cell. According to our preliminary data, the addition of NEDDylation inhibitor had no effect on the level of ubiquitylation of mRNA-crosslinked proteins, indicating that the Cullin-RING E3 ubiquitin-Ligases (CRLs) are not involved (Petroski and Deshaies, 2005). However, no ubiquitin E3 ligase is significantly recruited to ribosomes based on our preliminary polysome profiling MS results, suggesting no or only transient interaction between ribosomes and E3 ligases upon RPC induction.

To address the above question, a protein-protein crosslinker could be utilized to stabilize the interaction between E3 ligases and the substrates. Briefly, after 4-SU treatment and UVA irradiation, the protein-protein crosslinker is added to the cells, followed by polyA pull-down and MS measurement. This will allow us to determine the proteins that interact with RPCs and potentially capture of resolution factors that are recruited to RPCs that interact with their substrates. This would also enable the investigation of ubiquitylation-independent RPC resolution pathways. Alternatively, a proximity labelling method called TurboID could be utilized to identify proximal proteome of ribosomes after cells are challenged by RPCs. TurboID is a molecular biology tool that allows researchers to identify unknown interactors of a protein of interest. It consists of an engineered biotin ligase that catalyses biotin-AMP formation, which reacts with lysine residues of proximal proteins by forming covalent bonds. After that, protein pull-down using streptavidin-coupled beads and MS measurement are conducted to identify the interactome (Branon et al., 2018; Cho et al., 2020). This approach would identify proteins specifically associating with the ribosome upon RPC formation, which would be good candidates for factors involved in RPC resolution.

To gain more insight into how cells sense, respond to, and clear RPCs, a genome-wide CRISPR Cas9 screen would be an unbiased approach. Such a loss-of-function genetic screen will allow us to identify the network that provides RPC resistance. In brief, RPCs would be induced in cells after transduction with a lentiviral sgRNA library, followed by determining sgRNA frequencies by sequencing at several recovery time points. This will reveal sgRNAs that specifically dropped out when cells are challenged by RPC formation. Genes targeted by these sgRNAs will be promising candidates for an involvement in resistance to RPCs. However, such genome-wide genetic screens usually result in a large number of hits (Olivieri et al., 2020), making the selection and follow-up analysis complex and raising the risk of overlooking vital factors. To ensure optimal hit selection, a second genetic

screen in a different species, e.g. yeast, could be conducted. Focusing on common candidates across the two screens will ensure the selection of factors playing a role in evolutionarily conserved resistance mechanisms. Detailed functional assays can follow up the investigation of these hits, including cellular viability towards RPC formation, monitoring the resolution kinetics of mRNA-crosslinked protein, assessing *in vitro* RPC formation and clearance, etc. In conclusion, our study established tools to induce and monitor RPCs and revealed first principles of RPC quality control mechanisms, but there are still many open questions regarding involved factors and mechanisms of RPC clearance. Further studies will be required to address these questions to provide a full picture of cellular RPC resolution mechanisms.

4.5 Physiological and pathological roles of RPCs

The ribosome is an essential cellular machinery that performs protein synthesis. Our study demonstrated that RPCs trigger ribosome collisions and impede translation leading to cellular toxicity. Furthermore, we showed that formaldehyde generates RPCs and induces the same cellular stress responses triggered by RPCs, indicating that RPC is a major problem caused by endogenous formaldehyde. Therefore, we hypothesize that RPC formation contributes to formaldehyde-induced toxicity.

4.5.1 RPCs and ribosomopathies

Ribosome dysfunction leads to both congenital and acquired human disorders, known as ribosomopathies, including Diamond-Blackfan anemia (DBA), Schwachman-Diamond syndrome (SDS) and Treacher-Collins syndrome (TCS) (Liu and Ellis, 2006). DBA is a rare blood disorder characterized by bone marrow failure leading to decreased levels of erythroid precursors, anaemia and a predisposition to cancer (Lipton and Ellis, 2009; Narla and Ebert, 2010). Previous studies demonstrated that more than half of the DBA patients bear genetic mutations in various ribosomal protein-coding genes, which impair ribosome biogenesis and result in insufficient mature ribosomes in cells (Da Costa et al., 2018; Draptchinskaia et al., 1999; Ulirsch et al., 2018). The original idea suggests that the shortage of ribosomes affects the translation of proteins critical in erythropoiesis, or

Discussion

that non-ribosomal related functions of mutated ribosomal proteins are impeded (Narla et al., 2011; Warner and McIntosh, 2009). Emerging research suggested that the p53-mediated cellular stress response is essential when facing ribosomal protein insufficiency, wherein the ribosome biogenesis disruption results in the release of free RPL11 and other ribosomal proteins to the nucleoplasm, which bind to MDM2, leading to p53 accumulation and activation, ultimately triggering cycle arrest, senescence, autophagy and apoptosis (Narla et al., 2011; Zhang and Lu, 2009). Moreover, homozygous loss of p53 in the DBA mice model fully rescued the hematopoietic defects indicating the fundamental role of MDM2-p53 pathway in DBA pathomechanism (McGowan et al., 2008).

Mutations in ribosomal protein genes are expected to cause widespread phenotypes throughout the organism, but the clinical manifestations of DBA patients suggest DBA is a tissue-specific defect (Farley-Barnes et al., 2019). One explanation of the hematopoietic system-specific disorder is due to the tissue-restricted activation of the p53 pathway, which is more sensitive during hematopoietic stem cell (HSC) differentiation (Mills and Green, 2017). However, how the upstream signal of p53 leads to bone marrow failure but spares other types of cells remains undefined. Recent studies demonstrated that endogenous formaldehyde is released during HSC differentiation, which is highly reactive and damages DNA by forming ICLs and DPCs (Jung and Smogorzewska, 2021; Shen et al., 2020). In this context, it will be interesting to test whether the formaldehyde-induced formation of RPCs during HSC differentiation is a source of damage, enhancing the burden in DBA patients. Our data from this study suggests that the clearance of mRNA-crosslinked proteins is largely translation-dependent, which can be affected by the lack of mature ribosomes, leading to RPC persistence and translation defects. Furthermore, RPCs formed within ribosomes between ribosomal proteins and rRNAs can be an additional reason triggering translation collapse. Taken together, the burst of endogenously produced formaldehyde in HSCs and defects in ribosomal proteins may easily impair translation, leading to cell death and therefore impeding formation of erythrocytes by the hematopoietic system.

4.5.2 RPCs and aging

Translation dysfunction leads to nascent polypeptide chain misfolding, resulting in the formation of toxic protein aggregates, which eventually impairs cellular fitness and contributes to the development of age-related neurodegenerative diseases, such as Alzheimer's disease, Huntington's disease and Parkinson's disease. (Chiti and Dobson, 2006; Ishimura et al., 2014; Kim et al., 2015; Nedialkova and Leidel, 2015). However, the connection between aging and the decline of cellular proteostasis remains unclear. Emerging research demonstrated that aging exacerbates ribosome pausing, thereby increasing ribosome collisions. As a consequence the RQC pathway becomes overwhelmed, leading to co-translational proteostasis disruption and polypeptide aggregation (Stein et al., 2022). Nevertheless, the primary mechanism of how aging triggers ribosome stalling and interrupts cellular translation efficiency is unknown.

It has been reported that formaldehyde, a by-product of various metabolic reactions, appears in almost every vertebrate cell, and relatively high formaldehyde concentration have been detected in the brains of healthy adult animals (Kou et al., 2022; Wang et al., 2022). Previous studies suggested that aging induces memory decline associated with formaldehyde accumulation in mice models. Injection of formaldehyde into brains of healthy mice leads to spatial reference memory impairment, whereas adding formaldehyde scavenger, resveratrol, efficiently removes formaldehyde and attenuates the damage of learning and memory in the senile dementia mouse model (Tong et al., 2011). Moreover, endogenous formaldehyde is metabolized by alcohol dehydrogenase 5 (ADH5) and aldehyde dehydrogenase 2 (ALDH2) (Edenberg and Foroud, 2013; Pontel et al., 2015; Teng et al., 2001). Researchers observed that deficiency of ALDH2 or ADH5 induces age-dependent neurodegeneration in mice and also discovered a cell senescence-associated reduction of ADH5 expression (Ai et al., 2019; Ohsawa et al., 2008; Rizza et al., 2018). The above evidence indicates that formaldehyde-induced stress increases during aging, which may contribute to the risk of age-associated decline of brain function.

Even though it has been speculated that endogenous formaldehyde accelerates cell senescence and aging by impairing mitochondria quality control (Rizza et al., 2018), it will be interesting to understand whether increased

Discussion

formaldehyde levels lead to RPC formation and thereby also contribute to ribosome stalling, nascent protein misfolding and aggregating during aging. Detecting the cellular markers of senescence after RPC induction will be pivotal to address this question. Additionally, a method allowing the accurate detection of RPCs *in vivo* should be developed to investigate animal and cellular aging models. Moreover, it will be worthwhile to test whether the addition of formaldehyde scavengers alleviates the excess ribosome pausing and collisions reported in worm and yeast models of aging (Stein et al., 2022). To conclude, studying the resolution mechanism of formaldehyde-induced RPC will be helpful to understand the connection between aging and ribosome deceleration, providing new insights into the pathophysiology of aging-related neurodegenerative diseases and potential therapeutic targets.

Reference

Abbotts, R., Wilson, D.M., 2017. Coordination of DNA Single Strand Break Repair. *Free Radic Biol Med* 107, 228–244.

Adhikari, S., Karmahapatra, S.K., Karve, T.M., Bandyopadhyay, S., Woodrick, J., Manthena, P.V., Glasgow, E., Byers, S., Saha, T., Uren, A., 2012. Characterization of magnesium requirement of human 5'-tyrosyl DNA phosphodiesterase mediated reaction. *BMC Res Notes* 5, 134.

Ai, L., Tan, T., Tang, Y., Yang, J., Cui, D., Wang, R., Wang, A., Fei, X., Di, Y., Wang, X., Yu, Y., Zhao, S., Wang, W., Bai, S., Yang, X., He, R., Lin, W., Han, H., Cai, X., Tong, Z., 2019. Endogenous formaldehyde is a memory-related molecule in mice and humans. *Commun Biol* 2, 1–12.

Aitken, C.E., Lorsch, J.R., 2012. A mechanistic overview of translation initiation in eukaryotes. *Nat Struct Mol Biol* 19, 568–576.

Alabert, C., Bukowski-Wills, J.-C., Lee, S.-B., Kustatscher, G., Nakamura, K., de Lima Alves, F., Menard, P., Mejlvang, J., Rappsilber, J., Groth, A., 2014. Nascent chromatin capture proteomics determines chromatin dynamics during DNA replication and identifies unknown fork components. *Nat Cell Biol* 16, 281–291.

Alberts, B., Johnson, A., Lewis, J., Raff, M., Roberts, K., Walter, P., 2002. From RNA to Protein. *Molecular Biology of the Cell*. 4th edition.

Alcón, P., Shakeel, S., Chen, Z.A., Rappsilber, J., Patel, K.J., Passmore, L.A., 2020. FANCD2–FANCI is a clamp stabilized on DNA by monoubiquitination of FANCD2 during DNA repair. *Nat Struct Mol Biol* 27, 240–248.

Alseth, I., Osman, F., Korvald, H., Tsaneva, I., Whitby, M.C., Seeberg, E., Bjørås, M., 2005. Biochemical characterization and DNA repair pathway interactions of Mag1-mediated base excision repair in *Schizosaccharomyces pombe*. *Nucleic Acids Res* 33, 1123–1131.

Álvarez-Quilón, A., Wojtaszek, J.L., Mathieu, M.-C., Patel, T., Appel, C.D., Hustedt, N., Rossi, S.E., Wallace, B.D., Setiaputra, D., Adam, S., Ohashi, Y., Melo, H., Cho, T., Gervais, C., Muñoz, I.M., Grazzini, E., Young, J.T.F., Rouse, J., Zinda, M., Williams, R.S., Durocher, D., 2020. Endogenous DNA 3' Blocks Are Vulnerabilities for BRCA1 and BRCA2 Deficiency and Are Reversed by the APE2 Nuclease. *Molecular Cell* 78, 1152-1165.e8.

Reference

- Ambroggio, X.I., Rees, D.C., Deshaies, R.J., 2003. JAMM: A Metalloprotease-Like Zinc Site in the Proteasome and Signalosome. *PLoS Biol* 2, e2.
- Ameri, K., Harris, A.L., 2008. Activating transcription factor 4. *Int J Biochem Cell Biol* 40, 14–21.
- An, L., Jiang, Y., Ng, H.H.W., Man, E.P.S., Chen, J., Khoo, U.-S., Gong, Q., Huen, M.S.Y., n.d. Dual-utility NLS drives RNF169-dependent DNA damage responses. *CELL BIOLOGY* 10.
- Andersen, G.R., Valente, L., Pedersen, L., Kinzy, T.G., Nyborg, J., 2001. Crystal structures of nucleotide exchange intermediates in the eEF1A–eEF1B α complex. *Nat Struct Mol Biol* 8, 531–534.
- Andersen, P.L., Xu, F., Xiao, W., 2008. Eukaryotic DNA damage tolerance and translesion synthesis through covalent modifications of PCNA. *Cell Res* 18, 162–173.
- Anindya, R., Aygün, O., Svejstrup, J.Q., 2007. Damage-Induced Ubiquitylation of Human RNA Polymerase II by the Ubiquitin Ligase Nedd4, but Not Cockayne Syndrome Proteins or BRCA1. *Molecular Cell* 28, 386–397.
- Aquila, L., Atanassov, B.S., 2020. Regulation of Histone Ubiquitination in Response to DNA Double Strand Breaks. *Cells* 9, 1699.
- Araki, Y., Takahashi, S., Kobayashi, T., Kajihō, H., Hoshino, S., Katada, T., 2001. Ski7p G protein interacts with the exosome and the Ski complex for 3'-to-5' mRNA decay in yeast. *EMBO J* 20, 4684–4693.
- Ashour, M.E., Mosammaparast, N., 2021. Mechanisms of damage tolerance and repair during DNA replication. *Nucleic Acids Research* 49, 3033–3047.
- Aubert, M., O'Donohue, M.-F., Lebaron, S., Gleizes, P.-E., 2018. Pre-Ribosomal RNA Processing in Human Cells: From Mechanisms to Congenital Diseases. *Biomolecules* 8, 123.
- Bai, M., Ti, D., Mei, Q., Liu, J., Yan, X., Chen, D., Li, X., Wu, Z., Han, W., 2020. The Role of Posttranslational Modifications in DNA Repair. *BioMed Research International* 2020, 1–13.
- Baker, D.J., Wuenschell, G., Xia, L., Termini, J., Bates, S.E., Riggs, A.D., O'Connor, T.R., 2007. Nucleotide Excision Repair Eliminates Unique DNA-Protein Cross-links from Mammalian Cells. *Journal of Biological Chemistry* 282, 22592–22604.
- Balbo, S., Turesky, R.J., Villalta, P.W., 2014. DNA Adductomics. *Chem. Res. Toxicol.* 27, 356–366.

Reference

- Bantscheff, M., Schirle, M., Sweetman, G., Rick, J., Kuster, B., 2007. Quantitative mass spectrometry in proteomics: a critical review. *Anal Bioanal Chem* 389, 1017–1031.
- Bard, J.A.M., Goodall, E.A., Greene, E.R., Jonsson, E., Dong, K.C., Martin, A., 2018. Structure and Function of the 26S Proteasome. *Annu Rev Biochem* 87, 697–724.
- Bartel, D.P., 2018. Metazoan MicroRNAs. *Cell* 173, 20–51.
- Basbous, J., Constantinou, A., 2019. A tumor suppressive DNA translocase named FANCM. *Critical Reviews in Biochemistry and Molecular Biology* 54, 27–40.
- Bäumert, H.G., Sköld, S.E., Kurland, C.G., 1978. RNA-protein neighbourhoods of the ribosome obtained by crosslinking. *Eur J Biochem* 89, 353–359.
- Beard, W.A., Horton, J.K., Prasad, R., Wilson, S.H., 2019. Eukaryotic Base Excision Repair: New Approaches Shine Light on Mechanism. *Annu. Rev. Biochem.* 88, 137–162.
- Bębenek, A., Ziuzia-Graczyk, I., 2018. Fidelity of DNA replication—a matter of proofreading. *Curr Genet* 64, 985–996.
- Bebenek, K., Kunkel, T.A., 2004. Functions of DNA Polymerases, in: *Advances in Protein Chemistry, DNA Repair and Replication*. Academic Press, pp. 137–165.
- Becker, J.R., Clifford, G., Bonnet, C., Groth, A., Wilson, M.D., Chapman, J.R., 2021. BARD1 reads H2A lysine 15 ubiquitination to direct homologous recombination. *Nature* 596, 433–437.
- Begley, T.J., Samson, L.D., 2003. AlkB mystery solved: oxidative demethylation of N1-methyladenine and N3-methylcytosine adducts by a direct reversal mechanism. *Trends in Biochemical Sciences* 28, 2–5.
- Benard, L., Carroll, K., Valle, R.C., Masison, D.C., Wickner, R.B., 1999. The ski7 antiviral protein is an EF1-alpha homolog that blocks expression of non-Poly(A) mRNA in *Saccharomyces cerevisiae*. *J Virol* 73, 2893–2900.
- Bengtson, M.H., Joazeiro, C.A.P., 2010. Role of a ribosome-associated E3 ubiquitin ligase in protein quality control. *Nature* 467, 470–473.
- Bentley, D.L., 2014. Coupling mRNA processing with transcription in time and space. *Nat Rev Genet* 15, 163–175.
- Berg, M.D., Brandl, C.J., n.d. Transfer RNAs: diversity in form and function. *RNA Biol* 18, 316–339.

Reference

- Bernstein, E., Caudy, A.A., Hammond, S.M., Hannon, G.J., 2001. Role for a bidentate ribonuclease in the initiation step of RNA interference. *Nature* 409, 363–366.
- Best, K., Ikeuchi, K., Kater, L., Best, D., Musial, J., Matsuo, Y., Berninghausen, O., Becker, T., Inada, T., Beckmann, R., 2022. Clearing of ribosome collisions by the ribosome quality control trigger complex RQT.
- Betat, H., Long, Y., Jackman, J.E., Mörl, M., 2014. From End to End: tRNA Editing at 5'- and 3'-Terminal Positions. *Int J Mol Sci* 15, 23975–23998.
- Bhargava, V., Goldstein, C.D., Russell, L., Xu, L., Ahmed, M., Li, W., Casey, A., Servage, K., Kollipara, R., Picciarelli, Z., Kittler, R., Yatsenko, A., Carmell, M., Orth, K., Amatruda, J.F., Yanowitz, J.L., Buszczak, M., 2020. GCNA Preserves Genome Integrity and Fertility Across Species. *Developmental Cell* 52, 38-52.e10.
- Bi, X., 2015. Mechanism of DNA damage tolerance. *World J Biol Chem* 6, 48–56.
- Bogorad, A.M., Lin, K.Y., Marintchev, A., 2017. Novel mechanisms of eIF2B action and regulation by eIF2 α phosphorylation. *Nucleic Acids Res* 45, 11962–11979.
- Bohgaki, M., Bohgaki, T., El Ghamrasni, S., Srikumar, T., Maire, G., Panier, S., Fradet-Turcotte, A., Stewart, G.S., Raught, B., Hakem, A., Hakem, R., 2013. RNF168 ubiquitylates 53BP1 and controls its response to DNA double-strand breaks. *Proc Natl Acad Sci U S A* 110, 20982–20987.
- Boiteux, S., Guillet, M., 2004. Abasic sites in DNA: repair and biological consequences in *Saccharomyces cerevisiae*. *DNA Repair* 3, 1–12.
- Borgermann, N., Ackermann, L., Schwertman, P., Hendriks, I.A., 2019. SUMOylation promotes protective responses to DNA-protein crosslinks. *The EMBO Journal* 38, e101496.
- Bothmer, A., Robbiani, D.F., Feldhahn, N., Gazumyan, A., Nussenzweig, A., Nussenzweig, M.C., 2010. 53BP1 regulates DNA resection and the choice between classical and alternative end joining during class switch recombination. *Journal of Experimental Medicine* 207, 855–865.
- Botuyan, M.V., Lee, J., Ward, I.M., Kim, J.-E., Thompson, J.R., Chen, J., Mer, G., 2006. Structural Basis for the Methylation State-Specific Recognition of Histone H4-K20 by 53BP1 and Crb2 in DNA Repair. *Cell* 127, 1361–1373.
- Boye, E., Grallert, B., 2020. eIF2 α phosphorylation and the regulation of translation. *Curr Genet* 66, 293–297.

Reference

- Brandman, O., Hegde, R.S., 2016. Ribosome-associated protein quality control. *Nat Struct Mol Biol* 23, 7–15.
- Brandman, O., Stewart-Ornstein, J., Wong, D., Larson, A., Williams, C.C., Li, G.-W., Zhou, S., King, D., Shen, P.S., Weibezahn, J., Dunn, J.G., Rouskin, S., Inada, T., Frost, A., Weissman, J.S., 2012. A ribosome-bound quality control complex triggers degradation of nascent peptides and signals translation stress. *Cell* 151, 1042–1054.
- Branon, T.C., Bosch, J.A., Sanchez, A.D., Udeshi, N.D., Svinkina, T., Carr, S.A., Feldman, J.L., Perrimon, N., Ting, A.Y., 2018. Efficient proximity labeling in living cells and organisms with TurboID. *Nat Biotechnol* 36, 880–887.
- Branzei, D., 2011. Ubiquitin family modifications and template switching. *FEBS Letters* 585, 2810–2817.
- Branzei, D., Seki, M., Enomoto, T., 2004. Rad18/Rad5/Mms2-mediated polyubiquitination of PCNA is implicated in replication completion during replication stress. *Genes to Cells* 9, 1031–1042.
- Branzei, D., Szakal, B., 2016. DNA damage tolerance by recombination: Molecular pathways and DNA structures. *DNA Repair, Cutting-edge Perspectives in Genomic Maintenance III* 44, 68–75.
- Braten, O., Livneh, I., Ziv, T., Admon, A., Kehat, I., Caspi, L.H., Gonen, H., Bercovich, B., Godzik, A., Jahandideh, S., Jaroszewski, L., Sommer, T., Kwon, Y.T., Guharoy, M., Tompa, P., Ciechanover, A., 2016. Numerous proteins with unique characteristics are degraded by the 26S proteasome following monoubiquitination. *Proceedings of the National Academy of Sciences* 113, E4639–E4647.
- Bregman, D.B., Halaban, R., van Gool, A.J., Henning, K.A., Friedberg, E.C., Warren, S.L., 1996. UV-induced ubiquitination of RNA polymerase II: a novel modification deficient in Cockayne syndrome cells. *Proceedings of the National Academy of Sciences* 93, 11586–11590.
- Brosnan, C., Voinnet, O., 2009. The long and the short of noncoding RNAs. *Current opinion in cell biology* 21, 416–25.
- Brueckner, F., Hennecke, U., Carell, T., Cramer, P., 2007. CPD Damage Recognition by Transcribing RNA Polymerase II. *Science*.
- Burma, S., Chen, B.P., Murphy, M., Kurimasa, A., Chen, D.J., 2001. ATM Phosphorylates Histone H2AX in Response to DNA Double-strand Breaks. *Journal of Biological Chemistry* 276, 42462–42467.
- Caldecott, K.W., 2008. Single-strand break repair and genetic disease. *Nat Rev Genet* 9, 619–631.

Reference

- Callen, E., Di Virgilio, M., Kruhlak, M.J., Nieto-Soler, M., Wong, N., Chen, H.-T., Faryabi, R.B., Polato, F., Santos, M., Starnes, L.M., Wesemann, D.R., Lee, J.-E., Tubbs, A., Sleckman, B.P., Daniel, J.A., Ge, K., Alt, F.W., Fernandez-Capetillo, O., Nussenzweig, M.C., Nussenzweig, A., 2013. 53BP1 mediates productive and mutagenic DNA repair through distinct phosphoprotein interactions. *Cell* 153, 1266–1280.
- Cannan, W.J., Pederson, D.S., 2016. Mechanisms and Consequences of Double-strand DNA Break Formation in Chromatin. *J Cell Physiol* 231, 3–14.
- Carmell, M.A., Dokshin, G.A., Skaletsky, H., Hu, Y.-C., van Wolfswinkel, J.C., Igarashi, K.J., Bellott, D.W., Nefedov, M., Reddien, P.W., Enders, G.C., Uversky, V.N., Mello, C.C., Page, D.C., 2016. A widely employed germ cell marker is an ancient disordered protein with reproductive functions in diverse eukaryotes. *eLife* 5, e19993.
- Cass, I., Baldwin, R.L., Varkey, T., Moslehi, R., Narod, S.A., Karlan, B.Y., 2003. Improved survival in women with BRCA-associated ovarian carcinoma. *Cancer* 97, 2187–2195.
- Castello, A., Fischer, B., Eichelbaum, K., Horos, R., Beckmann, B.M., Strein, C., Davey, N.E., Humphreys, D.T., Preiss, T., Steinmetz, L.M., Krijgsveld, J., Hentze, M.W., 2012. Insights into RNA Biology from an Atlas of Mammalian mRNA-Binding Proteins. *Cell* 149, 1393–1406.
- Ceccaldi, R., Sarangi, P., D'Andrea, A.D., 2016. The Fanconi anaemia pathway: new players and new functions. *Nat Rev Mol Cell Biol* 17, 337–349.
- Cejka, D., Losert, D., Wacheck, V., 2006. Short interfering RNA (siRNA): tool or therapeutic? *Clin. Sci.* 110, 47–58.
- Centore, R.C., Yazinski, S.A., Tse, A., Zou, L., 2012. Spartan/C1orf124, a Reader of PCNA Ubiquitylation and a Regulator of UV-Induced DNA Damage Response. *Molecular Cell* 46, 625–635.
- Champoux, J.J., 2001. DNA Topoisomerases: Structure, Function, and Mechanism. *Annual Review of Biochemistry* 70, 369–413.
- Chandrasekaran, V., Juszkiwicz, S., Choi, J., Puglisi, J.D., Brown, A., Shao, S., Ramakrishnan, V., Hegde, R.S., 2019. Mechanism of ribosome stalling during translation of a poly(A) tail. *Nat Struct Mol Biol* 26, 1132–1140.
- Chapman, J.R., Barral, P., Vannier, J.-B., Borel, V., Steger, M., Tomas-Loba, A., Sartori, A.A., Adams, I.R., Batista, F.D., Boulton, S.J., 2013. RIF1 is essential for 53BP1-dependent nonhomologous end joining and suppression of DNA double-strand break resection. *Mol Cell* 49, 858–871.

Reference

- Chatterjee, N., Walker, G.C., 2017. Mechanisms of DNA damage, repair and mutagenesis. *Environ Mol Mutagen* 58, 235–263.
- Chau, V., Tobias, J.W., Bachmair, A., Marriott, D., Ecker, D.J., Gonda, D.K., Varshavsky, A., 1989. A multiubiquitin chain is confined to specific lysine in a targeted short-lived protein. *Science* 243, 1576–1583.
- Che, J., Hong, X., Rao, H., 2021. PCNA Ubiquitylation: Instructive or Permissive to DNA Damage Tolerance Pathways? *Biomolecules* 11, 1543.
- Chen, R.-H., Chen, Y.-H., Huang, T.-Y., 2019. Ubiquitin-mediated regulation of autophagy. *J Biomed Sci* 26, 80.
- Chitale, S., Richly, H., 2017. Timing of DNA lesion recognition: Ubiquitin signaling in the NER pathway. *Cell Cycle* 16, 163–171.
- Chiti, F., Dobson, C.M., 2006. Protein Misfolding, Functional Amyloid, and Human Disease. *Annu. Rev. Biochem.* 75, 333–366.
- Cho, K.F., Branon, T.C., Udeshi, N.D., Myers, S.A., Carr, S.A., Ting, A.Y., 2020. Proximity labeling in mammalian cells with TurboID and split-TurboID. *Nat Protoc* 15, 3971–3999.
- Choi, J.-H., Pfeifer, G.P., 2005. The role of DNA polymerase η in UV mutational spectra. *DNA Repair* 4, 211–220.
- Chukka, P.A.R., Wetmore, S.D., Thakor, N., 2021. Established and Emerging Regulatory Roles of Eukaryotic Translation Initiation Factor 5B (eIF5B). *Frontiers in Genetics* 12:737433.
- Chválková, K., Brabec, V., Kašpárková, J., 2007. Mechanism of the formation of DNA–protein cross-links by antitumor cisplatin. *Nucleic Acids Research* 35, 1812–1821.
- Ciccía, A., Nimonkar, A.V., Hu, Y., Hajdu, I., Achar, Y.J., Izhar, L., Petit, S.A., Adamson, B., Yoon, J.C., Kowalczykowski, S.C., Livingston, D.M., Haracska, L., Elledge, S.J., 2012. Polyubiquitinated PCNA Recruits the ZRANB3 Translocase to Maintain Genomic Integrity after Replication Stress. *Molecular Cell* 47, 396–409.
- Cipolla, L., Maffia, A., Bertoletti, F., Sabbioneda, S., 2016. The Regulation of DNA Damage Tolerance by Ubiquitin and Ubiquitin-Like Modifiers. *Frontiers in Genetics* 7:105.
- Clague, M.J., Urbé, S., Komander, D., 2019. Breaking the chains: deubiquitylating enzyme specificity begets function. *Nat Rev Mol Cell Biol* 20, 338–352.

Reference

- Clark, A.C., 2016. Caspase Allostery and Conformational Selection. *Chem. Rev.* 116, 6666–6706.
- Cleaver, J.E., Lam, E.T., Revet, I., 2009. Disorders of nucleotide excision repair: the genetic and molecular basis of heterogeneity. *Nat Rev Genet* 10, 756–768.
- Collins, G.A., Goldberg, A.L., 2017. The Logic of the 26S Proteasome. *Cell* 169, 792–806.
- Connelly, J.C., de Leau, E.S., Leach, D.R.F., 2003. Nucleolytic processing of a protein-bound DNA end by the *E. coli* SbcCD (MR) complex. *DNA Repair* 2, 795–807.
- Cooke, M.S., Evans, M.D., Dizdaroglu, M., Lunec, J., 2003. Oxidative DNA damage: mechanisms, mutation, and disease. *The FASEB Journal* 17, 1195–1214.
- Cortez, D., 2019. Replication-Coupled DNA Repair. *Molecular Cell* 74, 866–876.
- Costa-Mattioli, M., Walter, P., 2020. The integrated stress response: From mechanism to disease. *Science* 368, eaat5314.
- Crick, F.H., 1958. On protein synthesis. *Symp Soc Exp Biol* 12, 138–163.
- Crick, F.H.C., Watson, J.D., Bragg, W.L., 1954. The complementary structure of deoxyribonucleic acid. *Proceedings of the Royal Society of London. Series A. Mathematical and Physical Sciences* 223, 80–96.
- Cruz, L., Soares, P., Correia, M., 2021. Ubiquitin-Specific Proteases: Players in Cancer Cellular Processes. *Pharmaceuticals* 14, 848.
- Cruz-García, A., López-Saavedra, A., Huertas, P., 2014. BRCA1 Accelerates CtIP-Mediated DNA-End Resection. *Cell Reports* 9, 451–459.
- Cusack, S., 1999. RNA–protein complexes. *Current Opinion in Structural Biology* 9, 66–73.
- Da Costa, L., Narla, A., Mohandas, N., 2018. An update on the pathogenesis and diagnosis of Diamond-Blackfan anemia. *F1000Res* 7, F1000 Faculty Rev-1350.
- Dan, C., Pei, H., Zhang, B., Zheng, X., Ran, D., Du, C., 2021. Fanconi anemia pathway and its relationship with cancer. *GENOME INSTAB. DIS.* 2, 175–183.
- Dana, H., Chalbatani, G.M., Mahmoodzadeh, H., Karimloo, R., Rezaiean, O., Moradzadeh, A., Mehmandoost, N., Moazzen, F., Mazraeh, A., Marmari, V., Ebrahimi, M., Rashno, M.M., Abadi, S.J., Gharagouzlo, E., 2017. Molecular Mechanisms and Biological Functions of siRNA. *Int J Biomed Sci* 13, 48–57.

Reference

- D'Andrea, A., Pellman, D., 1998. Deubiquitinating enzymes: a new class of biological regulators. *Crit Rev Biochem Mol Biol* 33, 337–352.
- Darling, N.J., Cook, S.J., 2014. The role of MAPK signalling pathways in the response to endoplasmic reticulum stress. *Biochim Biophys Acta* 1843, 2150–2163.
- Darnell, J.C., Van Driesche, S.J., Zhang, C., Hung, K.Y.S., Mele, A., Fraser, C.E., Stone, E.F., Chen, C., Fak, J.J., Chi, S.W., Licatalosi, D.D., Richter, J.D., Darnell, R.B., 2011. FMRP stalls ribosomal translocation on mRNAs linked to synaptic function and autism. *Cell* 146, 247–261.
- Davidovic, L., Vodenicharov, M., Affar, E.B., Poirier, G.G., 2001. Importance of Poly(ADP-Ribose) Glycohydrolase in the Control of Poly(ADP-Ribose) Metabolism. *Experimental Cell Research* 268, 7–13.
- Davies, O., Mendes, P., Smallbone, K., Malys, N., 2012. Characterisation of multiple substrate-specific (d)ITP/(d)XTPase and modelling of deaminated purine nucleotide metabolism. *BMB Reports* 45, 259–264.
- Davies, R.J.H., 1995. Ultraviolet Radiation Damage in DNA. *Biochemical Society Transactions* 23, 407–418.
- Davis, E.J., Lachaud, C., Appleton, P., Macartney, T.J., Näthke, I., Rouse, J., 2012. DVC1 (C1orf124) recruits the p97 protein segregase to sites of DNA damage. *Nat Struct Mol Biol* 19, 1093–1100.
- De Bont, R., van Larebeke, N., 2004. Endogenous DNA damage in humans: a review of quantitative data. *Mutagenesis* 19, 169–185.
- de Graaf, B., Clore, A., McCullough, A.K., 2009. Cellular pathways for DNA repair and damage tolerance of formaldehyde-induced DNA-protein crosslinks. *DNA Repair* 8, 1207–1214.
- De, S., Mühlemann, O., 2022. A comprehensive coverage insurance for cells: revealing links between ribosome collisions, stress responses and mRNA surveillance. *RNA Biology* 19, 609–621.
- Deans, A.J., West, S.C., 2011. DNA interstrand crosslink repair and cancer. *Nat Rev Cancer* 11, 467–480.
- Debethune, L., 2002. Processing of nucleopeptides mimicking the topoisomerase I-DNA covalent complex by tyrosyl-DNA phosphodiesterase. *Nucleic Acids Research* 30, 1198–1204.
- Demple, B., DeMott, M.S., 2002. Dynamics and diversions in base excision DNA repair of oxidized abasic lesions. *Oncogene* 21, 8926–8934.

Reference

- Densham, R.M., Garvin, A.J., Stone, H.R., Strachan, J., Baldock, R.A., Daza-Martin, M., Fletcher, A., Blair-Reid, S., Beesley, J., Johal, B., Pearl, L.H., Neely, R., Keep, N.H., Watts, F.Z., Morris, J.R., 2016. Human BRCA1-BARD1 ubiquitin ligase activity counteracts chromatin barriers to DNA resection. *Nat Struct Mol Biol* 23, 647–655.
- Deol, K.K., Lorenz, S., Strieter, E.R., 2019. Enzymatic Logic of Ubiquitin Chain Assembly. *Frontiers in Physiology* 10:835.
- Deriano, L., Roth, D., 2013. Modernizing the nonhomologous end-joining repertoire: alternative and classical NHEJ share the stage. *Annual review of genetics*. 2013. 47:433–55
- Desai, S.D., Li, T.K., Rodriguez-Bauman, A., Rubin, E.H., Liu, L.F., 2001. Ubiquitin/26S proteasome-mediated degradation of topoisomerase I as a resistance mechanism to camptothecin in tumor cells. *Cancer Res* 61, 5926–5932.
- Desai, S.D., Liu, L.F., Vazquez-Abad, D., D'Arpa, P., 1997. Ubiquitin-dependent Destruction of Topoisomerase I Is Stimulated by the Antitumor Drug Camptothecin. *Journal of Biological Chemistry* 272, 24159–24164.
- Deshai, R.J., Joazeiro, C.A.P., 2009. RING Domain E3 Ubiquitin Ligases. *Annual Review of Biochemistry* 78, 399–434.
- Deshpande, R.A., Lee, J.-H., Arora, S., Paull, T.T., 2016. Nbs1 Converts the Human Mre11/Rad50 Nuclease Complex into an Endo/Exonuclease Machine Specific for Protein-DNA Adducts. *Molecular Cell* 64, 593–606.
- Dever, T.E., Dinman, J.D., Green, R., 2018. Translation Elongation and Recoding in Eukaryotes. *Cold Spring Harb Perspect Biol* 10, a032649.
- Dever, T.E., Green, R., 2012. The Elongation, Termination, and Recycling Phases of Translation in Eukaryotes. *Cold Spring Harbor Perspectives in Biology* 4, a013706–a013706.
- Dey, S., Baird, T.D., Zhou, D., Palam, L.R., Spandau, D.F., Wek, R.C., 2010. Both Transcriptional Regulation and Translational Control of ATF4 Are Central to the Integrated Stress Response. *Journal of Biological Chemistry* 285, 33165–33174.
- Dharap, A., Pokrzywa, C., Murali, S., Pandi, G., Vemuganti, R., 2013. MicroRNA miR-324-3p Induces Promoter-Mediated Expression of RelA Gene. *PLOS ONE* 8, e79467.
- Di Virgilio, M., Callen, E., Yamane, A., Zhang, W., Jankovic, M., Gitlin, A.D., Feldhahn, N., Resch, W., Oliveira, T.Y., Chait, B.T., Nussenzweig, A., Casellas, R., Robbiani, D.F., Nussenzweig, M.C., 2013. Rif1 Prevents Resection of DNA Breaks and Promotes Immunoglobulin Class Switching. *Science* 339, 10.1126

Reference

- Diefenbacher, M.E., Popov, N., Blake, S.M., Schülein-Völk, C., Nye, E., Spencer-Dene, B., Jaenicke, L.A., Eilers, M., Behrens, A., 2014. The deubiquitinase USP28 controls intestinal homeostasis and promotes colorectal cancer. *J Clin Invest* 124, 3407–3418.
- Dirac-Svejstrup, A.B., Walker, J., Faull, P., Encheva, V., Akimov, V., Puglia, M., Perkins, D., Kümper, S., Hunjan, S.S., Blagoev, B., Snijders, A.P., Powell, D.J., Svejstrup, J.Q., 2020. DDI2 Is a Ubiquitin-Directed Endoprotease Responsible for Cleavage of Transcription Factor NRF1. *Molecular Cell* 79, 332-341.e7.
- Dittmar, G., Winklhofer, K.F., 2020. Linear Ubiquitin Chains: Cellular Functions and Strategies for Detection and Quantification. *Front. Chem.* 7: 915.
- Dokshin, G.A., Davis, G.M., Sawle, A.D., Eldridge, M.D., Nicholls, P.K., Gourley, T.E., Romer, K.A., Molesworth, L.W., Tatnell, H.R., Ozturk, A.R., de Rooij, D.G., Hannon, G.J., Page, D.C., Mello, C.C., Carmell, M.A., 2020. GCNA Interacts with Spartan and Topoisomerase II to Regulate Genome Stability. *Developmental Cell* 52, 53-68.e6.
- Doma, M.K., Parker, R., 2007. RNA Quality Control in Eukaryotes. *Cell* 131, 660–668.
- Doma, M.K., Parker, R., 2006. Endonucleolytic cleavage of eukaryotic mRNAs with stalls in translation elongation. *Nature* 440, 561–564.
- Dong, J., Qiu, H., Garcia-Barrio, M., Anderson, J., Hinnebusch, A.G., 2000. Uncharged tRNA activates GCN2 by displacing the protein kinase moiety from a bipartite tRNA-binding domain. *Mol Cell* 6, 269–279.
- D’Orazio, K.N., Green, R., 2021. Ribosome states signal RNA quality control. *Molecular Cell* 81, 1372–1383.
- D’Orazio, K.N., Wu, C.C.-C., Sinha, N., Loll-Krippelber, R., Brown, G.W., Green, R., 2019. The endonuclease Cue2 cleaves mRNAs at stalled ribosomes during No Go Decay. *Elife* 8, e49117.
- Dorner, S., Brunelle, J.L., Sharma, D., Green, R., 2006. The hybrid state of tRNA binding is an authentic translation elongation intermediate. *Nat Struct Mol Biol* 13, 234–241.
- Drabløs, F., Feyzi, E., Aas, P.A., Vaagbø, C.B., Kavli, B., Bratlie, M.S., Peña-Díaz, J., Otterlei, M., Slupphaug, G., Krokan, H.E., 2004. Alkylation damage in DNA and RNA—repair mechanisms and medical significance. *DNA Repair* 3, 1389–1407.
- Draptchinskaja, N., Gustavsson, P., Andersson, B., Pettersson, M., Willig, T.N., Dianzani, I., Ball, S., Tchernia, G., Klar, J., Matsson, H., Tentler, D., Mohandas, N.,

Reference

- Carlsson, B., Dahl, N., 1999. The gene encoding ribosomal protein S19 is mutated in Diamond-Blackfan anaemia. *Nat Genet* 21, 169–175.
- Duch, A., de Nadal, E., Posas, F., 2012. The p38 and Hog1 SAPKs control cell cycle progression in response to environmental stresses. *FEBS Lett* 586, 2925–2931.
- Duxin, J.P., Dewar, J.M., Yardimci, H., Walter, J.C., 2014. Repair of a DNA-Protein Crosslink by Replication-Coupled Proteolysis. *Cell* 159, 346–357.
- Eastman, A., 1987. The formation, isolation and characterization of DNA adducts produced by anticancer platinum complexes. *Pharmacology & Therapeutics* 34, 155–166.
- Eberle, A.B., Lykke-Andersen, S., Mühlemann, O., Jensen, T.H., 2009. SMG6 promotes endonucleolytic cleavage of nonsense mRNA in human cells. *Nat Struct Mol Biol* 16, 49–55.
- Edenberg, H.J., Foroud, T., 2013. Genetics and alcoholism. *Nat Rev Gastroenterol Hepatol* 10, 487–494.
- El-Khamisy, S.F., Saifi, G.M., Weinfeld, M., Johansson, F., Helleday, T., Lupski, J.R., Caldecott, K.W., 2005. Defective DNA single-strand break repair in spinocerebellar ataxia with axonal neuropathy-1. *Nature* 434, 108–113.
- Ellison, K.S., Dogliotti, E., Connors, T.D., Basu, A.K., Essigmann, J.M., 1989. Site-specific mutagenesis by O6-alkylguanines located in the chromosomes of mammalian cells: influence of the mammalian O6-alkylguanine-DNA alkyltransferase. *Proc Natl Acad Sci U S A* 86, 8620–8624.
- Enoiu, M., Jiricny, J., Schärer, O.D., 2012. Repair of cisplatin-induced DNA interstrand crosslinks by a replication-independent pathway involving transcription-coupled repair and translesion synthesis. *Nucleic Acids Research* 40, 8953–8964.
- Escribano-Díaz, C., Orthwein, A., Fradet-Turcotte, A., Xing, M., Young, J.T.F., Tkáč, J., Cook, M.A., Rosebrock, A.P., Munro, M., Canny, M.D., Xu, D., Durocher, D., 2013. A cell cycle-dependent regulatory circuit composed of 53BP1-RIF1 and BRCA1-CtIP controls DNA repair pathway choice. *Mol Cell* 49, 872–883.
- Eshraghi, M., Karunadharma, P.P., Blin, J., Shahani, N., Ricci, E.P., Michel, A., Urban, N.T., Galli, N., Sharma, M., Ramírez-Jarquín, U.N., Florescu, K., Hernandez, J., Subramaniam, S., 2021. Mutant Huntingtin stalls ribosomes and represses protein synthesis in a cellular model of Huntington disease. *Nat Commun* 12, 1461.
- Fanconi, G., 1967. Familial constitutional panmyelocytopenia, Fanconi's anemia (F.A.). I. Clinical aspects. *Semin Hematol* 4, 233–240.

Reference

- Fang, Y., Fu, D., Shen, X.-Z., 2010. The potential role of ubiquitin c-terminal hydrolases in oncogenesis. *Biochim Biophys Acta* 1806, 1–6.
- Farley-Barnes, K.I., Ogawa, L.M., Baserga, S.J., 2019. Ribosomopathies: Old Concepts, New Controversies. *Trends in Genetics* 35, 754–767.
- Fessler, E., Eckl, E.-M., Schmitt, S., Mancilla, I.A., Meyer-Bender, M.F., Hanf, M., Philippou-Massier, J., Krebs, S., Zischka, H., Jae, L.T., 2020. A pathway coordinated by DELE1 relays mitochondrial stress to the cytosol. *Nature* 579, 433–437.
- Fielden, J., Wiseman, K., Torrecilla, I., Li, S., Hume, S., Chiang, S.-C., Ruggiano, A., Narayan Singh, A., Freire, R., Hassanieh, S., Domingo, E., Vendrell, I., Fischer, R., Kessler, B.M., Maughan, T.S., El-Khamisy, S.F., Ramadan, K., 2020. TEX264 coordinates p97- and SPRTN-mediated resolution of topoisomerase 1-DNA adducts. *Nat Commun* 11, 1274.
- Fine, D.A., Rozenblatt-Rosen, O., Padi, M., Korkhin, A., James, R.L., Adelmant, G., Yoon, R., Guo, L., Berrios, C., Zhang, Y., Calderwood, M.A., Velmurgan, S., Cheng, J., Marto, J.A., Hill, D.E., Cusick, M.E., Vidal, M., Florens, L., Washburn, M.P., Litovchick, L., DeCaprio, J.A., 2012. Identification of FAM111A as an SV40 Host Range Restriction and Adenovirus Helper Factor. *PLoS Pathog* 8, e1002949.
- Finley, D., 2009. Recognition and processing of ubiquitin-protein conjugates by the proteasome. *Annu Rev Biochem* 78, 477–513.
- Fischer, E.S., Scrima, A., Böhm, K., Matsumoto, S., Lingaraju, G.M., Faty, M., Yasuda, T., Cavadini, S., Wakasugi, M., Hanaoka, F., Iwai, S., Gut, H., Sugawara, K., Thomä, N.H., 2011. The Molecular Basis of CRL4DDB2/CSA Ubiquitin Ligase Architecture, Targeting, and Activation. *Cell* 147, 1024–1039.
- Fitch, M.E., Nakajima, S., Yasui, A., Ford, J.M., 2003. In Vivo Recruitment of XPC to UV-induced Cyclobutane Pyrimidine Dimers by the DDB2 Gene Product. *Journal of Biological Chemistry* 278, 46906–46910.
- Fradet-Turcotte, A., Canny, M.D., Escribano-Díaz, C., Orthwein, A., Leung, C.C.Y., Huang, H., Landry, M.-C., Kitevski-LeBlanc, J., Noordermeer, S.M., Sicheri, F., Durocher, D., 2013. 53BP1 is a reader of the DNA-damage-induced H2A Lys 15 ubiquitin mark. *Nature* 499, 50–54.
- Frank, J., 2003. Toward an understanding of the structural basis of translation. *Genome Biology* 4, 237.
- Frankenberg-Schwager, M., 1990. Induction, repair and biological relevance of radiation-induced DNA lesions in eukaryotic cells. *Radiat Environ Biophys* 29, 273–292.

Reference

- Franz, A., Ackermann, L., Hoppe, T., 2016. Ring of Change: CDC48/p97 Drives Protein Dynamics at Chromatin. *Frontiers in Genetics* 7:73.
- Frischmeyer, P.A., van Hoof, A., O'Donnell, K., Guerrero, A.L., Parker, R., Dietz, H.C., 2002. An mRNA Surveillance Mechanism That Eliminates Transcripts Lacking Termination Codons. *Science* 295, 2258–2261.
- Fu, D., Calvo, J.A., Samson, L.D., 2012. Balancing repair and tolerance of DNA damage caused by alkylating agents. *Nat Rev Cancer* 12, 104–120.
- Fu, Y.V., Yardimci, H., Long, D.T., Guainazzi, A., Bermudez, V.P., Hurwitz, J., van Oijen, A., Schärer, O.D., Walter, J.C., 2011. Selective Bypass of a Lagging Strand Roadblock by the Eukaryotic Replicative DNA Helicase. *Cell* 146, 931–941.
- Fugger, K., Hewitt, G., West, S.C., Boulton, S.J., 2021. Tackling PARP inhibitor resistance. *Trends in Cancer* 7, 1102–1118.
- Fulda, S., Gorman, A.M., Hori, O., Samali, A., 2010. Cellular Stress Responses: Cell Survival and Cell Death. *International Journal of Cell Biology* 2010, e214074.
- Gallina, I., Hendriks, I.A., Hoffmann, S., Larsen, N.B., Johansen, J., Colding-Christensen, C.S., Schubert, L., Sellés-Baiget, S., Fábíán, Z., Kühbacher, U., Gao, A.O., Räsche, M., Rasmussen, S., Nielsen, M.L., Mailand, N., Duxin, J.P., 2021. The ubiquitin ligase RFWF3 is required for translesion DNA synthesis. *Molecular Cell* 81, 442-458.e9.
- Galluzzi, L., Yamazaki, T., Kroemer, G., 2018. Linking cellular stress responses to systemic homeostasis. *Nat Rev Mol Cell Biol* 19, 731–745.
- Ganai, R.A., Johansson, E., 2016. DNA Replication—A Matter of Fidelity. *Molecular Cell* 62, 745–755.
- Ganoza, M.C., Kiel, M.C., Aoki, H., 2002. Evolutionary Conservation of Reactions in Translation. *Microbiol Mol Biol Rev* 66, 460–485.
- Gao, R., Huang, S.N., Marchand, C., Pommier, Y., 2012. Biochemical Characterization of Human Tyrosyl-DNA Phosphodiesterase 2 (TDP2/TTRAP). *Journal of Biological Chemistry* 287, 30842–30852.
- Garcia-Higuera, I., Taniguchi, T., Ganesan, S., Meyn, M.S., Timmers, C., Hejna, J., Grompe, M., D'Andrea, A.D., 2001. Interaction of the Fanconi Anemia Proteins and BRCA1 in a Common Pathway. *Molecular Cell* 7, 249–262.
- Gariépy, C.E., Dickinson, C.J., 2006. CHAPTER 2 - Translation and Posttranslational Processing of Gastrointestinal Peptides, in: Johnson, L.R. (Ed.),

Reference

Physiology of the Gastrointestinal Tract (Fourth Edition). Academic Press, Burlington, pp. 31–62.

Garshott, D.M., Sundaramoorthy, E., Leonard, M., Bennett, E.J., 2020. Distinct regulatory ribosomal ubiquitylation events are reversible and hierarchically organized. *eLife* 9, e54023.

Gates, K.S., 2009. An Overview of Chemical Processes That Damage Cellular DNA: Spontaneous Hydrolysis, Alkylation, and Reactions with Radicals. *Chem. Res. Toxicol.* 22, 1747–1760.

Gavrilov, K., Saltzman, W.M., 2012. Therapeutic siRNA: principles, challenges, and strategies. *Yale J Biol Med* 85, 187–200.

Geacintov, N.E., 1986. Is intercalation a critical factor in the covalent binding of mutagenic and tumorigenic polycyclic aromatic diol epoxides to DNA? *Carcinogenesis* 7, 759–766.

Gelot, C., Magdalou, I., Lopez, B., 2015. Replication Stress in Mammalian Cells and Its Consequences for Mitosis. *Genes* 6, 267–298.

Ghodgaonkar, M.M., Lazzaro, F., Olivera-Pimentel, M., Artola-Borán, M., Cejka, P., Reijns, M.A., Jackson, A.P., Plevani, P., Muzi-Falconi, M., Jiricny, J., 2013. Ribonucleotides misincorporated into DNA act as strand-discrimination signals in eukaryotic mismatch repair. *Mol Cell* 50, 323–332.

Ghosal, G., Leung, J.W.-C., Nair, B.C., Fong, K.-W., Chen, J., 2012. Proliferating Cell Nuclear Antigen (PCNA)-binding Protein C1orf124 Is a Regulator of Translesion Synthesis. *Journal of Biological Chemistry* 287, 34225–34233.

Ghosh, S., Saha, T., 2012. Central Role of Ubiquitination in Genome Maintenance: DNA Replication and Damage Repair. *ISRN Molecular Biology* 2012, 1–9.

Giegé, R., Frugier, M., 2013. Transfer RNA Structure and Identity, *Madame Curie Bioscience Database*. Landes Bioscience.

Glickman, M.H., Ciechanover, A., 2002. The Ubiquitin-Proteasome Proteolytic Pathway: Destruction for the Sake of Construction. *Physiological Reviews* 82, 373–428.

Gnyszka, A., Jastrzębski, Z., Flis, S., 2013. DNA Methyltransferase Inhibitors and Their Emerging Role in Epigenetic Therapy of Cancer. *ANTICANCER RESEARCH* 33: 2989-2996

Reference

- Goh, K.C., deVeer, M.J., Williams, B.R., 2000. The protein kinase PKR is required for p38 MAPK activation and the innate immune response to bacterial endotoxin. *EMBO J* 19, 4292–4297.
- Gómez-Herreros, F., Romero-Granados, R., Zeng, Z., Álvarez-Quilón, A., Quintero, C., Ju, L., Umans, L., Vermeire, L., Huylebroeck, D., Caldecott, K.W., Cortés-Ledesma, F., 2013. TDP2-Dependent Non-Homologous End-Joining Protects against Topoisomerase II-Induced DNA Breaks and Genome Instability in Cells and In Vivo. *PLoS Genet* 9, e1003226.
- Gopinath, P., Ohayon, S., Nawatha, M., Brik, A., 2016. Chemical and semisynthetic approaches to study and target deubiquitinases. *Chem. Soc. Rev.* 45, 4171–4198.
- Gopinath, S.C.B., 2009. Mapping of RNA-protein interactions. *Analytica Chimica Acta* 636, 117–128.
- Gordiyenko, Y., Llácer, J.L., Ramakrishnan, V., 2019. Structural basis for the inhibition of translation through eIF2 α phosphorylation. *Nat Commun* 10, 2640.
- Gouridis, G., Hetzert, B., Kiosze-Becker, K., de Boer, M., Heinemann, H., Nürenberg-Goloub, E., Cordes, T., Tampé, R., 2019. ABCE1 Controls Ribosome Recycling by an Asymmetric Dynamic Conformational Equilibrium. *Cell Reports* 28, 723-734.e6.
- Grady, W.M., Ulrich, C.M., 2007. DNA alkylation and DNA methylation: cooperating mechanisms driving the formation of colorectal adenomas and adenocarcinomas? *Gut* 56, 318–320.
- Granneman, S., 2004. Ribosome biogenesis: of knobs and RNA processing. *Experimental Cell Research* 296, 43–50.
- Groehler IV, A., Degner, A., Tretyakova, N.Y., 2017. Mass Spectrometry-Based Tools to Characterize DNA-Protein Cross-Linking by Bis-Electrophiles. *Basic & Clinical Pharmacology & Toxicology* 121, 63–77.
- Groettrup, M., Pelzer, C., Schmidtke, G., Hofmann, K., 2008. Activating the ubiquitin family: UBA6 challenges the field. *Trends in Biochemical Sciences* 33, 230–237.
- Groisman, R., Kuraoka, I., Chevallier, O., Gaye, N., Magnaldo, T., Tanaka, K., Kisselev, A.F., Harel-Bellan, A., Nakatani, Y., 2006. CSA-dependent degradation of CSB by the ubiquitin-proteasome pathway establishes a link between complementation factors of the Cockayne syndrome. *Genes Dev* 20, 1429–1434.
- Groisman, R., Polanowska, J., Kuraoka, I., Sawada, J., Saijo, M., Drapkin, R., Kisselev, A.F., Tanaka, K., Nakatani, Y., 2003. The Ubiquitin Ligase Activity in the

Reference

DDB2 and CSA Complexes Is Differentially Regulated by the COP9 Signalosome in Response to DNA Damage. *Cell* 113, 357–367.

Guo, H.J., Tadi, P., 2022. Biochemistry, Ubiquitination, StatPearls PMID: 32310512. StatPearls Publishing.

Guo, X., Aviles, G., Liu, Y., Tian, R., Unger, B.A., Lin, Y.-H.T., Wiita, A.P., Xu, K., Correia, M.A., Kampmann, M., 2020. Mitochondrial stress is relayed to the cytosol by an OMA1-DELE1-HRI pathway. *Nature* 579, 427–432.

Gutierrez, R., O'Connor, T.R., 2021. DNA direct reversal repair and alkylating agent drug resistance. *Cancer Drug Resist* 4, 414–423.

Guydosh, N.R., Green, R., 2017. Translation of poly(A) tails leads to precise mRNA cleavage. *RNA* 23, 749–761.

Hafner, M., Landthaler, M., Burger, L., Khorshid, M., Hausser, J., Berninger, P., Rothballer, A., Ascano, M., Jungkamp, A.-C., Munschauer, M., Ulrich, A., Wardle, G.S., Dewell, S., Zavolan, M., Tuschl, T., 2010. Transcriptome-wide Identification of RNA-Binding Protein and MicroRNA Target Sites by PAR-CLIP. *Cell* 141, 129–141.

Haglund, K., Dikic, I., 2005. Ubiquitylation and cell signaling. *EMBO J* 24, 3353–3359.

Haince, J.-F., McDonald, D., Rodrigue, A., Déry, U., Masson, J.-Y., Hendzel, M.J., Poirier, G.G., 2008. PARP1-dependent Kinetics of Recruitment of MRE11 and NBS1 Proteins to Multiple DNA Damage Sites *. *Journal of Biological Chemistry* 283, 1197–1208.

Halder, S., Torrecilla, I., Burkhalter, M.D., Popović, M., Fielden, J., Vaz, B., Oehler, J., Pilger, D., Lessel, D., Wiseman, K., Singh, A.N., Vendrell, I., Fischer, R., Philipp, M., Ramadan, K., 2019. SPRTN protease and checkpoint kinase 1 cross-activation loop safeguards DNA replication. *Nat Commun* 10, 3142.

Han, J., Back, S.H., Hur, J., Lin, Y.-H., Gildersleeve, R., Shan, J., Yuan, C.L., Krokowski, D., Wang, S., Hatzoglou, M., Kilberg, M.S., Sartor, M.A., Kaufman, R.J., 2013. ER-stress-induced transcriptional regulation increases protein synthesis leading to cell death. *Nat Cell Biol* 15, 481–490.

Hanawalt, P.C., 2002. Subpathways of nucleotide excision repair and their regulation. *Oncogene* 21, 8949–8956.

Hanpude, P., Bhattacharya, S., Dey, A.K., Maiti, T.K., 2015. Deubiquitinating enzymes in cellular signaling and disease regulation. *IUBMB Life* 67, 544–555.

Reference

- Hanssen-Bauer, A., Solvang-Garten, K., Sundheim, O., Peña-Diaz, J., Andersen, S., Slupphaug, G., Krokan, H.E., Wilson III, D.M., Akbari, M., Otterlei, M., 2011. XRCC1 coordinates disparate responses and multiprotein repair complexes depending on the nature and context of the DNA damage. *Environmental and Molecular Mutagenesis* 52, 623–635.
- Harding, H.P., Novoa, I., Zhang, Y., Zeng, H., Wek, R., Schapira, M., Ron, D., 2000. Regulated translation initiation controls stress-induced gene expression in mammalian cells. *Mol Cell* 6, 1099–1108.
- Harding, H.P., Ordonez, A., Allen, F., Parts, L., Inglis, A.J., Williams, R.L., Ron, D., 2019. The ribosomal P-stalk couples amino acid starvation to GCN2 activation in mammalian cells. *eLife* 8, e50149.
- Harding, H.P., Zhang, Y., Zeng, H., Novoa, I., Lu, P.D., Calton, M., Sadri, N., Yun, C., Popko, B., Paules, R., Stojdl, D.F., Bell, J.C., Hettmann, T., Leiden, J.M., Ron, D., 2003. An integrated stress response regulates amino acid metabolism and resistance to oxidative stress. *Mol Cell* 11, 619–633.
- Harreman, M., Taschner, M., Sigurdsson, S., Anindya, R., Reid, J., Somesh, B., Kong, S.E., Banks, C.A.S., Conaway, R.C., Conaway, J.W., Svejstrup, J.Q., 2009. Distinct ubiquitin ligases act sequentially for RNA polymerase II polyubiquitylation. *Proceedings of the National Academy of Sciences* 106, 20705–20710.
- Harrigan, J.A., Jacq, X., Martin, N.M., Jackson, S.P., 2018. Deubiquitylating enzymes and drug discovery: emerging opportunities. *Nat Rev Drug Discov* 17, 57–78.
- Hashimoto, S., Sugiyama, T., Yamazaki, R., Nobuta, R., Inada, T., 2020. Identification of a novel trigger complex that facilitates ribosome-associated quality control in mammalian cells. *Sci Rep* 10, 3422.
- He, J., Zhu, Q., Wani, G., Sharma, N., Han, C., Qian, J., Pentz, K., Wang, Q., Wani, A.A., 2014. Ubiquitin-specific Protease 7 Regulates Nucleotide Excision Repair through Deubiquitinating XPC Protein and Preventing XPC Protein from Undergoing Ultraviolet Light-induced and VCP/p97 Protein-regulated Proteolysis *. *Journal of Biological Chemistry* 289, 27278–27289.
- He, J., Zhu, Q., Wani, G., Sharma, N., Wani, A.A., 2016. Valosin-containing Protein (VCP)/p97 Segregase Mediates Proteolytic Processing of Cockayne Syndrome Group B (CSB) in Damaged Chromatin. *Journal of Biological Chemistry* 291, 7396–7408.

Reference

- He, M., Zhou, Z., Shah, A.A., Zou, H., Tao, J., Chen, Q., Wan, Y., 2016. The emerging role of deubiquitinating enzymes in genomic integrity, diseases, and therapeutics. *Cell Biosci* 6, 62.
- Hedglin, M., Aitha, M., Pedley, A., Benkovic, S.J., 2019. Replication protein A dynamically regulates monoubiquitination of proliferating cell nuclear antigen. *J Biol Chem* 294, 5157–5168.
- Hegde, M.L., Hazra, T.K., Mitra, S., 2008. Early steps in the DNA base excision/single-strand interruption repair pathway in mammalian cells. *Cell Res* 18, 27–47.
- Henle, E.S., Linn, S., 1997. Formation, Prevention, and Repair of DNA Damage by Iron/Hydrogen Peroxide. *Journal of Biological Chemistry* 272, 19095–19098.
- Henry, R.W., Mittal, V., Ma, B., Kobayashi, R., Hernandez, N., 1998. SNAP19 mediates the assembly of a functional core promoter complex (SNAPc) shared by RNA polymerases II and III. *Genes Dev* 12, 2664–2672.
- Hentze, M.W., Castello, A., Schwarzl, T., Preiss, T., 2018. A brave new world of RNA-binding proteins. *Nat Rev Mol Cell Biol* 19, 327–341.
- Hershey, J.W.B., Sonenberg, N., Mathews, M.B., 2012. Principles of Translational Control: An Overview. *Cold Spring Harb Perspect Biol* 4, a011528.
- Hershko, A., Ciechanover, A.. THE UBIQUITIN SYSTEM 57 *Annu. Rev. Biochem.* 1998. 67:425–79.
- Hicke, L., 2001. Protein regulation by monoubiquitin. *Nat Rev Mol Cell Biol* 2, 195–201.
- Hinnebusch, A.G., Lorsch, J.R., 2012. The Mechanism of Eukaryotic Translation Initiation: New Insights and Challenges. *Cold Spring Harb Perspect Biol* 4, a011544.
- Hirano, R., Interthal, H., Huang, C., Nakamura, T., Deguchi, K., Choi, K., Bhattacharjee, M.B., Arimura, K., Umehara, F., Izumo, S., Northrop, J.L., Salih, M.A.M., Inoue, K., Armstrong, D.L., Champoux, J.J., Takashima, H., Boerkoel, C.F., 2007. Spinocerebellar ataxia with axonal neuropathy: consequence of a Tdp1 recessive neomorphic mutation? *EMBO J* 26, 4732–4743.
- Hoa, N.N., Shimizu, T., Zhou, Z.W., Wang, Z.-Q., Deshpande, R.A., Paull, T.T., Akter, S., Tsuda, M., Furuta, R., Tsutsui, K., Takeda, S., Sasanuma, H., 2016. Mre11 Is Essential for the Removal of Lethal Topoisomerase 2 Covalent Cleavage Complexes. *Molecular Cell* 64, 580–592.

Reference

- Hoege, C., Pfander, B., Moldovan, G.-L., Pyrowolakis, G., Jentsch, S., 2002. RAD6-dependent DNA repair is linked to modification of PCNA by ubiquitin and SUMO. *Nature* 419, 135–141.
- Hoeller, D., Crosetto, N., Blagoev, B., Raiborg, C., Tikkanen, R., Wagner, S., Kowanez, K., Breitling, R., Mann, M., Stenmark, H., Dikic, I., 2006. Regulation of ubiquitin-binding proteins by monoubiquitination. *Nat Cell Biol* 8, 163–169.
- Hoffman, E.A., Frey, B.L., Smith, L.M., Auble, D.T., 2015. Formaldehyde Crosslinking: A Tool for the Study of Chromatin Complexes. *Journal of Biological Chemistry* 290, 26404–26411.
- Hoffmann, S., Pentakota, S., Mund, A., Haahr, P., Coscia, F., Gallo, M., Mann, M., Taylor, N.M., Mailand, N., 2020. FAM111 protease activity undermines cellular fitness and is amplified by gain - of - function mutations in human disease. *EMBO Rep* 21:e50662.
- Holloman, W.K., 2011. Unraveling the mechanism of BRCA2 in homologous recombination. *Nat Struct Mol Biol* 18, 748–754.
- Hopfield, J.J., 1974. Kinetic Proofreading: A New Mechanism for Reducing Errors in Biosynthetic Processes Requiring High Specificity. *Proc Natl Acad Sci U S A* 71, 4135–4139.
- Hsiang, Y.H., Lihou, M.G., Liu, L.F., 1989. Arrest of replication forks by drug-stabilized topoisomerase I-DNA cleavable complexes as a mechanism of cell killing by camptothecin. *Cancer Res* 49, 5077–5082.
- Hsieh, P., Yamane, K., 2008. DNA mismatch repair: Molecular mechanism, cancer, and ageing. *Mech Ageing Dev* 129, 391–407.
- Hu, Y., Scully, R., Sobhian, B., Xie, A., Shestakova, E., Livingston, D.M., 2011. RAP80-directed tuning of BRCA1 homologous recombination function at ionizing radiation-induced nuclear foci. *Genes Dev* 25, 685–700.
- Huang, J., Zhou, Q., Gao, M., Nowsheen, S., Zhao, F., Kim, W., Zhu, Q., Kojima, Y., Yin, P., Zhang, Y., Guo, G., Tu, X., Deng, M., Luo, K., Qin, B., Machida, Y., Lou, Z., 2020. Tandem Deubiquitination and Acetylation of SPRTN Promotes DNA-Protein Crosslink Repair and Protects against Aging. *Molecular Cell* 79, 824-835.e5.
- Huang, T.T., Nijman, S.M.B., Mirchandani, K.D., Galardy, P.J., Cohn, M.A., Haas, W., Gygi, S.P., Ploegh, H.L., Bernards, R., D'Andrea, A.D., 2006. Regulation of monoubiquitinated PCNA by DUB autocleavage. *Nat Cell Biol* 8, 341–347.
- Huang, Y., Li, L., 2013. DNA crosslinking damage and cancer - a tale of friend and foe. *Transl Cancer Res* 2, 144–154.

Reference

- Huertas, P., 2010. DNA resection in eukaryotes: deciding how to fix the break. *Nat Struct Mol Biol* 17, 11–16.
- Humphreys, D.T., Westman, B.J., Martin, D.I.K., Preiss, T., 2005. MicroRNAs control translation initiation by inhibiting eukaryotic initiation factor 4E/cap and poly(A) tail function. *Proceedings of the National Academy of Sciences* 102, 16961–16966.
- Huntzinger, E., Kashima, I., Fauser, M., Saulière, J., Izaurralde, E., 2008. SMG6 is the catalytic endonuclease that cleaves mRNAs containing nonsense codons in metazoan. *RNA* 14, 2609–2617.
- Hwang, B.J., Ford, J.M., Hanawalt, P.C., Chu, G., 1999. Expression of the *p48* xeroderma pigmentosum gene is p53-dependent and is involved in global genomic repair. *Proc. Natl. Acad. Sci. U.S.A.* 96, 424–428.
- Ide, H., Kotera, M., 2004. Human DNA Glycosylases Involved in the Repair of Oxidatively Damaged DNA. *Biological and Pharmaceutical Bulletin* 27, 480–485.
- Ide, H., Nakano, T., Shoukamy, M.I., Salem, A.M.H., 2015. Formation, Repair, and Biological Effects of DNA–Protein Cross-Link Damage. *Advances in DNA Repair*. ISBN:978-953-51-2209-8
- Ikeuchi, K., Izawa, T., Inada, T., 2019a. Recent Progress on the Molecular Mechanism of Quality Controls Induced by Ribosome Stalling. *Frontiers in Genetics* 9:743.
- Ikeuchi, K., Tesina, P., Matsuo, Y., Sugiyama, T., Cheng, J., Saeki, Y., Tanaka, K., Becker, T., Beckmann, R., Inada, T., 2019b. Collided ribosomes form a unique structural interface to induce Hel2 - driven quality control pathways. *The EMBO Journal* 38: e100276.
- Inada, T., 2017. The Ribosome as a Platform for mRNA and Nascent Polypeptide Quality Control. *Trends in Biochemical Sciences* 42, 5–15.
- Inada, T., 2013. Quality control systems for aberrant mRNAs induced by aberrant translation elongation and termination. *Biochim Biophys Acta* 1829, 634–642.
- Inada, T., Aiba, H., 2005. Translation of aberrant mRNAs lacking a termination codon or with a shortened 3'-UTR is repressed after initiation in yeast. *EMBO J* 24, 1584–1595.
- Inglis, A.J., Masson, G.R., Shao, S., Perisic, O., McLaughlin, S.H., Hegde, R.S., Williams, R.L., 2019. Activation of GCN2 by the ribosomal P-stalk. *Proc. Natl. Acad. Sci. U.S.A.* 116, 4946–4954.

Reference

- Interthal, H., Champoux, J.J., 2011. Effects of DNA and protein size on substrate cleavage by human tyrosyl-DNA phosphodiesterase 1. *Biochemical Journal* 436, 559–566.
- Interthal, H., Chen, H.J., Kehl-Fie, T.E., Zotzmann, J., Leppard, J.B., Champoux, J.J., 2005. SCAN1 mutant Tdp1 accumulates the enzyme–DNA intermediate and causes camptothecin hypersensitivity. *EMBO J* 24, 2224–2233.
- Interthal, H., Pouliot, J.J., Champoux, J.J., 2001. The tyrosyl-DNA phosphodiesterase Tdp1 is a member of the phospholipase D superfamily. *Proc Natl Acad Sci U S A* 98, 12009–12014.
- Iordanov, M.S., Pribnow, D., Magun, J.L., Dinh, T.H., Pearson, J.A., Chen, S.L., Magun, B.E., 1997. Ribotoxic stress response: activation of the stress-activated protein kinase JNK1 by inhibitors of the peptidyl transferase reaction and by sequence-specific RNA damage to the alpha-sarcin/ricin loop in the 28S rRNA. *Molecular and Cellular Biology* 17, 3373–3381.
- Iordanov, M.S., Pribnow, D., Magun, J.L., Dinh, T.-H., Pearson, J.A., Magun, B.E., 1998. Ultraviolet Radiation Triggers the Ribotoxic Stress Response in Mammalian Cells *. *Journal of Biological Chemistry* 273, 15794–15803.
- Ishiai, M., Kitao, H., Smogorzewska, A., Tomida, J., Kinomura, A., Uchida, E., Saberi, A., Kinoshita, E., Kinoshita-Kikuta, E., Koike, T., Tashiro, S., Elledge, S.J., Takata, M., 2008. FANCI phosphorylation functions as a molecular switch to turn on the Fanconi anemia pathway. *Nat Struct Mol Biol* 15, 1138–1146.
- Ishimura, R., Nagy, G., Dotu, I., Zhou, H., Yang, X.-L., Schimmel, P., Senju, S., Nishimura, Y., Chuang, J.H., Ackerman, S.L., 2014. Ribosome stalling induced by mutation of a CNS-specific tRNA causes neurodegeneration. *Science* 345, 455–459.
- Isono, M., Niimi, A., Oike, T., Hagiwara, Y., Sato, H., Sekine, R., Yoshida, Y., Isobe, S.-Y., Obuse, C., Nishi, R., Petricci, E., Nakada, S., Nakano, T., Shibata, A., 2017. BRCA1 Directs the Repair Pathway to Homologous Recombination by Promoting 53BP1 Dephosphorylation. *Cell Rep* 18, 520–532.
- Iyer, R.R., Pluciennik, A., 2021. DNA Mismatch Repair and its Role in Huntington's Disease. *Journal of Huntington's Disease* 10, 75–94.
- Jackson, R.J., Hellen, C.U.T., Pestova, T.V., 2010. The mechanism of eukaryotic translation initiation and principles of its regulation. *Nat Rev Mol Cell Biol* 11, 113–127.
- Jackson, S.P., Bartek, J., 2009. The DNA-damage response in human biology and disease. *Nature* 461, 1071–1078.

Reference

- Jandhyala, D.M., Ahluwalia, A., Obrig, T., Thorpe, C.M., 2008. ZAK: a MAP3Kinase that transduces Shiga toxin- and ricin-induced proinflammatory cytokine expression. *Cell Microbiol* 10, 1468–1477.
- Jennings, M.D., Zhou, Y., Mohammad-Qureshi, S.S., Bennett, D., Pavitt, G.D., 2013. eIF2B promotes eIF5 dissociation from eIF2•GDP to facilitate guanine nucleotide exchange for translation initiation. *Genes Dev* 27, 2696–2707.
- Jiricny, J., 2013. Postreplicative Mismatch Repair. *Cold Spring Harb Perspect Biol* 5, a012633.
- Juhasz, S., Balogh, D., Hajdu, I., Burkovics, P., Villamil, M.A., Zhuang, Z., Haracska, L., 2012. Characterization of human Spartan/C1orf124, an ubiquitin-PCNA interacting regulator of DNA damage tolerance. *Nucleic Acids Research* 40, 10795–10808.
- Jung, M., Smogorzewska, A., 2021. Endogenous formaldehyde destroys blood stem cells. *Blood* 137, 1988–1990.
- Juzskiewicz, S., Chandrasekaran, V., Lin, Z., Kraatz, S., Ramakrishnan, V., Hegde, R.S., 2018. ZNF598 Is a Quality Control Sensor of Collided Ribosomes. *Molecular Cell* 72, 469-481.e7.
- Juzskiewicz, S., Slodkowitz, G., Lin, Z., Freire-Pritchett, P., Peak-Chew, S.-Y., Hegde, R.S., 2020a. Ribosome collisions trigger cis-acting feedback inhibition of translation initiation. *eLife* 9, e60038.
- Juzskiewicz, S., Speldewinde, S.H., Wan, L., Svejstrup, J.Q., Hegde, R.S., 2020b. The ASC-1 Complex Disassembles Collided Ribosomes. *Molecular Cell* 79, 603-614.e8.
- Kaddar, T., Carreau, M., 2012. Fanconi Anemia Proteins and Their Interacting Partners: A Molecular Puzzle. *Anemia* 2012, 1–11.
- Kadyrov, F.A., Dzantiev, L., Constantin, N., Modrich, P., 2006. Endonucleolytic Function of MutL α in Human Mismatch Repair. *Cell* 126, 297–308.
- Kadyrov, F.A., Holmes, S.F., Arana, M.E., Lukianova, O.A., O'Donnell, M., Kunkel, T.A., Modrich, P., 2007. *Saccharomyces cerevisiae* MutL α Is a Mismatch Repair Endonuclease. *Journal of Biological Chemistry* 282, 37181–37190.
- Kais, Z., Rondinelli, B., Holmes, A., O'Leary, C., Kozono, D., D'Andrea, A.D., Ceccaldi, R., 2016. FANCD2 Maintains Fork Stability in BRCA1/2-Deficient Tumors and Promotes Alternative End-Joining DNA Repair. *Cell Reports* 15, 2488–2499.

Reference

- Kalb, R., Mallery, D.L., Larkin, C., Huang, J.T.J., Hiom, K., 2014. BRCA1 is a histone-H2A-specific ubiquitin ligase. *Cell Rep* 8, 999–1005.
- Kamiya, H., Miura, K., Ishikawa, H., Inoue, H., Nishimura, S., Ohtsuka, E., 1992. c-Ha-ras Containing 8-Hydroxyguanine at Codon 12 Induces Point Mutations at the Modified and Adjacent Positions. *Cancer Res* 52, 3483–3485.
- Kannouche, P.L., Wing, J., Lehmann, A.R., n.d. Interaction of Human DNA Polymerase η with Monoubiquitinated PCNA: A Possible Mechanism for the Polymerase Switch in Response to DNA Damage. *Molecular Cell* 14, 491–500.
- Kapp, L.D., Lorsch, J.R., 2004. The Molecular Mechanics of Eukaryotic Translation. *Annual Review of Biochemistry* 73, 657–704.
- Karamyshev, A.L., Karamysheva, Z.N., 2018. Lost in Translation: Ribosome-Associated mRNA and Protein Quality Controls. *Frontiers in Genetics* 9:431.
- Käshammer, L., Saathoff, J.-H., Lammens, K., Gut, F., Bartho, J., Alt, A., Kessler, B., Hopfner, K.-P., 2019. Mechanism of DNA End Sensing and Processing by the Mre11-Rad50 Complex. *Molecular Cell* 76, 382-394.e6.
- Kashima, I., Yamashita, A., Izumi, N., Kataoka, N., Morishita, R., Hoshino, S., Ohno, M., Dreyfuss, G., Ohno, S., 2006. Binding of a novel SMG-1-Upf1-eRF1-eRF3 complex (SURF) to the exon junction complex triggers Upf1 phosphorylation and nonsense-mediated mRNA decay. *Genes Dev* 20, 355–367.
- Kashiwagi, K., Yokoyama, T., Nishimoto, M., Takahashi, M., Sakamoto, A., Yonemochi, M., Shirouzu, M., Ito, T., 2019. Structural basis for eIF2B inhibition in integrated stress response. *Science* 364, 495–499.
- Katyal, S., El-Khamisy, S.F., Russell, H.R., Li, Y., Ju, L., Caldecott, K.W., McKinnon, P.J., 2007. TDP1 facilitates chromosomal single-strand break repair in neurons and is neuroprotective in vivo. *EMBO J* 26, 4720–4731.
- Kee, Y., D'Andrea, A.D., 2012. Molecular pathogenesis and clinical management of Fanconi anemia. *J. Clin. Invest.* 122, 3799–3806.
- Keeney, S., Giroux, C.N., Kleckner, N., 1997. Meiosis-Specific DNA Double-Strand Breaks Are Catalyzed by Spo11, a Member of a Widely Conserved Protein Family. *Cell* 88, 375–384.
- Kenner, L.R., Anand, A.A., Nguyen, H.C., Myasnikov, A.G., Klose, C.J., McGeever, L.A., Tsai, J.C., Miller-Vedam, L.E., Walter, P., Frost, A., 2019. eIF2B-catalyzed nucleotide exchange and phosphoregulation by the integrated stress response. *Science* 364, 491–495.

Reference

- Kervestin, S., Jacobson, A., 2012. NMD: a multifaceted response to premature translational termination. *Nat Rev Mol Cell Biol* 13, 700–712.
- Khaminets, A., Behl, C., Dikic, I., 2016. Ubiquitin-Dependent And Independent Signals In Selective Autophagy. *Trends Cell Biol* 26, 6–16.
- Khanna, K.K., Jackson, S.P., 2001. DNA double-strand breaks: signaling, repair and the cancer connection. *Nat Genet* 27, 247–254.
- Khatter, H., Myasnikov, A.G., Natchiar, S.K., Klaholz, B.P., 2015. Structure of the human 80S ribosome. *Nature* 520, 640–645.
- Khim, H.F, Chowdhury, M.K., Boerkoel C.F.. 2012. Spinocerebellar Ataxia with Axonal Neuropathy (SCAN1): A Disorder of Nuclear and Mitochondrial DNA Repair, , Spinocerebellar Ataxia. ISBN: 978-953-51-0542-8
- Kiiianitsa, K., Maizels, N., 2013. A rapid and sensitive assay for DNA–protein covalent complexes in living cells. *Nucleic Acids Research* 41, e104–e104.
- Kim, B., Kim, V.N., 2019. fCLIP-seq for transcriptomic footprinting of dsRNA-binding proteins: Lessons from DROSHA. *Methods* 152, 3–11.
- Kim, H., D’Andrea, A.D., 2012. Regulation of DNA cross-link repair by the Fanconi anemia/BRCA pathway. *Genes Dev.* 26, 1393–1408.
- Kim, M., Kim, J.M., 2016. The role of USP1 autocleavage in DNA interstrand crosslink repair. *FEBS Lett* 590, 340–348.
- Kim, M.S., Machida, Y., Vashisht, A.A., Wohlschlegel, J.A., Pang, Y.-P., Machida, Y.J., 2013. Regulation of error-prone translesion synthesis by Spartan/C1orf124. *Nucleic Acids Research* 41, 1661–1668.
- Kim, S.J., Yoon, J.S., Shishido, H., Yang, Z., Rooney, L.A., Barral, J.M., Skach, W.R., 2015. Translational tuning optimizes nascent protein folding in cells. *Science* 348, 444–448.
- Kirillov, S. v., Makarov, E. m., Semenov, Yu.P., 1983. Quantitative study of interaction of deacylated tRNA with Escherichia coli ribosomes. *FEBS Letters* 157, 91–94.
- Klauer, A.A., van Hoof, A., 2012. Degradation of mRNAs that lack a stop codon: A decade of nonstop progress. *Wiley Interdiscip Rev RNA* 3, 649–660.
- Kleiman, F.E., Wu-Baer, F., Fonseca, D., Kaneko, S., Baer, R., Manley, J.L., 2005. BRCA1/BARD1 inhibition of mRNA 3’ processing involves targeted degradation of RNA polymerase II. *Genes Dev.* 19, 1227–1237.

Reference

- Klein Douwel, D., Boonen, R.A.C.M., Long, D.T., Szypowska, A.A., Räschle, M., Walter, J.C., Knipscheer, P., 2014. XPF-ERCC1 Acts in Unhooking DNA Interstrand Crosslinks in Cooperation with FANCD2 and FANCP/SLX4. *Molecular Cell* 54, 460–471.
- Klinge, S., Woolford, J.L., 2019. Ribosome assembly coming into focus. *Nat Rev Mol Cell Biol* 20, 116–131.
- Klionsky, D.J., 2007. Autophagy: from phenomenology to molecular understanding in less than a decade. *Nat Rev Mol Cell Biol* 8, 931–937.
- Kloor, M., Staffa, L., Ahadova, A., von Knebel Doeberitz, M., 2014. Clinical significance of microsatellite instability in colorectal cancer. *Langenbecks Arch Surg* 399, 23–31.
- Knipscheer, P., Räschle, M., Smogorzewska, A., Enoiu, M., Ho, T.V., Schärer, O.D., Elledge, S.J., Walter, J.C., 2009. The Fanconi Anemia Pathway Promotes Replication-Dependent DNA Interstrand Cross-Link Repair. *Science* 326, 1698–1701.
- Kobaisi, F., Fayyad, N., Rezvani, H.R., Fayyad-Kazan, M., Sulpice, E., Badran, B., Fayyad-Kazan, H., Gidrol, X., Rachidi, W., 2019. Signaling Pathways, Chemical and Biological Modulators of Nucleotide Excision Repair: The Faithful Shield against UV Genotoxicity. *Oxidative Medicine and Cellular Longevity* 2019, e4654206.
- Koizumi, S., Irie, T., Hirayama, S., Sakurai, Y., Yashiroda, H., Naguro, I., Ichijo, H., Hamazaki, J., Murata, S., 2016. The aspartyl protease DDI2 activates Nrf1 to compensate for proteasome dysfunction. *eLife* 5, e18357.
- Kojima, Y., Machida, Y., Palani, S., Caulfield, T.R., Radisky, E.S., Kaufmann, S.H., Machida, Y.J., 2020. FAM111A protects replication forks from protein obstacles via its trypsin-like domain. *Nat Commun* 11, 1318.
- Kokic, G., Chernev, A., Tegunov, D., Dienemann, C., Urlaub, H., Cramer, P., 2019. Structural basis of TFIIH activation for nucleotide excision repair. *Nat Commun* 10, 2885.
- Kolas, N.K., Chapman, J.R., Nakada, S., Ylanko, J., Chahwan, R., Sweeney, F.D., Panier, S., Mendez, M., Wildenhain, J., Thomson, T.M., Pelletier, L., Jackson, S.P., Durocher, D., 2007. Orchestration of the DNA-damage response by the RNF8 ubiquitin ligase. *Science* 318, 1637–1640.
- Komander, D., Rape, M., 2012. The Ubiquitin Code. *Annual Review of Biochemistry* 81, 203–229.

Reference

- Kondo, N., Takahashi, A., Ono, K., Ohnishi, T., 2010. DNA Damage Induced by Alkylating Agents and Repair Pathways. *Journal of Nucleic Acids* 2010, 1–7.
- Korzhev, D.M., Hadden, M.K., 2016. Targeting the Translesion Synthesis Pathway for the Development of Anti-Cancer Chemotherapeutics. *J. Med. Chem.* 59, 9321–9336.
- Kou, Y., Zhao, H., Cui, D., Han, H., Tong, Z., 2022. Formaldehyde toxicity in age-related neurological dementia. *Ageing Research Reviews* 73, 101512.
- Koutmou, K.S., Schuller, A.P., Brunelle, J.L., Radhakrishnan, A., Djuranovic, S., Green, R., 2015. Ribosomes slide on lysine-encoding homopolymeric A stretches. *eLife* 4, e05534
- Krahn, N., Fischer, J.T., Söll, D., 2020. Naturally Occurring tRNAs With Non-canonical Structures. *Frontiers in Microbiology* 11:596914.
- Krasikova, Y., Rechkunova, N., Lavrik, O., 2021. Nucleotide Excision Repair: From Molecular Defects to Neurological Abnormalities. *International Journal of Molecular Sciences* 22, 6220.
- Krasikova, Y.S., Rechkunova, N.I., Maltseva, E.A., Petruseva, I.O., Lavrik, O.I., 2010. Localization of xeroderma pigmentosum group A protein and replication protein A on damaged DNA in nucleotide excision repair. *Nucleic Acids Research* 38, 8083–8094.
- Krastev, D.B., Li, S., Sun, Y., Wicks, A.J., Hoslett, G., Weekes, D., Badder, L.M., Knight, E.G., Marlow, R., Pardo, M.C., Yu, L., Talele, T.T., Bartek, J., Choudhary, J.S., Pommier, Y., Pettitt, S.J., Tutt, A.N.J., Ramadan, K., Lord, C.J., 2022. The ubiquitin-dependent ATPase p97 removes cytotoxic trapped PARP1 from chromatin. *Nat Cell Biol* 24, 62–73.
- Krijger, P.H.L., Lee, K.-Y., Wit, N., van den Berk, P.C.M., Wu, X., Roest, H.P., Maas, A., Ding, H., Hoeijmakers, J.H.J., Myung, K., Jacobs, H., 2011. HLTF and SHPRH are not essential for PCNA polyubiquitination, survival and somatic hypermutation: Existence of an alternative E3 ligase. *DNA Repair* 10, 438–444.
- Krishnamoorthy, T., Pavitt, G.D., Zhang, F., Dever, T.E., Hinnebusch, A.G., 2001. Tight binding of the phosphorylated alpha subunit of initiation factor 2 (eIF2alpha) to the regulatory subunits of guanine nucleotide exchange factor eIF2B is required for inhibition of translation initiation. *Mol Cell Biol* 21, 5018–5030.
- Krokan, H.E., Bjørås, M., 2013. Base Excision Repair. *Cold Spring Harb Perspect Biol* 5, a012583.

Reference

- Kröning, A., van den Boom, J., Kracht, M., Kueck, A.F., Meyer, H., 2022. Ubiquitin-directed AAA+ ATPase p97/VCP unfolds stable proteins crosslinked to DNA for proteolysis by SPRTN. *Journal of Biological Chemistry* 298, 101976.
- Kühbacher, U., Duxin, J.P., 2020. How to fix DNA-protein crosslinks. *DNA Repair* 94, 102924.
- Kültz, D., 2005. MOLECULAR AND EVOLUTIONARY BASIS OF THE CELLULAR STRESS RESPONSE. *Annu. Rev. Physiol.* 67, 225–257.
- Kunkel, T.A., Erie, D.A., 2005. DNA MISMATCH REPAIR. *Annu. Rev. Biochem.* 74, 681–710.
- Kuroha, K., Zinoviev, A., Hellen, C.U.T., Pestova, T.V., 2018. Release of Ubiquitinated and Non-ubiquitinated Nascent Chains from Stalled Mammalian Ribosomal Complexes by ANKZF1 and Pth1. *Mol Cell* 72, 286-302.e8.
- Kurosaki, T., Popp, M.W., Maquat, L.E., 2019. Quality and quantity control of gene expression by nonsense-mediated mRNA decay. *Nat Rev Mol Cell Biol* 20, 406–420.
- Kusakabe, M., Onishi, Y., Tada, H., Kurihara, F., Kusao, K., Furukawa, M., Iwai, S., Yokoi, M., Sakai, W., Sugawara, K., 2019. Mechanism and regulation of DNA damage recognition in nucleotide excision repair. *Genes and Environment* 41, 2.
- Kuznetsova, A.V., Meller, J., Schnell, P.O., Nash, J.A., Ignacak, M.L., Sanchez, Y., Conaway, J.W., Conaway, R.C., Czyzyk-Krzeska, M.F., 2003. von Hippel–Lindau protein binds hyperphosphorylated large subunit of RNA polymerase II through a proline hydroxylation motif and targets it for ubiquitination. *Proceedings of the National Academy of Sciences* 100, 2706–2711.
- Lafranchi, L., Boer, R de, H., 2014. APC/CCdh1 controls CtIP stability during the cell cycle and in response to DNA damage. *The EMBO Journal* 33, 2860–2879.
- Lamond, A.I., 1993. The Spliceosome. *BioEssays* 15, 595–603.
- Lapointe, C.P., Wilinski, D., Saunders, H.A.J., Wickens, M., 2015. Protein-RNA networks revealed through covalent RNA marks. *Nat Methods* 12, 1163–1170.
- Larsen, N.B., Gao, A.O., Sparks, J.L., Gallina, I., Wu, R.A., Mann, M., Räschle, M., Walter, J.C., Duxin, J.P., 2019. Replication-Coupled DNA-Protein Crosslink Repair by SPRTN and the Proteasome in *Xenopus* Egg Extracts. *Molecular Cell* 73, 574-588.e7.

Reference

- Le Hir, H., Izaurralde, E., Maquat, L.E., Moore, M.J., 2000. The spliceosome deposits multiple proteins 20-24 nucleotides upstream of mRNA exon-exon junctions. *EMBO J* 19, 6860–6869.
- Ledesma, F.C., El Khamisy, S.F., Zuma, M.C., Osborn, K., Caldecott, K.W., 2009. A human 5'-tyrosyl DNA phosphodiesterase that repairs topoisomerase-mediated DNA damage. *Nature* 461, 674–678.
- Lee, K.C., Padget, K., Curtis, H., Cowell, I.G., Moiani, D., Sondka, Z., Morris, N.J., Jackson, G.H., Cockell, S.J., Tainer, J.A., Austin, C.A., 2012. MRE11 facilitates the removal of human topoisomerase II complexes from genomic DNA. *Biology Open* 1, 863–873.
- Lehmann, A.R., 2006. Translesion synthesis in mammalian cells. *Experimental Cell Research* 312, 2673–2676.
- Lehrbach, N.J., Ruvkun, G., 2016. Proteasome dysfunction triggers activation of SKN-1A/Nrf1 by the aspartic protease DDI-1. *eLife* 5, e17721.
- Lejeune, F., Li, X., Maquat, L.E., 2003. Nonsense-Mediated mRNA Decay in Mammalian Cells Involves Decapping, Deadenylation, and Exonucleolytic Activities. *Molecular Cell* 12, 675–687.
- Lemonidis, K., Rennie, M.L., Arkinson, C., Chaugule, V.K., Clarke, M., Streetley, J., Walden, H., 2022. Structural and biochemical basis of FANCI-FANCD2 interdependent ubiquitination (preprint). *Biochemistry*.
- Leng, X., Duxin, J.P., 2022. Targeting DNA-Protein Crosslinks via Post-Translational Modifications. *Frontiers in Molecular Biosciences* 9:944775.
- Ler, A.A.L., Carty, M.P., 2022. DNA Damage Tolerance Pathways in Human Cells: A Potential Therapeutic Target. *Frontiers in Oncology* 11:822500.
- Lessel, D., Vaz, B., Halder, S., Lockhart, P.J., Marinovic-Terzic, I., Lopez-Mosqueda, J., Philipp, M., Sim, J.C.H., Smith, K.R., Oehler, J., Cabrera, E., Freire, R., Pope, K., Nahid, A., Norris, F., Leventer, R.J., Delatycki, M.B., Barbi, G., von Ameln, S., Högel, J., Degoricija, M., Fertig, R., Burkhalter, M.D., Hofmann, K., Thiele, H., Altmüller, J., Nürnberg, G., Nürnberg, P., Bahlo, M., Martin, G.M., Aalfs, C.M., Oshima, J., Terzic, J., Amor, D.J., Dikic, I., Ramadan, K., Kubisch, C., 2014. Mutations in SPRTN cause early onset hepatocellular carcinoma, genomic instability and progeroid features. *Nat Genet* 46, 1239–1244.
- Letzring, D.P., Dean, K.M., Grayhack, E.J., 2010. Control of translation efficiency in yeast by codon–anticodon interactions. *RNA* 16, 2516–2528.

Reference

- Leung, W., Baxley, R., Moldovan, G.-L., Bielinsky, A.-K., 2018. Mechanisms of DNA Damage Tolerance: Post-Translational Regulation of PCNA. *Genes* 10, 10.
- Lewis, C.J.T., Pan, T., Kalsotra, A., 2017. RNA modifications and structures cooperate to guide RNA–protein interactions. *Nat Rev Mol Cell Biol* 18, 202–210.
- Li, Faxiang, Raczynska, J.E., Chen, Z., Yu, H., 2019. Structural Insight into DNA-Dependent Activation of Human Metalloprotease Spartan. *Cell Reports* 26, 3336-3346.e4.
- Li, Fuyang, Wang, Q., Seol, J.-H., Che, J., Lu, X., Shim, E.Y., Lee, S.E., Niu, H., 2019. Apn2 resolves blocked 3' ends and suppresses Top1-induced mutagenesis at genomic rNMP sites. *Nat Struct Mol Biol* 26, 155–163.
- Li, J., Bhat, A., Xiao, W., 2011. Regulation of nucleotide excision repair through ubiquitination. *Acta Biochimica et Biophysica Sinica* 43, 919–929.
- Li, M., Chen, D., Shiloh, A., Luo, J., Nikolaev, A.Y., Qin, J., Gu, W., 2002. Deubiquitination of p53 by HAUSP is an important pathway for p53 stabilization. *Nature* 416, 648–653.
- Li, X., Cao, G., Liu, X., Tang, T.-S., Guo, C., Liu, H., 2022. Polymerases and DNA Repair in Neurons: Implications in Neuronal Survival and Neurodegenerative Diseases. *Frontiers in Cellular Neuroscience* 16:852002.
- Li, Z., Wu, J., Deleo, C.J., 2006. RNA damage and surveillance under oxidative stress. *IUBMB Life* 58, 581–588.
- Liao, Y., Sumara, I., Pangou, E., 2022. Non-proteolytic ubiquitylation in cellular signaling and human disease. *Commun Biol* 5, 114.
- Lin, C.-P., Ban, Y., Lyu, Y.L., Desai, S.D., Liu, L.F., 2008. A Ubiquitin-Proteasome Pathway for the Repair of Topoisomerase I-DNA Covalent Complexes. *J Biol Chem* 283, 21074–21083.
- Lindahl, T., 1993. Instability and decay of the primary structure of DNA. *Nature* 362, 709–715.
- Lindahl, T., Barnes, D.E., 2000. Repair of Endogenous DNA Damage. *Cold Spring Harbor Symposia on Quantitative Biology* 65, 127–134.
- Lindahl, T., Karlstrom, O., 1973. Heat-induced depyrimidination of deoxyribonucleic acid in neutral solution. *Biochemistry*, 12, 25, 5151–5154
- Lipton, J.M., Ellis, S.R., 2009. Diamond-Blackfan Anemia: Diagnosis, Treatment, and Molecular Pathogenesis. *Hematology/Oncology Clinics of North America, Bone Marrow Failure Syndromes* 23, 261–282.

Reference

- Liu, J.C.Y., Kühbacher, U., Larsen, N.B., Borgermann, N., Garvanska, D.H., Hendriks, I.A., Ackermann, L., Haahr, P., Gallina, I., Guérillon, C., Branigan, E., Hay, R.T., Azuma, Y., Nielsen, M.L., Duxin, J.P., Mailand, N., 2021. Mechanism and function of DNA replication - independent DNA - protein crosslink repair via the SUMO - RNF4 pathway. *The EMBO Journal* 40, e107413.
- Liu, J.M., Ellis, S.R., 2006. Ribosomes and marrow failure: coincidental association or molecular paradigm? *Blood* 107, 4583–4588.
- Liu, Y., Prasad, R., Beard, W.A., Kedar, P.S., Hou, E.W., Shock, D.D., Wilson, S.H., 2007. Coordination of Steps in Single-nucleotide Base Excision Repair Mediated by Apurinic/Apyrimidinic Endonuclease 1 and DNA Polymerase β . *J Biol Chem* 282, 13532–13541.
- Loeb, L.A., Harris, C.C., 2008. Advances in Chemical Carcinogenesis: A Historical Review and Prospective. *Cancer Res* 68, 6863–6872.
- Loeb, L.A., Monnat, R.J., 2008. DNA polymerases and human disease. *Nat Rev Genet* 9, 594–604.
- Loeb, L.A., Preston, B.D., 1986. MUTAGENESIS BY APURINIC/APYRIMIDINIC SITES. *Ann. Rev. Genet.* 20:201-30.
- Loechler, E.L., Green, C.L., Essigmann, J.M., 1984. In vivo mutagenesis by O⁶-methylguanine built into a unique site in a viral genome. *Proc. Natl. Acad. Sci. USA* Vol. 81, pp. 6271-6275.
- Lopez-Mosqueda, J., Maddi, K., Prgomet, S., Kalayil, S., Marinovic-Terzic, I., Terzic, J., Dikic, I., 2016. SPRTN is a mammalian DNA-binding metalloprotease that resolves DNA-protein crosslinks. *eLife* 5, e21491.
- Lu, J., Deutsch, C., 2008. Electrostatics in the Ribosomal Tunnel Modulate Chain Elongation Rates. *Journal of Molecular Biology* 384, 73–86.
- Lu, K., Ye, W., Zhou, L., Collins, L.B., Chen, X., Gold, A., Ball, L.M., Swenberg, J.A., 2010. Structural Characterization of Formaldehyde-Induced Cross-Links Between Amino Acids and Deoxynucleosides and Their Oligomers. *J. Am. Chem. Soc.* 132, 3388–3399.
- Lu, P.D., Harding, H.P., Ron, D., 2004. Translation reinitiation at alternative open reading frames regulates gene expression in an integrated stress response. *J Cell Biol* 167, 27–33.
- Lunde, B.M., Moore, C., Varani, G., 2007. RNA-binding proteins: modular design for efficient function. *Nat Rev Mol Cell Biol* 8, 479–490.

Reference

- Luo, Z., Zheng, J., Lu, Y., Bregman, D.B., 2001. Ultraviolet radiation alters the phosphorylation of RNA polymerase II large subunit and accelerates its proteasome-dependent degradation. *Mutation Research/DNA Repair* 486, 259–274.
- Ma, X., Tang, T.-S., Guo, C., 2020. Regulation of translesion DNA synthesis in mammalian cells. *Environmental and Molecular Mutagenesis* 61, 680–692.
- Machida, Y., Kim, M.S., Machida, Y.J., 2012. Spartan/C1orf124 is important to prevent UV-induced mutagenesis. *Cell Cycle* 11, 3395–3402.
- Machida, Y.J., Machida, Y., Chen, Y., Gurtan, A.M., Kupfer, G.M., D'Andrea, A.D., Dutta, A., 2006. UBE2T Is the E2 in the Fanconi Anemia Pathway and Undergoes Negative Autoregulation. *Molecular Cell* 23, 589–596.
- Mah, M.C.-M., Maher, V.M., Thomas, H., Reid, T.M., King, C.M., McCormick, J.J., 1989. Mutations induced by aminofluorene-DNA adducts during replication in human cells. *Carcinogenesis* 10, 2321–2328.
- Mailand, N., Bekker-Jensen, S., Faustrup, H., Melander, F., Bartek, J., Lukas, C., Lukas, J., 2007. RNF8 ubiquitylates histones at DNA double-strand breaks and promotes assembly of repair proteins. *Cell* 131, 887–900.
- Maiorano, D., El Etri, J., Franchet, C., Hoffmann, J.-S., 2021. Translesion Synthesis or Repair by Specialized DNA Polymerases Limits Excessive Genomic Instability upon Replication Stress. *IJMS* 22, 3924.
- Majumder, M., Palanisamy, V., 2021. Compendium of Methods to Uncover RNA-Protein Interactions In Vivo. *MPs* 4, 22.
- Malik, M., Nitiss, J.L., 2004. DNA Repair Functions That Control Sensitivity to Topoisomerase-Targeting Drugs. *Eukaryot Cell* 3, 82–90.
- Mao, Y., Desai, S.D., Ting, C.-Y., Hwang, J., Liu, L.F., 2001. 26 S Proteasome-mediated Degradation of Topoisomerase II Cleavable Complexes. *Journal of Biological Chemistry* 276, 40652–40658.
- Marchese, D., de Groot, N.S., Lorenzo Gotor, N., Livi, C.M., Tartaglia, G.G., 2016. Advances in the characterization of RNA - binding proteins. *Wiley Interdiscip Rev RNA* 7, 793–810.
- Maskey, R.S., Flatten, K.S., Sieben, C.J., Peterson, K.L., Baker, D.J., Nam, H.-J., Kim, M.S., Smyrk, T.C., Kojima, Y., Machida, Y., Santiago, A., van Deursen, J.M., Kaufmann, S.H., Machida, Y.J., 2017. Spartan deficiency causes accumulation of Topoisomerase 1 cleavage complexes and tumorigenesis. *Nucleic Acids Research* 45, 4564–4576.

Reference

- Maskey, R.S., Kim, M.S., Baker, D.J., Childs, B., Malureanu, L.A., Jeganathan, K.B., Machida, Y., van Deursen, J.M., Machida, Y.J., 2014. Spartan deficiency causes genomic instability and progeroid phenotypes. *Nat Commun* 5, 5744.
- Masutani, C., Kusumoto, R., Yamada, A., Dohmae, N., Yokoi, M., Yuasa, M., Araki, M., Iwai, S., Hanaoka, F., 1999. The XPV (xeroderma pigmentosum variant) gene encodes human DNA polymerase η . *Nature*, 399, 700-704.
- Mateyak, M.K., Kinzy, T.G., 2010. eEF1A: Thinking Outside the Ribosome. *J Biol Chem* 285, 21209–21213.
- Matos, J., West, S.C., 2014. Holliday junction resolution: Regulation in space and time. *DNA Repair* 19, 176–181.
- Matsumoto, S., Fischer, E.S., Yasuda, T., Dohmae, N., Iwai, S., Mori, T., Nishi, R., Yoshino, K., Sakai, W., Hanaoka, F., Thomä, N.H., Sugasawa, K., 2015. Functional regulation of the DNA damage-recognition factor DDB2 by ubiquitination and interaction with xeroderma pigmentosum group C protein. *Nucleic Acids Res* 43, 1700–1713.
- Matsunaga, F., Forterre, P., Ishino, Y., Myllykallio, H., 2001. In vivo interactions of archaeal Cdc6/Orc1 and minichromosome maintenance proteins with the replication origin. *Proceedings of the National Academy of Sciences* 98, 11152–11157.
- Matsuo, Y., Tesina, P., Nakajima, S., Mizuno, M., Endo, A., Buschauer, R., Cheng, J., Shounai, O., Ikeuchi, K., Saeki, Y., Becker, T., Beckmann, R., Inada, T., 2020. RQT complex dissociates ribosomes collided on endogenous RQC substrate SDD1. *Nat Struct Mol Biol* 27, 323–332.
- Mattiroli, F., Penengo, L., 2021. Histone Ubiquitination: An Integrative Signaling Platform in Genome Stability. *Trends in Genetics* 37, 566–581.
- Mattiroli, F., Vissers, J.H.A., van Dijk, W.J., Ikpa, P., Citterio, E., Vermeulen, W., Marteijn, J.A., Sixma, T.K., 2012. RNF168 ubiquitinates K13-15 on H2A/H2AX to drive DNA damage signaling. *Cell* 150, 1182–1195.
- Maynard, S., Fang, E.F., Scheibye-Knudsen, M., Croteau, D.L., Bohr, V.A., 2015. DNA Damage, DNA Repair, Aging, and Neurodegeneration. *Cold Spring Harb Perspect Med* 5, a025130.
- McDowell, G.S., Philpott, A., 2013. Non-canonical ubiquitylation: Mechanisms and consequences. *The International Journal of Biochemistry & Cell Biology* 45, 1833–1842.
- McGowan, K.A., Li, J.Z., Park, C.Y., Beaudry, V., Tabor, H.K., Sabnis, A.J., Zhang, W., Fuchs, H., de Angelis, M.H., Myers, R.M., Attardi, L.D., Barsh, G.S., 2008.

Reference

Ribosomal mutations cause p53-mediated dark skin and pleiotropic effects. *Nat Genet* 40, 963–970.

McHugh, C.A., Russell, P., Guttman, M., 2014. Methods for comprehensive experimental identification of RNA-protein interactions. *Genome Biol* 15, 203.

McMahon, A.C., Rahman, R., Jin, H., Shen, J.L., Fieldsend, A., Luo, W., Rosbash, M., 2016. TRIBE: Hijacking an RNA-Editing Enzyme to Identify Cell-Specific Targets of RNA-Binding Proteins. *Cell* 165, 742–753.

McVey, M., Khodaverdian, V.Y., Meyer, D., Cerqueira, P.G., Heyer, W.-D., 2016. Eukaryotic DNA Polymerases in Homologous Recombination. *Annu Rev Genet* 50, 393–421.

Mechanistic analysis of PCNA poly-ubiquitylation by the ubiquitin protein ligases Rad18 and Rad5, 2009. . *The EMBO Journal* 28, 3657–3666.

Meehan, T., Wolfe, A.R., Negrete, G.R., Song, Q., 1997. Benzo[a]pyrene diol epoxide-DNA cis adduct formation through a trans chlorohydrin intermediate. *Proceedings of the National Academy of Sciences* 94, 1749–1754.

Meetei, A.R., de Winter, J.P., Medhurst, A.L., Wallisch, M., Waisfisz, Q., van de Vrugt, H.J., Oostra, A.B., Yan, Z., Ling, C., Bishop, C.E., Hoatlin, M.E., Joenje, H., Wang, W., 2003. A novel ubiquitin ligase is deficient in Fanconi anemia. *Nat Genet* 35, 165–170.

Mehta, A., Haber, J.E., 2014. Sources of DNA Double-Strand Breaks and Models of Recombinational DNA Repair. *Cold Spring Harb Perspect Biol* 6, a016428.

Mei, C., Lei, L., Tan, L.-M., Xu, X.-J., He, B.-M., Luo, C., Yin, J.-Y., Li, X., Zhang, W., Zhou, H.-H., Liu, Z.-Q., 2020. The role of single strand break repair pathways in cellular responses to camptothecin induced DNA damage. *Biomedicine & Pharmacotherapy* 125, 109875.

Meisenheimer, K.M., Koch, T.H., 1997. Photocross-Linking of Nucleic Acids to Associated Proteins. *Critical Reviews in Biochemistry and Molecular Biology* 32, 101–140.

Melis, J.P.M., van Steeg, H., Luijten, M., 2013. Oxidative DNA Damage and Nucleotide Excision Repair. *Antioxidants & Redox Signaling* 18, 2409–2419.

Meyer, C., Garzia, A., Morozov, P., Molina, H., Tuschl, T., 2020. The G3BP1-Family-USP10 Deubiquitinase Complex Rescues Ubiquitinated 40S Subunits of Ribosomes Stalled in Translation from Lysosomal Degradation. *Mol Cell* 77, 1193-1205.e5.

Reference

- Miele, E., Mastronuzzi, A., Po, A., Carai, A., Alfano, V., Serra, A., Colafati, G.S., Strocchio, L., Antonelli, M., Buttarelli, F.R., Zani, M., Ferraro, S., Buffone, A., Vacca, A., Screpanti, I., Giangaspero, F., Giannini, G., Locatelli, F., Ferretti, E., 2015. Characterization of medulloblastoma in Fanconi Anemia: a novel mutation in the BRCA2 gene and SHH molecular subgroup. *Biomark Res* 3, 13.
- Miller, E.C., 1978. Some Current Perspectives on Chemical Carcinogenesis in Humans and Experimental Animals: Presidential Address. *Cancer Res* 38, 1479–1496.
- Mills, E.W., Green, R., 2017. Ribosomopathies: There's strength in numbers. *Science* 358, eaan2755.
- Mimitou, E.P., Symington, L.S., 2009. Nucleases and helicases take center stage in homologous recombination. *Trends in Biochemical Sciences* 34, 264–272.
- Minajigi, A., Froberg, J.E., Wei, C., Sunwoo, H., Kesner, B., Colognori, D., Lessing, D., Payer, B., Boukhali, M., Haas, W., Lee, J.T., 2015. A comprehensive Xist interactome reveals cohesin repulsion and an RNA-directed chromosome conformation. *Science* 349, aab2276.
- Minchin, S., Lodge, J., 2019. Understanding biochemistry: structure and function of nucleic acids. *Essays Biochem* 63, 433–456.
- Minko, I.G., Kurtz, A.J., Croteau, D.L., Van Houten, B., Harris, T.M., Lloyd, R.S., 2005. Initiation of Repair of DNA–Polypeptide Cross-Links by the UvrABC Nuclease. *Biochemistry* 44, 3000–3009.
- Minko, I.G., Yamanaka, K., Kozekov, I.D., Kozekova, A., Indiani, C., O'Donnell, M.E., Jiang, Q., Goodman, M.F., Rizzo, C.J., Lloyd, R.S., 2008. Replication Bypass of the Acrolein-Mediated Deoxyguanine DNA-Peptide Cross-Links by DNA Polymerases of the DinB Family. *Chem. Res. Toxicol.* 21, 1983–1990.
- Minko, I.G., Zou, Y., Lloyd, R.S., 2002. Incision of DNA–protein crosslinks by UvrABC nuclease suggests a potential repair pathway involving nucleotide excision repair. *PNAS* 99, 1905–1909.
- Mohni, K.N., Wessel, S.R., Zhao, R., Wojciechowski, A.C., Luzwick, J.W., Layden, H., Eichman, B.F., Thompson, P.S., Mehta, K.P.M., Cortez, D., 2019. HMCES Maintains Genome Integrity by Shielding Abasic Sites in Single-Strand DNA. *Cell* 176, 144-153.e13.
- Moldovan, G.-L., D'Andrea, A.D., 2009. How the Fanconi Anemia Pathway Guards the Genome. *Annu. Rev. Genet.* 43, 223–249.

Reference

Moldovan, G.-L., Pfander, B., Jentsch, S., 2007. PCNA, the Maestro of the Replication Fork. *Cell* 129, 665–679.

Montelone, B.A., 2015. DNA Repair and Mutagenesis. Second Edition. By Errol C Friedberg, Graham C Walker, Wolfram Siede, Richard D Wood, Roger A Schultz, and, Tom Ellenberger. Washington (DC): ISBN: 1-55581-319-4.

Moore, P.B., Steitz, T.A., 2002. The involvement of RNA in ribosome function. *Nature* 418, 229–235.

Mórocz, M., Zsigmond, E., Tóth, R., Enyedi, M.Z., Pintér, L., Haracska, L., 2017. DNA-dependent protease activity of human Spartan facilitates replication of DNA–protein crosslink-containing DNA. *Nucleic Acids Res* 45, 3172–3188.

Morreale, F.E., Walden, H., 2016. Types of Ubiquitin Ligases. *Cell* 165, 248-248.e1.

Morris, C., Cluet, D., Ricci, E.P., 2021. Ribosome dynamics and mRNA turnover, a complex relationship under constant cellular scrutiny. *WIREs RNA* 12: e1658.

Mosbech, A., Gibbs-Seymour, I., Kagias, K., Thorslund, T., Beli, P., Povlsen, L., Nielsen, S.V., Smedegaard, S., Sedgwick, G., Lukas, C., Hartmann-Petersen, R., Lukas, J., Choudhary, C., Pocock, R., Bekker-Jensen, S., Mailand, N., 2012. DVC1 (C1orf124) is a DNA damage–targeting p97 adaptor that promotes ubiquitin-dependent responses to replication blocks. *Nat Struct Mol Biol* 19, 1084–1092.

Moss, T., Stefanovsky, V.Y., 2002. At the Center of Eukaryotic Life. *Cell* 109, 545–548.

Nakamura, J., La, D.K., Swenberg, J.A., 2000. 5'-Nicked Apurinic/Apyrimidinic Sites Are Resistant to β -Elimination by β -Polymerase and Are Persistent in Human Cultured Cells after Oxidative Stress. *Journal of Biological Chemistry* 275, 5323–5328.

Nakano, T., Katafuchi, A., Matsubara, M., Terato, H., Tsuboi, T., Masuda, T., Tatsumoto, T., Pack, S.P., Makino, K., Croteau, D.L., Van Houten, B., Iijima, K., Tauchi, H., Ide, H., 2009. Homologous Recombination but Not Nucleotide Excision Repair Plays a Pivotal Role in Tolerance of DNA-Protein Cross-links in Mammalian Cells. *Journal of Biological Chemistry* 284, 27065–27076.

Nakano, T., Morishita, S., Katafuchi, A., Matsubara, M., Horikawa, Y., Terato, H., Salem, A.M.H., Izumi, S., Pack, S.P., Makino, K., Ide, H., 2007. Nucleotide Excision Repair and Homologous Recombination Systems Commit Differentially to the Repair of DNA-Protein Crosslinks. *Molecular Cell* 28, 147–158.

Reference

- Nakano, T., Xu, X., Salem, A.M.H., Shoukamy, M.I., Ide, H., 2017. Radiation-induced DNA–protein cross-links: Mechanisms and biological significance. *Free Radical Biology and Medicine, Oxidative DNA Damage & Repair* 107, 136–145.
- Nakazawa, Y., Hara, Y., Oka, Y., Komine, O., van den Heuvel, D., Guo, C., Daigaku, Y., Isono, M., He, Y., Shimada, M., Kato, K., Jia, N., Hashimoto, S., Kotani, Y., Miyoshi, Y., Tanaka, M., Sobue, A., Mitsutake, N., Suganami, T., Masuda, A., Ohno, K., Nakada, S., Mashimo, T., Yamanaka, K., Luijsterburg, M.S., Ogi, T., 2020. Ubiquitination of DNA Damage-Stalled RNAPII Promotes Transcription-Coupled Repair. *Cell* 180, 1228-1244.e24.
- Naldiga, S., Ji, S., Thomforde, J., Nicolae, C.M., Lee, M., Zhang, Z., Moldovan, G.-L., Tretyakova, N.Y., Basu, A.K., 2019. Error-prone replication of a 5-formylcytosine-mediated DNA-peptide cross-link in human cells. *Journal of Biological Chemistry* 294, 10619–10627.
- Nalepa, G., Clapp, D.W., 2018. Fanconi anaemia and cancer: an intricate relationship. *Nat Rev Cancer* 18, 168–185.
- Narla, A., Ebert, B.L., 2010. Ribosomopathies: human disorders of ribosome dysfunction. *Blood* 115, 3196–3205.
- Narla, A., Hurst, S.N., Ebert, B.L., 2011. Ribosome defects in disorders of erythropoiesis. *Int J Hematol* 93, 144–149.
- Nay, S.L., O'Connor, T.R., 2013. Direct Repair in Mammalian Cells, *New Research Directions in DNA Repair*. IntechOpen. ISBN: 978-953-51-1114-6.
- Neale, M.J., Pan, J., Keeney, S., 2005. Endonucleolytic processing of covalent protein-linked DNA double-strand breaks. *Nature* 436, 1053–1057.
- Nedialkova, D.D., Leidel, S.A., 2015. Optimization of Codon Translation Rates via tRNA Modifications Maintains Proteome Integrity. *Cell* 161, 1606–1618.
- Nicholson, P., Yepiskoposyan, H., Metze, S., Zamudio Orozco, R., Kleinschmidt, N., Mühlemann, O., 2010. Nonsense-mediated mRNA decay in human cells: mechanistic insights, functions beyond quality control and the double-life of NMD factors. *Cell. Mol. Life Sci.* 67, 677–700.
- Nickoloff, J.A., Sharma, N., Taylor, L., Allen, S.J., Hromas, R., 2021. The Safe Path at the Fork: Ensuring Replication-Associated DNA Double-Strand Breaks are Repaired by Homologous Recombination. *Frontiers in Genetics* 12:748033.
- Nie, M., Oravcová, M., Jami - Alahmadi, Y., Wohlschlegel, J.A., Lazzerini - Denchi, E., Boddy, M.N., 2021. FAM111A induces nuclear dysfunction in disease and viral restriction. *EMBO Rep* 22, e50803.

Reference

Niedernhofer, L.J., Lalai, A.S., Hoeijmakers, J.H.J., 2005. Fanconi Anemia (Cross)linked to DNA Repair. *Cell* 123, 1191–1198.

Niraj, J., Färkkilä, A., D'Andrea, A.D., 2019. The Fanconi Anemia Pathway in Cancer. *Annual Review of Cancer Biology* 3, 457–478.

Niranjanakumari, S., Lasda, E., Brazas, R., Garcia-Blanco, M.A., 2002. Reversible cross-linking combined with immunoprecipitation to study RNA–protein interactions in vivo. *Methods* 26, 182–190.

Nitiss, J.L., 2009. Targeting DNA topoisomerase II in cancer chemotherapy. *Nat Rev Cancer* 9, 338–350.

Noll, D.M., Mason, T.M., Miller, P.S., 2006. Formation and Repair of Interstrand Cross-Links in DNA. *Chem. Rev.* 106, 277–301.

Nowsheen, S., Aziz, K., Aziz, A., Deng, M., Qin, B., Luo, K., Jeganathan, K.B., Zhang, H., Liu, T., Yu, J., Deng, Y., Yuan, J., Ding, W., van Deursen, J.M., Lou, Z., 2018. L3MBTL2 orchestrates ubiquitin signalling by dictating the sequential recruitment of RNF8 and RNF168 after DNA damage. *Nat Cell Biol* 20, 455–464.

O'Brien, J., Hayder, H., Zayed, Y., Peng, C., 2018. Overview of MicroRNA Biogenesis, Mechanisms of Actions, and Circulation. *Frontiers in Endocrinology* 9:402.

Ohsawa, I., Nishimaki, K., Murakami, Y., Suzuki, Y., Ishikawa, M., Ohta, S., 2008. Age-Dependent Neurodegeneration Accompanying Memory Loss in Transgenic Mice Defective in Mitochondrial Aldehyde Dehydrogenase 2 Activity. *J. Neurosci.* 28, 6239–6249.

O'Keefe, E.P., 2021. siRNAs and shRNAs: Tools for Protein Knockdown by Gene Silencing. *Materials and Methods.* 3:197.

Oliveira, C., Faoro, H., Alves, L.R., Goldenberg, S., 2017. RNA-binding proteins and their role in the regulation of gene expression in *Trypanosoma cruzi* and *Saccharomyces cerevisiae*. *Genet Mol Biol* 40, 22–30.

Olivieri, M., Cho, T., Álvarez-Quilón, A., Li, K., Schellenberg, M.J., Zimmermann, M., Hustedt, N., Rossi, S.E., Adam, S., Melo, H., Heijink, A.M., Sastre-Moreno, G., Moatti, N., Szilard, R.K., McEwan, A., Ling, A.K., Serrano-Benitez, A., Ubhi, T., Feng, S., Pawling, J., Delgado-Sainz, I., Ferguson, M.W., Dennis, J.W., Brown, G.W., Cortés-Ledesma, F., Williams, R.S., Martin, A., Xu, D., Durocher, D., 2020. A Genetic Map of the Response to DNA Damage in Human Cells. *Cell* 182, 481-496.e21.

Reference

- Ortega-Atienza, S., Green, S.E., Zhitkovich, A., 2015. Proteasome activity is important for replication recovery, CHK1 phosphorylation and prevention of G2 arrest after low-dose formaldehyde. *Toxicology and Applied Pharmacology* 286, 135–141.
- Orthwein, A., Noordermeer, S.M., Wilson, M.D., Landry, S., Enchev, R.I., Sherker, A., Munro, M., Pinder, J., Salsman, J., Delleire, G., Xia, B., Peter, M., Durocher, D., 2015. A mechanism for the suppression of homologous recombination in G1 cells. *Nature* 528, 422–426.
- Osuna, B.A., Howard, C.J., KC, S., Frost, A., Weinberg, D.E., 2017. In vitro analysis of RQC activities provides insights into the mechanism and function of CAT tailing. *eLife* 6, e27949.
- Pakos-Zebrucka, K., Koryga, I., Mnich, K., 2016. The integrated stress response. *EMBO reports* 17, 1374–1395.
- Pal, S., 2020. Chapter 10 - RNA processing, in: Pal, S. (Ed.), *Fundamentals of Molecular Structural Biology*. Academic Press, pp. 277–309.
- Park, Jumin, Park, Jongmin, Lee, J., Lim, C., 2021. The trinity of ribosome-associated quality control and stress signaling for proteostasis and neuronal physiology. *BMB Rep* 54, 439–450.
- Paull, T.T., 2018. 20 Years of Mre11 Biology: No End in Sight. *Molecular Cell* 71, 419–427.
- Pavri, R., Zhu, B., Li, G., Trojer, P., Mandal, S., Shilatifard, A., Reinberg, D., 2006. Histone H2B Monoubiquitination Functions Cooperatively with FACT to Regulate Elongation by RNA Polymerase II. *Cell* 125, 703–717.
- Peng, Y., Pei, H., 2021. DNA alkylation lesion repair: outcomes and implications in cancer chemotherapy. *J. Zhejiang Univ. Sci. B* 22, 47–62.
- Penny, G.D., Kay, G.F., Sheardown, S.A., Rastan, S., Brockdorff, N., 1996. Requirement for Xist in X chromosome inactivation. *Nature* 379, 131–137.
- Perry, M., Biegert, M., Kollala, S.S., Mallard, H., Su, G., Kodavati, M., Kreiling, N., Holbrook, A., Ghosal, G., 2021. USP11 mediates repair of DNA–protein cross-links by deubiquitinating SPRTN metalloprotease. *Journal of Biological Chemistry* 296, 100396.
- Pestova, T.V., Kolupaeva, V.G., Lomakin, I.B., Pilipenko, E.V., Shatsky, I.N., Agol, V.I., Hellen, C.U.T., 2001. Molecular mechanisms of translation initiation in eukaryotes. *Proceedings of the National Academy of Sciences* 98, 7029–7036.

Reference

- Petroski, M.D., Deshaies, R.J., 2005. Function and regulation of cullin-RING ubiquitin ligases. *Nat Rev Mol Cell Biol* 6, 9–20.
- Pfeifer, G.P., Denissenko, M.F., Olivier, M., Tretyakova, N., Hecht, S.S., Hainaut, P., 2002. Tobacco smoke carcinogens, DNA damage and p53 mutations in smoking-associated cancers. *Oncogene* 21, 7435–7451.
- Phillips, D.H., 2005. DNA adducts as markers of exposure and risk. *Mutation Research/Fundamental and Molecular Mechanisms of Mutagenesis, Mechanisms of DNA Repair* 577, 284–292.
- Pickart, C.M., Fushman, D., 2004. Polyubiquitin chains: polymeric protein signals. *Current Opinion in Chemical Biology* 8, 610–616.
- Pilzecker, B., Buoninfante, O.A., Jacobs, H., 2019. DNA damage tolerance in stem cells, ageing, mutagenesis, disease and cancer therapy. *Nucleic Acids Res* 47, 7163–7181.
- Pisarev, A.V., Skabkin, M.A., Pisareva, V.P., Skabkina, O.V., Rakotondrafara, A.M., Hentze, M.W., Hellen, C.U.T., Pestova, T.V., 2010. The role of ABCE1 in eukaryotic posttermination ribosomal recycling. *Mol Cell* 37, 196–210.
- Pisareva, V.P., Skabkin, M.A., Hellen, C.U.T., Pestova, T.V., Pisarev, A.V., 2011. Dissociation by Pelota, Hbs1 and ABCE1 of mammalian vacant 80S ribosomes and stalled elongation complexes. *EMBO J* 30, 1804–1817.
- Pluciennik, A., Dzantiev, L., Iyer, R.R., Constantin, N., Kadyrov, F.A., Modrich, P., 2010. PCNA function in the activation and strand direction of MutL α endonuclease in mismatch repair. *PNAS* 107, 16066–16071.
- Poetsch, A.R., 2020. The genomics of oxidative DNA damage, repair, and resulting mutagenesis. *Computational and Structural Biotechnology Journal* 18, 207–219.
- Polacek, N., Mankin, A.S., 2005. The ribosomal peptidyl transferase center: structure, function, evolution, inhibition. *Crit Rev Biochem Mol Biol* 40, 285–311.
- Pommier, Y., Huang, S.N., Gao, R., Das, B.B., Murai, J., Marchand, C., 2014. Tyrosyl-DNA-phosphodiesterases (TDP1 and TDP2). *DNA Repair* 19, 114–129.
- Pommier, Y., Marchand, C., 2012. Interfacial inhibitors: targeting macromolecular complexes. *Nat Rev Drug Discov* 11, 25–36.
- Pontel, L.B., Rosado, I.V., Burgos-Barragan, G., Garaycochea, J.I., Yu, R., Arends, M.J., Chandrasekaran, G., Broecker, V., Wei, W., Liu, L., Swenberg, J.A., Crossan, G.P., Patel, K.J., 2015. Endogenous Formaldehyde Is a Hematopoietic Stem Cell Genotoxin and Metabolic Carcinogen. *Mol Cell* 60, 177–188.

Reference

- Poria, D.K., Ray, P.S., 2017. RNA-protein UV-crosslinking Assay. *Bio Protoc* 7, e2193.
- Pouliot, J.J., Robertson, C.A., Nash, H.A., 2001. Pathways for repair of topoisomerase I covalent complexes in *Saccharomyces cerevisiae*. *Genes Cells* 6, 677–687.
- Pouliot, J.J., Yao, K.C., Robertson, C.A., Nash, H.A., 1999. Yeast Gene for a Tyr-DNA Phosphodiesterase that Repairs Topoisomerase I Complexes. *Science* 286, 552–555.
- Poulsen, S.L., Hansen, R.K., Wagner, S.A., van Cuijk, L., van Belle, G.J., Streicher, W., Wikström, M., Choudhary, C., Houtsmuller, A.B., Marteijn, J.A., Bekker-Jensen, S., Mailand, N., 2013. RNF111/Arkadia is a SUMO-targeted ubiquitin ligase that facilitates the DNA damage response. *Journal of Cell Biology* 201, 797–807.
- Preiss, T., W Hentze, M., 2003. Starting the protein synthesis machine: eukaryotic translation initiation. *Bioessays* 25, 1201–1211.
- Putnam, C.D., 2021. Strand discrimination in DNA mismatch repair. *DNA Repair* 105, 103161.
- Puumalainen, M.-R., Lessel, D., Rütthemann, P., Kaczmarek, N., Bachmann, K., Ramadan, K., Naegeli, H., 2014. Chromatin retention of DNA damage sensors DDB2 and XPC through loss of p97 segregase causes genotoxicity. *Nat Commun* 5, 3695.
- Qian, J., Pentz, K., Zhu, Q., Wang, Q., He, J., Srivastava, A.K., Wani, A.A., 2015. USP7 modulates UV-induced PCNA monoubiquitination by regulating DNA polymerase eta stability. *Oncogene* 34, 4791–4796.
- Qiu, R., Sakato, M., Sacho, E.J., Wilkins, H., Zhang, X., Modrich, P., Hingorani, M.M., Erie, D.A., Weninger, K.R., 2015. MutL traps MutS at a DNA mismatch. *Proc Natl Acad Sci USA* 112, 10914–10919.
- Queiroz, R.M.L., Smith, T., Villanueva, E., Monti, M., Pizzinga, M., Marti-Solano, M., Mirea, D.-M., Ramakrishna, M., Harvey, R.F., Dezi, V., Degroeve, S., Martens, L., Thomas, G.H., Willis, A.E., Lilley, K.S., 2018. Unbiased dynamic characterization of RNA-protein interactions by OOPS (Preprint).
- Querido, J.B., Sokabe, M., Kraatz, S., Gordiyenko, Y., Skehel, J.M., Fraser, C.S., Ramakrishnan, V., 2020. Structure of a human 48S translational initiation complex. *Science* 369, 1220–1227.

Reference

- Quievryn, G., Zhitkovich, A., 2000. Loss of DNA-protein crosslinks from formaldehyde-exposed cells occurs through spontaneous hydrolysis and an active repair process linked to proteasome function. *Carcinogenesis* 21, 1573–1580.
- Rajalakshmi, T.R., Aravindh Babu, N., Shanmugam, K.T., Masthan, K.M.K., 2015. DNA adducts-chemical add-ons. *J Pharm Bioallied Sci* 7, S197–S199.
- Ramanathan, M., Majzoub, K., Rao, D.S., Neela, P.H., Zarnegar, B.J., Mondal, S., Roth, J.G., Gai, H., Kovalski, J.R., Sibrashvili, Z., Palmer, T.D., Carette, J.E., Khavari, P.A., 2018. RNA–protein interaction detection in living cells. *Nat Methods* 15, 207–212.
- Ramanathan, M., Porter, D.F., Khavari, P.A., 2019. Methods to study RNA–protein interactions. *Nat Methods* 16, 225–234.
- Rape, M., Hoppe, T., Gorr, I., Kalocay, M., Richly, H., Jentsch, S., 2001. Mobilization of Processed, Membrane-Tethered SPT23 Transcription Factor by CDC48UFD1/NPL4, a Ubiquitin-Selective Chaperone. *Cell* 107, 667–677.
- Reardon, J.T., Sancar, A., 2006. Repair of DNA–polypeptide crosslinks by human excision nuclease. *PNAS* 103, 4056–4061.
- Rechkunova, N.I., Maltseva, E.A., Lavrik, O.I., 2019. Post-translational Modifications of Nucleotide Excision Repair Proteins and Their Role in the DNA Repair. *Biochemistry Moscow* 84, 1008–1020.
- Reinking, H.K., Kang, H.-S., Götz, M.J., Li, H.-Y., Kieser, A., Zhao, S., Acampora, A.C., Weickert, P., Fessler, E., Jae, L.T., Sattler, M., Stingle, J., 2020. DNA Structure-Specific Cleavage of DNA-Protein Crosslinks by the SPRTN Protease. *Molecular Cell* 80, 102-113.e6.
- Rennie, M.L., Lemonidis, K., Arkinson, C., Chaugule, V.K., Clarke, M., Streetley, J., Spagnolo, L., Walden, H., 2020. Differential functions of FANCI and FANCD2 ubiquitination stabilize ID2 complex on DNA. *EMBO Rep* 21, e50133.
- Reynolds, J.J., El-Khamisy, S.F., Katyal, S., Clements, P., McKinnon, P.J., Caldecott, K.W., 2009. Defective DNA Ligation during Short-Patch Single-Strand Break Repair in Ataxia Oculomotor Apraxia 1. *Mol Cell Biol* 29, 1354–1362.
- Ribeiro, J., Crossan, G.P., 2022. GCNA is a histone binding protein required for spermatogonial stem cell maintenance (preprint). *Physiology*.
- Ribeiro-Silva, C., Sabatella, M., Helfricht, A., Marteiijn, J.A., Theil, A.F., Vermeulen, W., Lans, H., 2020. Ubiquitin and TFIIH-stimulated DDB2 dissociation drives DNA damage handover in nucleotide excision repair. *Nat Commun* 11, 4868.

Reference

- Riccio, A.A., Schellenberg, M.J., Williams, R.S., 2020. Molecular mechanisms of topoisomerase 2 DNA–protein crosslink resolution. *Cell. Mol. Life Sci.* 77, 81–91.
- Rickman, K.A., Lach, F.P., Abhyankar, A., Donovan, F.X., Sanborn, E.M., Kennedy, J.A., Sougnez, C., Gabriel, S.B., Elemento, O., Chandrasekharappa, S.C., Schindler, D., Auerbach, A.D., Smogorzewska, A., 2015. Deficiency of UBE2T, the E2 Ubiquitin Ligase Necessary for FANCD2 and FANCI Ubiquitination, Causes FA-T Subtype of Fanconi Anemia. *Cell Reports* 12, 35–41.
- Rios-Szwed, D.O., Garcia-Wilson, E., Sanchez-Pulido, L., Alvarez, V., Jiang, H., Bandau, S., Lamond, A., Ponting, C.P., Alabert, C., 2020. FAM111A regulates replication origin activation and cell fitness (Preprint).
- Ripley, B.M., Gildenberg, M.S., Washington, M.T., 2020. Control of DNA Damage Bypass by Ubiquitylation of PCNA. *Genes* 11, 138.
- Rizza, S., Cardaci, S., Montagna, C., Di Giacomo, G., De Zio, D., Bordi, M., Maiani, E., Campello, S., Borreca, A., Puca, A.A., Stamler, J.S., Cecconi, F., Filomeni, G., 2018. S-nitrosylation drives cell senescence and aging in mammals by controlling mitochondrial dynamics and mitophagy. *Proceedings of the National Academy of Sciences* 115, E3388–E3397.
- Rocha, C.R.R., Silva, M.M., Quinet, A., Cabral-Neto, J.B., Menck, C.F.M., 2018. DNA repair pathways and cisplatin resistance: an intimate relationship. *Clinics (Sao Paulo)* 73, e478s.
- Rogakou, E.P., Pilch, D.R., Orr, A.H., Ivanova, V.S., Bonner, W.M., 1998. DNA double-stranded breaks induce histone H2AX phosphorylation on serine 139. *J Biol Chem* 273, 5858–5868.
- Ronai, Z.A., 2016. Monoubiquitination in proteasomal degradation. *Proceedings of the National Academy of Sciences* 113, 8894–8896.
- Roux, P.P., Topisirovic, I., 2012. Regulation of mRNA Translation by Signaling Pathways. *Cold Spring Harb Perspect Biol* 4, a012252.
- Roy, B., Jacobson, A., 2013. The intimate relationships of mRNA decay and translation. *Trends in Genetics* 29, 691–699.
- Rozpędek, W., Pytel, D., Mucha, B., Leszczyńska, H., Diehl, J.A., Majsterek, I., 2016. The Role of the PERK/eIF2 α /ATF4/CHOP Signaling Pathway in Tumor Progression During Endoplasmic Reticulum Stress. *Curr Mol Med* 16, 533–544.
- Rubio, A., Ghosh, S., Mülleder, M., Ralser, M., Mata, J., 2021. Ribosome profiling reveals ribosome stalling on tryptophan codons and ribosome queuing upon oxidative stress in fission yeast. *Nucleic Acids Research* 49, 383–399.

Reference

- Ruggiano, A., Ramadan, K., 2021a. DNA–protein crosslink proteases in genome stability. *Commun Biol* 4, 11.
- Ruggiano, A., Ramadan, K., 2021b. The Trinity of SPRTN Protease Regulation. *Trends in Biochemical Sciences* 46, 2–4.
- Ruggiano, A., Vaz, B., Kilgas, S., Popović, M., Rodriguez-Berriguete, G., Singh, A.N., Higgins, G.S., Kiltie, A.E., Ramadan, K., 2021. The protease SPRTN and SUMOylation coordinate DNA-protein crosslink repair to prevent genome instability. *Cell Reports* 37, 110080.
- Ruijs, M.W.G., van Andel, R.N.J., Oshima, J., Madan, K., Nieuwint, A.W.M., Aalfs, C.M., 2003. Atypical progeroid syndrome: an unknown helicase gene defect? *Am J Med Genet A* 116A, 295–299.
- Rutkowski, D.T., Arnold, S.M., Miller, C.N., Wu, J., Li, J., Gunnison, K.M., Mori, K., Sadighi Akha, A.A., Raden, D., Kaufman, R.J., 2006. Adaptation to ER stress is mediated by differential stabilities of pro-survival and pro-apoptotic mRNAs and proteins. *PLoS Biol* 4, e374.
- Saito, S., Hosoda, N., Hoshino, S., 2013. The Hbs1-Dom34 Protein Complex Functions in Non-stop mRNA Decay in Mammalian Cells *. *Journal of Biological Chemistry* 288, 17832–17843.
- Sale, J.E., 2013. Translesion DNA Synthesis and Mutagenesis in Eukaryotes. *Cold Spring Harbor Perspectives in Biology* 5, a012708–a012708.
- Salem, A.M.H., Nakano, T., Takuwa, M., Matoba, N., Tsuboi, T., Terato, H., Yamamoto, K., Yamada, M., Nohmi, T., Ide, H., 2009. Genetic Analysis of Repair and Damage Tolerance Mechanisms for DNA-Protein Cross-Links in *Escherichia coli*. *Journal of Bacteriology* 191, 5657–5668.
- Sallmyr, A., Tomkinson, A.E., 2018. Repair of DNA double-strand breaks by mammalian alternative end-joining pathways. *J Biol Chem* 293, 10536–10546.
- Sancar, A., 1996. Dna Excision Repair. *Annual Review of Biochemistry* 65, 43–81.
- Santi, D.V., Norment, A., Garrett, C.E., 1984. Covalent bond formation between a DNA-cytosine methyltransferase and DNA containing 5-azacytosine. *Proceedings of the National Academy of Sciences* 81, 6993–6997.
- Sasaki, A.T., Carracedo, A., Locasale, J.W., Anastasiou, D., Takeuchi, K., Kahoud, E.R., Haviv, S., Asara, J.M., Pandolfi, P.P., Cantley, L.C., 2011. Ubiquitination of Ras enhances activation and facilitates binding to select downstream effectors. *SciSignal*. 4(163): ra13

Reference

- Scaggiante, B., Dapas, B., Farra, R., Tonon, F., Abrami, M., Grassi, M., Musiani, F., Zanconati, F., Pozzato, G., Grassi, G., 2014. Translation and Its Regulation in Cancer Biology and Medicine. Springer Netherlands, Dordrecht, pp. 241–265.
- Schellenberg, M.J., Lieberman, J.A., Herrero-Ruiz, A., Butler, L.R., Williams, J.G., Muñoz-Cabello, A.M., Mueller, G.A., London, R.E., Cortés-Ledesma, F., Williams, R.S., 2017. ZATT (ZNF451)-mediated resolution of topoisomerase 2 DNA-protein cross-links. *Science* 357, 1412–1416.
- Schmid, M., Jensen, T.H., 2008. The exosome: a multipurpose RNA-decay machine. *Trends in Biochemical Sciences* 33, 501–510.
- Schmidt, C., Beilsten-Edmands, V., Robinson, C.V., 2016. Insights into Eukaryotic Translation Initiation from Mass Spectrometry of Macromolecular Protein Assemblies. *Journal of Molecular Biology, Study of biomolecules and biological systems: Proteins* 428, 344–356.
- Schoof, M., Boone, M., Wang, L., Lawrence, R., Frost, A., Walter, P., 2021. eIF2B conformation and assembly state regulate the integrated stress response. *eLife* 10, e65703.
- Schwertman, P., Bekker-Jensen, S., Mailand, N., 2016. Regulation of DNA double-strand break repair by ubiquitin and ubiquitin-like modifiers. *Nat Rev Mol Cell Biol* 17, 379–394.
- Schwertman, P., Lagarou, A., Dekkers, D.H.W., Raams, A., van der Hoek, A.C., Laffeber, C., Hoeijmakers, J.H.J., Demmers, J.A.A., Fouteri, M., Vermeulen, W., Marteijn, J.A., 2012. UV-sensitive syndrome protein UVSSA recruits USP7 to regulate transcription-coupled repair. *Nat Genet* 44, 598–602.
- Scrima, A., Koníčková, R., Czyzewski, B.K., Kawasaki, Y., Jeffrey, P.D., Groisman, R., Nakatani, Y., Iwai, S., Pavletich, N.P., Thomä, N.H., 2008. Structural Basis of UV DNA-Damage Recognition by the DDB1–DDB2 Complex. *Cell* 135, 1213–1223.
- Semlow, D.R., Walter, J.C., 2021. Mechanisms of Vertebrate DNA Interstrand Cross-Link Repair. *Annu. Rev. Biochem.* 90, 107–135.
- Serbyn, N., Bagdiul, I., Noireterre, A., Michel, A.H., Suhandynata, R.T., Zhou, H., Kornmann, B., Stutz, F., 2021. SUMO orchestrates multiple alternative DNA-protein crosslink repair pathways. *Cell Reports* 37, 110034.
- Serbyn, N., Noireterre, A., Bagdiul, I., Plank, M., Michel, A.H., Loewith, R., Kornmann, B., Stutz, F., 2020. The Aspartic Protease Ddi1 Contributes to DNA-Protein Crosslink Repair in Yeast. *Molecular Cell* 77, 1066-1079.e9.

Reference

- Serdar, L.D., Whiteside, D.L., Baker, K.E., 2016. ATP hydrolysis by UPF1 is required for efficient translation termination at premature stop codons. *Nat Commun* 7, 14021.
- Sergiev, P.V., Lavrik, I.N., Dokudovskaya, S.S., Dontsova, O.A., Bogdanov, A.A., 1998. Structure of the decoding center of the ribosome. *Biochemistry (Mosc)* 63, 963–976.
- Shaham, J., Bomstein, Y., Melzer, A., Ribak, J., 1997. DNA–Protein Crosslinks and Sister Chromatid Exchanges as Biomarkers of Exposure to Formaldehyde. *International Journal of Occupational and Environmental Health* 3, 95–104.
- Shao, S., Brown, A., Santhanam, B., Hegde, R.S., 2015. Structure and Assembly Pathway of the Ribosome Quality Control Complex. *Molecular Cell* 57, 433–444.
- Shao, S., Murray, J., Brown, A., Taunton, J., Ramakrishnan, V., Hegde, R.S., 2016. Decoding Mammalian Ribosome-mRNA States by Translational GTPase Complexes. *Cell* 167, 1229-1240.e15.
- Shao, S., von der Malsburg, K., Hegde, R.S., 2013. Listerin-dependent nascent protein ubiquitination relies on ribosome subunit dissociation. *Mol Cell* 50, 637–648.
- Shapiro, R., Yamaguchi, H., 1972. Nucleic acid reactivity and conformation I. Deamination of cytosine by nitrous acid. *Biochimica et Biophysica Acta (BBA) - Nucleic Acids and Protein Synthesis* 281, 501–506.
- Sharp, S.J., Schaack, J., Cooley, L., Burke, D.J., Soil, D., 1985. Structure and Transcription of Eukaryotic tRNA Gene. *Critical Reviews in Biochemistry* 19, 107–144.
- Shatkin, A.J., Manley, J.L., 2000. The ends of the affair: capping and polyadenylation. *Nat Struct Biol* 7, 838–842.
- Shen, J.C., Rideout, W.M., Jones, P.A., 1994. The rate of hydrolytic deamination of 5-methylcytosine in double-stranded DNA. *Nucleic Acids Res* 22, 972–976.
- Shen, P.S., Park, J., Qin, Y., Li, X., Parsawar, K., Larson, M.H., Cox, J., Cheng, Y., Lambowitz, A.M., Weissman, J.S., Brandman, O., Frost, A., 2015. Protein synthesis. Rqc2p and 60S ribosomal subunits mediate mRNA-independent elongation of nascent chains. *Science* 347, 75–78.
- Shen, X., Wang, R., Kim, M.J., Hu, Q., Hsu, C.-C., Yao, J., Klages-Mundt, N., Tian, Y., Lynn, E., Brewer, T.F., Zhang, Y., Arun, B., Gan, B., Andreeff, M., Takeda, S., Chen, J., Park, J., Shi, X., Chang, C.J., Jung, S.Y., Qin, J., Li, L., 2020. A Surge of DNA Damage Links Transcriptional Reprogramming and Hematopoietic Deficit in Fanconi Anemia. *Molecular Cell* 80, 1013-1024.e6.

Reference

Sherker, A., Chaudhary, N., Adam, S., 2021. Two redundant ubiquitin-dependent pathways of BRCA1 localization to DNA damage sites. *EMBO reports* 22, e53679.

Shifrin, V.I., Anderson, P., 1999. Trichothecene Mycotoxins Trigger a Ribotoxic Stress Response That Activates c-Jun N-terminal Kinase and p38 Mitogen-activated Protein Kinase and Induces Apoptosis *. *Journal of Biological Chemistry* 274, 13985–13992.

Shimamura, A., de Oca, R.M., Svenson, J.L., Haining, N., Moreau, L.A., Nathan, D.G., D'Andrea, A.D., 2002. A novel diagnostic screen for defects in the Fanconi anemia pathway. *Blood* 100, 4649–4654.

Shoemaker, C.J., Eyler, D.E., Green, R., 2010. Dom34:Hbs1 promotes subunit dissociation and peptidyl-tRNA drop-off to initiate no-go decay. *Science* 330, 369–372.

Shoemaker, C.J., Green, R., 2012. Translation drives mRNA quality control. *Nat Struct Mol Biol* 19, 594–601.

Shrestha, R.K., Ronau, J.A., Davies, C.W., Guenette, R.G., Strieter, E.R., Paul, L.N., Das, C., 2014. Insights into the Mechanism of Deubiquitination by JAMM Deubiquitinases from Cocystal Structures of the Enzyme with the Substrate and Product. *Biochemistry* 53, 3199–3217.

Shrivastav, N., Li, D., Essigmann, J.M., 2010. Chemical biology of mutagenesis and DNA repair: cellular responses to DNA alkylation. *Carcinogenesis* 31, 59–70.

Shuker, D.E.G., Margison, G.P., 1997. Nitrosated Glycine Derivatives as a Potential Source of O6-Methylguanine in DNA. *Cancer Res* 57, 366–369.

Simms, C.L., Thomas, E.N., Zaher, H.S., 2017a. Ribosome-based quality control of mRNA and nascent peptides. *Wiley Interdiscip Rev RNA* 8, 10.1002.

Simms, C.L., Yan, L.L., Zaher, H.S., 2017b. Ribosome Collision Is Critical for Quality Control during No-Go Decay. *Molecular Cell* 68, 361-373.e5.

Simpson, L.J., Ross, A., Szüts, D., Alviani, C.A., Oestergaard, V.H., Patel, K.J., Sale, J.E., 2006. RAD18 - independent ubiquitination of proliferating - cell nuclear antigen in the avian cell line DT40. *EMBO Rep* 7, 927–932.

Singh, S., Vanden Broeck, A., Miller, L., Chaker-Margot, M., Klinge, S., 2021. Nucleolar maturation of the human small subunit processome. *Science* 373, eabj5338.

Sinha, N.K., Ordureau, A., Best, K., Saba, J.A., Zinshteyn, B., Sundaramoorthy, E., Fulzele, A., Garshott, D.M., Denk, T., Thoms, M., Paulo, J.A., Harper, J.W., Bennett,

Reference

- E.J., Beckmann, R., Green, R., 2020. EDF1 coordinates cellular responses to ribosome collisions. *eLife* 9, e58828.
- Sitron, C.S., Brandman, O., 2020. Detection and Degradation of Stalled Nascent Chains via Ribosome-Associated Quality Control. *Annu. Rev. Biochem.* 89, 417–442.
- Sitron, C.S., Brandman, O., 2019. CAT tails drive degradation of stalled polypeptides on and off the ribosome. *Nat Struct Mol Biol* 26, 450–459.
- Siu, F., Bain, P.J., LeBlanc-Chaffin, R., Chen, H., Kilberg, M.S., 2002. ATF4 Is a Mediator of the Nutrient-sensing Response Pathway That Activates the Human Asparagine Synthetase Gene *. *Journal of Biological Chemistry* 277, 24120–24127.
- Smela, M.E., Currier, S.S., Bailey, E.A., Essigmann, J.M., 2001. The chemistry and biology of aflatoxin B(1): from mutational spectrometry to carcinogenesis. *Carcinogenesis* 22, 535–545.
- Smogorzewska, A., Matsuoka, S., Vinciguerra, P., McDonald, E.R., Hurov, K.E., Luo, J., Ballif, B.A., Gygi, S.P., Hofmann, K., D’Andrea, A.D., Elledge, S.J., 2007. Identification of the FANCI Protein, a Monoubiquitinated FANCD2 Paralog Required for DNA Repair. *Cell* 129, 289–301.
- Sobhian, B., Shao, G., Lilli, D.R., Culhane, A.C., Moreau, L.A., Xia, B., Livingston, D.M., Greenberg, R.A., 2007. RAP80 Targets BRCA1 to Specific Ubiquitin Structures at DNA Damage Sites. *Science* 316, 1198–1202.
- Solomon, M.J., Larsen, P.L., Varshavsky, A., 1988. Mapping protein-DNA interactions in vivo with formaldehyde: Evidence that histone H4 is retained on a highly transcribed gene. *Cell* 53, 937–947.
- Song, L., Luo, Z.-Q., 2019. Post-translational regulation of ubiquitin signaling. *J Cell Biol* 218, 1776–1786.
- Spahn, C.M., GomezLorenzo, M.G., Grassucci, R.A., 2004. Domain movements of elongation factor eEF2 and the eukaryotic 80S ribosome facilitate tRNA translocation. *The EMBO Journal* 23, 1008–1019.
- Sparks, J.L., Chistol, G., Gao, A.O., Räschele, M., Larsen, N.B., Mann, M., Duxin, J.P., Walter, J.C., 2019. The CMG Helicase Bypasses DNA-Protein Cross-Links to Facilitate Their Repair. *Cell* 176, 167-181.e21.
- Spielmann, M., Kakar, N., Tayebi, N., Leettola, C., Nürnberg, G., Sowada, N., Lupiáñez, D.G., Harabula, I., Flöttmann, R., Horn, D., Chan, W.L., Wittler, L., Yilmaz, R., Altmüller, J., Thiele, H., van Bokhoven, H., Schwartz, C.E., Nürnberg, P., Bowie, J.U., Ahmad, J., Kubisch, C., Mundlos, S., Borck, G., 2016. Exome sequencing and

Reference

- CRISPR/Cas genome editing identify mutations of ZAK as a cause of limb defects in humans and mice. *Genome Res* 26, 183–191.
- Spivak, G., 2015. Nucleotide excision repair in humans. *DNA Repair (Amst)* 36, 13–18.
- Starita, L.M., Horwitz, A.A., Keogh, M.-C., Ishioka, C., Parvin, J.D., Chiba, N., 2005. BRCA1/BARD1 ubiquitinate phosphorylated RNA polymerase II. *J Biol Chem* 280, 24498–24505.
- Stein, K.C., Morales-Polanco, F., van der Lienden, J., Rainbolt, T.K., Frydman, J., 2022. Ageing exacerbates ribosome pausing to disrupt cotranslational proteostasis. *Nature* 601(7894), 637-642.
- Steinacher, R., Osman, F., Lorenz, A., Bryer, C., Whitby, M.C., 2013. Slx8 Removes Pli1-Dependent Protein-SUMO Conjugates Including SUMOylated Topoisomerase I to Promote Genome Stability. *PLOS ONE* 8, e71960.
- Stewart, G.S., Wang, B., Bignell, C.R., Taylor, A.M.R., Elledge, S.J., 2003. MDC1 is a mediator of the mammalian DNA damage checkpoint. *Nature* 421, 961–966.
- Stewart, L., Redinbo, M.R., Qiu, X., Hol, W.G.J., Champoux, J.J., 1998. A Model for the Mechanism of Human Topoisomerase I. *Science* 279, 1534–1541.
- Stingele, J., Bellelli, R., Alte, F., Hewitt, G., Sarek, G., Maslen, S.L., Tsutakawa, S.E., Borg, A., Kjær, S., Tainer, J.A., Skehel, J.M., Groll, M., Boulton, S.J., 2016. Mechanism and Regulation of DNA-Protein Crosslink Repair by the DNA-Dependent Metalloprotease SPRTN. *Molecular Cell* 64, 688–703.
- Stingele, J., Bellelli, R., Boulton, S.J., 2017. Mechanisms of DNA–protein crosslink repair. *Nat Rev Mol Cell Biol* 18, 563–573.
- Stingele, J., Habermann, B., Jentsch, S., 2015. DNA–protein crosslink repair: proteases as DNA repair enzymes. *Trends in Biochemical Sciences* 40, 67–71.
- Stingele, J., Jentsch, S., 2015. DNA–protein crosslink repair. *Nat Rev Mol Cell Biol* 16, 455–460.
- Stingele, J., Schwarz, M.S., Bloemeke, N., Wolf, P.G., Jentsch, S., 2014. A DNA-Dependent Protease Involved in DNA-Protein Crosslink Repair. *Cell* 158, 327–338.
- Stohr, B.A., Kreuzer, K.N., 2001. Repair of topoisomerase-mediated DNA damage in bacteriophage T4. *Genetics* 158, 19–28.
- Stolz, A., Ernst, A., Dikic, I., 2014. Cargo recognition and trafficking in selective autophagy. *Nat Cell Biol* 16, 495–501.

Reference

- Stoneley, M., Harvey, R.F., Mulroney, T.E., Mordue, R., Jukes-Jones, R., Cain, K., Lilley, K.S., Sawarkar, R., Willis, A.E., 2022. Unresolved stalled ribosome complexes restrict cell-cycle progression after genotoxic stress. *Molecular Cell* 82, 1–16.
- Stucki, M., Clapperton, J.A., Mohammad, D., Yaffe, M.B., Smerdon, S.J., Jackson, S.P., 2005. MDC1 Directly Binds Phosphorylated Histone H2AX to Regulate Cellular Responses to DNA Double-Strand Breaks. *Cell* 123, 1213–1226.
- Su, D., Ma, S., Shan, L., Wang, Yue, Wang, Yuejiao, Cao, C., Liu, B., Yang, C., Wang, L., Tian, S., Ding, X., Liu, X., Yu, N., Song, N., Liu, L., Yang, S., Zhang, Q., Yang, F., Zhang, K., Shi, L., 2018. Ubiquitin-specific protease 7 sustains DNA damage response and promotes cervical carcinogenesis. *J Clin Invest* 128, 4280–4296.
- Su, T., Izawa, T., Thoms, M., Yamashita, Y., Cheng, J., Berninghausen, O., Hartl, F.U., Inada, T., Neupert, W., Beckmann, R., 2019. Structure and function of Vms1 and Arb1 in RQC and mitochondrial proteome homeostasis. *Nature* 570, 538–542.
- Su, Y.-T., Gao, C., Liu, Y., Guo, S., Wang, A., Wang, B., Erdjument-Bromage, H., Miyagi, M., Tempst, P., Kao, H.-Y., 2013. Monoubiquitination of Filamin B Regulates Vascular Endothelial Growth Factor-Mediated Trafficking of Histone Deacetylase 7. *Mol Cell Biol* 33, 1546–1560.
- Sugasawa, K., Ng, J.M.Y., Masutani, C., Iwai, S., van der Spek, P.J., Eker, A.P.M., Hanaoka, F., Bootsma, D., Hoeijmakers, J.H.J., 1998. Xeroderma Pigmentosum Group C Protein Complex Is the Initiator of Global Genome Nucleotide Excision Repair. *Molecular Cell* 2, 223–232.
- Sugasawa, K., Okuda, Y., Saijo, M., Nishi, R., Matsuda, N., Chu, G., Mori, T., Iwai, S., Tanaka, Keiji, Tanaka, Kiyoji, Hanaoka, F., 2005. UV-Induced Ubiquitylation of XPC Protein Mediated by UV-DDB-Ubiquitin Ligase Complex. *Cell* 121, 387–400.
- Sun, Y., Miller Jenkins, L.M., Su, Y.P., Nitiss, K.C., Nitiss, J.L., Pommier, Y., 2020a. A conserved SUMO pathway repairs topoisomerase DNA-protein cross-links by engaging ubiquitin-mediated proteasomal degradation. *Sci. Adv.* 6, eaba6290.
- Sun, Y., Saha, S., Wang, W., Saha, L.K., Huang, S.-Y.N., Pommier, Y., 2020b. Excision Repair of Topoisomerase DNA-Protein Crosslinks (TOP-DPC). *DNA Repair (Amst)* 89, 102837.
- Sundaramoorthy, E., Leonard, M., Mak, R., Liao, J., Fulzele, A., Bennett, E.J., 2017. ZNF598 and RACK1 Regulate Mammalian Ribosome-Associated Quality Control Function by Mediating Regulatory 40S Ribosomal Ubiquitylation. *Molecular Cell* 65, 751-760.e4.

Reference

- Sung, J.-S., Demple, B., 2006. Roles of base excision repair subpathways in correcting oxidized abasic sites in DNA. *The FEBS Journal* 273, 1620–1629.
- Svilar, D., Goellner, E.M., Almeida, K.H., Sobol, R.W., 2011. Base Excision Repair and Lesion-Dependent Subpathways for Repair of Oxidative DNA Damage. *Antioxidants & Redox Signaling* 14, 2491–2507.
- Svoboda, M., Konvalinka, J., Trempe, J.-F., Grantz Saskova, K., 2019. The yeast proteases Ddi1 and Wss1 are both involved in the DNA replication stress response. *DNA Repair* 80, 45–51.
- Szyfter, K., Hemminki, K., Szyfter, W., Szmeja, Z., Banaszewski, J., Pabiszczak, M., 1996. Tobacco smoke-associated *N* 7-alkylguanine in DNA of larynx tissue and leucocytes. *Carcinogenesis* 17, 501–506.
- Takahata, C., Masuda, Y., Takedachi, A., Tanaka, K., Iwai, S., Kuraoka, I., 2015. Repair synthesis step involving ERCC1-XPF participates in DNA repair of the Top1-DNA damage complex. *CARCIN* 36, 841–851.
- Takashima, H., Boerkoel, C.F., John, J., Saifi, G.M., Salih, M.A.M., Armstrong, D., Mao, Y., Quiocho, F.A., Roa, B.B., Nakagawa, M., Stockton, D.W., Lupski, J.R., 2002. Mutation of TDP1, encoding a topoisomerase I-dependent DNA damage repair enzyme, in spinocerebellar ataxia with axonal neuropathy. *Nat Genet* 32, 267–272.
- Takeshita, T., Wu, W., Koike, A., Fukuda, M., Ohta, T., 2009. Perturbation of DNA repair pathways by proteasome inhibitors corresponds to enhanced chemosensitivity of cells to DNA damage-inducing agents. *Cancer Chemother Pharmacol* 64, 1039–1046.
- Talpaert-Borlè, M., 1987. Formation, detection and repair of AP sites. *Mutation Research/Fundamental and Molecular Mechanisms of Mutagenesis* 181, 45–56.
- Tan, W., Deans, A.J., 2021. The ubiquitination machinery of the Fanconi Anemia DNA repair pathway. *Progress in Biophysics and Molecular Biology* 163, 5–13.
- Tan, W., van Twest, S., Leis, A., Bythell-Douglas, R., Murphy, V.J., Sharp, M., Parker, M.W., Crismani, W., Deans, A.J., 2020. Monoubiquitination by the human Fanconi anemia core complex clamps FANCI:FANCD2 on DNA in filamentous arrays. *eLife* 9, e54128.
- Tang, J., Chu, G., 2002. Xeroderma pigmentosum complementation group E and UV-damaged DNA-binding protein. *DNA Repair (Amst)* 1, 601–616.

Reference

Taniguchi, T., Garcia-Higuera, I., Xu, B., Andreassen, P.R., Gregory, R.C., Kim, S.-T., Lane, W.S., Kastan, M.B., D'Andrea, A.D., 2002. Convergence of the Fanconi Anemia and Ataxia Telangiectasia Signaling Pathways. *Cell* 109, 459–472.

Taylor, D.J., Nilsson, J., Merrill, A.R., 2007. Structures of modified eEF2-80S ribosome complexes reveal the role of GTP hydrolysis in translocation. *The EMBO Journal* 26, 2421–2431.

Teng, S., Beard, K., Pourahmad, J., Moridani, M., Easson, E., Poon, R., O'Brien, P.J., 2001. The formaldehyde metabolic detoxification enzyme systems and molecular cytotoxic mechanism in isolated rat hepatocytes. *Chemico-Biological Interactions* 130–132, 285–296.

Terai, K., Abbas, T., Jazaeri, A.A., Dutta, A., 2010. CRL4Cdt2 E3 Ubiquitin Ligase Monoubiquitinates PCNA to Promote Translesion DNA Synthesis. *Molecular Cell* 37, 143–149.

Thorslund, T., Ripplinger, A., Hoffmann, S., Wild, T., Uckelmann, M., Villumsen, B., Narita, T., Sixma, T.K., Choudhary, C., Bekker-Jensen, S., Mailand, N., 2015. Histone H1 couples initiation and amplification of ubiquitin signalling after DNA damage. *Nature* 527, 389–393.

Tian, X., Zhang, S., Zhou, L., Seyhan, A.A., Hernandez Borrero, L., Zhang, Y., El-Deiry, W.S., 2021. Targeting the Integrated Stress Response in Cancer Therapy. *Frontiers in Pharmacology* 12:747837.

Tong, Z., Zhang, J., Luo, W., Wang, W., Li, F., Li, H., Luo, H., Lu, J., Zhou, J., Wan, Y., He, R., 2011. Urine formaldehyde level is inversely correlated to mini mental state examination scores in senile dementia. *Neurobiology of Aging* 32, 31–41.

Tong, Z.-B., Ai, H.-S., Li, J.-B., 2020. The Mechanism of Chromatin Remodeler SMARCAD1/Fun30 in Response to DNA Damage. *Frontiers in Cell and Developmental Biology* 8:560098.

Torgovnick, A., Schumacher, B., 2015. DNA repair mechanisms in cancer development and therapy. *Frontiers in Genetics* 6:157.

Trendel, J., Schwarzl, T., Horos, R., Prakash, A., Bateman, A., Hentze, M.W., Krijgsveld, J., 2019. The Human RNA-Binding Proteome and Its Dynamics during Translational Arrest. *Cell* 176, 391-403.e19.

Tsuboi, T., Kuroha, K., Kudo, K., Makino, S., Inoue, E., Kashima, I., Inada, T., 2012. Dom34:Hbs1 Plays a General Role in Quality-Control Systems by Dissociation of a Stalled Ribosome at the 3' End of Aberrant mRNA. *Molecular Cell* 46, 518–529.

Reference

- Tsuda, M., Kitamasu, K., Hosokawa, S., Nakano, T., Ide, H., 2020. Repair of trapped topoisomerase II covalent cleavage complexes: Novel proteasome-independent mechanisms. *Nucleosides, Nucleotides & Nucleic Acids* 39, 170–184.
- Tubbs, A., Nussenzweig, A., 2017. Endogenous DNA Damage as a Source of Genomic Instability in Cancer. *Cell* 168, 644–656.
- Tufegdžić Vidaković, A., Mitter, R., Kelly, G.P., Neumann, M., Harreman, M., Rodríguez-Martínez, M., Herlihy, A., Weems, J.C., Boeing, S., Encheva, V., Gaul, L., Milligan, L., Tollervey, D., Conaway, R.C., Conaway, J.W., Snijders, A.P., Stewart, A., Svejstrup, J.Q., 2020. Regulation of the RNAPII Pool Is Integral to the DNA Damage Response. *Cell* 180, 1245-1261.e21.
- Turcu, F.E.R., Ventii, K.H., Wilkinson, K.D., 2009. Regulation and Cellular Roles of Ubiquitin-specific Deubiquitinating Enzymes. *Annu Rev Biochem* 78, 363–397.
- Ule, J., Hwang, H.-W., Darnell, R.B., 2018. The Future of Cross-Linking and Immunoprecipitation (CLIP). *Cold Spring Harb Perspect Biol* 10, a032243.
- Ule, J., Jensen, K.B., Ruggiu, M., Mele, A., Ule, A., Darnell, R.B., 2003. CLIP Identifies Nova-Regulated RNA Networks in the Brain. *Science* 302, 1212–1215.
- Ulirsch, J.C., Verboon, J.M., Kazerounian, S., Guo, M.H., Yuan, D., Ludwig, L.S., Handsaker, R.E., Abdulhay, N.J., Fiorini, C., Genovese, G., Lim, E.T., Cheng, A., Cummings, B.B., Chao, K.R., Beggs, A.H., Genetti, C.A., Sieff, C.A., Newburger, P.E., Niewiadomska, E., Matysiak, M., Vlachos, A., Lipton, J.M., Atsidaftos, E., Glader, B., Narla, A., Gleizes, P.-E., O'Donohue, M.-F., Montel-Lehry, N., Amor, D.J., McCarroll, S.A., O'Donnell-Luria, A.H., Gupta, N., Gabriel, S.B., MacArthur, D.G., Lander, E.S., Lek, M., Da Costa, L., Nathan, D.G., Korostelev, A.A., Do, R., Sankaran, V.G., Gazda, H.T., 2018. The Genetic Landscape of Diamond-Blackfan Anemia. *Am J Hum Genet* 103, 930–947.
- Unger, S., Gónna, M.W., Le Béhec, A., Do Vale-Pereira, S., Bedeschi, M.F., Geiberger, S., Grigelioniene, G., Horemuzova, E., Lalatta, F., Lausch, E., Magnani, C., Nampoothiri, S., Nishimura, G., Petrella, D., Rojas-Ringeling, F., Utsunomiya, A., Zabel, B., Pradervand, S., Harshman, K., Campos-Xavier, B., Bonafé, L., Superti-Furga, G., Stevenson, B., Superti-Furga, A., 2013. FAM111A Mutations Result in Hypoparathyroidism and Impaired Skeletal Development. *The American Journal of Human Genetics* 92, 990–995.
- Unk, I., Hajdú, I., Fátyol, K., Hurwitz, J., Yoon, J.-H., Prakash, L., Prakash, S., Haracska, L., 2008. Human HLTF functions as a ubiquitin ligase for proliferating cell nuclear antigen polyubiquitination. *Proceedings of the National Academy of Sciences* 105, 3768–3773.

Reference

Unk, I., Hajdú, I., Fátyol, K., Szakál, B., Blastyák, A., Bermudez, V., Hurwitz, J., Prakash, L., Prakash, S., Haracska, L., 2006. Human SHPRH is a ubiquitin ligase for Mms2–Ubc13-dependent polyubiquitylation of proliferating cell nuclear antigen. *Proceedings of the National Academy of Sciences* 103, 18107–18112.

Unterholzner, L., Izaurralde, E., 2004. SMG7 Acts as a Molecular Link between mRNA Surveillance and mRNA Decay. *Molecular Cell* 16, 587–596.

Urdaneta, E.C., Vieira-Vieira, C.H., Hick, T., Wessels, H.-H., Figini, D., Moschall, R., Medenbach, J., Ohler, U., Granneman, S., Selbach, M., Beckmann, B.M., 2019. Purification of cross-linked RNA-protein complexes by phenol-toluol extraction. *Nat Commun* 10, 990.

Valadkhan, S., Gunawardane, L.S., 2013. Role of small nuclear RNAs in eukaryotic gene expression. *Essays in Biochemistry* 54, 79–90.

Valles, G.J., Bezsonova, I., Woodgate, R., Ashton, N.W., 2020. USP7 Is a Master Regulator of Genome Stability. *Frontiers in Cell and Developmental Biology* 8:717.

van Cuijk, L., van Belle, G.J., Turkyilmaz, Y., Poulsen, S.L., Janssens, R.C., Theil, A.F., Sabatella, M., Lans, H., Mailand, N., Houtsmuller, A.B., Vermeulen, W., Marteijn, J.A., 2015. SUMO and ubiquitin-dependent XPC exchange drives nucleotide excision repair. *Nat Commun* 6, 7499.

van den Boom, J., Meyer, H., 2018. VCP/p97-Mediated Unfolding as a Principle in Protein Homeostasis and Signaling. *Molecular Cell* 69, 182–194.

van der Weegen, Y., de Lint, K., van den Heuvel, D., Nakazawa, Y., Mevissen, T.E.T., van Schie, J.J.M., San Martin Alonso, M., Boer, D.E.C., González-Prieto, R., Narayanan, I.V., Klaassen, N.H.M., Wondergem, A.P., Roohollahi, K., Dorsman, J.C., Hara, Y., Vertegaal, A.C.O., de Lange, J., Walter, J.C., Noordermeer, S.M., Ljungman, M., Ogi, T., Wolthuis, R.M.F., Luijsterburg, M.S., 2021. ELOF1 is a transcription-coupled DNA repair factor that directs RNA polymerase II ubiquitylation. *Nat Cell Biol* 23, 595–607.

van der Weegen, Y., Golan-Berman, H., Mevissen, T.E.T., Apelt, K., González-Prieto, R., Goedhart, J., Heilbrun, E.E., Vertegaal, A.C.O., van den Heuvel, D., Walter, J.C., Adar, S., Luijsterburg, M.S., 2020. The cooperative action of CSB, CSA, and UVSSA target TFIIH to DNA damage-stalled RNA polymerase II. *Nat Commun* 11, 2104.

van Hoof, A., Frischmeyer, P.A., Dietz, H.C., Parker, R., 2002. Exosome-Mediated Recognition and Degradation of mRNAs Lacking a Termination Codon. *Science* 295, 2262–2264.

Reference

- Vattem, K.M., Wek, R.C., 2004. Reinitiation involving upstream ORFs regulates ATF4 mRNA translation in mammalian cells. *Proceedings of the National Academy of Sciences* 101, 11269–11274.
- Vaz, B., Popovic, M., Newman, J.A., Fielden, J., Aitkenhead, H., Halder, S., Singh, A.N., Vendrell, I., Fischer, R., Torrecilla, I., Drobnitzky, N., Freire, R., Amor, D.J., Lockhart, P.J., Kessler, B.M., McKenna, G.W., Gileadi, O., Ramadan, K., 2016. Metalloprotease SPRTN/DVC1 Orchestrates Replication-Coupled DNA-Protein Crosslink Repair. *Molecular Cell* 64, 704–719.
- Vaz, B., Popovic, M., Ramadan, K., 2017. DNA–Protein Crosslink Proteolysis Repair. *Trends in Biochemical Sciences* 42, 483–495.
- Verma, R., Oania, R.S., Kolawa, N.J., Deshaies, R.J., 2013. Cdc48/p97 promotes degradation of aberrant nascent polypeptides bound to the ribosome. *eLife* 2, e00308.
- Verma, R., Reichermeier, K.M., Burroughs, A.M., Oania, R.S., Reitsma, J.M., Aravind, L., Deshaies, R.J., 2018. Vms1 and ANKZF1 peptidyl-tRNA hydrolases release nascent chains from stalled ribosomes. *Nature* 557, 446–451.
- Verma, S., Dixit, R., Pandey, K.C., 2016. Cysteine Proteases: Modes of Activation and Future Prospects as Pharmacological Targets. *Frontiers in Pharmacology* 7:107.
- Vind, A.C., Genzor, A.V., Bekker-Jensen, S., 2020a. Ribosomal stress-surveillance: three pathways is a magic number. *Nucleic Acids Research* 48, 10648–10661.
- Vind, A.C., Snieckute, G., Blasius, M., Tiedje, C., Krogh, N., Bekker-Jensen, D.B., Andersen, K.L., Nordgaard, C., Tollenaere, M.A.X., Lund, A.H., Olsen, J.V., Nielsen, H., Bekker-Jensen, S., 2020b. ZAK α Recognizes Stalled Ribosomes through Partially Redundant Sensor Domains. *Molecular Cell* 78, 700-713.e7.
- Vítor, A.C., Huertas, P., Legube, G., de Almeida, S.F., 2020. Studying DNA Double-Strand Break Repair: An Ever-Growing Toolbox. *Frontiers in Molecular Biosciences* 7:24.
- Vujanovic, M., Krietsch, J., Raso, M.C., Terraneo, N., Zellweger, R., Schmid, J.A., Taglialatela, A., Huang, J.-W., Holland, C.L., Zwicky, K., Herrador, R., Jacobs, H., Cortez, D., Ciccia, A., Penengo, L., Lopes, M., 2017. Replication Fork Slowing and Reversal upon DNA Damage Require PCNA Polyubiquitination and ZRANB3 DNA Translocase Activity. *Molecular Cell* 67, 882-890.e5.
- Walden, H., Rittinger, K., 2018. RBR ligase–mediated ubiquitin transfer: a tale with many twists and turns. *Nat Struct Mol Biol* 25, 440–445.

Reference

- Walker, J.R., Corpina, R.A., Goldberg, J., 2001. Structure of the Ku heterodimer bound to DNA and its implications for double-strand break repair. *Nature* 412, 607–614.
- Wang, D., Farhana, A., 2022. Biochemistry, RNA Structure, in: StatPearls. StatPearls Publishing, Treasure Island (FL).
- Wang, J., Aroumougame, A., Lobrich, M., Li, Y., Chen, D., Chen, J., Gong, Z., 2014. PTIP associates with Artemis to dictate DNA repair pathway choice. *Genes Dev* 28, 2693–2698.
- Wang, J.C., 2002. Cellular roles of DNA topoisomerases: a molecular perspective. *Nat Rev Mol Cell Biol* 3, 430–440.
- Wang, M., Dingler, F.A., Patel, K.J., 2022. Genotoxic aldehydes in the hematopoietic system. *Blood* 139, 2119–2129.
- Wang, R., Wang, S., Dhar, A., Peralta, C., Pavletich, N.P., 2020. DNA clamp function of the monoubiquitinated Fanconi anaemia ID complex. *Nature* 580, 278–282.
- Wang, X., Andreassen, P.R., D'Andrea, A.D., 2004. Functional Interaction of Monoubiquitinated FANCD2 and BRCA2/FANCD1 in Chromatin. *Molecular and Cellular Biology* 24, 5850–5862.
- Wang, X., Jin, C., Tang, Y., Tang, L.-Y., Zhang, Y.E., 2013. Ubiquitination of Tumor Necrosis Factor Receptor-associated Factor 4 (TRAF4) by Smad Ubiquitination Regulatory Factor 1 (Smurf1) Regulates Motility of Breast Epithelial and Cancer Cells. *Journal of Biological Chemistry* 288, 21784–21792.
- Wang, X., Mader, M.M., Toth, J.E., Yu, X., Jin, N., Campbell, R.M., Smallwood, J.K., Christe, M.E., Chatterjee, A., Goodson, T., Vlahos, C.J., Matter, W.F., Bloem, L.J., 2005. Complete Inhibition of Anisomycin and UV Radiation but Not Cytokine Induced JNK and p38 Activation by an Aryl-substituted Dihydropyrrlopyrazole Quinoline and Mixed Lineage Kinase 7 Small Interfering RNA *. *Journal of Biological Chemistry* 280, 19298–19305.
- Wang, Y., Liu, L., Wu, C., Bulgar, A., Somoza, E., Zhu, W., Gerson, S.L., 2009. Direct Detection and Quantification of Abasic Sites for In Vivo Studies of DNA Damage and Repair. *Nucl Med Biol* 36, 975–983.
- Wang, Z., Kang, W., You, Y., Pang, J., Ren, H., Suo, Z., Liu, H., Zheng, Y., 2019. USP7: Novel Drug Target in Cancer Therapy. *Frontiers in Pharmacology* 10:427.
- Warner, J.R., McIntosh, K.B., 2009. How Common Are Extraribosomal Functions of Ribosomal Proteins? *Molecular Cell* 34, 3–11.

Reference

- Watanabe, K., Tateishi, S., Kawasuji, M., 2004. Rad18 guides pol η to replication stalling sites through physical interaction and PCNA monoubiquitination. *The EMBO Journal* 23, 3886–3896.
- Weber, F., Wagner, V., Rasmussen, S.B., Hartmann, R., Paludan, S.R., 2006. Double-stranded RNA is produced by positive-strand RNA viruses and DNA viruses but not in detectable amounts by negative-strand RNA viruses. *J Virol* 80, 5059–5064.
- Weber, J., Polo, S., Maspero, E., 2019. HECT E3 Ligases: A Tale With Multiple Facets. *Frontiers in Physiology* 10:370.
- Wei, X., Peng, Y., Bryan, C., Yang, K., 2021. Mechanisms of DNA–protein cross-link formation and repair. *Biochimica et Biophysica Acta (BBA) - Proteins and Proteomics* 1869, 140669.
- Weickert, P., Stinglele, J., 2022. DNA–Protein Crosslinks and Their Resolution. *Annu. Rev. Biochem.* 91, annurev-biochem-032620-105820.
- Weissinger, R., Heinold, L., Akram, S., Jansen, R.-P., Hermesh, O., 2021. RNA Proximity Labeling: A New Detection Tool for RNA–Protein Interactions. *Molecules* 26, 2270.
- Wek, R.C., 2018. Role of eIF2 α Kinases in Translational Control and Adaptation to Cellular Stress. *Cold Spring Harb Perspect Biol* 10, a032870.
- Wek, S.A., Zhu, S., Wek, R.C., 1995. The histidyl-tRNA synthetase-related sequence in the eIF-2 alpha protein kinase GCN2 interacts with tRNA and is required for activation in response to starvation for different amino acids. *Mol Cell Biol* 15, 4497–4506.
- Wells, S.E., Hillner, P.E., Vale, R.D., Sachs, A.B., 1998. Circularization of mRNA by Eukaryotic Translation Initiation Factors. *Molecular Cell* 2, 135–140.
- Weston, R., Peeters, H., Ahel, D., 2012. ZRANB3 is a structure-specific ATP-dependent endonuclease involved in replication stress response. *Genes Dev.* 26, 1558–1572.
- Wickramaratne, S., Ji, S., Mukherjee, S., Su, Y., Pence, M.G., Lior-Hoffmann, L., Fu, I., Broyde, S., Guengerich, F.P., Distefano, M., Schäerer, O.D., Sham, Y.Y., Tretyakova, N., 2016. Bypass of DNA-Protein Cross-links Conjugated to the 7-Deazaguanine Position of DNA by Translesion Synthesis Polymerases. *Journal of Biological Chemistry* 291, 23589–23603.

Reference

- Wilson, D.M., Barsky, D., 2001. The major human abasic endonuclease: formation, consequences and repair of abasic lesions in DNA. *Mutation Research/DNA Repair* 485, 283–307.
- Wilson, M.D., Harreman, M., Svejstrup, J.Q., 2013. Ubiquitylation and degradation of elongating RNA polymerase II: The last resort. *Biochimica et Biophysica Acta (BBA) - Gene Regulatory Mechanisms, RNA polymerase II Transcript Elongation* 1829, 151–157.
- Wood, R.D., 2010. Nucleotide excision repair proteins and interstrand crosslink repair. *Environ Mol Mutagen* 51, 520–526.
- Woodworth, D.L., Kreuzer, K.N., 1996. Bacteriophage T4 Mutants Hypersensitive to an Antitumor Agent That Induces Topoisomerase-DNA Cleavage Complexes. *Genetics* 143, 1081–1090.
- Wower, I., Wower, J., Meinke, M., Brimacombe, R., 1981. The use of 2-iminothiolane as an RNA-protein cross-linking agent in *Escherichia coli* ribosomes, and the localisation on 23S RNA of sites cross-linked to proteins L4, L6, L21, L23, L27 and L29. *Nucleic Acids Res* 9, 4285–4302.
- Woźniak, K., Walter, Z., 2000. Induction of DNA-Protein Cross-Links by Platinum Compounds. *Zeitschrift für Naturforschung C* 55, 731–736.
- Wu, C.C.-C., Peterson, A., Zinshteyn, B., Regot, S., Green, R., 2020. Ribosome Collisions Trigger General Stress Responses to Regulate Cell Fate. *Cell* 182, 404-416.e14.
- Wu, P.-Y., Hanlon, M., Eddins, M., Tsui, C., Rogers, R.S., Jensen, J.P., Matunis, M.J., Weissman, A.M., Wolberger, C.P., Pickart, C.M., 2003. A conserved catalytic residue in the ubiquitin-conjugating enzyme family. *The EMBO Journal* Vol. 22 No. 19 pp. 5241-5250.
- Wu, X., Brewer, G., 2012. The Regulation of mRNA Stability in Mammalian Cells: 2.0. *Gene* 500, 10–21.
- Wyatt, M.D., Pittman, D.L., 2006. Methylating agents and DNA repair responses: methylated bases and sources of strand breaks. *Chem Res Toxicol* 19, 1580–1594.
- Xia, B., Sheng, Q., Nakanishi, K., Ohashi, A., Wu, J., Christ, N., Liu, X., Jasin, M., Couch, F.J., Livingston, D.M., 2006. Control of BRCA2 cellular and clinical functions by a nuclear partner, PALB2. *Mol Cell* 22, 719–729.
- Yamaguchi, H., Uchihori, Y., Yasuda, N., Takada, M., Kitamura, H., 2005. Estimation of Yields of OH Radicals in Water Irradiated by Ionizing Radiation. *Journal of Radiation Research* 46, 333–341.

Reference

- Yan, L.L., Simms, C.L., McLoughlin, F., Vierstra, R.D., Zaher, H.S., 2019. Oxidation and alkylation stresses activate ribosome-quality control. *Nat Commun* 10, 5611.
- Yan, L.L., Zaher, H.S., 2019. How do cells cope with RNA damage and its consequences? *Journal of Biological Chemistry* 294, 15158–15171.
- Ye, N., Holmquist, G.P., O'Connor, T.R., 1998. Heterogeneous repair of N-methylpurines at the nucleotide level in normal human cells¹¹Edited by M. Yahiv. *Journal of Molecular Biology* 284, 269–285.
- Yip, M.C.J., Bodnar, N.O., Rapoport, T.A., 2020. Ddi1 is a ubiquitin-dependent protease. *Proc. Natl. Acad. Sci. U.S.A.* 117, 7776–7781.
- Yip, M.C.J., Shao, S., 2021. Detecting and Rescuing Stalled Ribosomes. *Trends in Biochemical Sciences* 46, 731–743.
- Youngman, E.M., He, S.L., Nikstad, L.J., Green, R., 2007. Stop Codon Recognition by Release Factors Induces Structural Rearrangement of the Ribosomal Decoding Center that Is Productive for Peptide Release. *Molecular Cell* 28, 533–543.
- Yu, J., Qin, B., Lou, Z., 2020. Ubiquitin and ubiquitin-like molecules in DNA double strand break repair. *Cell Biosci* 10, 13.
- Yu, S.-L., Kang, M.-S., Kim, H.-Y., Gorospe, C.M., Kim, T.-S., Lee, S.-K., 2014. The PCNA binding domain of Rad2p plays a role in mutagenesis by modulating the cell cycle in response to DNA damage. *DNA Repair* 16, 1–10.
- Yu, X., Fu, S., Lai, M., Baer, R., Chen, J., 2006. BRCA1 ubiquitinates its phosphorylation-dependent binding partner CtIP. *Genes Dev* 20, 1721–1726.
- Yuan, J., Ghosal, G., Chen, J., 2012. The HARP-like Domain-Containing Protein AH2/ZRANB3 Binds to PCNA and Participates in Cellular Response to Replication Stress. *Molecular Cell* 47, 410–421.
- Yun, B.H., Guo, J., Bellamri, M., Turesky, R.J., 2020. DNA Adducts: formation, biological effects, and new biospecimens for mass spectrometric measurements in humans. *Mass Spectrom Rev* 39, 55–82.
- Zagnoli-Vieira, G., Caldecott, K.W., 2020. Untangling trapped topoisomerases with tyrosyl-DNA phosphodiesterases. *DNA Repair* 94, 102900.
- Zaman, U., Richter, F.M., Hofele, R., Kramer, K., Sachsenberg, T., Kohlbacher, O., Lenz, C., Urlaub, H., 2015. Dithiothreitol (DTT) Acts as a Specific, UV-inducible Cross-linker in Elucidation of Protein-RNA Interactions. *Mol Cell Proteomics* 14, 3196–3210.

Reference

- Zeng, Z., Cortés-Ledesma, F., El Khamisy, S.F., Caldecott, K.W., 2011. TDP2/TTRAP Is the Major 5'-Tyrosyl DNA Phosphodiesterase Activity in Vertebrate Cells and Is Critical for Cellular Resistance to Topoisomerase II-induced DNA Damage. *Journal of Biological Chemistry* 286, 403–409.
- Zhang, H., Koch, C.J., Wallen, C.A., Wheeler, K.T., 1995. Radiation-induced DNA damage in tumors and normal tissues. III. Oxygen dependence of the formation of strand breaks and DNA-protein crosslinks. *Radiat Res* 142, 163–168.
- Zhang, H., Xiong, Y., Chen, J., 2020. DNA–protein cross-link repair: what do we know now? *Cell Biosci* 10, 3.
- Zhang, J., Zhou, W., Liu, Y., Liu, T., Li, C., Wang, L., 2018. Oncogenic role of microRNA-532-5p in human colorectal cancer via targeting of the 5'UTR of RUNX3. *Oncology Letters* 15, 7215–7220.
- Zhang, S., Chea, J., Meng, X., Zhou, Y., Lee, E.Y.C., Lee, M.Y.W.T., 2008. PCNA is ubiquitinated by RNF8. *Cell Cycle* 7, 3399–3404.
- Zhang, X., Horibata, K., Saijo, M., Ishigami, C., Ukai, A., Kanno, S., Tahara, H., Neilan, E.G., Honma, M., Nohmi, T., Yasui, A., Tanaka, K., 2012. Mutations in UVSSA cause UV-sensitive syndrome and destabilize ERCC6 in transcription-coupled DNA repair. *Nat Genet* 44, 593–597.
- Zhang, Y., Lu, H., 2009. Signaling to p53: Ribosomal Proteins Find Their Way. *Cancer Cell* 16, 369–377.
- Zhang, Y., Yuan, F., Presnell, S.R., Tian, K., Gao, Y., Tomkinson, A.E., Gu, L., Li, G.-M., 2005. Reconstitution of 5'-Directed Human Mismatch Repair in a Purified System. *Cell* 122, 693–705.
- Zhao, B., Rothenberg, E., Ramsden, D.A., Lieber, M.R., 2020. The molecular basis and disease relevance of non-homologous DNA end joining. *Nat Rev Mol Cell Biol* 21, 765–781.
- Zhao, F., Kim, W., Kloeber, J.A., Lou, Z., 2020. DNA end resection and its role in DNA replication and DSB repair choice in mammalian cells. *Exp Mol Med* 52, 1705–1714.
- Zhao, S., Kieser, A., Li, H.-Y., Reinking, H.K., Weickert, P., Euteneuer, S., Yaneva, D., Acampora, A.C., Götz, M.J., Feederle, R., Stingle, J., 2021. A ubiquitin switch controls autocatalytic inactivation of the DNA–protein crosslink repair protease SPRTN. *Nucleic Acids Research* 49, 902–915.
- Zheng, N., Shabek, N., 2017. Ubiquitin Ligases: Structure, Function, and Regulation. *Annual Review of Biochemistry* 86, 129–157.

Reference

- Zhou, H.-R., He, K., Landgraf, J., Pan, X., Pestka, J.J., 2014. Direct Activation of Ribosome-Associated Double-Stranded RNA-Dependent Protein Kinase (PKR) by Deoxynivalenol, Anisomycin and Ricin: A New Model for Ribotoxic Stress Response Induction. *Toxins (Basel)* 6, 3406–3425.
- Zhou, H.-R., Jia, Q., Pestka, J.J., 2005. Ribotoxic stress response to the trichothecene deoxynivalenol in the macrophage involves the SRC family kinase Hck. *Toxicol Sci* 85, 916–926.
- Zhou, H.-R., Lau, A.S., Pestka, J.J., 2003. Role of Double-Stranded RNA-Activated Protein Kinase R (PKR) in Deoxynivalenol-Induced Ribotoxic Stress Response. *Toxicological Sciences* 74, 335–344.
- Zhu, Q., Ding, N., Wei, S., Li, P., Wani, G., He, J., Wani, A.A., 2020. USP7-mediated deubiquitination differentially regulates CSB but not UVSSA upon UV radiation-induced DNA damage. *Cell Cycle* 19, 124–141.
- Zhu, Q., Sharma, N., He, J., Wani, G., Wani, A.A., 2015. USP7 deubiquitinase promotes ubiquitin-dependent DNA damage signaling by stabilizing RNF168*. *Cell Cycle* 14, 1413–1425.
- Zimmermann, M., Lottersberger, F., Buonomo, S.B., Sfeir, A., de Lange, T., 2013. 53BP1 regulates DSB repair using Rif1 to control 5' end resection. *Science* 339, 700–704.
- Zlatanou, A., Sabbioneda, S., Miller, E.S., Greenwalt, A., Aggathangelou, A., Maurice, M.M., Lehmann, A.R., Stankovic, T., Reverdy, C., Colland, F., Vaziri, C., Stewart, G.S., 2016. USP7 is essential for maintaining Rad18 stability and DNA damage tolerance. *Oncogene* 35, 965–976.
- Zorio, D., 2004. The link between mRNA processing and transcription: communication works both ways. *Experimental Cell Research* 296, 91–97.
- Zurita Rendón, O., Fredrickson, E.K., Howard, C.J., Van Vranken, J., Fogarty, S., Tolley, N.D., Kalia, R., Osuna, B.A., Shen, P.S., Hill, C.P., Frost, A., Rutter, J., 2018. Vms1p is a release factor for the ribosome-associated quality control complex. *Nat Commun* 9, 2197.

Acknowledgments

Time goes by so quickly. From October 2018 until now, it has already been more than four years. In more than one thousand days, I think I did innumerable western blots, scraped countless big dishes, picked up thousands of single colonies, well might also make some tiny contributions to scientific work. The friendship I gained and the spirit of scientific research I learned are more indelible than that. I would say this four-year period was the most unforgettable time that ever happened in my life. I appreciate everyone I met in my life. You have made my life unique.

First, I would like to give my deepest thanks to my PhD supervisor, Julian Stingele, who was the only PI that gave me a chance to have an interview five years ago. I really appreciate and cherish the opportunity you gave me to start an exciting scientific journey in your group. I do not want to say too much that you are the best boss ever because everyone knows that. I want to say that you are not only a great scientist who always has creative ideas about science but also a wonderful friend and a reliable spiritual guide that always being optimistic and motivating everyone. I want to appreciate every inspirational discussion, great advice, unconditional support and enthusiastic encouragement from you. I feel fortunate that I can work with so many lovely colleagues in this homely warm atmosphere.

Moreover, I am deeply thankful to all our most fantastic collaborators for the perfect collaborations, which contribute to a nice scientific story! Graeme, thank you for generating all the inducible knock-out cell lines that significantly contribute to the RPC story. I also appreciate that you hosted me in London even though we experienced a lot of pain because of ATAS certificate, I would say I had a wonderful time in the UK! Timur, I really appreciate your patience when I kept asking you numerous basic questions and your time helping us run countless sucrose gradients. Especially I want to thank you for proofreading my thesis and giving me many detailed and great comments. Karolina, I am highly grateful for measuring our hundreds of mass spectrums samples, which must have scared other people off. Thank you for all the effort and patience when we kept saying “the last samples” all the time.

I also want to express my sincere thanks to my colleagues in Stingele lab. Jackie, my best teammate. I know we suffered a lot, but I believe it is also enjoyable

Acknowledgments

most of the time. I am really glad that we are together to overcome the difficulties and that we finally managed. Thanks for all the support. You know the thing that I appreciate the most is your strong ability to empathize and you never skimp on your compliments. I really enjoyed the time working with such an energetic and enthusiastic person. Anja, I am deeply impressed by how well-organized you are. I want to say that you are my lucky star. Without you, the USP7 project won't exist. Thanks for doing all the preparation, which allowed me to start the work so quickly! Ricky, I want to say I am incredibly fortunate that I met you in the lab. You taught me every basic technique, answered my every stupid question and reviewed my thesis. I cannot imagine how can I adapt myself to the new environment and initiate my work so fast without you. Also, I am happy that we can always share cooking recipes, parenting experiences and practical life lessons with each other. Pedro, I don't know how many roles you played in my life. You are my taxi driver, chef, real estate agent, moving company and project advisor, but my best friend is the most critical one. I greatly admire your enthusiasm, warm heart and confidence, which are the qualities I want to learn from you. Thanks for always trying to cheer me up and organizing amazing activities which brought infinite joy to my life. Max, I would say I cannot finish my thesis without you, which is definitely true since you saved it from the bus. I sincerely appreciate you for analyzing our MS data which impressed me a lot that you learned all by yourself. Also, I am thankful for spending many hours in the evening discussing the projects with me, which is super inspirational. Denitsa, thank you for always being there to help me, driving me home in the night, helping me move homes, preparing stuff for dumpling evening, etc. Moreover, you must be the person who saw me cry the most. Thanks for your warm hugs, which comforted me a lot and made me feel emotionally safe. Sophie (the most precise person in the world) and MaxD (my best in vitro assay teacher), you are my best running partners. I want to say I really enjoyed the time when we were running, which made me feel at absolute liberty and in a relaxed mood. In addition, I am really glad that we spent many great times together, we went to the lake, we went to the best salad bar, I wish we can do more activities in the future, and please don't forget our ice cream date! Katharina, even though you just joined the lab for one year, I would say you did an excellent job. Thanks for always helping us order stuff so fast, which makes our life much easier. Eva, "supernumerary member of AG Stingele", my best weekend partner, working together with you makes me never feel lonely during the

Acknowledgments

weekend. Thanks for always helping and encouraging me. You are a sweet person and I am lucky to meet you in my life. Fabian, my first master student. I regret that I didn't spend much time with you when you were here. But I am also glad that you grow up quite fast independently. I appreciate all your contribution to the project. Hannah, our first PhD student, even though you have left the lab, I am glad that you are still in Munich and that we can meet as frequently as we can. For me, you were like an elder sister who took care of everyone's emotions. I am really grateful that you always listened to my complaints, brought me outside to relax and encouraged me. Every time when I talked with you, I feel incomparably calm, comfortable and warm. I wish you enjoy your new journey in life.

I especially would like to show my heartfelt gratitude to my family and friends who supported and encouraged me throughout my life. To my parents: thanks for your unconditional love and for being my solid backing. Without you, I will never be brave to come abroad and realize my dream. I want to say: that you are the best parents in the world, and I love you! To Mr. Zheng, who has already become Dr. Zheng: you are the role model I try to pursue in my life. Your perseverance, broad and profound knowledge, calm and wittiness have deeply attracted me. Thank you for always being together with me. I am sincerely grateful to have you in my life, with whom I start a new small family.

Finally, I want to thank the members of my thesis defense committee, Prof. Dr. Roland Beckmann, Prof. Dr. Andreas Ladurner, Prof. Dr. Danny Nedialkova, Prof. Dr. Klaus Förstemann and PD. Dr. Dietmar Martin, thank you for spending time refereeing and evaluating my thesis. In addition, I am very grateful to my TAC members, Andreas Ladurner and Stephan Hamperl, for the discussion and suggestions on my projects, which inspired me a lot. In the end, I would like to appreciate China Scholarship Council for supporting my study in Germany, I wish I fulfilled the initial expectations and I am looking forward to coming back to devote my efforts to society.

Publication

2021

Shubo Zhao, Anja Kieser, Hao-Yi Li, Hannah K Reinking, Pedro Weickert, Simon Euteneuer, Denitsa Yaneva, Aleida C Acampora, Maximilian J Götz, Regina Feederle, Julian Stingele. A ubiquitin switch controls autocatalytic inactivation of the DNA-protein cross-link repair protease SPRTN. *Nucleic Acids Res.* 2021 Jan 25; 49 (2): 902-915.

2022

Shubo Zhao[#], Jacqueline Cordes[#], Karolina M. Caban, Maximilian J. Götz, Timur Mackens-Kiani, Anthony J. Veltri, Niladri K. Sinha, Pedro Weickert, Graeme Hewitt, Thomas Fröhlich, Roland Beckmann, Allen R. Buskirk, Rachel Green, Julian Stingele. Translation-coupled sensing and degradation of RNA-protein crosslinks. Manuscript.

[#]These authors contributed equally to this work

A ubiquitin switch controls autocatalytic inactivation of the DNA–protein crosslink repair protease SPRTN

Shubo Zhao^{1,2}, Anja Kieser^{1,2}, Hao-Yi Li^{1,2}, Hannah K. Reinking^{1,2}, Pedro Weickert^{1,2}, Simon Euteneuer^{1,2}, Denitsa Yaneva^{1,2}, Aleida C. Acampora^{1,2}, Maximilian J. Götz^{1,2}, Regina Feederle³ and Julian Stinglele^{1,2,*}

¹Department of Biochemistry, Ludwig-Maximilians-University, 81377 Munich, Germany, ²Gene Center, Ludwig-Maximilians-University, 81377 Munich, Germany and ³Institute for Diabetes and Obesity, Monoclonal Antibody Core Facility, Helmholtz Zentrum München, 85764 Neuherberg, Germany

Received April 29, 2020; Revised December 02, 2020; Editorial Decision December 03, 2020; Accepted December 04, 2020

ABSTRACT

Repair of covalent DNA–protein crosslinks (DPCs) by the metalloprotease SPRTN prevents genome instability, premature aging and carcinogenesis. SPRTN is specifically activated by DNA structures containing single- and double-stranded features, but degrades the protein components of DPCs promiscuously and independent of amino acid sequence. This lack of specificity is useful to target diverse protein adducts, however, it requires tight control in return, in order to prohibit uncontrolled proteolysis of chromatin proteins. Here, we discover the components and principles of a ubiquitin switch, which negatively regulates SPRTN. We demonstrate that monoubiquitylation is induced in an E3 ligase-independent manner and, in contrast to previous assumptions, does not control chromatin access of the enzyme. Data obtained in cells and *in vitro* reveal that monoubiquitylation induces inactivation of the enzyme by triggering autocatalytic cleavage *in trans* while also priming SPRTN for proteasomal degradation *in cis*. Finally, we show that the deubiquitylating enzyme USP7 antagonizes this negative control of SPRTN in the presence of DPCs.

INTRODUCTION

Covalent DNA–protein crosslinks (DPCs) are particularly dangerous DNA lesions, which interfere with all basic chromatin transactions including transcription and replication (1–3). Endogenous DPCs are not only caused by toxic metabolites such as reactive aldehydes but also by entrapment of covalent reaction intermediates of enzymes such as topoisomerases (4). Moreover, crosslinking can be induced by exogenous agents such as ionizing radiation as well as by various widely-used chemotherapeutics (5,6). The

protein component of DPCs is targeted for repair by proteases of the Wss1/SPRTN family (7–14). The human protease SPRTN is essential for viability in mammalian cells, which highlights the scale of the threat posed by endogenous DPCs (15). Moreover, germline mutations in *SPRTN*, which result in the deletion of the enzyme's C-terminal tail, are causative for Ruijs-Aalfs syndrome (RJALS) (16,17). RJALS is characterized by premature aging and early-onset hepatocellular carcinomas with similar phenotypes being observed in hypomorphic *Sprtn* mutant mice (16–18). SPRTN is a DNA-dependent metalloprotease, which is activated by DNA structures containing single- (ss) and double-stranded (ds) features, such as ss-/dsDNA junctions or frayed dsDNA ends (19). However, SPRTN's proteolytic activity is highly promiscuous (8,9,11). The lack of preference for certain amino acid sequences is required to target diverse DPCs, but it demands tight control in return. A substantial fraction of SPRTN (30–50%) is constitutively monoubiquitylated (20–22). The modification is strongly reduced in SPRTN variants with amino acid replacements in the enzyme's C-terminal ubiquitin-binding zinc finger (UBZ) (20–22). Attempts to identify the site of monoubiquitylation by mass spectrometry revealed four potentially-modified lysine (K) residues, but SPRTN variants with collective lysine-to-arginine (KR) substitutions retained the modification (8). It has been proposed that monoubiquitylation regulates chromatin access of the enzyme because the recruitment of SPRTN to chromatin upon DPC induction is accompanied by rapid deubiquitylation (8). However, testing this model directly, has not been possible because the involved deubiquitylating enzyme (DUB) is unknown. Accordingly, the mechanistic principles of SPRTN's regulation by monoubiquitylation remain unclear.

Here, we identify the DUB USP7 as the factor responsible for deubiquitylating SPRTN when cells are challenged by DPCs. Moreover, we reveal that monoubiquitylation induces direct inactivation of SPRTN rather than regulating chromatin recruitment of the enzyme. The modifica-

*To whom correspondence should be addressed. Tel: +49 89 2180 71080; Email: stinglele@genzentrum.lmu.de

tion triggers autocleavage of the protease while also enhancing proteasomal degradation by priming polyubiquitylation. Finally, *in vitro* experiments suggest that the constitutive monoubiquitylation occurs in a highly promiscuous E3 ligase-independent manner. Taken together, we unravel the principles and components of a regulatory switch, which allows safe operation of a potentially dangerous enzymatic activity in human cells.

MATERIALS AND METHODS

Antibodies and inhibitors

Anti-Strep (ab76949) and anti-Histone H3 (ab10799) antibodies were purchased from Abcam; anti-Tubulin (T6074), anti-Flag (F3165) and anti-Rat IgG (A9037) antibodies were purchased from Sigma; anti-GAPDH (2118) antibody was purchased from Cell Signaling; anti-USP7 (sc-137008) and anti-Histone H1 (sc-377468) were purchased from Santa Cruz; Goat Anti-Mouse Immunoglobulins/HRP (P0447), Swine Anti-Rabbit Immunoglobulins/HRP (P0399) antibodies were purchased from Dako and anti-GFP (PABG1, used for detection of YFP) was purchased from Chromotek. Rat monoclonal anti-human SPRTN antibody (6F2) was generated by immunization of Wistar rats with purified GST-tagged SPRTN- Δ C, which was expressed in insect cells as described previously (8). Hybridoma supernatants were screened by ELISA for binding to purified untagged SPRTN protein and further validated by western blot analysis on HeLa cell lysates as well as recombinant protein. Clone SPRT 6F2 (IgG2a) was subcloned twice by limited dilution to obtain a stable monoclonal hybridoma cell line. For inhibition of the ubiquitin-activating enzyme E1 MLN7243 (TAK-243) was purchased from Chemietek and used at 1 μ M final concentration (23). For inhibition of proteasomal degradation MG132 was purchased from Sigma (M7449) and used at 5 μ M final concentration. For inhibition of protein synthesis cycloheximide was purchased from Sigma (C4859) and used at 100 μ g/ml final concentration.

Cell lines

HCT116 wild-type (WT), HCT116 *USP7* KO and HAP1 WT, *VCPIP1* KO, *USP11* KO cells were purchased from Horizon Discovery. HeLa T-REx Flp-In, 293 T-REx Flp-In and DLD1 cells were provided by Cell Services, The Francis Crick Institute. HeLa T-REx Flp-In cells stably expressing YFP-SPRTN-Strep-tag variants were generated using the Flp-In system (Thermo Fisher) according to manufacturer's instructions.

Transient transfection

For transient transfections cells were grown to 70–90% confluency in 12-well plates. Plasmids (1 μ g plasmid) and Lipofectamine 2000 reagent (Invitrogen, 1 μ l/ μ g plasmid) were diluted in 50 μ l Opti-MEM Medium each. Plasmid and Lipofectamine 2000 dilutions were mixed following a 5 min incubation. After an additional 15 min incubation, the transfection mix was added to the cells.

siRNA transfection

Cells were grown to 20–30% confluency in 6-well plates. 3 μ l siRNA (20 μ M, ON TARGETplus SMARTpool, Horizon, USP7 (L-006097-00-0005), USP11 (L-006063-00-0005), VCPIP1 (L-019137-00-0005), Control (D-001810-10-05)) and 3 μ l Lipofectamine RNAiMAX Transfection Reagent (Invitrogen) were each diluted in 100 μ l Opti-MEM Medium. siRNA and Lipofectamine RNAiMAX Transfection Reagent dilutions were mixed following a 5 min incubation. After an additional 15 min incubation, the transfection mix was added to the cells. After 48 h, cells were reseeded into 60 mm dishes, followed by chromatin fractionation the following day.

Generation of USP7 knock-out cells

USP7 gRNA1 (GGTCTGTCTGGATAAAAGCG) and gRNA2 (GAGTGATGGACACAACACCG) were inserted into Lenti-multi-CRISPR plasmid (Addgene #85402; RRID: Addgene.85402) as described previously (24). The resulting plasmid was then transiently transfected into HAP1 or DLD1 cells using Lipofectamine 2000 (Invitrogen) to generate USP7 knock-out cells. One day after transfection, cells were selected by Puromycin for 48 h. Selected cells were then reseeded in 96-well plates (0.5 cell/well) to generate single clones. Single clones were then screened using western blotting with anti-USP7 antibody.

Purification of partially ubiquitylated YFP-SPRTN-EQ-Strep

293 T-REx Flp-In cells expressing YFP-SPRTN-EQ-Strep were grown in two 245 \times 245 mm dishes to 50% confluency before overnight induction of protein expression by addition of 1 μ g/ml doxycycline. Cells were harvested by scraping, washed twice in PBS and stored at -80° C. For purification, cells were thawed and resuspended in 10 ml lysis buffer (50 mM HEPES/NaOH pH 7.2, 1 M NaCl, 10% glycerol, 1% IGEPAL CA-630, cOmplete EDTA free protease inhibitors, 0.04 mg/ml Pefabloc SC and 20 mM iodoacetamide). Following sonication and Benzonase (4 U/ml) digestion for 30 min at 4° C, lysates were cleared by centrifugation (23 500 g, 45 min, 4° C). 60 μ l MagStrep type3 XT beads (5% (v/v) suspension) were incubated with the supernatant for 1 h at 4° C prior to three wash steps with wash buffer (50 mM HEPES/NaOH pH 7.2, 0.5 M NaCl, 10% glycerol). Finally, purified YFP-SPRTN-EQ-Strep was eluted in 3 \times 80 μ l elution buffer (50 mM HEPES/NaOH pH 7.2, 0.5 M NaCl, 10% glycerol, 50 mM biotin).

DUB screen

71 cDNAs encoding human DUBs (hORFeome v8.1 Deubiquitinating Enzymes collection + seven additional ORFeome clones: CloneIds: 100011387, 100010734, 100002718, 100066416, 100070362, 100068239) were sub-cloned into pDEST17 using Gateway LR Clonase II (Invitrogen). Plasmids were then transformed into *Escherichia coli* BL21 (DE3) cells for protein expression in 50 ml cultures. Cell pellets were resuspended in BugBuster reagent (Merck Millipore, 5 ml/g). Benzonase (25 U/ml)

and DTT (5 mM) were added prior to an incubation of 20 min at room temperature. Lysates were then cleared by centrifugation (16 000 g, 20 min, 4°C). Lysates were mixed in pools of three prior to assessing their ability of deubiquitylating YFP-SPRTN-EQ-Strep. To this end, purified partially ubiquitylated YFP-SPRTN-EQ-Strep was incubated with lysate pools for 30 min at 25°C. Lysates of non-transformed BL21 cells served as negative control, the unspecific deubiquitylating activity of the catalytic domain of USP2 (USP2^{cd}, BostonBiochem, E-504) as positive control. Deubiquitylation was then assessed using SDS-PAGE followed by western blotting using anti-Strep antibody.

DUB activity assays

Candidate DUBs were partially purified using a standard Ni-NTA-purification strategy and then tested for their activity either using a ubiquitin–rhodamine cleavage assay kit (BostonBiochem) following the manufacturer's instructions or by incubation with partially ubiquitylated YFP-SPRTN-EQ-Strep for 30 min at 25°C followed by SDS-PAGE and western blotting using anti-Strep antibody.

Expression and purification of recombinant proteins

SPRTN codon-optimized for bacterial expression (using GeneOptimizer) was expressed from a pNIC-Strep-ZB-SPRTN plasmid as previously described (19). SPRTN-Ub^{LF} was generated using Gibson assembly cloning. Flag-SPRTN was generated using insertional mutagenesis. For protein expression plasmids were transformed into BL21(DE3) *E. coli* cells and grown at 37°C in Terrific broth (TB) medium until they reached OD 0.7. Protein expression was induced by addition of 0.5 mM IPTG over night at 18°C. Next, cells were harvested, resuspended in buffer A (50 mM HEPES/KOH pH 7.2, 500 mM KCl, 1 mM MgCl₂, 10% glycerol, 0.1% IGEPAL, 0.04 mg/ml Pefabloc SC, cOmplete EDTA-free protease inhibitors, 1 mM Tris(2-carboxyethyl)phosphine hydrochloride (TCEP), pH 7.2) and lysed by sonication. All steps were carried out at 4°C. Cell lysate was incubated with benzonase (45 U/ml lysate) for 30 min on ice prior to the removal of cell debris by centrifugation at 18 000 g for 30 min. Cleared supernatant was applied to Strep-Tactin[®] XT Superflow[®] high capacity cartridges, washed with 3 column volumes (CV) of buffer A and 4 CV of buffer B (50 mM HEPES/KOH pH 7.2, 500 mM KCl, 10% Glycerol, 1 mM TCEP, pH 7.2). Proteins were eluted in 6 CV buffer C (50 mM HEPES/KOH pH 7.2, 500 mM KCl, 10% glycerol, 1 mM TCEP and 50 mM biotin, pH 7.2). Eluted proteins were further applied to HiTrap Heparin HP affinity columns and washed with 3 CV buffer B before eluting in buffer D (50 mM HEPES/KOH pH 7.2, 1 M KCl, 10% glycerol, 1 mM TCEP, pH 7.2). Eluted fractions containing recombinant SPRTN protein were desalted against buffer B using PD-10 desalting columns. The affinity tag was cleaved off over night at 4°C by the addition of His-tagged TEV protease with 1:10 mass ratio. Cleaved recombinant SPRTN protein was further purified by size exclusion chromatography using a HiLoad 16/600 Superdex 200 pg column equilibrated in buffer E (50 mM

HEPES/KOH pH 7.2, 500 mM KCl, 10% Glycerol, 0.5 mM TCEP, pH 7.2). Eluted proteins were concentrated with 10 kDa cutoff Amicon Ultra centrifugal filters before snap-freezing in liquid nitrogen and storing at –80°C.

UBE2D3 was sub-cloned into pDEST17 using Gateway LR Clonase II (Invitrogen). For protein expression plasmids were transformed into BL21(DE3) *E. coli* cells and grown at 37°C in Terrific broth (TB) medium until they reached OD 0.7. Protein expression was induced by addition of 0.5 mM IPTG for 3 h at 37°C. Next, cells were harvested, resuspended in buffer A (50 mM NaH₂PO₄ pH 8, 150 mM NaCl, 10 mM Imidazol and 0.5 mM TCEP), with the addition of 0.04 mg/ml Pefabloc SC and cOmplete EDTA-free protease inhibitors. The cells were then lysed by sonication. All steps were carried out at 4°C. Cell lysate was incubated with benzonase (45 U/ml lysate) for 30 min at 4°C prior to the removal of cell debris by centrifugation at 16 000 g for 30 min. Cleared supernatant was applied twice to Ni-NTA beads equilibrated in buffer A, washed with 5 CV of buffer A and 7 CV of buffer B (50 mM NaH₂PO₄ pH 8, 500 mM NaCl, 20 mM Imidazol, 0.5 mM TCEP). Proteins were eluted in 5 CV buffer C (50 mM NaH₂PO₄ pH 8, 500 mM NaCl, 250 mM Imidazol, 0.5 mM TCEP). Eluted fractions containing recombinant His-UBE2D3 protein were desalted against buffer D (20 mM Tris pH 7.5, 150 mM NaCl, 10% glycerol, 2 mM TCEP) using PD-10 desalting columns. The recombinant protein was further purified by size exclusion chromatography using a HiLoad 16/600 Superdex 200 pg column equilibrated in buffer D. Eluted proteins were concentrated with 3 kDa cutoff Amicon Ultra centrifugal filters before snap-freezing in liquid nitrogen and storing at –80°C.

In vitro ubiquitylation assay

The E2 screen was conducted using the E2 screening kit (UBPBio) according to the manufacturer's instructions. In brief, human E2 ubiquitin conjugating enzymes (2 μM) were incubated together with catalytically inactive SPRTN-E112Q (EQ) (2 μM), E1 ubiquitin activating enzyme (100 nM), ubiquitin (R&D Systems, U-100H, 50 μM) or no lysines N-Terminal Biotin ubiquitin (R&D Systems, UB-NOK-050, 50 μM), DNA (11.1 nM ΦX174 virion) and ATP (2 mM) for 1.5 h at 30°C. All other *in vitro* ubiquitylation assays contained the indicated SPRTN variants, E1 ubiquitin activating enzyme (300 nM), ubiquitin (50 μM), ATP (2 mM) and purified His-tagged UBE2D3 (concentrations as indicated in figure legends) and were incubated for 1.5 h at 30°C. The catalytic domain of USP2 (USP2^{cd}) was purchased from BostonBiochem and was included as indicated. Ubiquitylation reactions were stopped by addition of 4× LDS sample buffer supplemented with β-mercaptoethanol and boiling at 95°C for 10 min and then subjected to SDS-PAGE followed by staining with Instant-Blue Coomassie protein stain. Contrast of scanned images was adjusted globally using Adobe Photoshop software

In vitro protease assays

Reactions were performed in 20 μl containing the indicated SPRTN variants (500 nM), histone H1 (500 nM, NEB) as

indicated and either Φ X174 Virion ssDNA or RFI dsDNA (11.1 nM, NEB). The reaction buffer comprised 19.5 mM HEPES/KOH pH 7.2, 2.9% glycerol, 5 mM TCEP and either 80 mM or 150 mM KCl. Reactions were incubated at 25°C for 1 h and stopped by the addition of 4x LDS sample buffer supplemented with β -mercaptoethanol. Samples were boiled at 95°C for 10 min, resolved on 4–12% Bis-Tris NuPAGE gradient gels and stained using InstantBlue Coomassie protein stain or analysed by western blotting using anti-SPRTN, anti-Flag and anti-H1 antibodies. The intensity of western blots and scanned gels was adjusted globally using Adobe Photoshop. Cleavage reactions were quantified by dividing the amount of cleaved protein by the total amount of protein (cleaved and uncleaved) as determined by analysis of western blot results using ImageJ.

Protein-oligonucleotide conjugate cleavage assay

Protein G was conjugated to the 5'-terminal, 3'-terminal or an internal base of a 30mer oligonucleotide (5'-Cy5-AC CAGTGCCTTGCTAGGACATCTTTGCCCA-3') as described previously (19). Double-stranded DPCs were generated by annealing a complementary reverse oligonucleotide. Annealing was carried out immediately prior to cleavage reactions by mixing conjugates and reverse oligonucleotides at a ratio of 1:1.2 in annealing buffer (25 mM HEPES/KOH pH 7.2, 50 mM KCl, 5% Glycerol, and 0.2 mg/ml BSA) followed by an incubation for 2 min at 37°C and a subsequent decrease in temperature of 1°C/min until 25°C were reached. Cleavage reactions with model DPCs were performed in a reaction volume of 10 μ l containing 6.25 nM SPRTN and 25 nM DPC in a final reaction buffer of 17.5 mM HEPES/KOH pH 7.2, 80 mM KCl, 3.5% glycerol, 5 mM TCEP and 0.1 mg/ml BSA. Reactions were incubated for 2 h at 25°C. 2 μ l of 6x Orange G loading dye was added before reactions were resolved on 20% TBE gels using 1x TBE as running buffer at 4°C. Gels were photographed using a BioRad Chemidoc MP system using filter settings for Cy5 fluorescence. The intensity of scanned gels was adjusted globally using ImageJ, which was also used to quantify cleavage by dividing the amount of cleaved conjugate by the total amount of conjugate (cleaved and uncleaved) and subtraction of background signal (determined from lanes without SPRTN).

Co-immuno-precipitation

To test binding between USP7/VCPIP1/USP11 and SPRTN, HeLa-T-REx Flp-In cells stably expressing YFP-SPRTN-Strep variants were seeded in 60 mm tissue culture plates, grown to 50% confluency and then transiently transfected with pcDNA5-FRT/TO plasmids encoding Flag/Flag-USP7/VCPIP1/USP11 variants using Lipofectamine 2000 (Invitrogen) according to the manufacturer's instructions. Sixteen hours after transfection and concurrent induction of protein expression by doxycycline (1 μ g/ml), cells were washed once with ice-cold PBS and harvested by scraping in lysis buffer (20 mM Tris/HCl pH 7.5, 137 mM NaCl, 1% IGEPAL CA-630, 2 mM EDTA, 2 mM MgCl₂, 4 U/ml Benzonase, cOmplete EDTA free protease inhibitors, 0.04 mg/ml PefaBloc SC and 20 mM

iodoacetamide). Lysates were incubated for 30 min on ice, before centrifugation at 16 000 g for 30 min. Supernatants were then used for immuno-precipitation using 5 μ l magnetic anti-Flag M2 beads (Sigma) at 4°C for 1 h. The beads were then washed three times with wash buffer (10 mM Tris/HCl pH 7.5, 150 mM NaCl, 0.5 mM EDTA and 0.5% IGEPAL CA-630). Finally, samples were resuspended in 100 μ l 1x LDS sample buffer, analysed by SDS-PAGE and western blotting with anti-Flag, anti-GAPDH and anti-Strep antibodies.

Cellular autocleavage assay

pcDNA5-FRT/TO plasmids encoding YFP-SPRTN-Strep or YFP-SPRTN-Ub^{LF} variants (1 μ g) and Flag/Flag-USP7^{WT/C223S} (3 μ g) were transiently transfected using Lipofectamine 2000 (Invitrogen) according to the manufacturer's instructions. Protein expression was induced by overnight (16 h) incubation with doxycycline (final concentration 1 μ g/ml). Cells were lysed on ice in 1 ml lysis buffer (50 mM HEPES pH 7.5, 1 M NaCl, 10% glycerol, 1% IGEPAL CA-630, 2 mM MgCl₂, 20 mM iodoacetamide, 0.04 mg/ml PefaBloc SC and cOmplete EDTA-free protease inhibitors). After addition of benzonase (4 U/ml), lysates were incubated for 30 min on ice. Lysates were cleared by centrifugation (16 000 g, 30 min) at 4°C and applied to 15 μ l GFP-trap Magnetic Agarose (Chromotek) and processed according to manufacturer's instructions. Finally, samples were resuspended in 65 μ l 1x LDS sample buffer, subjected to analysis by SDS-PAGE and western blotting with anti-GFP antibody (PABG1, Chromotek).

Chromatin fractionation

Cells in the mid-exponential phase of growth were collected by scraping in ice-cold 1X PBS. Cells were then equally split and either directly resuspended in 1X LDS buffer or incubated for 10 min in ice-cold CSK buffer (10 mM PIPES, 100 mM NaCl, 1.5 mM MgCl₂, 5 mM EDTA, 300 mM sucrose and 0.5% Triton X-100, 0.04 mg/ml PefaBloc SC and cOmplete EDTA free protease inhibitors). Chromatin-bound proteins were then isolated by low speed centrifugation (3000 rpm, 5 min at 4°C).

Cycloheximide chase

Cells were seeded in 12-well tissue culture plates, grown to 80% confluency and then treated with 5 μ M MG132. After 2 h cells were treated with 100 μ g/ml cycloheximide (Sigma) for the indicated amount of time. Finally, cells were lysed in 150 μ l 1X LDS sample buffer, followed by SDS-PAGE and western blotting with the indicated antibodies.

Formaldehyde sensitivity assay

Long term treatment: 10⁴ cells were seeded per well in 12-well plates and treated with the indicated formaldehyde concentration the next day. After 72 h, medium was replaced with alamarBlue cell viability reagent (36 μ g/ml resazurin in PBS) and plates kept for an additional 1 h incubation at 37°C. Cell viability was then assessed by measuring fluorescence (560 nm excitation/590 nm emission). Short term

treatment: 5×10^4 cells were seeded per well in 12-well plates and treated with 1 mM formaldehyde concentration the next day for 2 h. After 48 h, medium was replaced with alamarBlue cell viability reagent (36 μ g/ml resazurin in PBS) and plates kept for an additional 1 h incubation at 37°C. Cell viability was then assessed by measuring fluorescence (560 nm excitation/590 nm emission).

Detection of formaldehyde-induced DNA–protein crosslinks

DPCs were induced by treating HAP1 WT or *USP7* KO cells with 75 μ M formaldehyde for 2 h. DPCs were measured using a KCl/SDS precipitation assay as described before (25). Briefly, cells were washed twice with PBS and lysed in 400 μ l denaturing lysis buffer (2% SDS, 20 mM Tris/HCl, pH 7.5), frozen in liquid nitrogen and stored at -80°C until further processing. Lysates were thawed at 55°C for 5 min with 1200 rpm shaking, followed by pipetting samples up and down 30 times. Cellular protein was then precipitated by adding 400 μ l precipitation buffer (200 mM KCl, 20 mM Tris pH 7.5) and incubation on ice for 5 min. The precipitated protein was separated by full speed centrifugation at 4°C for 5 min. Next, 400 μ l supernatant was saved and used for soluble DNA measurement. The pellet was resuspended in 400 μ l precipitation buffer and resolved by shaking at 55°C for 5 min followed by cooling down on ice for 5 min and full speed centrifugation at 4°C for 5 min. After repeating the wash procedure 3 times, protein precipitate was resuspended in 400 μ l Proteinase K buffer (200 mM KCl, 20 mM Tris pH 7.5, Proteinase K 0.2 mg/ml) and incubated at 55°C for 45 min. Finally, 10 μ l BSA (50 mg/ml) was added to the solution followed by cooling down on ice for 5 min followed full speed centrifugation at 4°C for 5 min. Next, supernatant containing crosslinked DNA was collected. Total DNA and crosslinked DNA were treated with 0.2 mg/ml RNase A for 30 min at 37°C. DNA concentrations were determined using Qubit™ dsDNA HS Assay Kit (Thermo Fisher) according to the manufacturer's instructions. The amount of DPCs was calculated as the ratio between crosslinked DNA and total DNA (crosslinked plus soluble DNA).

Complementation of *USP7* KO cells

DLD1 WT or *USP7* KO cells were seeded in six-well plates, grown to 50% confluency before transient transfection with pcDNA5-FRT/TO plasmids encoding YFP/YFP-*USP7*^{WT/C223S} (2 μ g) using Lipofectamine 2000 (Invitrogen) according to the manufacturer's instructions. 16 h after transfection, cells were reseeded into 12-well plates (5×10^4 cells per well) followed by treatment with 1 mM formaldehyde for 2 h the next day. After 48 h cell viability was determined using alamarBlue cell viability assay.

RESULTS

The monoubiquitylation of SPRTN's C-terminal tail is promiscuous

In order to understand the regulation of SPRTN by monoubiquitylation, we first attempted to map the mod-

ified lysine residue(s) using protein truncations. Ubiquitylation of full length SPRTN (N-terminally YFP-, C-terminally Strep-tagged) is readily observed upon transient transfection and is sensitive to inhibition of the ubiquitin-activating enzyme (E1) (Figure 1A). The truncated SPRTN variant found in RJALS patients (SPRTN- Δ C) is not ubiquitylated, while the isolated C-terminal tail (SPRTN- Δ N) is modified (Figure 1A). The modification can be further mapped to a small 7 kDa fragment, which contains the UBZ domain and five lysine residues (SPRTN- Δ 425). Surprisingly, substitution of all five lysines (5KR) does not alter the level of modification (Figure 1A). The N-terminal YFP-tag and linker contain various lysines and we suspected that these residues might undergo modification as well. Indeed, deletion of the YFP-tag leads to a severe reduction in ubiquitylation of the SPRTN- Δ 425-5KR fragment (Figure 1B). However, a slightly extended variant (SPRTN- Δ 400) with the same lysine replacements (SPRTN- Δ 400-5KR) remains ubiquitylated, unless all additional lysines are replaced as well (SPRTN- Δ 400-9KR) (Figure 1C). Full-length SPRTN with the 9KR replacement is unstably expressed, but appears to remain monoubiquitylated (Figure 1D). Notably, a SPRTN- Δ 400-8KR fragment with only one remaining lysine residue displays multiple modifications, which indicates that the monoubiquitylation can be further modified (Supplementary Figure S1A). We conclude that the monoubiquitylation of SPRTN can target various lysine residues (even those of the YFP-tag) and can be extended to a ubiquitin chain.

E3-independent monoubiquitylation of SPRTN

Monoubiquitylation of proteins bearing ubiquitin-binding domains is frequently observed and has been proposed to occur in an E3-independent manner (26–28). Thus, we tested a collection of human recombinant ubiquitin-conjugating enzymes (E2s) for their ability to ubiquitylate catalytically-inactive SPRTN *in vitro*. Strikingly, ten out of twenty-nine E2s induce SPRTN monoubiquitylation in the absence of an E3 ubiquitin ligase (Figure 1E and Supplementary Figure S1B). *In vitro* ubiquitylation by the E2 UBE2D3 even triggers multi-monoubiquitylation of SPRTN, as indicated by multiple modifications with a ubiquitin variant containing no lysines and a biotinylated N-terminus (Supplementary Figure S1C). Notably, a SPRTN variant with an altered UBZ domain (UBZ*, D473A) undergoes modification *in vitro*, but its modification is sensitive to the addition of an unspecific deubiquitylation activity (USP2 catalytic domain) (Figure 1F). This could indicate that SPRTN-UBZ* variants lack monoubiquitylation in cells because a functional UBZ domain is important to shield the modification from cellular DUB activities. The fact that monoubiquitylation of SPRTN occurs in an E3-independent manner (although an involvement of E3 ligases in cells cannot be excluded) and the high level of modification in basal conditions argues that the generation of ubiquitylated SPRTN (SPRTN-Ub) is a constitutive process. In turn, this infers that cellular control of the modification must occur through deubiquitylation.

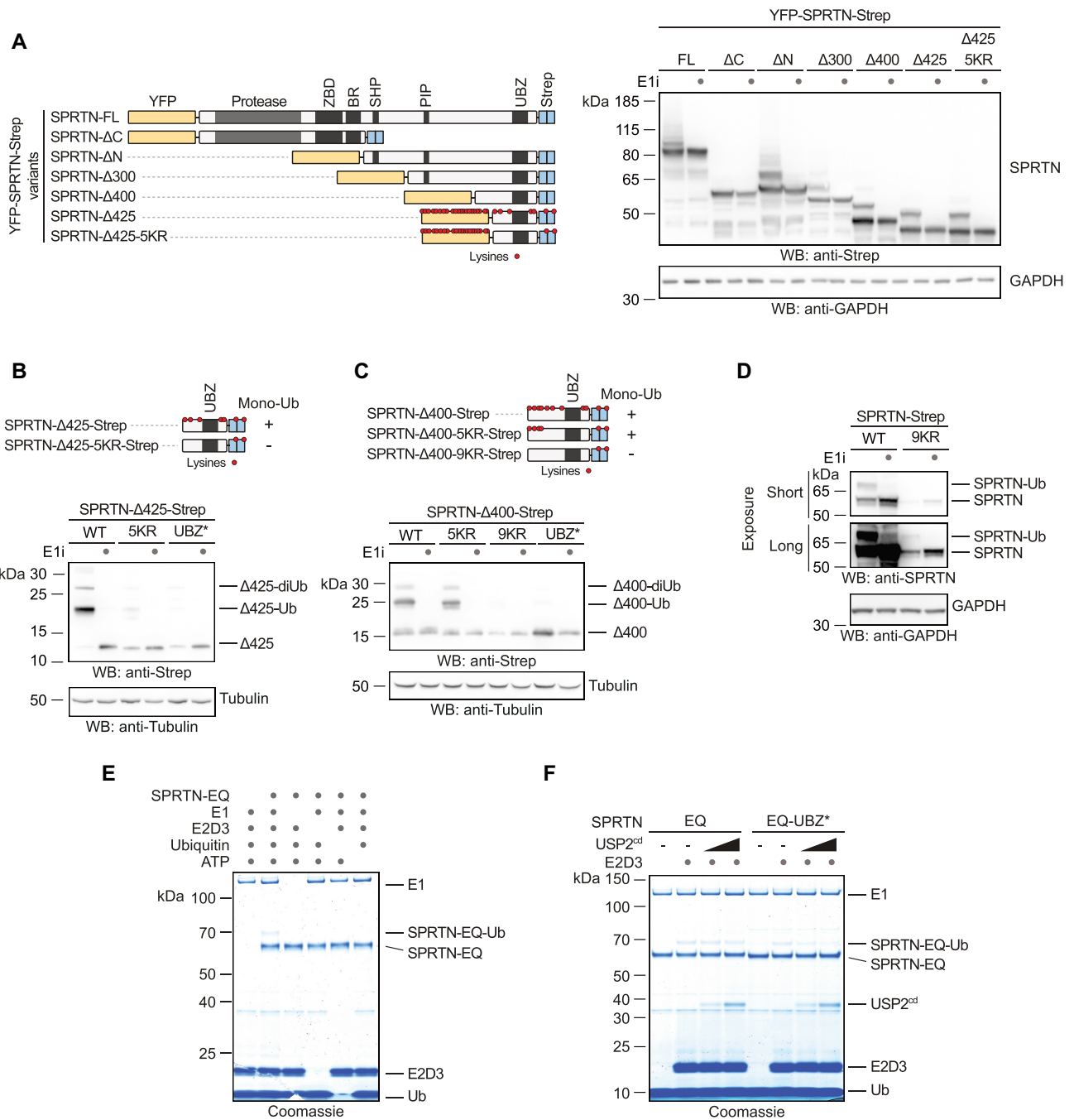


Figure 1. Promiscuous E3-independent monoubiquitylation of SPRTN's C-terminal tail. (A–D) Monoubiquitylation status of truncated SPRTN variants. Plasmids encoding tagged full-length (FL) SPRTN or truncations (carrying the indicated lysine to arginine (KR) substitutions or the UBZ* variant, D473A) were transiently transfected in HeLa T-REx Flp-In cells. Expression of SPRTN was induced by addition of doxycycline for 6 h prior to cell lysis (including a co-treatment with a ubiquitin-activating enzyme E1 inhibitor (E1i) as indicated) and analysed by SDS-PAGE and western blotting. (E) *In vitro* ubiquitylation assays containing SPRTN-EQ (410 nM), UBE2D3 (4 μM), E1 ubiquitin activating enzyme (300 nM), ubiquitin (50 μM) and ATP (2 mM) as indicated were incubated for 1.5 h at 30°C. Reactions were stopped by addition of LDS sample buffer and subjected to SDS-PAGE followed by staining with InstantBlue Coomassie protein stain. (F) *In vitro* ubiquitylation assays containing SPRTN-EQ or SPRTN-EQ-UBZ* (410 nM), E1 ubiquitin activating enzyme (300 nM), ubiquitin (50 μM), ATP (2 mM), UBE2D3 as indicated (8 μM) and increasing amounts of the catalytic domain of USP2 (USP2^{cd}) (0, 250 or 500 nM) were incubated for 1.5 h at 30°C. Reactions were stopped by addition of LDS sample buffer and subjected to SDS-PAGE followed by staining with InstantBlue Coomassie protein stain.

An *in vitro* screen reveals that USP7 targets ubiquitylated SPRTN

To identify the DUB responsible for deubiquitylating SPRTN, we designed an *in vitro* screen (Figure 2A). We subcloned an arrayed cDNA library containing sequences of seventy-one human DUBs into bacterial expression plasmids. Upon expression in *E. coli*, lysates were prepared and pooled in twenty-four sets of three. Deubiquitylation activity was assessed by incubating each pool with partially monoubiquitylated SPRTN-EQ purified from human cells. Addition of five out of twenty-four pools triggered SPRTN deubiquitylation (Supplementary Figure S2A). Each positive pool contained one lysate able to deubiquitylate SPRTN (Figure 2B). The respective plasmids were re-isolated and determined to encode four different DUBs: USP4, USP7, USP15 and USP42. All four candidates were re-expressed, partially purified and successfully re-tested for their ability to deubiquitylate SPRTN (Supplementary Figure S2B-C). To test whether these DUBs possess the ability to act on SPRTN-Ub in cells, we monitored SPRTN monoubiquitylation in cells upon overexpression of the respective candidates. Overexpression of USP7 but not of the other candidates leads to a loss of endogenous and exogenously-expressed SPRTN-Ub and a concurrent increase in unmodified SPRTN (Figure 3A-B). Of note, whether USP42 can deubiquitylate SPRTN in cells remains unclear, given that it was not expressed at significant levels. Importantly, overexpression of a catalytically inactive variant of the DUB (USP7^{CS}, C223S) does not trigger deubiquitylation (Figure 3C-D). Consistently, USP7 binds to SPRTN in co-immunoprecipitation experiments (Figure 3E). Notably, catalytically inactive USP7 (USP7^{CS}) binds preferentially to ubiquitylated SPRTN. Interestingly, monoubiquitylated species of SPRTN-UBZ* and SPRTN-ΔC co-immunoprecipitate with USP7^{CS}, although this modification is not detectable in input samples (Figure 3E). This observation is in agreement with our finding that SPRTN-UBZ* can be monoubiquitylated *in vitro*, but then fails to protect the modification (Figure 1F). USP7 bears an N-terminal TRAF domain, which precedes the catalytic domain (CD) and five C-terminal ubiquitin-like domains (UBLs). Deletion of the CD or the UBLs abrogates preferential binding of USP7 to SPRTN-Ub indicating that these domains are important to provide specificity for modified SPRTN, but are not essential for the interaction per se (Figure 3F). A USP7 variant lacking the TRAF domain (USP7-ΔTRAF) is deficient in SPRTN binding. However, interpretation of this result is complicated by the fact that this truncation is expressed at low levels, which may indicate more general defects (Figure 3F). We conclude that USP7 interacts specifically with SPRTN-Ub and has the ability to deubiquitylate the protease *in vitro* and in cells.

USP7 deubiquitylates SPRTN upon DPC induction

Next, we tested whether USP7 is the DUB responsible for regulating SPRTN's chromatin access by deubiquitylation upon DPC induction. Thus, we treated HCT116 WT and USP7 knock-out (KO) cells for 2 h with formaldehyde before assessing recruitment of SPRTN by chromatin fractionation. Indeed, endogenous SPRTN fails to be deubiqui-

tylated in the absence of USP7 upon formaldehyde exposure (Figure 4A). Unexpectedly however, the lack of deubiquitylation does not result in impaired recruitment. In USP7 KO cells, also SPRTN-Ub is found on chromatin. These results indicate that deubiquitylation occurs downstream or in parallel to recruitment and is not preceding SPRTN's re-localization to chromatin. To understand the contribution of USP7-mediated deubiquitylation to DPC repair, we generated DLD1 and HAP1 USP7 KO cells because sensitivity of HCT116 USP7 KO cells is difficult to assess due to their strong growth defect. HAP1 and DLD1 USP7 KO cells show defective SPRTN deubiquitylation and hypersensitivity towards formaldehyde exposure (Figure 4B-E). Importantly, the formaldehyde sensitivity of DLD1 USP7 KO cells is complemented by transient transfection of USP7^{WT} but not of USP7^{CS} (Figure 4F and Supplementary Figure S3A). Furthermore, HAP1 USP7 KO cells accumulate higher levels of DPCs following a 2-h exposure to formaldehyde as determined using a KCl-SDS precipitation assays (Figure 4G).

Of note, while this study was under consideration, it was proposed that SPRTN is deubiquitylated by VCPIP1 (29). In addition, a recent preprint argued that USP11 is responsible for SPRTN deubiquitylation (30). Given our identification of USP7, we compared the contribution of all three enzymes to SPRTN deubiquitylation. Neither VCPIP1 nor USP11 induce SPRTN deubiquitylation when overexpressed, while USP7 does (Supplementary Figure S3B). VCPIP1 and USP11 interact weakly with SPRTN in co-immunoprecipitating experiments, but show no (VCPIP1) or only weak (USP11) preference for SPRTN-Ub (Supplementary Figure S3B). siRNA-mediated depletion of VCPIP1 or USP11 has no effect on SPRTN deubiquitylation in DLD1 cells, while depletion of USP7 does (Supplementary Figure S3C). Moreover, we obtained HAP1 USP11 and VCPIP1 KO cells which show sensitivity towards formaldehyde but no defects in SPRTN deubiquitylation (Supplementary Figure S3D-E).

To conclude, under the conditions tested here, USP7 but not VCPIP1 or USP11 has a prominent role in deubiquitylating SPRTN in cells. Finally, the formaldehyde sensitivity and DPC accumulation observed in USP7 KO cells argue that deubiquitylation, although not involved in SPRTN's chromatin recruitment, must have an important function in DPC repair. Therefore, we further explored the effects of monoubiquitylation on the SPRTN protease.

Monoubiquitylation promotes degradation and autocleavage of SPRTN

Monoubiquitylation can lead to proteasomal degradation by priming polyubiquitylation (31,32). Thus, we assessed whether monoubiquitylation destabilizes SPRTN using cycloheximide-chase experiments. Indeed, endogenous SPRTN-Ub has a shorter half-life than non-ubiquitylated SPRTN, with degradation being blocked by proteasome inhibition (Figure 5A and Supplementary Figure S4A). Degradation is not affected by loss of USP7, which indicates that deubiquitylation is not involved in SPRTN protein stability under basal conditions (Supplementary Figure S4A). Proteasomal inhibition leads to accumulation of polyubiq-

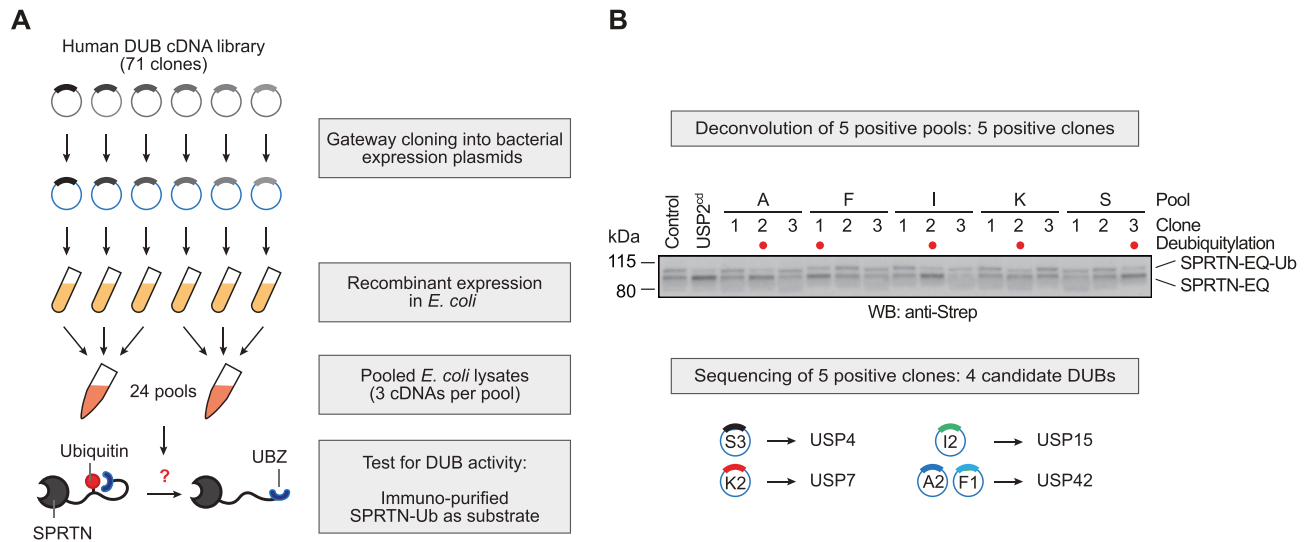


Figure 2. An *in vitro* screen identifies DUBs targeting ubiquitylated SPRTN. (A) Schematic depiction of the screening strategy employed to test seventy-one human deubiquitylating enzymes (DUBs) for their ability to deubiquitylate SPRTN. (B) Deconvolution of positive pools identified in Supplementary Figure S2A reveals four candidate DUBs. Lysates prepared from fifteen clones present in the five positive pools were incubated for 30 min at 25°C together with purified partially-monoubiquitylated YFP-SPRTN-EQ-Strep. Reactions were stopped by addition of LDS sample buffer and analysed by SDS-PAGE and western blotting using anti-Strep antibody. Lysates of BL21 cells served as negative control, the unspecific deubiquitylating activity of the catalytic domain of USP2 (USP2^{cd}) as positive control.

ubiquitylated SPRTN species, which are strongly reduced in the SPRTN-UBZ* variant, which provides further support for monoubiquitylation inducing degradation by priming polyubiquitylation (Figure 5B and Supplementary Figure S4B). Furthermore, a linear fusion of SPRTN with ubiquitin (SPRTN-Ub^{LF}, omitting the two C-terminal glycines), which has been previously suggested to mimic monoubiquitylation, destabilizes the entire SPRTN pool (Figure 5C) (21).

While conducting these experiments, we noted that cells expressing SPRTN-Ub^{LF} display various protein fragments, which are recognized by an antibody specific for the N-terminal YFP-tag (Figure 5D). These fragments become even more obvious when enriched on GFP-trap resins and correspond to the previously reported autocatalytic fragments seen in cells, which express WT SPRTN but are absent in cells expressing catalytically inactive SPRTN-EQ (Figure 5D) (8,9). These results raise the possibility that monoubiquitylation of SPRTN triggers enhanced autocleavage of the enzyme. In agreement, autocleavage of the non-ubiquitylated SPRTN-UBZ* variant is barely detectable, unless linearly-fused to ubiquitin (SPRTN-UBZ*-Ub^{LF}) (Figure 5D). Furthermore, deubiquitylation of SPRTN induced by overexpression of USP7^{WT}, but not of catalytically inactive USP7^{CS}, leads to reduced formation of autocatalytic SPRTN fragments (Figure 5E). Autocleavage of endogenous SPRTN is induced by formaldehyde exposure and is more prominent at lower concentrations while deubiquitylation is observable at higher concentrations (Figure 5F) (8). Remarkably, if monoubiquitylation of endogenous SPRTN is blocked by pre-treating cells with ubiquitin E1 inhibitor, autocleavage is strongly reduced (Figure 5F). Interestingly, autocleavage of endogenous SPRTN also increases in cells, which have been treated with proteasome inhibitors (Figure 5G and Supplementary

Figure S4C and D). This observation provides support for a model in which monoubiquitylated SPRTN is either degraded by the proteasome or undergoes autocleavage. In agreement, the short half-life of SPRTN-Ub is independent of the enzyme's catalytic activity and a SPRTN truncation (SPRTN^{aa1-227}) corresponding to the shortest autocleaved fragment is not particularly unstable (Supplementary Figure S4E-F). Taken together, proteasomal degradation and autocleavage appear to be independent outcomes induced by monoubiquitylation.

Next, we tested whether enhancement of SPRTN autocleavage by monoubiquitylation stems from a direct effect on the enzyme's activity. To this end, we produced recombinant SPRTN-Ub^{LF} and compared its autocleavage and substrate cleavage activity to WT SPRTN. Indeed, SPRTN-Ub^{LF} displays markedly increased DNA-dependent autocatalytic cleavage *in vitro* (Figure 6A). The effect is particularly strong in the presence of dsDNA and in high salt conditions. In contrast, cleavage of histone H1 or that of model DPC substrates (fluorescently-labelled protein G-oligonucleotide conjugates) is not significantly increased (Figure 6A and B). SPRTN autocleavage occurs *in trans* with one SPRTN molecule cleaving a second (8,9). A catalytically inactive Flag-tagged SPRTN-EQ variant is cleaved more efficiently by SPRTN-Ub^{LF} than by WT SPRTN. This suggests that modification of the SPRTN molecule cleaving *in trans* is sufficient to enhance autocleavage (Figure 6C). These *in vitro* data demonstrate that enhanced autocleavage of SPRTN-Ub in cells is caused by a direct effect of the modification on SPRTN activity. Thus, we conclude that monoubiquitylation negatively controls the SPRTN pool not only by inducing proteasomal degradation *in cis* but also by triggering the inactivation of other SPRTN molecules through *in trans* autocleavage.

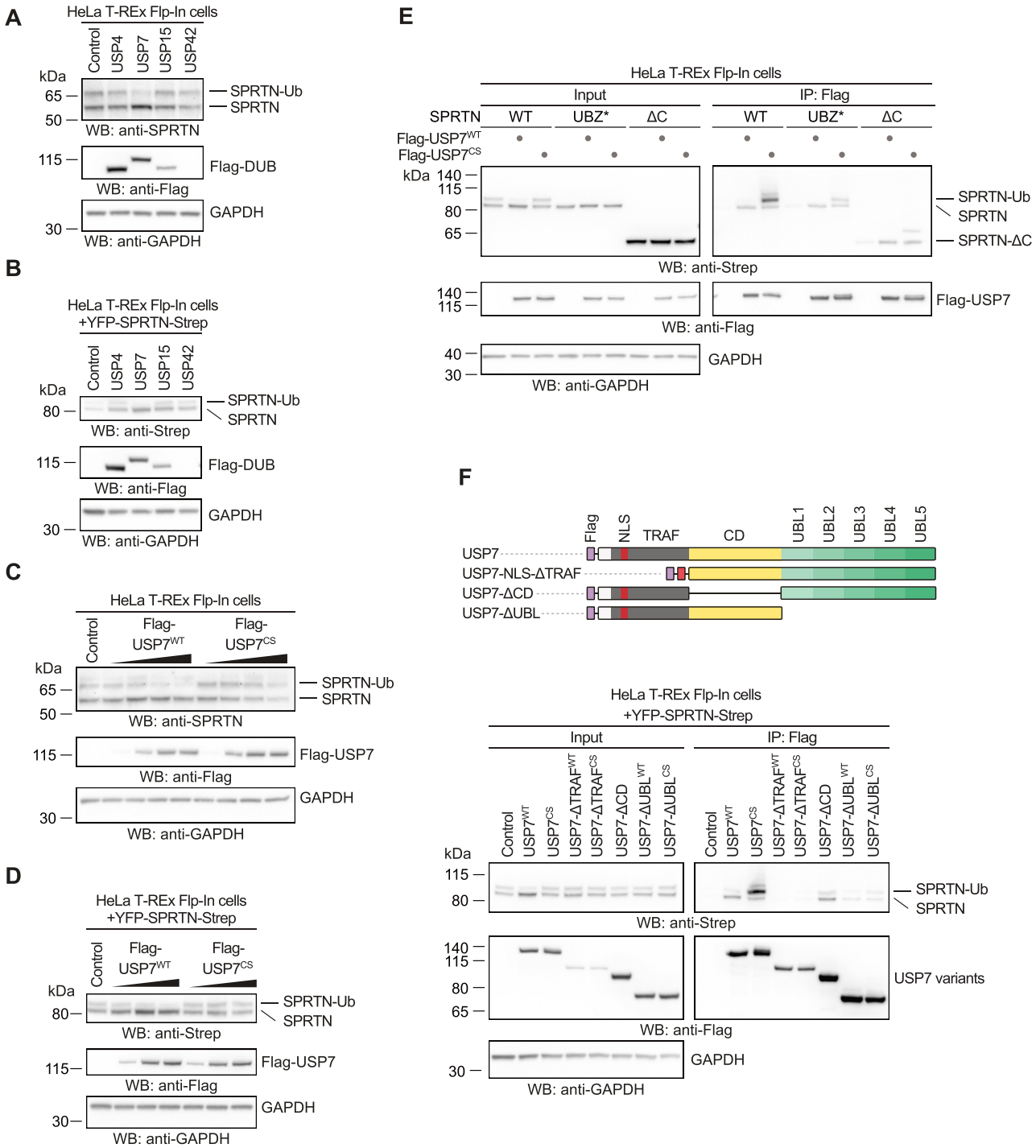


Figure 3. USP7 interacts with and targets ubiquitylated SPRTN in human cells. **(A)** Analysis of DUB overexpression-induced deubiquitylation of endogenous SPRTN in HeLa T-REx Flp-In cells. Indicated N-terminally Flag-tagged DUBs were transiently expressed for one day before cells were lysed and analysed by western blotting. **(B)** Analysis of DUB overexpression-induced deubiquitylation of doxycycline-inducible YFP-SPRTN-Strep stably expressed in HeLa T-REx Flp-In cells. Indicated N-terminally Flag-tagged DUBs were transiently expressed for one day before cells were lysed and analysed by western blotting. **(C)** Increasing amounts of N-terminally Flag-tagged USP7 (or the catalytically inactive CS variant) were transiently expressed in HeLa T-REx Flp-In cells for one day before cells were lysed and analysed by western blotting. **(D)** Increasing amounts of N-terminally Flag-tagged USP7 (or the catalytically inactive CS variant) were transiently expressed in HeLa T-REx Flp-In cells stably expressing doxycycline-inducible YFP-SPRTN-Strep for one day before cells were lysed and analysed by western blotting. **(E)** Plasmids encoding Flag-tagged full-length USP7 (WT or the catalytically inactive CS variant) were transiently transfected in HeLa T-REx Flp-In cells stably expressing the indicated doxycycline-inducible YFP-SPRTN-Strep variants. Binding was analysed by co-immunoprecipitation using anti-Flag beads followed by western blotting. **(F)** Schematic depiction of USP7's domain structure and protein truncations used for co-immunoprecipitation analysis with SPRTN (upper panel). Plasmids encoding Flag-tagged full-length USP7 (WT or the catalytically inactive CS variant) or the respective truncations were transiently transfected in HeLa T-REx Flp-In cells stably expressing doxycycline-inducible YFP-SPRTN-Strep. Binding was analysed by co-immunoprecipitation using anti-Flag beads followed by western blotting (lower panel).

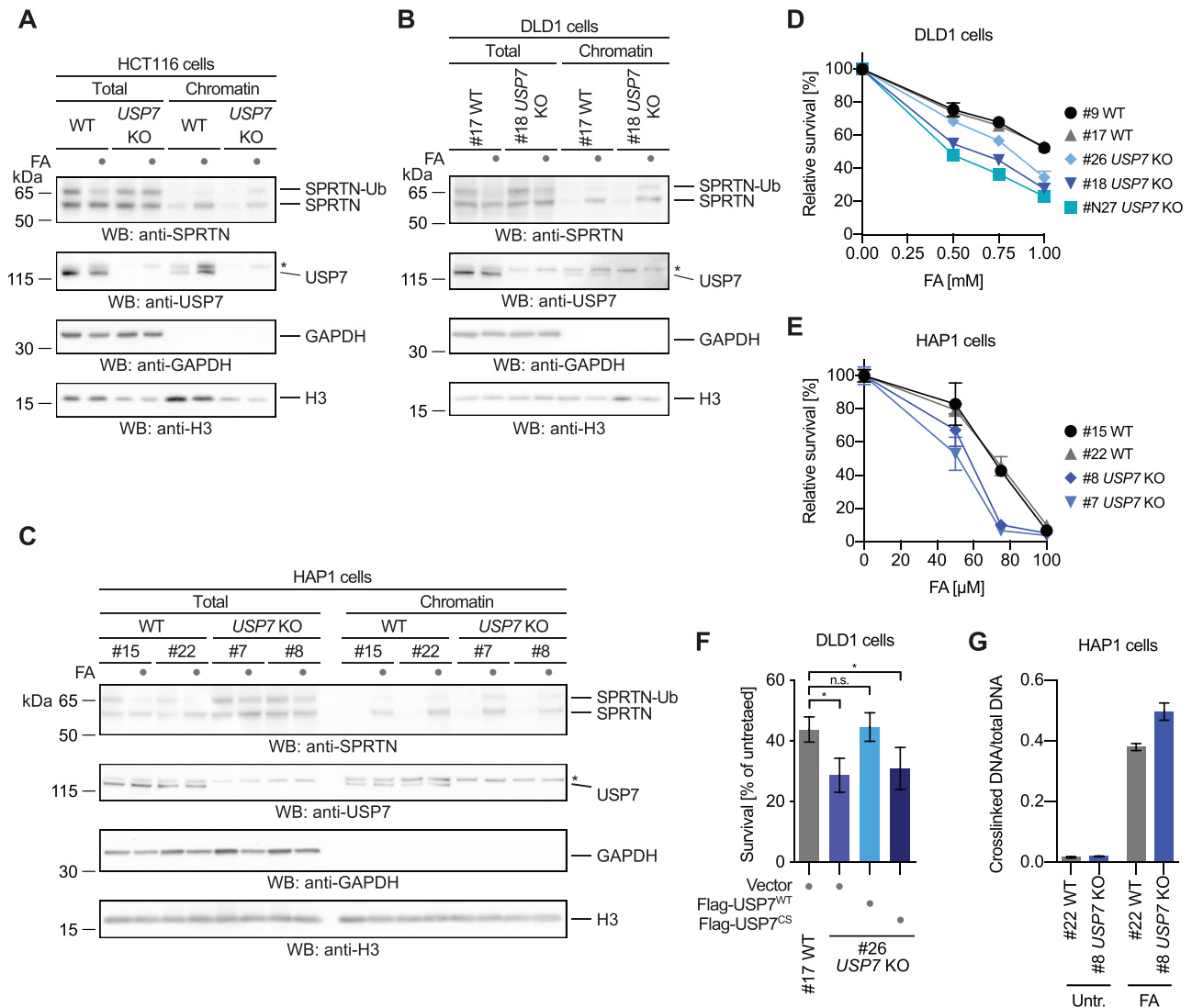


Figure 4. USP7 deubiquitylates SPRTN upon DPC induction. (A) HCT116 WT or *USP7* knock-out (KO) cells were treated with 2 mM formaldehyde (FA) for 2 h. Cells were either lysed directly in LDS sample buffer (total) or subjected to chromatin fractionation. Samples were then analyzed by SDS-PAGE followed by western blotting. Asterisks indicates a cross-reactive band. (B) Clonal DLD1 *USP7* KO cells and matched WT control cells were treated with 2 mM formaldehyde (FA) for 3 h. Cells were either lysed directly in LDS sample buffer (total) or subjected to chromatin fractionation. Samples were then analysed by SDS-PAGE followed by western blotting. Asterisks indicates a cross-reactive band. (C) Clonal HAP1 *USP7* KO cells and matched WT control cells were treated with 2 mM formaldehyde (FA) for 2 h. Cells were either lysed directly in LDS sample buffer (total) or subjected to chromatin fractionation. Samples were then analysed by SDS-PAGE followed by western blotting. Asterisks indicates a cross-reactive band. (D) Clonal DLD1 *USP7* KO cells and matched WT control cells were treated with the indicated formaldehyde concentrations for 2 h. After 48 h cell viability was determined using the alamarBlue cell viability assay. Values represent the mean \pm SD of three technical replicates normalized to the mean of untreated controls of each cell line (E) Clonal HAP1 *USP7* KO cells and matched WT control cells were treated with the indicated formaldehyde concentrations for 72 h. Cell viability was then determined using the alamarBlue cell viability assay. Values represent the mean \pm SD of three technical replicates normalized to the mean of untreated controls of each cell line. (F) YFP-tagged full-length USP7 (WT or the catalytically inactive CS variant) or the empty vector were transiently transfected in DLD1 *USP7* KO cells and matched WT control cells. Cells were treated with 1 mM formaldehyde for 2 h. After 48 h cell viability was determined using the alamarBlue cell viability assay. Values represent the mean \pm SEM of four independent biological replicates normalized to the mean of untreated controls of each cell line. Significance was determined using a paired *t*-test (**P*-value < 0.05). (G) Cellular DPCs were quantified in clonal HAP1 *USP7* KO cells and matched WT control cells treated with 75 μ M formaldehyde for 2 h using a KCl/SDS precipitation assay. DPCs were measured as the ratio of crosslinked DNA compared to total DNA. Values represent the mean \pm SD of three technical replicates.

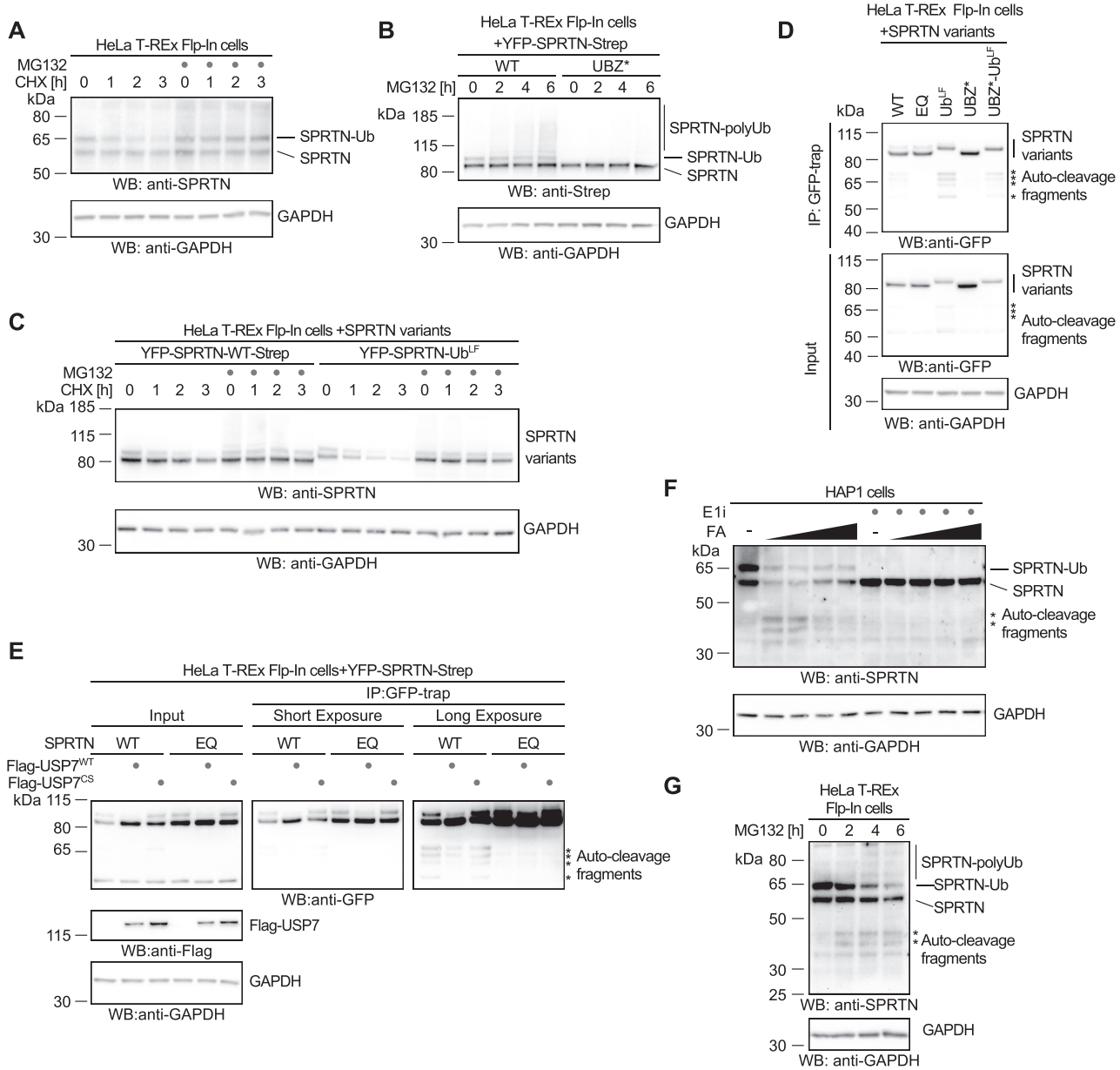


Figure 5. Monoubiquitylation promotes SPRTN degradation and autocleavage. (A) Stability of endogenous SPRTN was determined with a cycloheximide-chase experiment in HeLa-T-REx Flp-In cells. Cells were incubated with cycloheximide for the indicated amount of time (with or without a 2-h pre-treatment with the proteasome inhibitor MG132) prior to cell lysis and analysis by western blotting. (B) Polyubiquitylation of stably expressed doxycycline-inducible YFP-SPRTN-Strep or of YFP-SPRTN-UBZ*-Strep was determined in HeLa-T-REx Flp-In cells upon treatment with proteasome inhibitor MG132 for the indicated amount of time prior to cell lysis and analysis by western blotting. (C) Stability of stably expressed doxycycline-inducible YFP-SPRTN-Strep or a linear SPRTN-Ubiquitin fusion (YFP-SPRTN-Ub^L) was determined in HeLa-T-REx Flp-In cells using a cycloheximide-chase experiment. Cells were incubated in the presence of cycloheximide for the indicated amount of time (with or without a 2-h pre-treatment with the proteasome inhibitor MG132) prior to cell lysis and analysis by western blotting. (D) Indicated YFP-SPRTN-Strep or linear SPRTN-Ubiquitin fusion (YFP-SPRTN-Ub^L) variants were transiently transfected in HeLa-T-REx Flp-In cells. SPRTN auto-cleavage fragments were enriched on GFP-trap resins, followed by western blotting against the N-terminal YFP-tag. Western blotting of cell lysates against GAPDH serves as loading control. Asterisks indicate auto-cleavage fragments. (E) Indicated YFP-SPRTN-Strep variants were transiently transfected in HeLa-T-REx Flp-In cells in combination with Flag-tagged full-length USP7 (WT or the catalytically inactive CS variant) or the empty vector. SPRTN auto-cleavage fragments were enriched on GFP-trap resins, followed by western blotting against the N-terminal YFP-tag. Western blotting against GAPDH of cell lysates serves as loading control. Asterisks indicate auto-cleavage fragments. (F) HAP1 cells were treated with increasing amounts of formaldehyde (FA, 0.25, 0.5, 1 and 2 mM) for 2 h (either with or without a 2-h pre-treatment with ubiquitin-activating enzyme E1 inhibitor as indicated) prior to cell lysis and analysis by western blotting. Asterisks indicate auto-cleavage fragments. (G) HeLa-T-REx Flp-In cells were treated with proteasome inhibitor MG132 for the indicated amount of time prior to cell lysis and analysis by western blotting. Asterisks indicate auto-cleavage fragments.

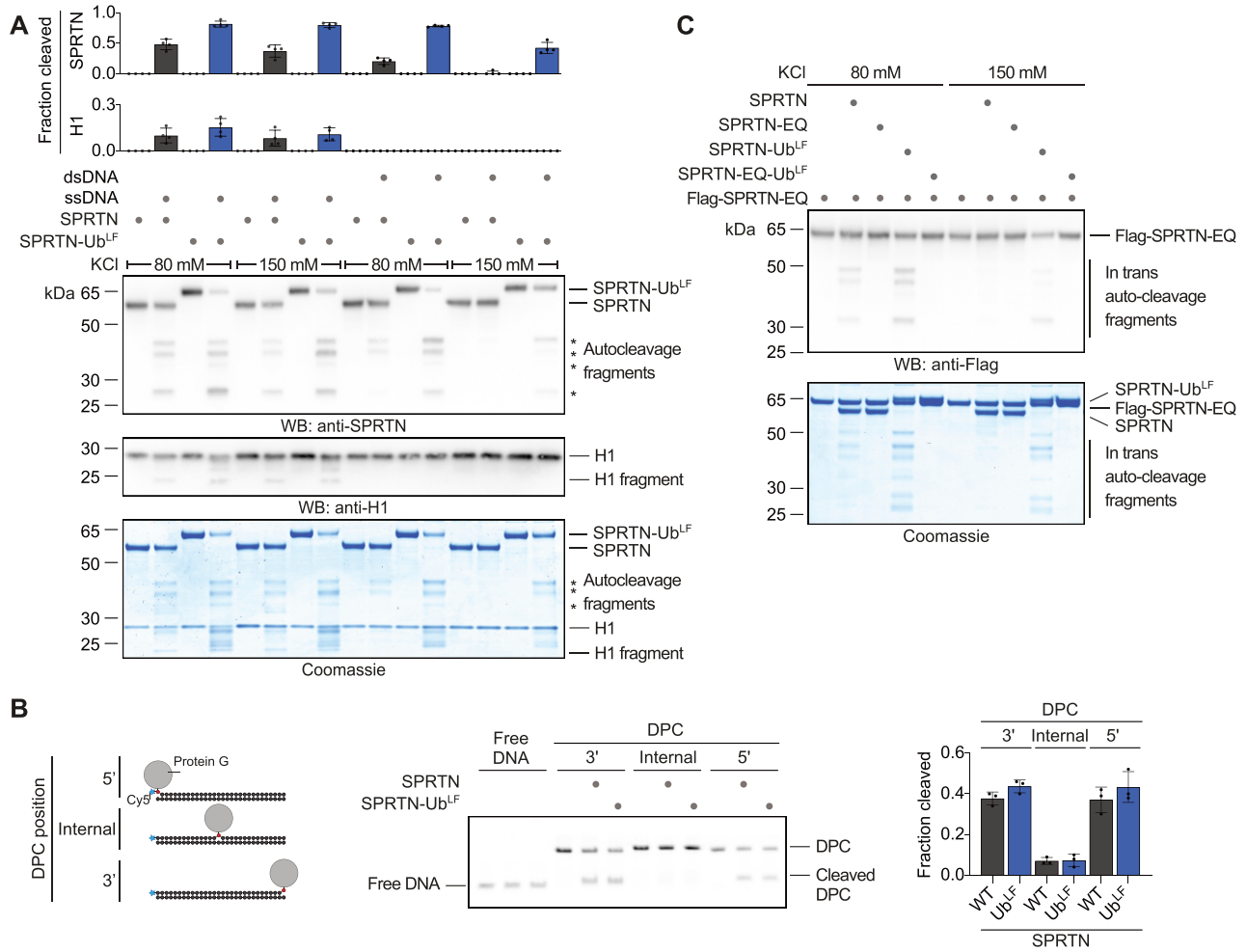


Figure 6. Monoubiquitylation promotes SPRTN autocleavage *in trans*. (A) Recombinant SPRTN or a linear SPRTN-Ubiquitin fusion (SPRTN-Ub^{LF}) (500 nM) were incubated with histone H1 alone or in the presence of either single- (ss) or double-stranded (ds) RFI Φ X174 DNA (11.1 nM) for 60 min at 25°C. Salt concentrations were as indicated. Reactions were analysed by SDS-PAGE followed by western blotting and staining with InstantBlue Coomassie protein stain. Quantification of western blots of results of SPRTN and histone H1 cleavage: values represent the mean \pm SD of four independent experiments. (B) Indicated model protein G-oligonucleotide conjugates (25nM) were incubated alone or in the presence of recombinant SPRTN (6.25 nM, WT or a linear SPRTN-Ubiquitin fusion (SPRTN-Ub^{LF})) for 2 h at 25°C prior to separation by native PAGE. Right panel, quantification of DPC cleavage: values represent the mean \pm SD of three independent experiments. (C) Recombinant catalytically inactive Flag-SPRTN-EQ (500 nM) was incubated alone or in combination with active SPRTN (500 nM, WT or a linear SPRTN-Ubiquitin fusion (SPRTN-Ub^{LF})) in the presence of DNA (Φ X174 RFI dsDNA, 11.1 nM) for 60 min at 25°C. Salt concentrations were as indicated. Reactions were subjected to SDS-PAGE followed by staining with InstantBlue Coomassie protein stain and western blotting.

DISCUSSION

The regulatory ubiquitin switch revealed here is distinct from other prominent types of monoubiquitylation events occurring during genome maintenance. FANCD2 and FANCI are ubiquitylated by the Fanconi anemia core complex in a site-specific manner upon recruitment to chromatin during the repair of inter-strand crosslinks (33). PCNA is site-specifically monoubiquitylated as a response to stalled DNA synthesis, which fosters recruitment of translesion synthesis polymerases (34–37). In contrast, SPRTN monoubiquitylation is not triggered by DPC induction but instead appears to be a constitutive process. Our data demonstrate that the modification can have two distinct outcomes, both of which lead to inactivation of the enzyme (Figure 7). Firstly, monoubiquitylation primes

SPRTN *in cis* for proteasomal degradation by fostering polyubiquitylation. Secondly, it further reduces the amount of active SPRTN by promoting autocleavage *in trans*. Importantly, SPRTN autocleavage requires the presence of DNA *in vitro*, which infers that monoubiquitylation-triggered autocleavage in cells is specifically affecting DNA-bound SPRTN molecules. If cells face DPC induction, USP7-mediated deubiquitylation appears to be important to stall this negative regulation in order to prolong the half-life of active DNA-bound SPRTN. Formaldehyde exposure triggers wide-spread ubiquitylation events in cells (38). It is thus attractive to speculate that in the presence of DPCs SPRTN's UBZ domain engages with specific ubiquitylation signals. In turn, this would expose the monoubiquitylation and thereby allow USP7 to remove the modification. Al-

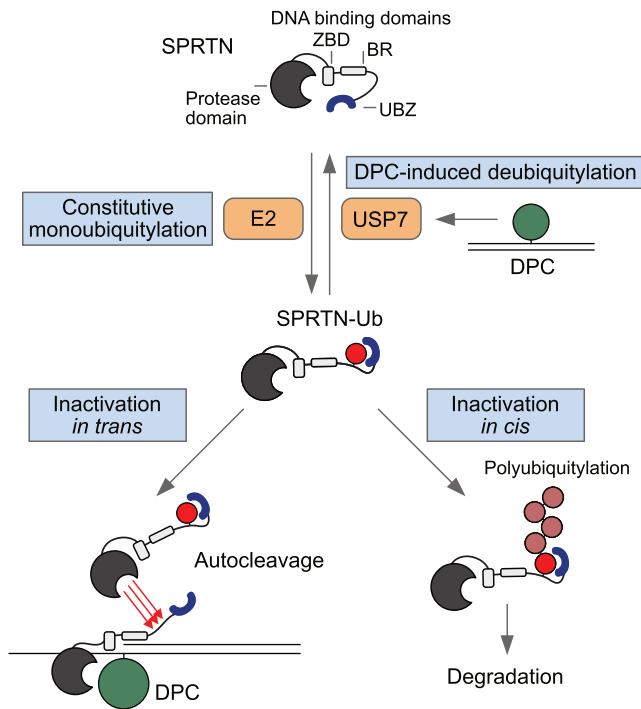


Figure 7. Regulation of SPRTN by monoubiquitylation and USP7. Proposed model for the regulation of SPRTN by monoubiquitylation and USP7-mediated deubiquitylation. SPRTN is subjected to constitutive promiscuous monoubiquitylation of its C-terminal tail. The modification is shielded by SPRTN's ubiquitin binding zinc-finger (UBZ). Monoubiquitylation affects SPRTN twofold. It primes SPRTN *in cis* for proteasomal degradation by inducing polyubiquitylation while also triggering inactivation by fostering autocleavage of other SPRTN molecules *in trans*. USP7 relieves this inhibition by deubiquitylating SPRTN upon induction of DNA–protein crosslinks (DPCs).

though the regulation described here is important to control SPRTN protein levels, it does not participate in the recruitment of SPRTN to chromatin. This finding is further supported by the fact that the RJALS syndrome variant SPRTN- Δ C retains a large degree of function despite lacking the UBZ and not being monoubiquitylated. In this context, it will be interesting to investigate whether the phenotypes observed in RJALS are caused, at least in part, by the loss of the negative regulation of SPRTN and not only by a reduction in DPC repair capacity. Notably, recruitment of SPRTN to UV-induced lesions (but not DPCs) has been shown to depend on the UBZ domain potentially indicating that this domain serves dual purposes (20–22). However, how SPRTN is recruited to DPCs remains controversial with evidence pointing towards ubiquitylation or SUMOylation signals (39,40). Understanding how the presence of crosslinks is signalled to DPC repair enzymes will be critical to decipher decision making during DPC repair. The recent identification of several additional proteases targeting DPCs implies that DPC repair pathway choice is a complex cellular process (13,39,41–45). At any rate, the intricate negative regulation described here highlights not only the complexity of DPC repair but also the importance of controlling SPRTN's potentially toxic proteolytic activity.

DATA AVAILABILITY

Data are available from the corresponding author upon reasonable request.

SUPPLEMENTARY DATA

Supplementary Data are available at NAR Online.

ACKNOWLEDGEMENTS

We thank S. Panier, G. Hewitt and R. Bellelli for discussions and comments on the manuscript.

FUNDING

LMU – China Scholarship Council Program [to S.Z.]; Peter and Traudl Engelhorn Foundation [to H.L.]; International Max-Planck Research School for Molecular Life Sciences [to A.C.A., P.W.]; European Research Council [ERC Starting Grant 801750 DNAProteinCrosslinks to J.S.]; Alfried Krupp Prize for Young University Teachers awarded by the Alfried Krupp von Bohlen and Halbach-Stiftung [to J.S.]; Center for Integrated Protein Sciences Munich (CIPSM) [to J.S.]. Funding for open access charge: ERC [Starting Grant 801750 DNAProteinCrosslinks].

Conflict of interest statement. None declared.

REFERENCES

- Nakano, T., Miyamoto-Matsubara, M., Shoulkamy, M.I., Salem, A.M., Pack, S.P., Ishimi, Y. and Ide, H. (2013) Translocation and stability of replicative DNA helicases upon encountering DNA–protein cross-links. *J. Biol. Chem.*, **288**, 4649–4658.
- Nakano, T., Ouchi, R., Kawazoe, J., Pack, S.P., Makino, K. and Ide, H. (2012) T7 RNA polymerases backed up by covalently trapped proteins catalyze highly error prone transcription. *J. Biol. Chem.*, **287**, 6562–6572.
- Duxin, J.P., Dewar, J.M., Yardimci, H. and Walter, J.C. (2014) Repair of a DNA–protein crosslink by replication-coupled proteolysis. *Cell*, **159**, 346–357.
- Barker, S., Weinfeld, M. and Murray, D. (2005) DNA–protein crosslinks: their induction, repair, and biological consequences. *Mutat. Res.*, **589**, 111–135.
- Stinglee, J., Bellelli, R. and Boulton, S.J. (2017) Mechanisms of DNA–protein crosslink repair. *Nat. Rev. Mol. Cell Biol.*, **18**, 563–573.
- Nakano, T., Xu, X., Salem, A.M.H., Shoulkamy, M.I. and Ide, H. (2017) Radiation-induced DNA–protein cross-links: mechanisms and biological significance. *Free Radic. Biol. Med.*, **107**, 136–145.
- Stinglee, J., Schwarz, M.S., Bloemke, N., Wolf, P.G. and Jentsch, S. (2014) A DNA-dependent protease involved in DNA–protein crosslink repair. *Cell*, **158**, 327–338.
- Stinglee, J., Bellelli, R., Alte, F., Hewitt, G., Sarek, G., Maslen, S.L., Tsutakawa, S.E., Borg, A., Kjaer, S., Tainer, J.A. *et al.* (2016) Mechanism and regulation of DNA–Protein crosslink repair by the DNA-dependent metalloprotease SPRTN. *Mol. Cell*, **64**, 688–703.
- Vaz, B., Popovic, M., Newman, J.A., Fielden, J., Aitkenhead, H., Halder, S., Singh, A.N., Vendrell, I., Fischer, R., Torrecilla, I. *et al.* (2016) Metalloprotease SPRTN/DVC1 orchestrates replication-coupled DNA–protein crosslink repair. *Mol. Cell*, **64**, 704–719.
- Lopez-Mosqueda, J., Maddi, K., Prgomet, S., Kalayil, S., Marinovic-Terzic, I., Terzic, J. and Dikic, I. (2016) SPRTN is a mammalian DNA-binding metalloprotease that resolves DNA–protein crosslinks. *Elife*, **5**, e21491.
- Mórocz, M., Zsigmond, E., Tóth, R., Enyedi, M.Z., Pintér, L. and Haracska, L. (2017) DNA-dependent protease activity of human Spartan facilitates replication of DNA–protein crosslink-containing DNA. *Nucleic Acids Res.*, **45**, 3172–3188.

12. Reinking, H.K., Hofmann, K. and Stinglele, J. (2020) Function and evolution of the DNA–protein crosslink proteases Wss1 and SPRTN. *DNA Repair (Amst.)*, **88**, 102822–102822.
13. Larsen, N.B., Gao, A.O., Sparks, J.L., Gallina, I., Wu, R.A., Mann, M., Raschle, M., Walter, J.C. and Duxin, J.P. (2019) Replication-coupled DNA-protein crosslink repair by SPRTN and the proteasome in xenopus egg extracts. *Mol. Cell*, **73**, 574–588.
14. Sparks, J.L., Chistol, G., Gao, A.O., Raschle, M., Larsen, N.B., Mann, M., Duxin, J.P. and Walter, J.C. (2019) The CMG helicase bypasses DNA-protein cross-links to facilitate their repair. *Cell*, **176**, 167–181.
15. Maskey, R.S., Kim, M.S., Baker, D.J., Childs, B., Malureanu, L.A., Jeganathan, K.B., Machida, Y., van Deursen, J.M. and Machida, Y.J. (2014) Spartan deficiency causes genomic instability and progeroid phenotypes. *Nat. Commun.*, **5**, 5744.
16. Lessel, D., Vaz, B., Halder, S., Lockhart, P.J., Marinovic-Terzic, I., Lopez-Mosqueda, J., Philipp, M., Sim, J.C., Smith, K.R., Oehler, J. et al. (2014) Mutations in SPRTN cause early onset hepatocellular carcinoma, genomic instability and progeroid features. *Nat. Genet.*, **46**, 1239–1244.
17. Ruijs, M.W.G., van Andel, R.N.J., Oshima, J., Madan, K., Nieuwint, A.W.M. and Aalfs, C.M. (2003) Atypical progeroid syndrome: an unknown helicase gene defect? *Am. J. Med. Genet. A*, **116A**, 295–299.
18. Maskey, R.S., Flatten, K.S., Sieben, C.J., Peterson, K.L., Baker, D.J., Nam, H.-J., Kim, M.S., Smyrk, T.C., Kojima, Y., Machida, Y. et al. (2017) Spartan deficiency causes accumulation of Topoisomerase I cleavage complexes and tumorigenesis. *Nucleic Acids Res.*, **45**, 4564–4576.
19. Reinking, H.K., Kang, H.S., Götz, M.J., Li, H.Y., Kieser, A., Zhao, S., Acampora, A.C., Weickert, P., Fessler, E., Jae, L.T. et al. (2020) DNA structure-specific cleavage of DNA-protein crosslinks by the SPRTN protease. *Mol. Cell*, **80**, 102–113.
20. Centore, R.C., Yazinski, S.A., Tse, A. and Zou, L. (2012) Spartan/C1orf124, a reader of PCNA ubiquitylation and a regulator of UV-induced DNA damage response. *Mol. Cell*, **46**, 625–635.
21. Mosbech, A., Gibbs-Seymour, I., Kagias, K., Thorslund, T., Beli, P., Povlsen, L., Nielsen, S.V., Smedegaard, S., Sedgwick, G., Lukas, C. et al. (2012) DVC1 (C1orf124) is a DNA damage-targeting p97 adaptor that promotes ubiquitin-dependent responses to replication blocks. *Nat. Struct. Mol. Biol.*, **19**, 1084–1092.
22. Davis, E.J., Lachaud, C., Appleton, P., Macartney, T.J., Nathke, I. and Rouse, J. (2012) DVC1 (C1orf124) recruits the p97 protein segregase to sites of DNA damage. *Nat. Struct. Mol. Biol.*, **19**, 1093–1100.
23. Hyer, M.L., Milhollen, M.A., Ciavarrri, J., Fleming, P., Traore, T., Sappal, D., Huck, J., Shi, J., Gavin, J., Brownell, J. et al. (2018) A small-molecule inhibitor of the ubiquitin activating enzyme for cancer treatment. *Nat. Med.*, **24**, 186–193.
24. Cao, J., Wu, L., Zhang, S.M., Lu, M., Cheung, W.K., Cai, W., Gale, M., Xu, Q. and Yan, Q. (2016) An easy and efficient inducible CRISPR/Cas9 platform with improved specificity for multiple gene targeting. *Nucleic Acids Res.*, **44**, e149.
25. Zhitkovich, A. and Costa, M. (1992) A simple, sensitive assay to detect DNA–protein crosslinks in intact cells and in vivo. *Carcinogenesis*, **13**, 1485–1489.
26. Hoeller, D., Crosetto, N., Blagoev, B., Raiborg, C., Tikkanen, R., Wagner, S., Kowanetz, K., Breitling, R., Mann, M., Stenmark, H. et al. (2006) Regulation of ubiquitin-binding proteins by monoubiquitination. *Nat. Cell Biol.*, **8**, 163–169.
27. Woelk, T., Oldrini, B., Maspero, E., Confalonieri, S., Cavallaro, E., Di Fiore, P.P. and Polo, S. (2006) Molecular mechanisms of coupled monoubiquitination. *Nat. Cell Biol.*, **8**, 1246–1254.
28. Hoeller, D., Hecker, C.M., Wagner, S., Rogov, V., Dotsch, V. and Dikic, I. (2007) E3-independent monoubiquitination of ubiquitin-binding proteins. *Mol. Cell*, **26**, 891–898.
29. Huang, J., Zhou, Q., Gao, M., Newshean, S., Zhao, F., Kim, W., Zhu, Q., Kojima, Y., Yin, P., Zhang, Y. et al. (2020) Tandem deubiquitination and acetylation of sprtn promotes dna-protein crosslink repair and protects against aging. *Mol. Cell*, **79**, 824–835.
30. Perry, M., Kollala, S.S., Biegert, M., Su, G., Kodavati, M., Mallard, H., Kreiling, N., Holbrook, A. and Ghosal, G. (2020) USP11 deubiquitinates monoubiquitinated SPRTN to repair DNA–protein crosslinks. bioRxiv doi: <https://doi.org/10.1101/2020.06.30.180471>, 01 July 2020, preprint: not peer reviewed.
31. Koegl, M., Hoppe, T., Schlenker, S., Ulrich, H.D., Mayer, T.U. and Jentsch, S. (1999) A novel ubiquitination factor, E4, is involved in multiubiquitin chain assembly. *Cell*, **96**, 635–644.
32. Braten, O., Livneh, I., Ziv, T., Admon, A., Kehat, I., Caspi, L.H., Gonen, H., Bercovich, B., Godzik, A., Jahandideh, S. et al. (2016) Numerous proteins with unique characteristics are degraded by the 26S proteasome following monoubiquitination. *PNAS*, **113**, E4639–E4647.
33. Cecaldi, R., Sarangi, P. and D’Andrea, A.D. (2016) The Fanconi anaemia pathway: new players and new functions. *Nat. Rev. Mol. Cell Biol.*, **17**, 337–349.
34. Moldovan, G.-L., Pfander, B. and Jentsch, S. (2007) PCNA, the maestro of the replication fork. *Cell*, **129**, 665–679.
35. Bienko, M., Green, C.M., Crosetto, N., Rudolf, F., Zapart, G., Coull, B., Kannouche, P., Wider, G., Peter, M., Lehmann, A.R. et al. (2005) Ubiquitin-binding domains in Y-family polymerases regulate translesion synthesis. *Science*, **310**, 1821–1824.
36. Stelter, P. and Ulrich, H.D. (2003) Control of spontaneous and damage-induced mutagenesis by SUMO and ubiquitin conjugation. *Nature*, **425**, 188–191.
37. Plosky, B.S., Vidal, A.E., Fernandez de Henestrosa, A.R., McLenigan, M.P., McDonald, J.P., Mead, S. and Woodgate, R. (2006) Controlling the subcellular localization of DNA polymerases ι and η via interactions with ubiquitin. *EMBO J.*, **25**, 2847–2855.
38. Ortega-Atienza, S., Rubis, B., McCarthy, C. and Zhitkovich, A. (2016) Formaldehyde is a potent proteotoxic stressor causing rapid heat shock transcription factor 1 activation and lys48-linked polyubiquitination of proteins. *Am. J. Pathol.*, **186**, 2857–2868.
39. Borgermann, N., Ackermann, L., Schwertman, P., Hendriks, I.A., Thijssen, K., Liu, J.C., Lans, H., Nielsen, M.L. and Mailand, N. (2019) SUMOylation promotes protective responses to DNA–protein crosslinks. *EMBO J.*, **38**, e101496.
40. Fielden, J., Wiseman, K., Torrecilla, I., Li, S., Hume, S., Chiang, S.-C., Ruggiano, A., Narayan Singh, A., Freire, R., Hassanieh, S. et al. (2020) TEX264 coordinates p97- and SPRTN-mediated resolution of topoisomerase I-DNA adducts. *Nat. Commun.*, **11**, 1274.
41. Bhargava, V., Goldstein, C.D., Russell, L., Xu, L., Ahmed, M., Li, W., Casey, A., Servage, K., Kollipara, R., Picciarelli, Z. et al. (2020) GCNA preserves genome integrity and fertility across species. *Dev. Cell*, **52**, 38–52.
42. Dokshin, G.A., Davis, G.M., Sawle, A.D., Eldridge, M.D., Nicholls, P.K., Gourley, T.E., Romer, K.A., Molesworth, L.W., Tatnell, H.R., Ozturk, A.R. et al. (2020) GCNA interacts with spartan and topoisomerase II to regulate genome stability. *Dev. Cell*, **52**, 53–68.
43. Serbyn, N., Noireterre, A., Bagdiul, I., Plank, M., Michel, A.H., Loewith, R., Kornmann, B. and Stutz, F. (2019) The aspartic protease ddi1 contributes to dna-protein crosslink repair in yeast. *Mol. Cell*, **77**, 1066–1079.
44. Svoboda, M., Konvalinka, J., Trempe, J.F. and Grantz Saskova, K. (2019) The yeast proteases Ddi1 and Wss1 are both involved in the DNA replication stress response. *DNA Repair (Amst.)*, **80**, 45–51.
45. Kojima, Y., Machida, Y., Palani, S., Caulfield, T.R., Radisky, E.S., Kaufmann, S.H. and Machida, Y.J. (2020) FAM111A protects replication forks from protein obstacles via its trypsin-like domain. *Nat. Commun.*, **11**, 1318.

SUPPLEMENTARY DATA

A ubiquitin switch controls autocatalytic inactivation of the DNA-protein crosslink repair protease SPRTN

Shubo Zhao, Anja Kieser, Hao-Yi Li, Hannah K. Reinking, Pedro Weickert, Simon Euteneuer, Denitsa Yaneva, Aleida C. Acampora, Maximilian J. Götz, Regina Feederle and Julian Stingele

Figure S1 (related to Figure 1). E3-independent monoubiquitylation SPRTN *in vitro*.

A. Analysis of monoubiquitylation of truncated SPRTN variants. Plasmids encoding the Strep-tagged SPRTN- Δ 400 truncation (carrying the indicated lysine to arginine (KR) substitutions. K407 was not replaced in the SPRTN- Δ 400-8KR variant) were transiently transfected in HeLa T-REx Flp-In cells. Expression of SPRTN was induced by addition of doxycycline for 16 hours before cells were lysed and subjected to immunoprecipitation using anti-Strep beads followed by western blotting. Western blotting of cell lysates against Tubulin serves as loading control.

B. Twenty-nine human E2 ubiquitin conjugating enzymes (2 μ M) were incubated together with SPRTN-EQ (2 μ M), E1 ubiquitin activating enzyme (100 nM), ubiquitin (50 μ M), DNA (11.1 nM Φ X174 single-stranded DNA) and ATP (2 mM) for 1.5 hours at 30°C. Reactions were stopped by addition of LDS sample buffer and subjected to SDS-PAGE followed by staining with InstantBlue Coomassie protein stain.

C. *In vitro* ubiquitylation assays containing SPRTN-EQ (410 nM), E1 ubiquitin activating enzyme (300 nM), UBE2D3 (16 μ M), ubiquitin WT or no-Lys, N-terminally biotinylated ubiquitin (50 μ M) and ATP (2 mM) were incubated for 1.5 hours at 30°C. Reactions were stopped by addition of LDS sample buffer and subjected to SDS-PAGE followed by staining with InstantBlue Coomassie protein stain.

Figure S2 (related to Figure 2). An *in vitro* screen reveals that USP7 targets ubiquitylated SPRTN.

A. Result of the primary screen schematically depicted in Figure 2A. Twenty-four pools (each containing three different lysates of *E. coli* cells expressing different DUB cDNAs) were incubated for 30 min at 25°C together with purified partially-ubiquitylated YFP-SPRTN-EQ-Strep in three experimental sets (A-K, L-N, O-X). Reactions were stopped by addition of LDS sample buffer and analysed by SDS-PAGE and western blotting using anti-Strep antibody. Lysates of BL21 cells served as negative control, the unspecific deubiquitylating activity of the catalytic domain of the USP2 (USP2^{cd}) as positive control.

B. Deubiquitylation activity of indicated partially purified DUBs was compared using the commercial Ubiquitin-Rhodamine cleavage assay, which measures the release of a rhodamine fluorophore C-terminally conjugated to ubiquitin with cleavage resulting in increased fluorescence. Left panel, increase in rhodamine fluorescence over time. Right panel, initial velocities of the deubiquitylating reactions. The catalytic domain of the USP2 (USP2^{cd}) served as positive control. Values represent the mean \pm SD of two technical replicates.

C. Indicated partially purified DUBs were incubated for 30 min at 25°C together with purified partially-ubiquitylated YFP-SPRTN-EQ-Strep. Reactions were stopped by addition of LDS sample buffer and analysed by SDS-PAGE and western blotting using anti-Strep antibody.

Figure S2 (related to Figure 2)

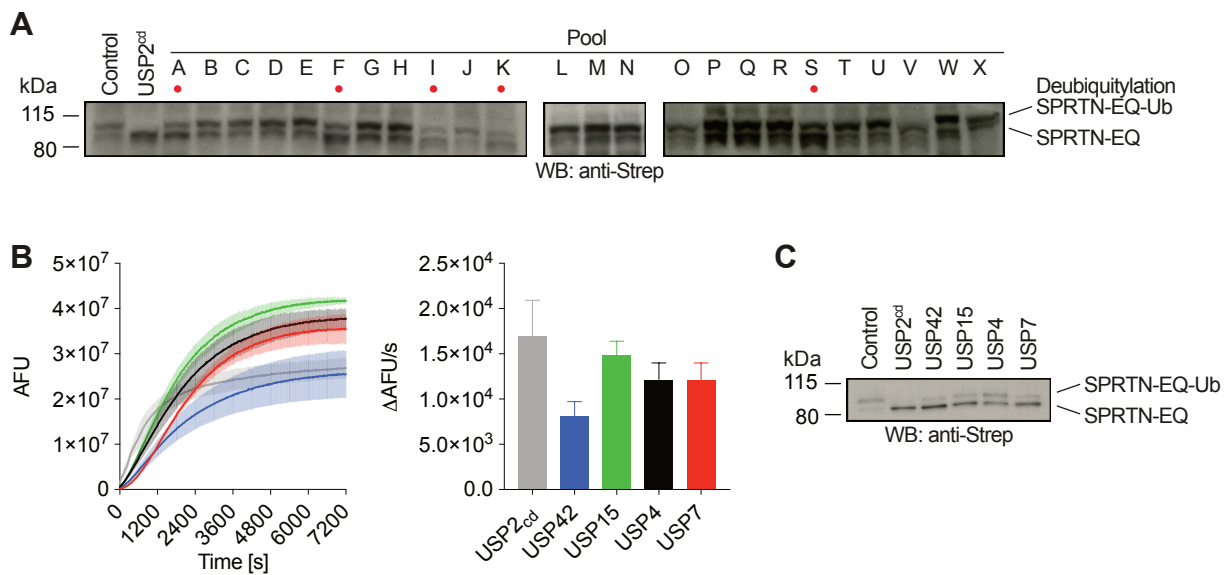


Figure S3 (related to Figure 4). USP7 deubiquitylates SPRTN upon DPC induction.

A. Western blot analysis of DLD1 WT or *USP7* KO cells transiently transfected with empty vector, YFP-tagged USP7 WT or the catalytically inactive USP7 CS variant, as indicated. Asterisks indicate a cross-reactive band.

B. Plasmids encoding Flag-tagged full-length USP7, VCPIP1 or USP11 (WT or catalytically inactive variants) or the empty vector were transiently transfected in HeLa T-REx Flp-In cells stably expressing doxycycline-inducible YFP-SPRTN-Strep. Binding was analysed by co-immunoprecipitation using anti-Flag beads followed by western blotting.

C. DLD1 cells transfected with siRNA pools targeting USP7, VCPIP1 or USP11 were treated for 2 hours with 2 mM formaldehyde (FA) 72 hours after transfection. Cells were lysed in LDS sample buffer and analysed by SDS-PAGE followed by western blotting.

D. HAP1 WT, *USP11* KO and *VCPIP1* KO cells were treated with the indicated formaldehyde concentrations for 72 hours. Cell viability was then determined using the alamarBlue cell viability assay. Values represent the mean \pm SD of three technical replicates normalized to the mean of untreated controls of each cell line.

E. HAP1 WT, *USP7* KO, *VCPIP1* KO and *USP11* KO cells were treated with 2 mM formaldehyde (FA) for 3 hours. Cells were either lysed directly in LDS sample buffer (total) or subjected to chromatin fractionation. Samples were then analysed by SDS-PAGE followed by western blotting. Asterisks indicate a cross-reactive band.

Figure S3 (related to Figure 4)

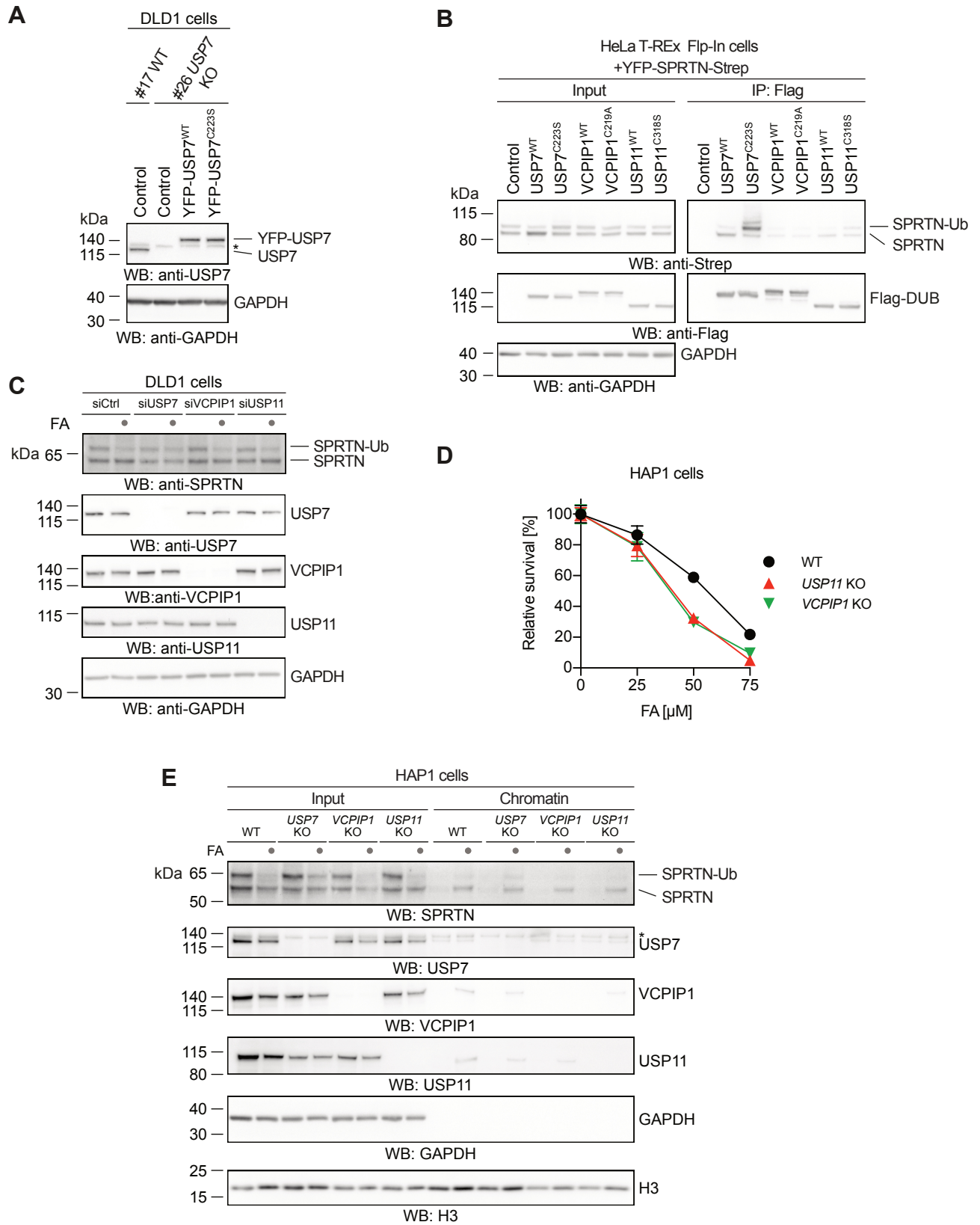


Figure S4 (related to Figure 5). Monoubiquitylation promotes SPRTN degradation and autocleavage.

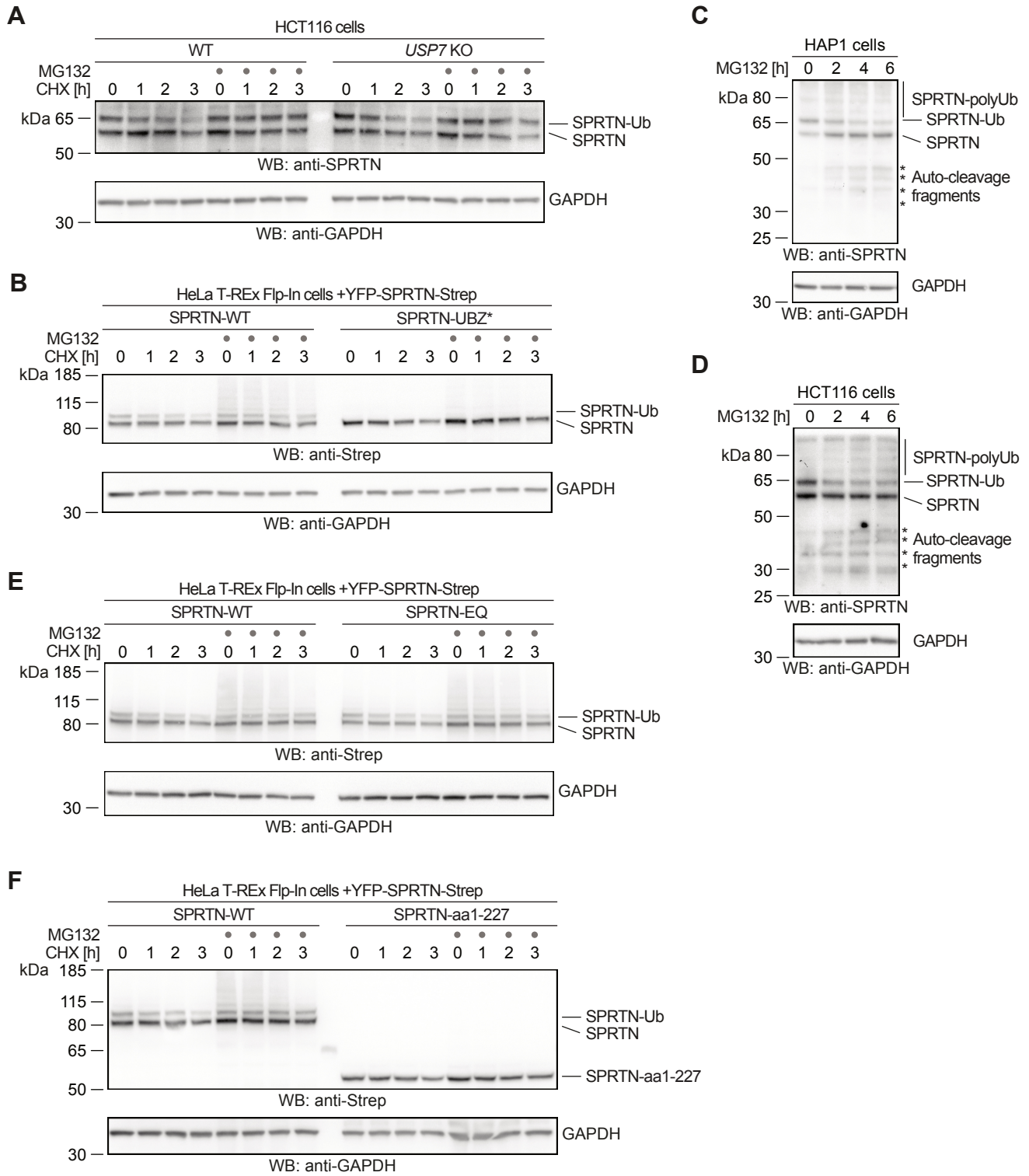
A. Stability of endogenous SPRTN was determined in HCT116 WT or *USP7* KO cells using a cycloheximide-chase experiment. Cells were incubated in the presence of cycloheximide for the indicated amount of time (with or without a 2-hour pre-treatment with the proteasome inhibitor MG132) prior to cell lysis and analysis by western blotting.

B. Stability of stably expressed doxycycline-inducible YFP-SPRTN-Strep and YFP-SPRTN-UBZ*-Strep was determined in HeLa-T-REx Flp-In cells using a cycloheximide-chase experiment. Cells were incubated in the presence of cycloheximide for the indicated amount of time (with or without a 2-hour pre-treatment with the proteasome inhibitor MG132) prior to cell lysis and analysis by western blotting.

C-D. HAP1 or HCT116 cells were treated with proteasome inhibitor MG132 for the indicated amount of time prior to cell lysis and analysis by western blotting. Asterisks indicate autocleavage fragments.

E-F. Stability of stably expressed doxycycline-inducible YFP-SPRTN-Strep and catalytically inactive YFP-SPRTN-EQ-Strep or the truncated YFP-SPRTN-aa1-227-Strep was determined in HeLa-T-REx Flp-In cells using a cycloheximide-chase experiment. Cells were incubated in the presence of cycloheximide for the indicated amount of time (with or without a 2-hour pre-treatment with the proteasome inhibitor MG132) prior to cell lysis and analysis by western blotting.

Figure S4 (related to Figure 5)



1 **Translation-coupled sensing and degradation of RNA-protein crosslinks**

2

3 Shubo Zhao^{1,2#}, Jacqueline Cordes^{1,2#}, Karolina M. Caban², Maximilian J. Götz^{1,2}, Timur

4 Mackens-Kiani^{1,2}, Anthony J. Veltri³, Niladri K. Sinha³, Pedro Weickert^{1,2}, Graeme Hewitt⁴,

5 Thomas Fröhlich², Roland Beckmann^{1,2}, Allen R. Buskirk³, Rachel Green^{3,5}, and Julian

6 Stingele^{1,2*}

7

8 ¹Department of Biochemistry, Ludwig-Maximilians-University Munich, Munich, Germany

9 ²Gene Center, Ludwig-Maximilians-University Munich, Munich, Germany

10 ³Department of Molecular Biology and Genetics, Johns Hopkins University School of Medicine, Baltimore,

11 USA

12 ⁴King's College London School of Cancer & Pharmaceutical Sciences, London, UK

13 ⁵Howard Hughes Medical Institute, Johns Hopkins University School of Medicine, Baltimore, USA

14

15 [#]These authors contributed equally to this work

16 ^{*}Corresponding author. Email: stingele@genzentrum.lmu.de

17

18

19 **Reactive aldehydes are abundant cytotoxic metabolites which challenge homeostasis by**
20 **crosslinking cellular macromolecules^{1,2}. Aldehyde-induced DNA-DNA crosslinks cause**
21 **cancer and bone marrow failure in Fanconi anemia³⁻⁶ while DNA-protein crosslinks**
22 **require proteolytic repair to prevent liver tumours and premature ageing⁷⁻⁹. It is**
23 **unknown whether RNA damage contributes to the toxicity of aldehydes and whether**
24 **cells possess mechanisms to specifically resolve RNA-protein crosslinks. Here, we**
25 **establish photoactivatable ribonucleoside-enhanced crosslinking as a tractable model**
26 **system to study aldehyde-mimicking RNA damage in the absence of confounding DNA**
27 **damage. We find that RNA crosslinking damage causes translational stress by stalling**
28 **elongating ribosomes, which causes cell death through ZAK α -dependent activation of**
29 **the ribotoxic stress response and GCN2-dependent activation of the integrated stress**
30 **response. Moreover, we discover the principles of a translation-coupled cellular quality**
31 **control mechanism that targets RNA-protein crosslinks. Collisions between translating**
32 **ribosomes and crosslinked mRNA-binding proteins trigger their ubiquitylation and**
33 **subsequent proteasomal degradation. Our findings identify RNA damage and RNA-**
34 **protein crosslink formation as central components of aldehyde-induced toxicity and lay**
35 **the groundwork for further research into the cellular responses to these threats.**

36

37 Reactive aldehydes arise endogenously in substantial quantities despite being highly toxic
38 and carcinogenic^{1,10,11}. Formaldehyde is continuously generated in cells as a by-product of
39 various demethylation reactions and one-carbon metabolism^{2,12,13}, resulting in formaldehyde
40 concentrations in the micromolar range in mammalian serum¹⁴. Formaldehyde is detoxified
41 by ADH5 and ALDH2, dehydrogenases that are defective in individuals with aldehyde
42 degradation deficiency syndrome leading to bone marrow failure and leukemia^{14,15}. This first-
43 tier of protection against aldehydes by metabolic detoxification is complemented by a

44 second-tier provided by DNA repair mechanisms². Aldehydes induce DNA inter-strand
45 crosslinks that stall advancing replication forks and are resolved by multiple repair
46 pathways^{16,17}. DNA-protein crosslinks are degraded by the proteasome as well as by
47 specialized proteases (Wss1 in yeast, SPRTN in mammals)¹⁸⁻²¹. SPRTN is essential for
48 cellular viability^{9,22}, indicating that endogenous crosslinking levels are sufficiently high to be
49 life-threatening. Formaldehyde also crosslinks proteins to RNA; such crosslinks have been
50 used to study RNA-protein interactions^{23,24}. However, it is unknown whether RNA damage is
51 a significant component of aldehyde-induced stress and toxicity. One of the challenges in
52 studying the specific consequences of RNA damage is that most reactive agents also damage
53 DNA²⁵.

54

55 **Photoactivatable-ribonucleoside-enhanced crosslinking recapitulates formaldehyde-** 56 **induced RNA-protein crosslink formation**

57 To study the specific consequences of RNA-protein crosslink (RPC) formation in the absence
58 of DNA damage, we repurposed the photoactivatable-ribonucleoside-enhanced crosslinking
59 (PAR-CL) strategy which was initially developed to probe RNA-protein interactions^{26,27}.
60 Cells were incubated for 16 hours with the uridine analogue 4-thiouridine (4-SU) which is
61 incorporated specifically into RNA, after which crosslinking was induced by UVA irradiation
62 (365 nm) (Fig 1a). Irradiation of cells labelled with 4-SU resulted in dose-dependent toxicity
63 in HAP1, HeLa T-REx Flp-In, and HCT116 cells, while either treatment alone did not
64 markedly affect viability (Fig. 1b, c, Extended Data Fig. 1a-d). Next, we exposed cells to
65 doses of PAR-CL (5 μ M 4-SU + 6 kJ/m² UVA) or formaldehyde (0.5 mM, 1 hour) that
66 affected viability to a similar degree (Fig. 1c, Extended Data Fig. 1e). Crosslinked RNA and
67 protein were then purified using the protein-x-linked RNAs extraction (XRNAX) protocol
68 (Fig 1d and ref²⁸). We observed that both treatments induced RPCs to a similar degree (Fig.

69 1d). In contrast to formaldehyde, however, PAR-CL did not result in detectable levels of
 70 DNA-protein crosslink formation in the KCl-SDS precipitation assay (Fig. 1e and Extended
 71 Data Fig. 1f). To compare the identity of PAR-CL- and formaldehyde-induced RPCs, we
 72 combined XRNAX with label-free quantitative mass spectrometry (MS). Formaldehyde

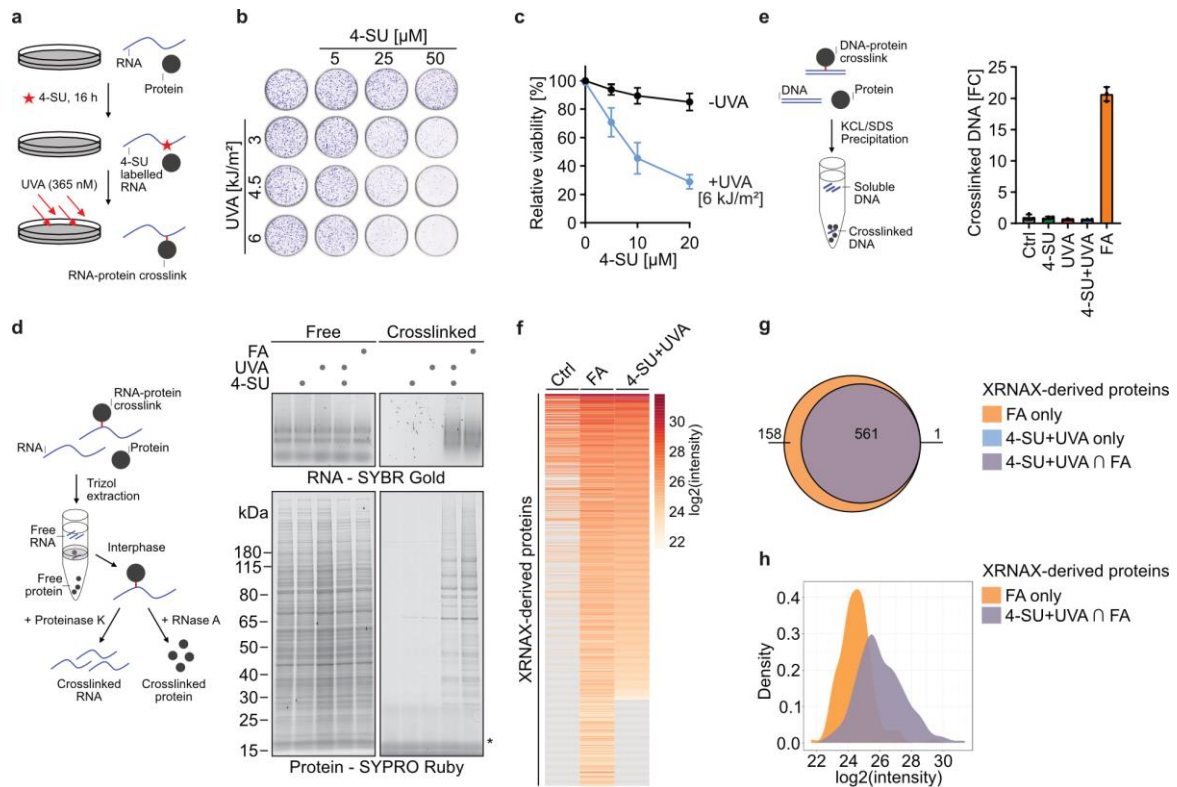


Figure 1. Photoactivatable-ribonucleoside-enhanced crosslinking (PAR-CL) recapitulates formaldehyde-induced RNA-protein crosslink formation. **a:** Schematic depiction of RNA-protein crosslink (RPC) induction. Cellular RNAs are labelled with the photoactivatable ribonucleoside 4-thiouridine (4-SU) and crosslinked by UVA irradiation. **b-c:** Colony formation assay (b) and cell viability measurement (c) of HAP1 cells after treatment with indicated doses of 4-SU and UVA. Values in (c) represent the mean \pm SD of three biological replicates normalised to the mean of corresponding control of each replicate. **d:** PAR-CL (4-SU+UVA) and formaldehyde-induced RPCs analysed by XRNAX. Left panel: schematic depiction of RPC purification by XRNAX. Right panel: RPC purification by XRNAX in HAP1 cells treated with 4-SU (5 μ M, 16 h, estimated to result in replacement of 0.125 % of uridines by 4-SU based on previous work²⁶), UVA (6 kJ/m²), or 0.5 mM formaldehyde (FA) for 1 h, as indicated. Purified RPCs were digested with proteinase K or RNase A prior to running on an agarose gel (RNA) and SDS-PAGE gel (protein), respectively. Asterisk indicates RNase A. **e:** DNA-protein-crosslink formation quantified by KCl-SDS precipitation assay. Left: schematic depiction of DNA-protein-crosslink quantification by KCl-SDS assay. Right: KCl-SDS assays of HAP1 cells treated as in (d). Crosslinked DNA was measured using Qubit DNA HS assay. Values represent the mean \pm SD of the fold change of crosslinked DNA of three technical replicates normalised to the mean of untreated controls. **f:** Heatmap of XRNAX-derived proteins crosslinked to RNA from HAP1 cells treated as in (d). Proteins identified in XRNAX samples, sorted by decreasing log₂ intensity in 4-SU+UVA samples. Values represent the mean of three biological replicates. **g-h:** Venn diagram (g) and density plot (h) for XRNAX-derived proteins crosslinked to RNA. Numbers indicate proteins identified in different treatments, formaldehyde (FA, orange), PAR-CL (4-SU+UVA, blue) or both (4-SU+UVA \cap FA, purple). Density plot shows the probability distribution of log₂ intensities for proteins crosslinked to RNA in formaldehyde (FA, orange) or formaldehyde and PAR-CL (4-SU+UVA \cap FA, purple).

73 induced crosslinking of 719 proteins to RNA, the majority of which (561) were also
74 crosslinked by PAR-CL (Fig 1f, g). Crosslinks were primarily formed by RNA-binding
75 proteins and structural constituents of the ribosome (Extended Data Fig. 1g). Formaldehyde-
76 induced RPCs not captured by PAR-CL (158) were in general of low abundance (Fig. 1h).
77 We conclude that PAR-CL mimics formaldehyde-induced RPC formation in the absence of
78 DNA-protein crosslinking and thus represents a clean model system which allows for the
79 analysis of this aspect of aldehyde toxicity.

80

81 **PAR-CL and formaldehyde induce ZAK α - and GCN2-dependent stress responses**

82 To understand how aldehyde-induced RNA damage affects cellular physiology, we
83 monitored PAR-CL-induced signalling responses in HAP1 cells by quantitative
84 phosphoproteomics using TMT-based multiplexing (Fig. 2a, b, Supplementary Table 2, 3).
85 Kinase-substrate enrichment analysis of significantly altered phospho-sites implicated the
86 p38 and JNK kinases as well as their corresponding upstream MAP2 kinases (Extended Data
87 Fig. 2a, Supplementary Table 4). The observed signatures were reminiscent of recent studies
88 reporting ZAK α -dependent activation of the ribotoxic stress response (RSR)^{29,30}. ZAK α
89 activates p38 and JNK upon sensing ribosome stalling caused by RNA damage or translation
90 elongation inhibitors²⁹⁻³¹. Indeed, in ZAK knock-out (KO) cells, the majority of PAR-CL-
91 induced phospho-site changes were abrogated (Fig. 2b). We confirmed p38 activation in
92 HAP1, HeLa T-REx Flp-In, and HCT116 cells using antibodies specific for phosphorylated
93 p38 (p-p38), using an intermediate dose of the translation elongation inhibitor anisomycin
94 (ANS) as positive control (Fig. 2c, Extended Data Fig. 2b, c). Phosphorylation of p38 was
95 lost in ZAK KO cells and restored upon re-expression of ZAK α ^{WT}, but not catalytically
96 inactive ZAK α ^{K45R} (Fig. 2c, Extended Data Fig. 2b, c). Activation of the RSR is typically
97 accompanied by activation of the integrated stress response (ISR) through phosphorylation of

98 eIF2 α by GCN2²⁹. In agreement, we detected phosphorylated eIF2 α (p-eIF2 α) upon PAR-CL
 99 treatment; this phosphorylation was lost in *GCN2* KO cells and restored upon re-expression
 100 of GCN2^{WT} but not catalytically inactive GCN2^{D848N} (Fig. 2c, Extended Data Fig. 2d, e). To
 101 corroborate these data, we generated inducible *ZAK* and *GCN2 iCas9* eHAP KO cells
 102 (Extended Data Fig. 2f, g). Upon induction of Cas9 expression using doxycycline, we saw a

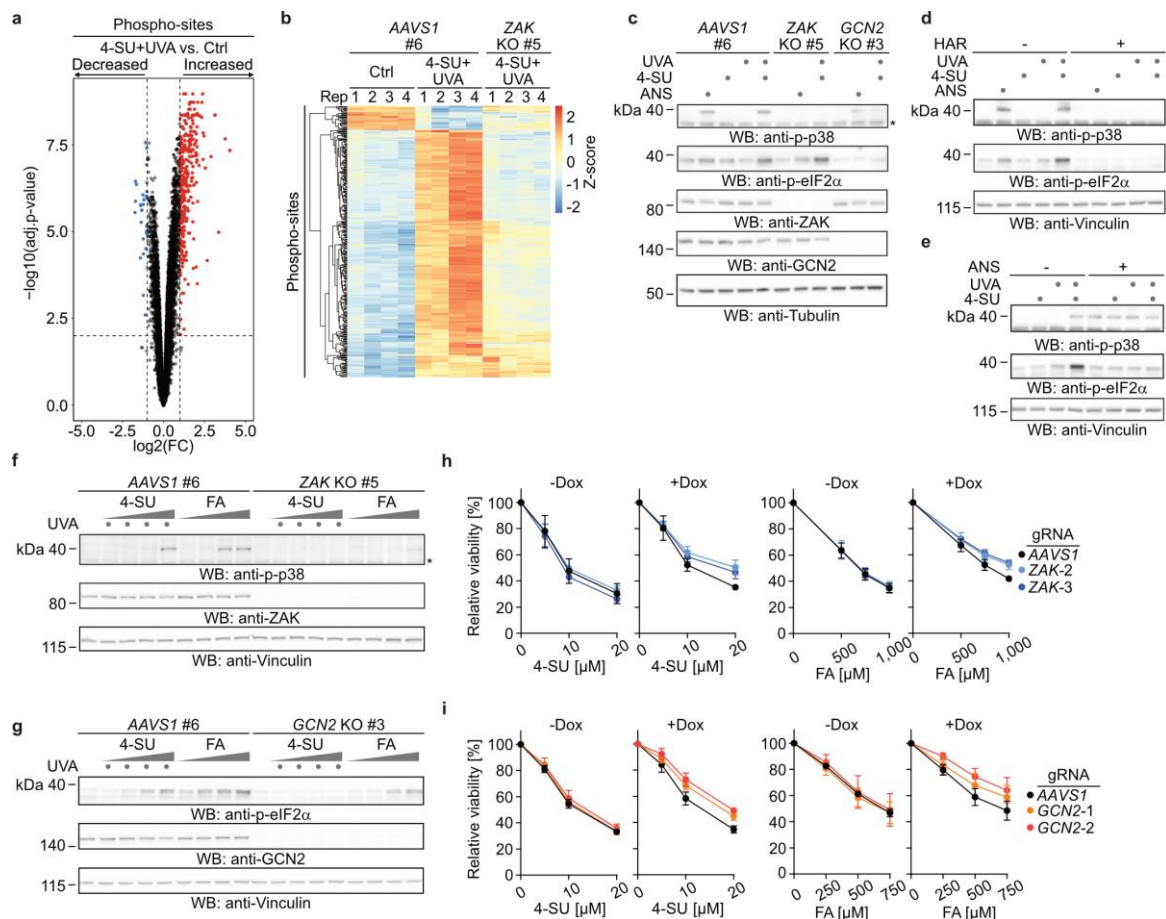


Figure 2. PAR-CL and formaldehyde induce ZAK α - and GCN2-dependent stress responses. **a:** Volcano plot indicating differentially modified phospho-sites 0.5 h after treatment with PAR-CL (4-SU (5 μ M, 16 h) + UVA (6 kJ/m²)) in HAP1 cells. Statistically significantly changed sites (adj. p-value \leq 0.01, $-1 \geq \log_2$ fold change \geq 1) are highlighted in red for increased and blue for decreased phospho-sites. **b:** Heatmap depicting Z-scored intensities for significantly affected phospho-sites in *AAVS1* control and *ZAK* KO HAP1 cells treated as in (a). **c:** Representative western blot analysis of clonal HAP1 *ZAK* KO, *GCN2* KO and matched *AAVS1* control cells treated with 4-SU (5 μ M, 16 h), UVA (6 kJ/m²), or anisomycin (ANS, 1 μ M, 0.5 h), as indicated. Asterisk indicates unspecific band. **d-e:** Representative western blot analysis of HAP1 cells treated with 4-SU (5 μ M, 16 h) followed by harringtonine (HAR, 2 μ g/ml, 0.5 h) prior to irradiation with UVA (6 kJ/m²) and anisomycin (ANS, 1 μ M, 0.5 h) (d) or anisomycin treatment (ANS, 375 μ M, 0.5 h) prior to irradiation with UVA (6 kJ/m²) (e), as indicated. Asterisk indicates unspecific band. **f-g:** Representative western blot analysis of clonal HAP1 *ZAK* KO (f) and *GCN2* KO (g) cells and matched *AAVS1* control cells treated with increasing doses of 4-SU (0.04, 0.2, 1 and 5 μ M, 16 h), followed by UVA irradiation (6 kJ/m²) or increasing doses of formaldehyde (FA, 100, 200, 500, 1000 μ M, 1 h). Asterisk indicates unspecific band. **h-i:** eHAP cells expressing doxycycline-inducible Cas9 and *AAVS1* or *ZAK* gRNAs (h) or *GCN2* gRNAs (i) were incubated with doxycycline (Dox, 1 μ g/ml, 48 h) followed by treatment with indicated doses of 4-SU (16 h) and UVA irradiation (6 kJ/m²) or indicated doses of formaldehyde (FA, 1 h). After 24 h, viability was determined using AlamarBlue assay. Values represent the mean \pm SD of three (4-SU+UVA) or four (formaldehyde, FA) biological replicates normalised to the mean of corresponding controls of each replicate.

103 reduction in PAR-CL-induced p38 phosphorylation in cells expressing gRNAs targeting *ZAK*
104 and in eIF2 α phosphorylation in cells expressing gRNAs targeting *GCN2* (Extended Data
105 Fig. 2f, g).

106 Given that *ZAK* α and *GCN2* are known to be activated by ribosome stalling^{30,31} and
107 subsequent collisions with trailing ribosomes²⁹, we asked next whether their activation by
108 PAR-CL also originates at ribosomes. We pre-treated cells with harringtonine (HAR), which
109 depletes translating ribosomes from mRNAs by trapping ribosomes at sites of translation
110 initiation, allowing other ribosomes to run off, or a high dose of anisomycin, which globally
111 stalls ribosomes on mRNA, before inducing RPCs. We observed that harringtonine
112 suppressed phosphorylation of eIF2 α and p38 (Fig. 2d, Extended Data Fig. 2h). A high dose
113 of anisomycin blocked eIF2 α phosphorylation while itself inducing p38-phosphorylation
114 which was not further increased by PAR-CL (Fig. 2e, Extended Data Fig. 2i). Consistent with
115 PAR-CL mimicking key features of aldehyde crosslinking stress, formaldehyde also induced
116 p38 and eIF2 α phosphorylation (Fig. 2f, g, Extended Data Fig. 3a, b), which was largely
117 dependent on *ZAK* and *GCN2*, respectively, and suppressed by harringtonine pre-treatment
118 (Fig. 2f, g, Extended Data Fig. 3a-d).

119 Taken together, these results suggest that the pleiotropically-acting agent
120 formaldehyde induces activation of the RSR and ISR primarily through a *ZAK* α - and *GCN2*-
121 dependent response which is recapitulated by PAR-CL and originates at the ribosome. To
122 understand the consequences of these signalling responses, we monitored viability upon
123 conditional depletion of *ZAK* or *GCN2* in iCas9 eHAP cells and observed modestly increased
124 viability upon treatment with PAR-CL or formaldehyde (Fig. 2h, i). These results suggest
125 that ISR and RSR influence cell fate in response to high levels of crosslinking stress and also
126 that RNA damage is a component of aldehyde toxicity.

127

128 **PAR-CL induces translational stress and ribosome collisions**

129 Intrigued by the requirement for actively translating ribosomes to generate signalling
130 responses in response to PAR-CL, we next explored its effects on translation. First, we
131 monitored protein synthesis levels by measuring incorporation of O-propargyl-puromycin
132 (OPP) into nascent peptide chains³² and observed a dose-dependent shutdown of translation
133 upon PAR-CL treatment (Fig. 3a, Extended Data Fig. 4a). Second, we monitored ribosome
134 populations using sucrose gradients and found that polysomes collapsed to monosomes
135 within thirty minutes after crosslinking (Fig. 3b).

136 To better understand how PAR-CL induces these clear signs of translational stress, we
137 observed ribosome densities across open reading frames (ORFs) using ribosome profiling. In
138 PAR-CL-treated cells (but not upon treatment with either 4-SU or UVA alone), ribosome
139 protected fragments (RPFs) were enriched in the 5'-region of ORFs while the density
140 dropped off downstream (Fig. 3c). This pattern of ribosome density loss is consistent with
141 roadblocks that stall elongating ribosomes.

142 To understand whether ribosome stalling within ORFs was related to the formation of
143 RPCs, we searched for T-C conversions within RPFs. When reverse transcriptase encounters
144 an amino acid-nucleotide crosslink, it often misreads the modified U as a C, leading to T-C
145 conversions in the final reads^{24,26}. As expected, the frequency of T-C conversions in the
146 standard monosome RPFs (30 nt) was higher in the PAR-CL-treated sample compared with
147 the other treatments. This was also true for RPFs from collided disomes (> 58 nt). Although
148 there was also an increase in the sample treated with 4-SU alone, consistent with the
149 tendency of reverse transcriptase to sometimes misread even unreacted 4-SU, the PAR-CL
150 samples showed the highest conversion rates (Fig. 3d). As a negative control, we counted the
151 opposite conversion (C to T) in 30-mer RPFs and found that they occurred at similar rates in

152 all conditions, as expected (Extended Data Fig. 4b). These findings show that there is an
 153 enrichment of ribosome footprints that include crosslinking sites in PAR-CL samples.

154 The position of the T-C conversions within the RPFs sheds light onto the ribosome
 155 stalling that we observed. In samples treated with 4-SU alone, the T-C conversions were
 156 randomly distributed across the 30-mer footprints, but upon PAR-CL treatment, the
 157 conversions were specifically enriched around position 18 in 30-mers (Fig. 3e, left panel).

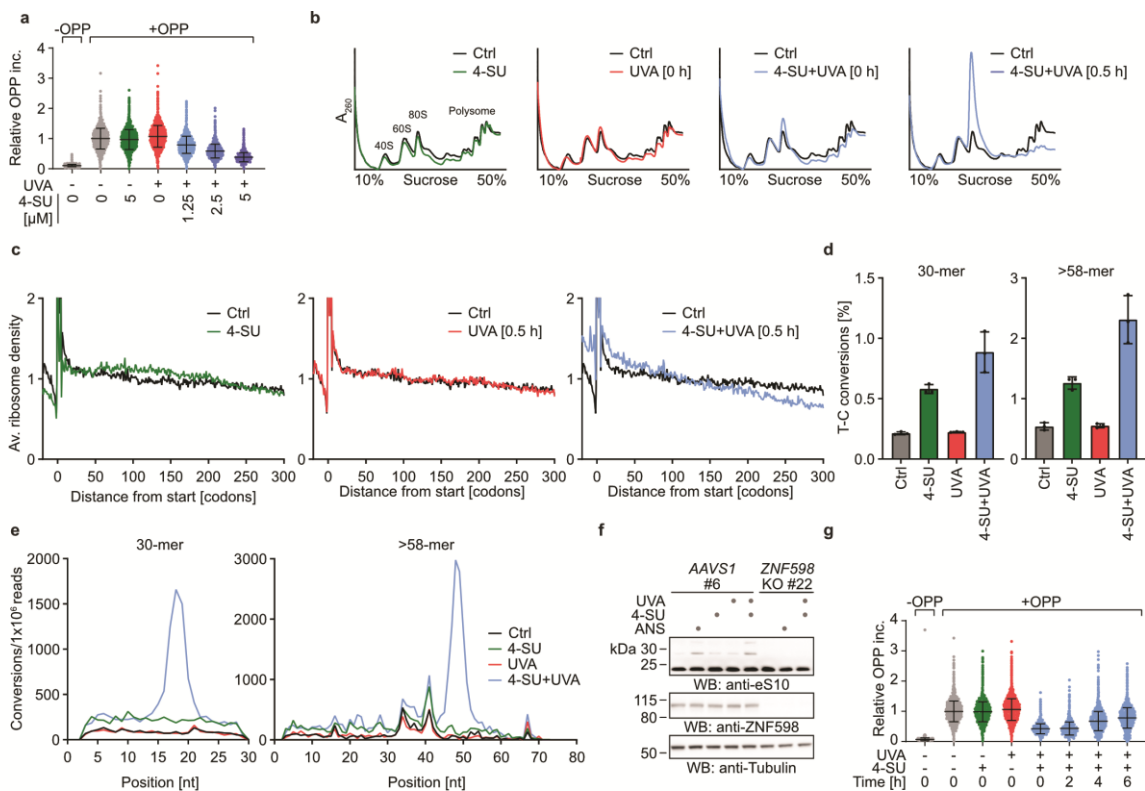


Figure 3. PAR-CL induces translation stress and ribosome collisions. **a:** Relative levels of O-propargyl-puromycin (OPP) incorporation measured by flow cytometry to determine protein synthesis rate in HAP1 cells following treatment with indicated doses of 4-SU (16 h) followed by UVA irradiation (6 kJ/m²). Values represent fluorescence intensities of live, single cells normalised to the mean of untreated controls. **b:** Polysome profiles of HAP1 cells treated with 4-SU (5 μM, 16 h) and UVA (6 kJ/m²) as indicated. Cells were harvested 0 h or 0.5 h after irradiation. Lysates were fractionated over 10-50% sucrose gradients followed by UV(A₂₆₀) absorbance measurement. **c:** Ribosome profiles of HAP1 cells treated with 4-SU (5 μM, 18 h) and UVA (6 kJ/m²) harvested 0.5 h after irradiation. Meta-gene analysis of ribosome footprints shows average ribosome density across ORFs in indicated conditions compared to control. Average ribosome density represents mean of three replicates. **d:** Frequency of T-C conversion in the sequencing of 30-mer (left) or > 58-mer (right) ribosome footprints from HAP1 cells treated with 4-SU (5 μM, 18 h) and UVA (6 kJ/m²) compared to controls. Values represent the mean ± SD of three replicates. **e:** Representative T-C conversion distribution across positions in 30-mer (left) or >58-mer (right) ribosome footprints from HAP1 cells treated with 4-SU (5 μM, 18 h) and UVA (6 kJ/m²) compared to controls. **f:** Representative western blot analysis of clonal HAP1 *ZNF598* KO cells and matched *AAVS1* control cells treated with 4-SU (5 μM, 16 h), UVA (6 kJ/m²) or anisomycin (ANS, 1 μM, 0.5 h), as indicated. **g:** O-propargyl-puromycin (OPP) incorporation analysed by flow cytometry in HAP1 cells treated with 4-SU (5 μM, 16 h) and UVA (6 kJ/m²) at different timepoints after irradiation. Values represent fluorescence intensities of live, single cells normalised to the mean of controls.

158 This position corresponds to the A site of the ribosome, where T-C conversions may arise
159 from crosslinks that block decoding. Consistent with decoding defects in PAR-CL treated
160 cells, we observed an increase in short RPFs of ~22 nt upon crosslinking corresponding to
161 ribosomes awaiting a tRNA with an empty A site³³, while longer RPFs (~30 nt)
162 corresponding to ribosomes with an occupied A site were reciprocally reduced (Extended
163 Data Fig. 4c). While it is likely that RPCs are also present in front of stalled ribosomes,
164 leading to translational arrest, these crosslinks are invisible to our analysis because the
165 associated T-C conversions occur outside the RPFs. Taken together, these data are consistent
166 with a model wherein PAR-CL treatment triggers translation stress by blocking the
167 progression of ribosomes.

168 In addition, we analysed T-C conversion frequency in the longer RPFs (more than 58
169 nt) corresponding to the footprint of two adjacent ribosomes and observed a peak of
170 conversions at position 48 in PAR-CL treated cells (Fig. 3e, right panel) corresponding to the
171 A site of the leading ribosome in the disome. Again, this suggests that ribosome stalling at
172 crosslinks results in collisions with trailing ribosomes. This interpretation is in line with our
173 observation that PAR-CL induces ZAK α -dependent RSR and GCN2-dependent ISR
174 activation, both of which are linked to ribosome collisions²⁹, and with the increase in the
175 level of RNase-resistant disomes after treatment with PAR-CL (Extended Data Fig. 4d).

176 In addition to RSR and ISR activation, ribosome collisions trigger ribosome quality
177 control (RQC) mechanisms to maintain proteostasis by splitting stalled ribosomes, degrading
178 incomplete nascent polypeptide chains, and recycling ribosomal subunits^{25,34}. RQC is
179 initiated in mammalian cells by ubiquitylation of the small ribosomal subunit protein eS10 by
180 the ZNF598 E3 ligase (Hel2 in yeast) which specifically recognizes an interface formed by
181 two collided ribosomes^{35,36}. As expected, we observed ZNF598-dependent monoubiquitylation
182 of eS10 upon PAR-CL treatment (Fig. 3f, Extended Data Fig. 4e, f) or upon addition of an

183 intermediate dose of anisomycin as a positive control. In addition, anti-ubiquitin antibodies
184 revealed ZNF598-dependent accumulation of multiple additional ubiquitylation events
185 (Extended Data Fig. 4e, f), as was previously noted in yeast upon RQC activation³⁷. The loss
186 of RQC in *ZNF598* KO cells was rescued by re-expression of ZNF598^{WT} but not catalytically
187 inactive ZNF598^{C29A} (Extended Data Fig. 4e, f). Notably, we did not observe any discernible
188 interdependencies between RQC, RSR and ISR under the conditions tested here; ZNF598-
189 dependent ubiquitylation events were not affected by loss of ZAK or GCN2, p38-
190 phosphorylation was not affected by loss of ZNF598 or GCN2, and eIF2 α -phosphorylation
191 was not affected by loss of ZAK or ZNF598 (Extended Data Fig. 4g-l).

192 Collectively, our data demonstrate that aldehyde-mimicking RNA damage triggers
193 ribosome stalling and collisions, activating ribosomal stress surveillance mechanisms.
194 Although RQC pathways are activated, their activity appears insufficient to resolve ribosome
195 stalling and prevent ISR- and RSR-dependent induction of cell death. In agreement with a
196 non-essential role for RQC in response to aldehyde stress, inducible loss of ZNF598 in eHAP
197 iCas9 cells did not result in significant changes in viability upon PAR-CL or formaldehyde
198 treatment (Extended Data Fig. 5a, b), which matches recent data showing that ribosomes
199 stalled at bulky RNA lesions are refractory to splitting³¹. Together with the fact that cells
200 recovered from the shutdown of protein synthesis caused by an intermediate dose of PAR-CL
201 over the course of six hours (Fig. 3g, Extended Data Fig. 5c), this suggested to us that
202 additional, uncharacterized quality control mechanisms that resolve aldehyde-induced RNA
203 damage may exist.

204

205 **Translation-coupled resolution of mRNA-protein crosslinks**

206 To understand how cells recover from aldehyde-induced translation stress, we focused on the
207 resolution of crosslinks between proteins and poly-adenylated mRNAs (mRPCs). We

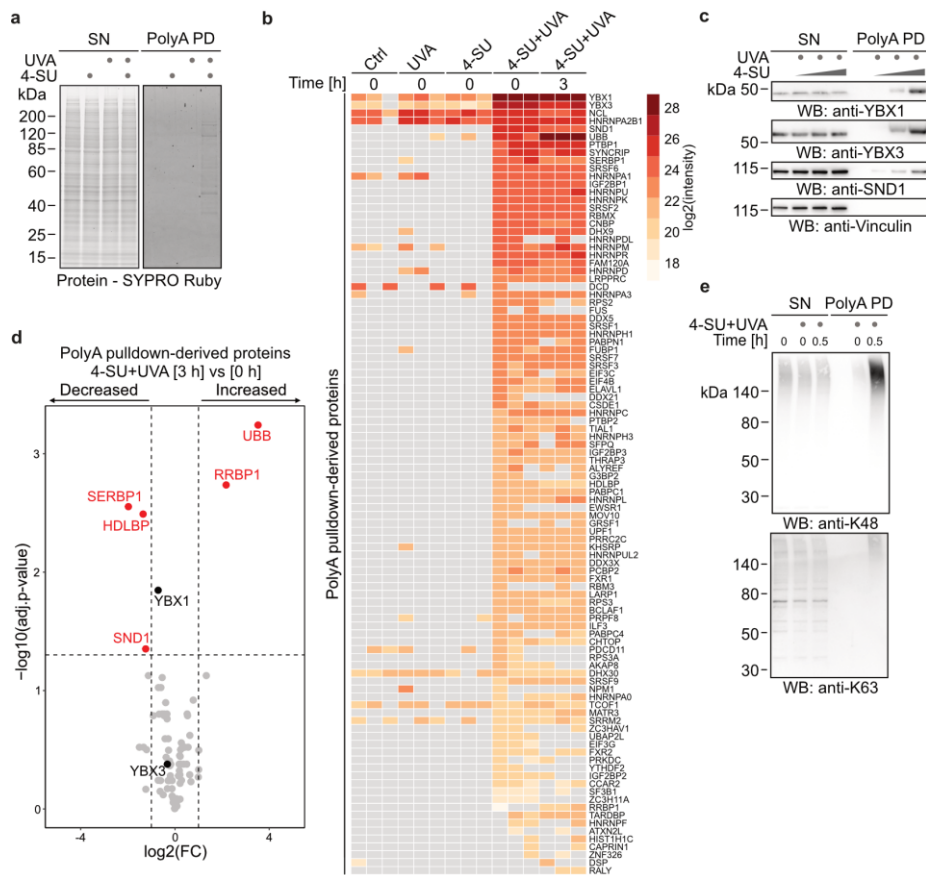


Figure 4. Ubiquitylation of mRNA-protein crosslinks. **a:** mRNA-protein crosslinks (mRPCs) isolated by poly-A pulldown from HAP1 cells treated with 4-SU (5 μ M, 16 h) and UVA (6 kJ/m²), as indicated. Crosslinked proteins were visualized by SDS-PAGE followed by SYPRO Ruby staining. **b:** Heatmap depicting abundance of mRPCs isolated using poly-A pulldown. Proteins are sorted by average log₂ intensity in 4-SU+UVA 0 h samples. **c:** Representative western blot analysis of mRPCs isolated by poly-A pulldown from HAP1 cells treated with increasing doses of 4-SU (1.25, 2.5, 5 μ M, 16 h) and UVA (6 kJ/m²). **d:** Volcano plot comparing crosslinked proteins after PAR-CL (4-SU (5 μ M, 16 h) +UVA (6 kJ/m²)) at 3 h vs 0 h after irradiation. **e:** Representative western blot analysis of poly-A pulldown samples from HAP1 cells treated with 4-SU (2.5 μ M, 16 h) and UVA (6 kJ/m²), as indicated and followed by recovery for 0 or 0.5 h.

208 monitored the fate of mRPCs using denaturing polyA-pulldowns (polyA-PD)^{38,39}, which
 209 require significantly less material than RPC-purification by XRNAX and can thus be used to
 210 test various experimental conditions. As expected, PAR-CL, but not 4-SU or UVA alone,
 211 triggered co-precipitation of crosslinked proteins in polyA-pulldown samples (Fig. 4a). Using
 212 quantitative label-free MS we determined the identity and abundance of proteins crosslinked
 213 to mRNA either immediately after crosslinking or three hours later. Among the 99 mRPCs
 214 we identified, the mRNA-binding proteins YBX1 and YBX3⁴⁰ formed the most abundant
 215 crosslinks (Fig. 4b, Supplementary Table 5). Dose-dependent formation of several mRPCs
 216 was confirmed by western blotting of polyA-pulldowns (Fig. 4c).

217 Three hours after irradiation, crosslinks formed by the mRNA- or ribosome-
218 associated proteins SND1⁴¹, SERBP1⁴², and HDLBP⁴³ decreased in abundance (Fig. 4d,
219 Supplementary Table 6), indicating their resolution. Strikingly, we observed a strong
220 concurrent increase in ubiquitin (UBB) in polyA-pulldown samples (Fig. 4b, d). These results
221 suggest that proteins crosslinked to mRNAs may undergo covalent modification with
222 ubiquitin. To test this idea, we monitored ubiquitylation in polyA-pulldown samples using
223 western blotting with chain-specific antibodies (anti-K48 and anti-K63) upon treatment with
224 a sublethal dose of PAR-CL (2.5 μ M 4-SU + 6 kJ/m² UVA). No ubiquitylation was detected
225 in the absence of crosslinking, while little ubiquitylation was seen directly after crosslinking
226 (Fig. 4e). However, thirty minutes after irradiation, we observed a strong increase in
227 ubiquitylation, primarily formed by K48-linked chains (Fig. 4e).

228 Next, we asked whether mRPC ubiquitylation is linked to their resolution. We
229 induced mRPCs by PAR-CL and monitored their fate in control cells or in cells treated with a
230 specific inhibitor for ubiquitin activating enzyme 1 (Ub-E1i, TAK-243, ref⁴⁴). PolyA-
231 pulldowns followed by mass spectrometry and western blot analysis confirmed that Ub-E1i
232 fully blocked mRPC-ubiquitylation (Fig. 5a-c, Supplementary Table 7, 8). In addition,
233 resolution of mRPCs formed by SND1 and HDLBP was inhibited, indicating that these
234 crosslinks are removed in a ubiquitin-dependent manner (Fig. 5a-c; we failed to detect
235 HDLBP-mRPCs by western blot due to their low abundance). In contrast, resolution of
236 mRPCs formed by YBX1 or YBX3 was not affected (Fig. 5a-c, Extended Data Fig. 6a).

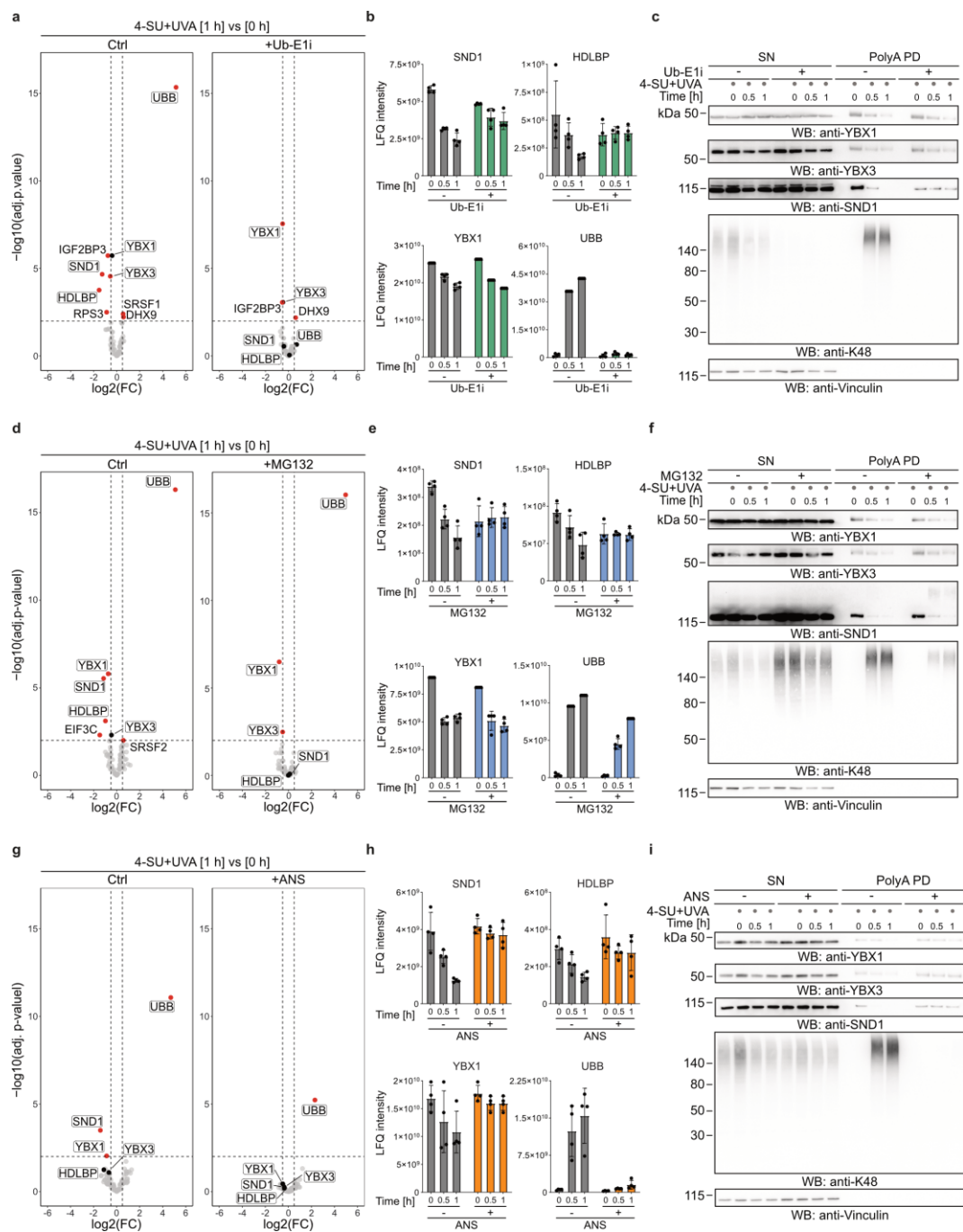


Figure 5. Translation-coupled degradation of mRNA-protein crosslinks. **a-c:** Volcano plot (a) comparing mRPCs isolated by poly-A pulldown from HAP1 cells treated with 4-SU (2.5 μ M, 16 h) and ubiquitin E1 inhibitor (Ub-E1i, TAK-243, 1 μ M, 1 h), as indicated, prior to irradiation with UVA (6 kJ/m²) at 1 h vs 0 h after irradiation. Bar graphs depicting normalised label free quantification (LFQ) intensities (b) and representative western blot analysis (c) showing indicated timepoints of recovery of mRPCs isolated by poly-A pulldown from HAP1 cells. **d-f:** Volcano plot (d) comparing mRPCs isolated by poly-A pulldown from HAP1 cells treated with 4-SU (2.5 μ M, 16 h) and proteasome inhibitor (MG132, 5 μ M, 1 h), as indicated, prior to irradiation with UVA (6 kJ/m²) at 1 h vs 0 h after irradiation. Bar graphs depicting normalised label free quantification (LFQ) intensities (e) and representative western blot analysis (f) showing indicated timepoints of recovery of mRPCs isolated by poly-A pulldown from HAP1 cells. **g-i:** Volcano plot (g) comparing mRPCs isolated by poly-A pulldown from HAP1 cells treated with 4-SU (2.5 μ M, 16 h) and translation inhibitor anisomycin (ANS, 375 μ M, 1 h), as indicated, prior to irradiation with UVA (6 kJ/m²) at 1 h vs 0 h after irradiation. Bar graphs depicting normalised label free quantification (LFQ) intensities (h) and representative western blot analysis (i) showing indicated timepoints of recovery of mRPCs isolated by poly-A pulldown from HAP1 cells. Statistically significantly changed proteins (adj. p-value \leq 0.01, $-0.5 \geq \log_2$ fold change \geq 0.5) in (a, d, g) are highlighted in red. Bar graphs depict mean \pm SD of four biological replicates.

238 Given that K48-linked ubiquitin chains are a potent signal to trigger protein
239 degradation by the proteasome⁴⁵, we asked whether the ubiquitin-dependent turnover of
240 mRPCs was dependent on proteasome activity. Indeed, proteasome inhibition (using pre-
241 treatment with MG132), abolished resolution of mRPCs formed by SND1 and HDLBP (Fig
242 5d, e, Supplementary Table 9, 10). Moreover, slower migrating SND1-species appeared in
243 western blots of polyA-pulldown samples upon proteasome inhibition, likely representing
244 accumulating poly-ubiquitylated SND1-mRPCs (Fig 5f). Inhibition of autophagy, the second
245 major cellular protein degradation system⁴⁵, using Bafilomycin A1 (BAF) had no effect on
246 mRPC resolution (Extended Data Fig. 6b). In line with their resolution being ubiquitin-
247 independent, YBX1 and YBX3 crosslinks were not affected by proteasome inhibition (Fig
248 5d-f, Extended Data Fig. 6c).

249 The swift ubiquitylation of mRPCs following crosslinking raises the question as to
250 how cells detect mRPCs and distinguish crosslinked proteins from proteins merely interacting
251 non-covalently with mRNAs. First, we tested a potential involvement of RSR, ISR, and RQC
252 factors by analysing mRPC resolution in *ZAK*, *GCN2* or *ZNF598* KO cells, but did not
253 observe any effects on mRPC ubiquitylation or stability (Extended Data Fig. 6d). We
254 speculated that the collisions between translating ribosomes and mRPCs might serve as the
255 sensing mechanism for crosslink detection, by analogy with DNA-protein crosslinks that are
256 detected in cells because they stall advancing DNA replication forks⁴⁶. To test this idea, we
257 globally stalled ribosomes on mRNAs using a high-dose of anisomycin, induced RPCs and
258 followed their resolution using polyA-pulldowns, MS, and western blotting. Remarkably,
259 pre-treatment with anisomycin not only abolished mRPC ubiquitylation, but also blocked
260 degradation of rapidly turned-over mRPCs (SND1, HDLBP) and more stable mRPCs
261 (YBX1, YBX3) (Fig. 5g-i, Extended Data Fig. 6e, Supplementary Table 11, 12). To exclude
262 that anisomycin treatment interferes with ubiquitylation in an indirect or unspecific manner,

263 we tested its effect on UVC-induced ubiquitylation of the DNA damage sensor protein XPC⁴⁷
264 and observed XPC ubiquitylation was not affected (Extended Data Fig. 6f). Together, these
265 data suggest a model wherein translating ribosomes serve as a sensor for the detection of
266 mRPCs triggering their resolution, either through their rapid ubiquitylation and subsequent
267 proteasomal degradation or through a slower ubiquitin- and proteasome-independent
268 mechanism.

269

270 **Conclusions**

271 In this study, we found that PAR-CL can be used to mimic the consequences of reactive
272 aldehydes on RNA in the absence of DNA damage. The data we obtained using this system
273 allows the formulation of a first model on crosslinking-induced translation stress and the
274 resulting cellular responses (Fig. 6). Aldehyde-induced RNA damage causes ribosome
275 stalling and subsequent ribosome collisions, which triggers diverse ribosomal stress
276 surveillance mechanisms, including ZAK α -dependent RSR activation and GCN2-dependent
277 ISR activation, both of which appear to drive cell death (although the ISR is primarily
278 thought to promote survival, it can drive cell death upon severe stress⁴⁸). Our observation that
279 loss of *ZAK* or *GCN2* confers slightly increased resistance to PAR-CL and formaldehyde
280 indicates that RNA-damage is a critical component of the cytotoxicity of reactive aldehydes.

281 By investigating the resolution of crosslinks between RNA-binding proteins and poly-
282 adenylated mRNAs, we provide evidence for two distinct mRPC quality control mechanisms.
283 mRPCs formed by the proteins SND1 and HDLBP are subjected to translation-coupled
284 ubiquitylation, which results in their rapid proteasomal degradation (Fig. 6). It is conceivable
285 that ribosomes advance further once the protein block on the mRNA is trimmed by
286 degradation and then stall again when the peptide remnant blocks decoding within the A site.
287 Our observation that crosslinks accumulate within the ribosomal A site thirty minutes after

288 PAR-CL treatment provides support for this idea. In contrast, mRPCs formed by YBX1 and
289 YBX3 are resolved more slowly and independent of ubiquitylation and proteasomal activity.
290 How YBX1/3-mRPCs are removed, the identity of the E3 ligase(s) ubiquitylating SND1- and
291 HDLBP-mRPCs, and what dictates the choice between these mechanisms are exciting future
292 questions.

293 The existence of mRPC-resolution mechanisms highlights these lesions as relevant
294 quality control problems with broad implications. Aldehyde-induced RPCs may be sources of
295 endogenous ribosome collisions, which increase during ageing⁴⁹, and could activate innate
296 immune responses⁵⁰. Therefore, RPC resolution mechanisms may constitute a critical
297 additional tier in cellular protection against reactive aldehydes in addition to DNA repair and
298 metabolic detoxification.

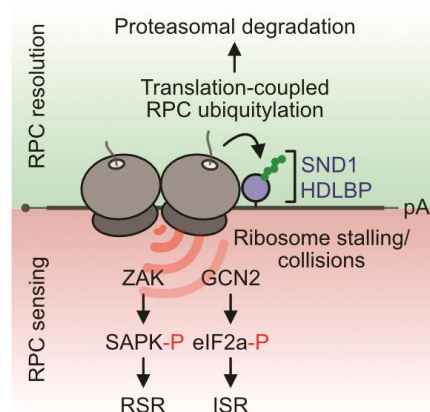


Figure 6. Model of translation-coupled sensing and resolution of mRNA-protein crosslinks.

299 **References**

- 300 1 O'Brien, P. J., Siraki, A. G. & Shangari, N. Aldehyde sources, metabolism, molecular toxicity
301 mechanisms, and possible effects on human health. *Crit Rev Toxicol* **35**, 609-662,
302 doi:10.1080/10408440591002183 (2005).
- 303 2 Wang, M., Dingler, F. A. & Patel, K. J. Genotoxic aldehydes in the hematopoietic system. *Blood* **139**,
304 2119-2129, doi:10.1182/blood.2019004316 (2022).
- 305 3 Langevin, F., Crossan, G. P., Rosado, I. V., Arends, M. J. & Patel, K. J. Fancd2 counteracts the toxic
306 effects of naturally produced aldehydes in mice. *Nature* **475**, 53-58, doi:10.1038/nature10192 (2011).
- 307 4 Garaycochea, J. I. *et al.* Genotoxic consequences of endogenous aldehydes on mouse haematopoietic
308 stem cell function. *Nature* **489**, 571-575, doi:10.1038/nature11368 (2012).
- 309 5 Pontel, L. B. *et al.* Endogenous Formaldehyde Is a Hematopoietic Stem Cell Genotoxin and Metabolic
310 Carcinogen. *Mol Cell* **60**, 177-188, doi:10.1016/j.molcel.2015.08.020 (2015).
- 311 6 Hira, A. *et al.* Variant ALDH2 is associated with accelerated progression of bone marrow failure in
312 Japanese Fanconi anemia patients. *Blood* **122**, 3206-3209, doi:10.1182/blood-2013-06-507962 (2013).
- 313 7 Weickert, P. & Stinglele, J. DNA-Protein Crosslinks and Their Resolution. *Annu Rev Biochem* **91**, 157-
314 181, doi:10.1146/annurev-biochem-032620-105820 (2022).
- 315 8 Lessel, D. *et al.* Mutations in SPRTN cause early onset hepatocellular carcinoma, genomic instability
316 and progeroid features. *Nat Genet* **46**, 1239-1244, doi:10.1038/ng.3103 (2014).
- 317 9 Maskey, R. S. *et al.* Spartan deficiency causes genomic instability and progeroid phenotypes. *Nat*
318 *Commun* **5**, 5744, doi:10.1038/ncomms6744 (2014).
- 319 10 Garaycochea, J. I. *et al.* Alcohol and endogenous aldehydes damage chromosomes and mutate stem
320 cells. *Nature* **553**, 171-177, doi:10.1038/nature25154 (2018).
- 321 11 Swenberg, J. A. *et al.* Formaldehyde carcinogenicity research: 30 years and counting for mode of
322 action, epidemiology, and cancer risk assessment. *Toxicol Pathol* **41**, 181-189,
323 doi:10.1177/0192623312466459 (2013).
- 324 12 Walport, L. J., Hopkinson, R. J. & Schofield, C. J. Mechanisms of human histone and nucleic acid
325 demethylases. *Curr Opin Chem Biol* **16**, 525-534, doi:10.1016/j.cbpa.2012.09.015 (2012).
- 326 13 Burgos-Barragan, G. *et al.* Mammals divert endogenous genotoxic formaldehyde into one-carbon
327 metabolism. *Nature* **548**, 549-554, doi:10.1038/nature23481 (2017).
- 328 14 Dingler, F. A. *et al.* Two Aldehyde Clearance Systems Are Essential to Prevent Lethal Formaldehyde
329 Accumulation in Mice and Humans. *Mol Cell* **80**, 996-1012 e1019, doi:10.1016/j.molcel.2020.10.012
330 (2020).
- 331 15 Oka, Y. *et al.* Digenic mutations in ALDH2 and ADH5 impair formaldehyde clearance and cause a
332 multisystem disorder, AMeD syndrome. *Sci Adv* **6**, doi:10.1126/sciadv.abd7197 (2020).
- 333 16 Hodskinson, M. R. *et al.* Alcohol-derived DNA crosslinks are repaired by two distinct mechanisms.
334 *Nature* **579**, 603-608, doi:10.1038/s41586-020-2059-5 (2020).
- 335 17 Semlow, D. R. & Walter, J. C. Mechanisms of Vertebrate DNA Interstrand Cross-Link Repair. *Annu*
336 *Rev Biochem* **90**, 107-135, doi:10.1146/annurev-biochem-080320-112510 (2021).
- 337 18 Stinglele, J., Schwarz, M. S., Bloemke, N., Wolf, P. G. & Jentsch, S. A DNA-dependent protease
338 involved in DNA-protein crosslink repair. *Cell* **158**, 327-338, doi:10.1016/j.cell.2014.04.053 (2014).
- 339 19 Stinglele, J. *et al.* Mechanism and Regulation of DNA-Protein Crosslink Repair by the DNA-Dependent
340 Metalloprotease SPRTN. *Mol Cell* **64**, 688-703, doi:10.1016/j.molcel.2016.09.031 (2016).
- 341 20 Vaz, B. *et al.* Metalloprotease SPRTN/DVC1 Orchestrates Replication-Coupled DNA-Protein
342 Crosslink Repair. *Mol Cell* **64**, 704-719, doi:10.1016/j.molcel.2016.09.032 (2016).
- 343 21 Larsen, N. B. *et al.* Replication-Coupled DNA-Protein Crosslink Repair by SPRTN and the
344 Proteasome in Xenopus Egg Extracts. *Mol Cell* **73**, 574-588 e577, doi:10.1016/j.molcel.2018.11.024
345 (2019).
- 346 22 Hart, T. *et al.* High-Resolution CRISPR Screens Reveal Fitness Genes and Genotype-Specific Cancer
347 Liabilities. *Cell* **163**, 1515-1526, doi:10.1016/j.cell.2015.11.015 (2015).
- 348 23 Au, P. C., Helliwell, C. & Wang, M. B. Characterizing RNA-protein interaction using cross-linking
349 and metabolite supplemented nuclear RNA-immunoprecipitation. *Mol Biol Rep* **41**, 2971-2977,
350 doi:10.1007/s11033-014-3154-1 (2014).
- 351 24 Hafner, M. *et al.* CLIP and complementary methods. *Nature Reviews Methods Primers* **1**, 20,
352 doi:10.1038/s43586-021-00018-1 (2021).
- 353 25 Yan, L. L. & Zaher, H. S. How do cells cope with RNA damage and its consequences? *J Biol Chem*
354 **294**, 15158-15171, doi:10.1074/jbc.REV119.006513 (2019).
- 355 26 Hafner, M. *et al.* Transcriptome-wide identification of RNA-binding protein and microRNA target sites
356 by PAR-CLIP. *Cell* **141**, 129-141, doi:10.1016/j.cell.2010.03.009 (2010).

357 27 Castello, A. *et al.* Insights into RNA biology from an atlas of mammalian mRNA-binding proteins.
358 *Cell* **149**, 1393-1406, doi:10.1016/j.cell.2012.04.031 (2012).

359 28 Trendel, J. *et al.* The Human RNA-Binding Proteome and Its Dynamics during Translational Arrest.
360 *Cell* **176**, 391-403 e319, doi:10.1016/j.cell.2018.11.004 (2019).

361 29 Wu, C. C., Peterson, A., Zinshteyn, B., Regot, S. & Green, R. Ribosome Collisions Trigger General
362 Stress Responses to Regulate Cell Fate. *Cell* **182**, 404-416 e414, doi:10.1016/j.cell.2020.06.006 (2020).

363 30 Vind, A. C. *et al.* ZAKalpha Recognizes Stalled Ribosomes through Partially Redundant Sensor
364 Domains. *Mol Cell* **78**, 700-713 e707, doi:10.1016/j.molcel.2020.03.021 (2020).

365 31 Stoneley, M. *et al.* Unresolved stalled ribosome complexes restrict cell-cycle progression after
366 genotoxic stress. *Mol Cell* **82**, 1557-1572 e1557, doi:10.1016/j.molcel.2022.01.019 (2022).

367 32 Liu, J., Xu, Y., Stoleru, D. & Salic, A. Imaging protein synthesis in cells and tissues with an alkyne
368 analog of puromycin. *Proc Natl Acad Sci U S A* **109**, 413-418, doi:10.1073/pnas.1111561108 (2012).

369 33 Wu, C. C., Zinshteyn, B., Wehner, K. A. & Green, R. High-Resolution Ribosome Profiling Defines
370 Discrete Ribosome Elongation States and Translational Regulation during Cellular Stress. *Mol Cell* **73**,
371 959-970 e955, doi:10.1016/j.molcel.2018.12.009 (2019).

372 34 Joazeiro, C. A. P. Mechanisms and functions of ribosome-associated protein quality control. *Nat Rev*
373 *Mol Cell Biol* **20**, 368-383, doi:10.1038/s41580-019-0118-2 (2019).

374 35 Juszkiwicz, S. *et al.* ZNF598 Is a Quality Control Sensor of Collided Ribosomes. *Mol Cell* **72**, 469-
375 481 e467, doi:10.1016/j.molcel.2018.08.037 (2018).

376 36 Ikeuchi, K. *et al.* Collided ribosomes form a unique structural interface to induce Hel2-driven quality
377 control pathways. *EMBO J* **38**, doi:10.15252/embj.2018100276 (2019).

378 37 Yan, L. L. & Zaher, H. S. Ribosome quality control antagonizes the activation of the integrated stress
379 response on colliding ribosomes. *Mol Cell* **81**, 614-628 e614, doi:10.1016/j.molcel.2020.11.033 (2021).

380 38 Castello, A. *et al.* System-wide identification of RNA-binding proteins by interactome capture. *Nat*
381 *Protoc* **8**, 491-500, doi:10.1038/nprot.2013.020 (2013).

382 39 Perez-Perri, J. I. *et al.* Global analysis of RNA-binding protein dynamics by comparative and enhanced
383 RNA interactome capture. *Nat Protoc* **16**, 27-60, doi:10.1038/s41596-020-00404-1 (2021).

384 40 Mordovkina, D. *et al.* Y-Box Binding Proteins in mRNP Assembly, Translation, and Stability Control.
385 *Biomolecules* **10**, doi:10.3390/biom10040591 (2020).

386 41 Baquero-Perez, B. *et al.* The Tudor SND1 protein is an m(6)A RNA reader essential for replication of
387 Kaposi's sarcoma-associated herpesvirus. *Elife* **8**, doi:10.7554/eLife.47261 (2019).

388 42 Brown, A., Baird, M. R., Yip, M. C., Murray, J. & Shao, S. Structures of translationally inactive
389 mammalian ribosomes. *Elife* **7**, doi:10.7554/eLife.40486 (2018).

390 43 Frey, S., Pool, M. & Sedorf, M. Scp160p, an RNA-binding, polysome-associated protein, localizes to
391 the endoplasmic reticulum of *Saccharomyces cerevisiae* in a microtubule-dependent manner. *J Biol*
392 *Chem* **276**, 15905-15912, doi:10.1074/jbc.M009430200 (2001).

393 44 Hyer, M. L. *et al.* A small-molecule inhibitor of the ubiquitin activating enzyme for cancer treatment.
394 *Nat Med* **24**, 186-193, doi:10.1038/nm.4474 (2018).

395 45 Pohl, C. & Dikic, I. Cellular quality control by the ubiquitin-proteasome system and autophagy.
396 *Science* **366**, 818-822, doi:10.1126/science.aax3769 (2019).

397 46 Duxin, J. P., Dewar, J. M., Yardimci, H. & Walter, J. C. Repair of a DNA-protein crosslink by
398 replication-coupled proteolysis. *Cell* **159**, 346-357, doi:10.1016/j.cell.2014.09.024 (2014).

399 47 Sugasawa, K. *et al.* UV-induced ubiquitylation of XPC protein mediated by UV-DDB-ubiquitin ligase
400 complex. *Cell* **121**, 387-400, doi:10.1016/j.cell.2005.02.035 (2005).

401 48 Pakos-Zebrucka, K. *et al.* The integrated stress response. *EMBO Rep* **17**, 1374-1395,
402 doi:10.15252/embr.201642195 (2016).

403 49 Stein, K. C., Morales-Polanco, F., van der Lienden, J., Rainbolt, T. K. & Frydman, J. Ageing
404 exacerbates ribosome pausing to disrupt cotranslational proteostasis. *Nature* **601**, 637-642,
405 doi:10.1038/s41586-021-04295-4 (2022).

406 50 Wan, L. *et al.* Translation stress and collided ribosomes are co-activators of cGAS. *Mol Cell* **81**, 2808-
407 2822 e2810, doi:10.1016/j.molcel.2021.05.018 (2021).

409

410 **Materials and Methods**

411

412 **Cell lines**

413 HeLa T-REx Flp-In cells were provided by Cell Services, The Francis Crick Institute, and
414 maintained in Dulbecco's Modified Eagle Medium (DMEM) and supplemented with 10%
415 (v/v) fetal bovine serum (FBS). HCT116 and HAP1 cells were purchased from Horizon
416 Discovery and grown in RPMI-1640 Medium supplemented with 10% FBS, and Iscove's
417 Modified Dulbecco's Medium (IMDM) supplemented with 10% FBS and Penicillin-
418 Streptomycin-Glutamine, respectively. eHAP iCas9 cells were generated as described
419 previously¹ and maintained in IMDM medium supplemented with 10% Tet-Free FBS and
420 Penicillin-Streptomycin.

421

422 **Western blotting**

423 2×10^5 HAP1 cells/ 10^5 HeLa T-REx Flp-In cells/ 2×10^5 HCT116 cells per well were seeded in
424 12-well plates. The following day, fresh medium with indicated concentrations of 4-SU (Jena
425 Bioscience (N-1090-250)) was added and cells were incubated for 16 h; translation inhibitors
426 (harringtonine, HAR, 2 μ g/ml; anisomycin, ANS, 375 μ M) were added to 4-SU containing
427 medium for 0.5 h prior to irradiation, as indicated. Cells were washed once with 1 ml PBS
428 followed by 365 nm UVA irradiation (BS-02 UV/VIS irradiation chamber, Opsytec / Dr.
429 Gröbel) in an additional 1 ml PBS and incubated in fresh media for 0.5 h. Alternatively, 40 h
430 after seeding, cells were treated with indicated concentrations of formaldehyde for 1 h. Cells
431 were directly lysed in 150 μ l LDS sample buffer (Thermo Fisher Scientific, NP0007)
432 containing NuPAGE Sample Reducing Agent (Thermo Fisher Scientific, NP0009).

433 After boiling the samples for 15 minutes at 95°C, they were resolved on NuPAGE-
434 SDS-PAGE gels (Thermo Fisher Scientific). Electrophoresis was followed by transfer to 0.45

435 μm PVDF membranes (Merck, IPVH00010). Membranes were blocked in 5 % milk in TBS-
436 T for 1 h at room temperature before incubation with the following primary antibodies at 4 °C
437 overnight: Anti-GCN2 (Santa Cruz, sc-374609, 1:1000 dilution), Anti-K48 poly-Ub linkage
438 (Cell Signaling, #8081, 1:1000 dilution), anti-K63 poly-Ub linkage (Cell Signaling, #5621,
439 1:1000 dilution), Anti-Ubiquitin (Santa Cruz, Sc-8017, 1:2000 dilution), Anti-Phospho-eIF2a
440 (Ser51) (Cell Signaling, #3597, 1:1000 dilution), Anti-phospho-p38 MAPK (Thr180/Tyr82)
441 (Cell Signaling, #9216, 1:1000 dilution), Anti-eS10/Ribosomal protein S10 (LS-Bio, LS-
442 C335612, 1:1000 dilution), Anti-SND1/TudorSN (Santa Cruz, Sc-166676, 1:500 dilution),
443 Anti-Tubulin (Sigma-Aldrich, T6074, 1:2000 dilution), Anti-Vinculin (Santa Cruz, Sc-73614,
444 1:1000 dilution), Anti-XPC (Santa Cruz, Sc-74410, 1:500 dilution), Anti-YBX1 (Cell
445 Signaling, #4202, 1:500 dilution), Anti-YBX3/ZONAB (Bethyl, #303-070A, 1:1000
446 dilution), Anti-ZAK (Bethyl, #A301-993A, 1:1000), Anti-ZNF598 (Sigma-Aldrich,
447 HPA041760, 1:2500 dilution). Afterwards, membranes were washed with TBS-T and
448 incubated with corresponding horseradish peroxidase (HRP)-conjugated secondary antibodies
449 for 1 h at room temperature: Goat-anti-Mouse Immunoglobulins/HRP (Dako, Cat#P0447,
450 1:3000-5000 dilution), Swine-anti-Rabbit Immunoglobulins/HRP (DAKO, Cat#P0399,
451 1:3000-5000 dilution). Finally, membranes were imaged using the ChemiDoc MP Imaging
452 System (Bio-Rad).

453

454 **Cell viability measurement**

455 For PAR-CL treatment, 10^5 HAP1 cells/ 5×10^4 HeLa T-REx Flp-In cells/ 2×10^5 HCT116 cells
456 per well were seeded in 12-well plates. Medium was changed with the indicated
457 concentrations of 4-SU the following day. 16 h later, cells were washed once with 1 ml PBS
458 followed by UVA irradiation in an additional 1 ml PBS and fresh medium was added.
459 Alternatively, 5×10^4 eHAP iCas9 cells per well were seeded in 12-well plates with or without

460 1 µg/ml doxycycline. 48 h later, the media was changed to media containing indicated
461 concentrations of 4-SU, again with or without 1 µg/ml doxycycline. After 16 h, cells were
462 washed once with PBS followed by UVA irradiation in 1 ml no-phenol-red medium with or
463 without 1 µg/ml doxycycline. For formaldehyde treatment, 10⁵ HAP1 cells per well were
464 seeded in 12-well plates. Cells were treated with the indicated concentrations of
465 formaldehyde for 1 h the following day. Alternatively, 5×10⁴ eHAP cells per well were
466 seeded in 12-well plates with or without 1 µg/ml doxycycline for two days. Cells were treated
467 with the indicated concentrations of formaldehyde for 1 h. After 24 h, cellular viability was
468 measured by AlamarBlue assay: the medium was replaced with AlamarBlue cell viability
469 reagent (40 µg/ml resazurin in PBS, Resazurin, R7017, Sigma) and plates were incubated for
470 1 h at 37°C. Cell viability was then assessed by measuring fluorescence (560 nm
471 excitation/590 nm emission) using Tecan Spark plate reader. For colony formation assay, 10³
472 HAP1/ HeLa T-REx Flp-In/HCT116 cells were seeded into one 6 cm dish. Medium was
473 changed with the indicated concentrations of 4-SU the following day. 16 h later, cells were
474 washed once with 1 ml PBS followed by UVA irradiation in an additional 1 ml PBS and
475 fresh medium was added. 7 days later, cells were dried and scanned following crystal violet
476 staining.

477

478 **XRNAX (protein-x-linked RNA extraction)**

479 Three 15 cm dishes per condition with each 1.5×10⁷ HAP1 cells were seeded in medium with
480 or without 4-SU (5 µM, 16 h). Cells were then irradiated with UVA (6 kJ/m²) or treated with
481 formaldehyde (500 µM, 1 h). Cells were then washed twice in PBS and scraped in 5 ml ice-
482 cold PBS on ice, transferred to a 50 ml tube and spun down at 500 g for 5 minutes at 4°C.
483 The pellet was then lysed in 8 mL TRI reagent (T9424, Sigma-Aldrich) by pipetting up and
484 down. Subsequently, 1.6 mL chloroform were added, mixed by vigorous shaking and

485 incubated for 5 minutes at room temperature until phase separation was complete. Samples
486 were spun down at 7,000 g for 10 minutes at 4°C. 400µl of the aqueous phase was transferred
487 to a 1.5 ml tube, total RNA was extracted using isopropanol precipitation and resuspended in
488 200 µl nuclease-free water. The white sticky interphase was transferred to a 2 mL tube and
489 washed twice with 1 mL low SDS buffer (50 mM Tris-Cl, 1 mM EDTA, 0.1% SDS),
490 flushing protein off the walls of the tube while retaining the integrity of the interphase.
491 Samples were spun down at 5,000 g for 2 minutes at room temperature and the supernatant
492 discarded. After the washing, the interphase pellet was solubilized by adding 1 mL of low
493 SDS buffer and pipetting up and down approx. 20 times. The interphase was spun down with
494 5,000 g for 2 minutes at room temperature and the supernatant saved as interphase eluate 1.
495 Solubilization of the interphase was repeated with another 1 mL of low SDS buffer, then
496 twice with 1 mL of high SDS buffer (50 mM Tris-Cl, 1 mM EDTA, 0.5% SDS) each time
497 yielding approx. 1 mL of interphase eluates. NaCl was added to a final concentration of 300
498 mM to each of the four interphase eluates, along with 1 µl GlycoBlue (AM9515, Invitrogen)
499 and 1 mL isopropanol before mixing by inversion. Samples were spun down for 15 minutes
500 at 18,000 g at -10°C. The supernatants were discarded and pellets from all four elutes were
501 combined in 2 mL of 70% ethanol. The combined sample was again centrifuged for 1 minute
502 at 18,000 g at room temperature, supernatant discarded, and all residual ethanol removed.
503 The pellet was taken up in 1.8 mL of nuclease-free water and allowed to swell for 1 hour on
504 ice with occasional mixing by inversion and eventually dissolved by pipetting. 200 µl 10 x
505 NEB DNase I buffer was added along with 2 µl RNasin Plus, 100 µl NEB DNase and
506 incubated for 1.5 h at 37°C and 700 rpm. Subsequently, the sample was isopropanol
507 precipitated as described above without further addition of GlycoBlue. Pellets were taken up
508 in 400µl nuclease-free water and dissolved by pipetting. Samples were flash frozen and
509 stored at -80° C. For further analysis, the samples either digested with Proteinase K or RNase

510 A for 1 h shaking at 700 rpm at 60°C or 37°C, respectively. RNase-digested samples were
511 either directly subjected to MS or combined with 2x LDS sample buffer and boiled at 95°C
512 for 10 minutes to be analysed by SDS-PAGE and Sypro Ruby staining. ProteinaseK-digested
513 samples were combined with 2x RNA loading dye and boiled for 2 minutes at 85°C and
514 immediately placed on ice. The samples were analysed on an agarose gel and stained with
515 SYBR Gold according to manufacturer.

516

517 **Detection of DNA-protein crosslinks by KCl/SDS assay**

518 10⁵ HAP1 or HeLa T-REx Flp-In cells were seeded per well in 6-well plates. The following
519 day, cells were treated with 5 µM 4-SU for 16 h prior to irradiation with 6 kJ/m² UVA in 1 ml
520 PBS following one wash with PBS or cells were treated 40 h after seeding with 500 µM
521 formaldehyde for 1 h followed by two washes with PBS prior to KCl/SDS assay. To quantify
522 DPC induction, cells were collected in 400 µl denaturing lysis buffer (2% SDS, 20 mM
523 Tris/HCl, pH 7.5), frozen in liquid nitrogen and stored at -80°C until further processing. Cell
524 lysates were thawed at 55°C for 5 minutes with 1,200 rpm shaking, followed by pipetting
525 samples up and down 30 times. Cellular proteins were precipitated by adding 400 µl
526 precipitation buffer (200 mM KCl, 20 mM Tris pH 7.5) followed by incubation on ice for 5
527 minutes. Precipitated proteins were pelleted by full-speed centrifugation at 4°C for 5 minutes.
528 Next, 400 µl supernatant was saved and used for soluble DNA measurements. The pellet was
529 dissolved in 400 µl precipitation buffer by cooling down on ice for 5 minutes following
530 incubation at 55°C for 5 minutes with 1,200 rpm shaking and subsequent re-pelleting by full-
531 speed centrifugation at 4°C for 5 minutes. After repeating the washing procedure three times,
532 protein precipitate was resuspended in 400 µl Proteinase K-containing precipitation buffer
533 (200 mM KCl, 20 mM Tris pH 7.5. Proteinase K 0.2 mg/ml) followed by incubation at 55°C
534 for 45 minutes with 1,200 rpm shaking. Finally, 10 µl BSA (50 mg/ml) was added to the

535 solution followed by cooling down on ice for 5 minutes. Following a full-speed
536 centrifugation at 4°C for 5 minutes, crosslinked DNA in the supernatant was collected. RNA
537 contaminants in total DNA and crosslinked DNA were digested with 0.2 mg/ml RNase A for
538 30 minutes at 37°C. DNA concentrations were measured using Qubit™ dsDNA HS Assay
539 Kit (Thermo Fisher) according to the manufacturer's instructions. The proportion of
540 crosslinked DNA was calculated as the ratio between crosslinked DNA and total DNA
541 (crosslinked plus soluble DNA). Fold change represents the value of treated samples
542 normalised to the mean value of untreated control.

543

544 **Quantitative phosphoproteomics**

545 1.5×10^7 HAP1 cells were seeded into 15 cm dish with medium containing 4-SU (5 μM, 16 h),
546 followed by 10 ml PBS wash once prior to 6 kJ/m² UVA irradiation in additional 10 ml PBS
547 to induce RPCs. Cells were then incubated for 0.5 h in fresh medium at 37°C. To harvest,
548 cells were washed once in 10 ml PBS and then scraped in 5 ml ice-cold PBS on ice,
549 transferred to a 15 ml tube and spun down at 500 g for 5 minutes at 4°C. Cell pellets were
550 flash-frozen in liquid nitrogen and stored at -80°C until further processing. For TMT
551 labelling, cell pellets were lysed in modified RIPA buffer (50 mM Tris pH 7.5, 150 mM
552 NaCl, 1 mM EDTA, 1% NP-40, 0.1% sodium deoxycholate, containing Complete protease
553 inhibitor cocktail, 1 mM sodium orthovanadate, 5 mM β-glycerophosphate, and 5 mM
554 sodium fluoride) and homogenized and cleared by sonication and centrifugation,
555 respectively. A minimum of 5 mg of protein from individual whole cell lysates were trypsin-
556 digested and used for downstream 16-plex TMT-labelling, and phosphopeptide enrichment.
557 Briefly, acetone precipitated protein samples were digested to peptides using MS-approved
558 trypsin (Serva) at 1:150 and desalted through the reversed-phase Sep-Pak C18 cartridges
559 (Waters). Next, a total 150 ug of peptides for each individual sample were subjected to TMT

560 labelling at 1:1 for 1 h in 150 mM HEPES, pH 8.5. TMT-labelling was terminated with the
561 addition of 0.4 % hydroxylamine solution and excess labels were cleaned up through the
562 reversed-phase Sep-Pak C18 cartridges. Finally, equal amount of the TMT-labelled peptides
563 were combined for subsequent titanium dioxide (TiO₂)-based phosphopeptide enrichment².
564 The enriched phosphopeptides were eluted from the TiO₂ spheres using 5% NH₄OH and 10%
565 NH₄OH / 25% ACN, concentrated, acidified and fractionated using micro-column-based
566 SCX prior to C18 Stage tipping. For phosphopeptide measurements, peptide fractions were
567 analysed on a quadrupole Orbitrap mass spectrometer (Orbitrap Exploris 480, Thermo
568 Scientific) equipped with a UHPLC system (EASY-nLC 1000, Thermo Scientific), as
569 described^{3,4}. Peptide samples were loaded onto C18 reversed-phase columns (15 cm length,
570 75 µm inner diameter, 1.9 µm bead size) and eluted with a linear gradient from 8 to 40%
571 acetonitrile containing 0.1% formic acid in 2 h. The mass spectrometer was operated in data-
572 dependent mode, automatically switching between MS and MS2 acquisition. Survey full scan
573 MS spectra (m/z 300-1650) were acquired in the Orbitrap. The 10 most intense ions were
574 sequentially isolated and fragmented by higher-energy C-trap dissociation (HCD)⁵. Peptides
575 with unassigned charge states, as well as with charge state less than +2 were excluded from
576 fragmentation. Fragment spectra were acquired in the Orbitrap mass analyzer.

577

578 **Generation of knock-out cells**

579 To generate *ZAK*, *GCN2*, *ZNF598* knock-out and *AAVS1* control clones, gRNA_ZAK_1
580 (GGAGTGTTTATCGAGCCAAA), gRNA_ZAK_2 (TCGAGCCAAATGGATATCAC),
581 gRNA_GCIN2 (GCTACCGGTCCGCAAGCGTC), gRNA_ZNF598_1
582 (GTGGTACTCGCGCAAGGACC), gRNA_ZNF598_2 (CTACTGCGCCGTGTGCCGCG)
583 and gRNA_AAVS1 (GTCCCTAGTGGCCCCACTGT) were cloned into pX330-Puro
584 (Addgene #82580). gRNA_ZAK_1, gRNA_GCIN2, gRNA_ZNF598_2 and gRNA_AAVS1

585 were transfected into HAP1 cells, gRNA_ZAK_1, gRNA_GCN2, gRNA_ZNF598_1 and
586 gRNA_AAVS1 were transfected into HeLa T-REx Flp-In cells, gRNA_ZAK_2,
587 gRNA_GCN2, gRNA_ZNF598_1 and gRNA_AAVS1 were transfected into HCT116 cells,
588 using Lipofectamine 2000 (Invitrogen) according to the manufacturer's instructions. 16 h
589 after transfection, cells were selected in 0.75 µg/ml puromycin-containing IMDM media
590 (HAP1 cells) or 1 µg/ml puromycin-containing DMEM media (HeLa T-REx Flp-In cells) or
591 1 µg/ml puromycin-containing RPMI 1640 media (HCT116 cells) for 2-3 days until un-
592 transfected cells had died. To generate single clones, puromycin-selected cells were reseeded
593 in 96-well plates (0.5 cell/well). Single clones were expanded and validated by western
594 blotting using corresponding antibodies.

595

596 **Complementation of knock-out cells**

597 Clonal HeLa T-REx Flp-In or HCT116 ZAK/GCN2/ZNF598 knock-out cells were seeded in
598 6-well plates, and grown to 50% confluency, followed by transient transfection with 2 µg
599 pIRES-FRT plasmids (encoding GFP-Flag-NES, GFP-Flag-GCN2^{WT}, GFP-Flag-GCN2^{D848N})
600 or pcDNA5-FRT/TO plasmids (encoding YFP-ZAK^{WT}, YFP-ZA^{K45A} YFP-ZNF598^{WT}, YFP-
601 ZNF598^{C29A}) using Lipofectamine 2000 (Invitrogen) according to the manufacturer's
602 instructions. 16 h after transfection, cells were reseeded into 12-well plates (10⁵ HeLa T-REx
603 Flp-In cells with 1 µg/ml doxycycline or 2×10⁵ HCT116 cells per well) followed by indicated
604 treatments and after 0.5 h cells were lysed in 150 µl LDS sample buffer and analysed by
605 western blot.

606

607 **Cloning of expression plasmids and site-directed mutagenesis**

608 pcDNA4-TO-Strep-HA-ZAKα-K45A, pcDNA4-TO-GFP-ZNF598 were provided by
609 Addgene (#141194, #141191). ZAKα-K45A and ZNF598 WT were amplified by PCR and

610 cloned into pDONR221 vector using Gateway BP clonase followed by shuttling into
611 pcDNA5-FRT/TO-YFP vector using LR clonase. GCN2 fragments were cloned from cDNA
612 and inserted into pIRES-FRT-GFP-Flag vector (a gift from Boulton lab) using Gibson
613 assembly protocol. ZAK α ^{WT}, ZNF598^{C29A}, GCN2^{D848N} were generated by Q5 site-directed
614 mutagenesis (NEB, #E0554S) according to the manufacturer's instructions.

615

616 **Generation of eHAP iCas9 knock-out cells**

617 To generate eHAP inducible knock-out cell lines, the following gRNAs were cloned into
618 lenti-sgRNA vector (addgene # 104990) following Zhang lab protocol⁶:

619 gRNA_ZAK_1 (GH_CRp_4, TCGAGCCAAATGGATATCAC),

620 gRNA_ZAK_3 (GH_CRp_250, TGCATGGACGGAAGACGATG),

621 gRNA_GCN2_1 (GH_CRp_1, CCTACCGGTCCGCAAGCGTC),

622 gRNA_GCN2_2 (GH_CRp_2, ACTGGCCAAGAAACACTGTG),

623 gRNA_ZNF598_1 (GH_CRp_5, GTGGTACTCGCGCAAGGACC),

624 gRNA_ZNF598_2 (GH_CRp_6 CTACTGCGCCGTGTGCCGCG),

625 gRNA_AAVS1 (GH_CRp_38, GGGGCCACTAGGGACAGGAT).

626 To produce lentivirus, 8 x10⁵ 293FT cells in 6-well were transfected with packaging plasmids
627 (0.566 μ g pLP1, 0.26 μ g pLP2 and 0.37 μ g pLP/VSVG) along with 1 μ g of gRNA-expression
628 plasmid using 4 μ l Lipofectamine 2000 (Life Technologies/Thermo Fisher) following
629 manufacturer's instructions. Medium was refreshed 12-16 h after transfection. Virus-
630 containing supernatant was collected approximately 36-40 h post transfection and cleared
631 through a 0.45- μ m filter. eHAP iCas9 cells were transduced with 50 μ l of viral supernatant in
632 media supplemented with 8 μ g/ml polybrene (Sigma). 0.4 μ g/ml puromycin was used for the
633 selection of transductants 24 h following transduction.

634

635 **Measurements of protein synthesis rates**

636 1×10^6 HeLa T-REx Flp-In/ 1.5×10^6 HAP1 cells were seeded in one 6 cm dish per condition in
637 medium with or without indicated concentrations of 4-SU. Cells were irradiated with 6 kJ/m^2
638 UVA following 16 h incubation with 4-SU and washed twice with PBS directly after
639 irradiation or at indicated recovery time points, followed by 2 ml of medium containing OPP
640 ($20 \text{ }\mu\text{M}$ final concentration) incubation for 30 minutes at 37°C . Cells were then washed twice
641 with PBS, trypsinised and collected in a 1.5 ml tube. Samples were spun down at 500 g for 5
642 minutes and supernatant was discarded. The pellet was washed in 1 ml PBS once and
643 subsequently spun down again. Cells were then resuspended in $200 \text{ }\mu\text{l}$ PBS containing 1x
644 eFluor780 viability dye (Thermo, 65-0865-14) and incubated for 30 minutes in the dark at
645 4°C with occasional mixing. Afterwards cells were spun down and washed with 1 ml 1%
646 BSA in PBS. Subsequently the cells were fixed by resuspending the pellet in $200 \text{ }\mu\text{l}$ 4%
647 Formaldehyde in PBS and incubated for 15 minutes at room temperature. Cells were again
648 washed with 1 ml 1% BSA in PBS and stored in 1% BSA in PBS in the fridge.

649 For click-labelling, fixed cells were spun down and the pellet was resuspended in 250
650 μl 0.25% Triton-X in PBS and incubated for 20 minutes at room temperature for
651 permeabilization. In the meantime, click-chemistry mix was prepared using freshly dissolved
652 ascorbic acid ($113,5 \text{ mM}$, 50 mg in 2.5 ml water). For each condition $250 \text{ }\mu\text{l}$ of click-
653 chemistry mix was prepared with final concentration of 39.5 mM Tris-HCl pH 8.0, $60 \text{ }\mu\text{M}$
654 Alexa Fluor 488-Azide, 4 mM CuSO_4 , 11 mM ascorbic acid and 10 nM DAPI. After
655 permeabilization, cells were spun down, washed with 1 ml 1% BSA in PBS and supernatant
656 was removed. Cells were then resuspended in $250 \text{ }\mu\text{l}$ click-chemistry mix, and reactions were
657 incubated for 30 minutes at room temperature in the dark and mixed by occasional flicking of
658 the tube. After incubation, cells were washed in 1 ml 1% BSA in PBS and finally
659 resuspended in $200 \text{ }\mu\text{l}$ 1% BSA in PBS and analysed by flow cytometry.

660 For flow cytometry, samples were analysed on a BD LSRFortessa (BD Bioscience)
661 equipped with 355/405/488/561/640 nm lasers with a minimum count of 10,000 events. Flow
662 cytometry results were analysed using FlowJo™ v10.7 Software (BD Life Sciences).
663 Staining with fixable viability dye eFluor780 was used to exclude dead cells, and the mean
664 fluorescence intensity (MFI) in FITC channel was measured for single and live cells.

665

666 **Polysome Profiling**

667 7×10^6 HAP1 cells were seeded into 15 cm dishes in no-phenol-red medium, with or without 5
668 μM 4-SU. Two dishes were prepared per condition. Cells were irradiated with 6 kJ/m^2 UVA
669 following 16 h incubation of 4-SU treatment. Cells were harvested immediately or 0.5 h after
670 irradiation on ice. Cells were pelleted with 500 g centrifugation for 5 minutes at $4 \text{ }^\circ\text{C}$. From
671 then, all steps were performed at $4 \text{ }^\circ\text{C}$. Pelleted cells were resuspended in 500 μl of lysis
672 buffer (5 mM Tris-HCl pH 7.5, 1.5 mM KCl, 2.5 mM MgCl_2 , 2 mM DTT, 0.5% v/v Triton
673 X-100, 0.25% w/v sodium deoxycholate, 20 U/ml SUPERase-In RNase Inhibitor
674 (Invitrogen), complete EDTA-free protease inhibitor cocktail (Roche) and spun down at
675 15,000 g for 5 minutes. The nucleic acid content of the supernatants was measured by
676 determining absorption at 260 nm (A_{260}) in an Eppendorf BioPhotometer. Equal volumes of
677 each supernatant were then applied to 10%-50% continuous sucrose density gradients (20
678 mM HEPES pH 7.5, 100 mM KOAc, 5 mM $\text{Mg}(\text{OAc})_2$, 1 mM DTT, and protease inhibitor
679 cocktail). The gradients were centrifuged in an SW40Ti rotor (Beckman Coulter) at 202,408
680 g for 135 minutes and fractionated using a BioComp Gradient Station while A_{260} was
681 recorded using a Triax Flow Cell FC-2. Measured absorption values were normalised to the
682 soluble fraction containing no ribosomal material.

683

684

685 **Disome profiling**

686 Cell culture and treatments were carried out as described below. Briefly, 0.75×10^6 HAP1
687 cells were seeded onto 6×10 cm plates and grown overnight at 37°C . The next day, cells were
688 supplemented with fresh medium containing 10% dialyzed FBS and supplemented with $5 \mu\text{M}$
689 4-SU. After approx. 18 h of 4-SU incorporation, cells were re-supplemented with fresh IMEM
690 (containing dialyzed FBS and $5 \mu\text{M}$ 4-SU) without phenol-red. 1 h later, plates were treated
691 with 0 or 6 kJ/m^2 UVA, and allowed to recover for 0.5h. Cells were lysed by aspirating
692 media, immediately rinsed with 10 ml warm PBS supplemented with $378 \mu\text{M}$ anisomycin to
693 freeze ribosomes *in situ*, and lysed by adding $250 \mu\text{l}$ ice-cold lysis buffer (50 mM HEPES pH
694 7.4, 100 mM KOAc, 5% glycerol, 0.25% NP-40, 15 mM $\text{Mg}(\text{OAc})_2$, $378 \mu\text{M}$ anisomycin, 8
695 units/ml Turbo DNase (Thermo Fisher), 1x protease and phosphatase inhibitor (Cell
696 Signaling), $0.2 \mu\text{l/ml}$ SUPERase IN, and 1 mM TCEP dropwise to the plate. Plates were
697 swirled to distribute lysis buffer, and cells were scraped from the plate using a cell scraper,
698 gently pipetted to homogenize the cell lysate, and transferred to ice for 10 minutes to
699 complete lysis. Lysates were clarified by brief centrifugation at $8,000 \text{ g}$ for 10 minutes, and
700 the clarified supernatant was transferred to a fresh tube on ice. Clarified cell lysates were
701 treated with RNase A (Ambion) using the following condition: $1 \mu\text{g}$ RNase A was added per
702 $100 \mu\text{g}$ RNA in a $250 \mu\text{l}$ reaction volume, shaken at 500 rpm (20 minutes, 25°C) on a table-
703 top thermo-mixer (Eppendorf); the reaction was quenched by the addition of
704 SUPERaseIn RNase inhibitor (~ 200 units per $100 \mu\text{g}$ RNA). RNase A digested lysates were
705 layered on top of 10-35% sucrose gradients and ultra-centrifuged in a Beckman SW41
706 swinging bucket rotor ($40,000 \text{ rpm}$; 105 minutes). UV (A_{260}) absorbance across 10-35%
707 sucrose gradients was measured using a top-down Biocomp Piston Gradient Fractionator as
708 per manufacturer's instructions.

709

710 **Ribosome profiling**

711 1.5×10^6 HAP1 cells were seeded onto twelve 10 cm plates and grown overnight. The next
712 day, the media was changed to fresh IMEM media with or without 5 μ M 4-SU. After 18 h,
713 the media was changed to media without phenol red (with or without 5 μ M 4SU). 30 minutes
714 later, half of the plates of cells were irradiated with 6 kJ/m² UVA. After a 0.5 h recovery
715 period, the plates were washed with 10 mL warm PBS buffer and cells from each plate were
716 resuspended with vigorous scraping in 250 μ L lysis buffer (50 mM HEPES pH 7.4, 100 mM
717 KOAc, 5% glycerol, 0.25% NP40, 15 mM Mg (OAc)₂, 100 μ g/mL cycloheximide, protease
718 and phosphatase inhibitor (Cell Signaling), 0.2 μ L/mL SUPERase IN, and 1 mM TCEP).
719 Lysates were digested with Turbo DNase I (2 units/mL) for 15 minutes on ice and clarified
720 by centrifugation at 20,000 g for 10 min. 30 μ g of RNA was digested with 150 units of
721 RNase I for 1 h at 25 °C. The ribosomes were pelleted through a 1 mL sucrose cushion (1 M
722 sucrose, 20 mM Tris-HCl pH 8, 150 mM KCl, 5 mM MgCl₂, 1 mM DTT, and 100 μ g/mL
723 cycloheximide) in a TLA100.3 rotor at 100,000 rpm for 1 h at 4 °C. The ribosome pellets
724 were resuspended in 250 μ L proteinase K buffer (50 mM Tris-HCl pH 7.5, 75 mM NaCl,
725 12.5 mM EDTA, 1% SDS, and 1.2 mg/mL proteinase K) and digested for 30 minutes at 55
726 °C. Following phenol extraction, RNA was size-selected on 15% denaturing PAGE gels,
727 isolating between 15-70 nt fragments. Library construction was carried out as described
728 previously⁷. The libraries were sequenced on the Illumina NovaSeq6000 instrument at the
729 Johns Hopkins University Genetic Resources Core Facility.

730

731 **Data processing for RNA-seq**

732 Reads in the raw FASTQ files were trimmed to remove the adaptor and UMI sequence
733 NNNNNNCACTCGGGCACCAAGGAC using the bbdduk script in the BBtools suite
734 (<https://jgi.doe.gov/data-and-tools/bbtools/>). rRNA sequences were removed by aligned to a

735 non-coding RNA library, after which trimmed reads failing to align were then were then
736 aligned to the hg38 human genome sequence using STAR⁸. Subsequent analyses were
737 performed with custom Python scripts. For metagene plots, the transcript with the highest
738 level of evidence in the ensemble database was selected for each gene. For each transcript
739 with more than an average of 0.1 reads per codon, the average ribosome density surrounding
740 the start codon (100 nt upstream and 1,000 nt downstream) was calculated with each gene
741 contributing equally to the average. To identify T to C conversions, sites where the HAP1
742 cells differ from the hg38 annotation were first compiled in a VCF file from RNAseq data
743 from three untreated samples using the mpileup and call command from bcftools. From the
744 BAM alignment files, reads containing T to C conversions were identified; if the site of
745 conversion corresponds to a known SNP in the VCF file, these reads were ignored. The
746 position of the remaining T to C conversions in the reads that are standard ribosome
747 footprints (30 nt) or disomes (> 58 nt) were counted.

748

749 **Poly-A pulldown**

750 1.5×10^7 HAP1 cells were seeded into 15 cm dish with indicated concentration of 4-SU for 16
751 h prior to UVA (6 kJ/m²) irradiation; inhibitors (TAK-243, Ub-E1i, 1 μ M; MG132, 5 μ M;
752 anisomycin, ANS, 375 μ M,) were added to 4-SU containing medium for 1 h prior to
753 irradiation, as indicated. Cells were washed once in 10 ml PBS prior to irradiation in fresh 10
754 ml of PBS. Cells were then scraped in 5 ml ice-cold PBS on ice at indicated time points,
755 transferred to a 15 ml tube and spun down at 500 g for 5 minutes at 4°C. PBS was removed
756 and cells were lysed in 5 ml ice-cold lysis buffer (20 mM Tris-HCl pH 7.5; 500 mM LiCl; 1
757 mM EDTA pH 8.0; 0.5 % LiDS; add fresh: 5 mM DTT, Protease-inhibitor cocktail, RNase
758 Inhibitor 20U/ml) by pipetting up and down. Subsequently lysates were homogenized using a
759 syringe with five consecutive strokes and flash frozen in liquid nitrogen. For processing,

760 samples were thawed at 60°C in a water bath for 5 minutes and placed on ice. 200 µl NEB
761 oligo d(T) beads per conditions were equilibrated in lysis buffer and added to the lysates.
762 Binding of the beads was performed at 4°C on a rotation wheel at 20 rpm for 1 h. After
763 binding, lysates were placed on a magnetic rack to collect the beads. A 100 µl sample (SN)
764 was taken from each sample and 3x LDS sample buffer was added to a final volume of 150
765 µl. Beads were then washed twice with wash buffer 1 (20 mM Tris-HCl pH 7.5; 500 mM
766 LiCl; 1 mM EDTA pH 8.0; 0.1 % LiDS; add fresh: 5 mM DTT, Protease-inhibitor cocktail),
767 then twice with wash buffer 2 (20 mM Tris-HCl pH 7.5; 500 mM LiCl; 1 mM EDTA pH 8.0;
768 0.02% IGEPAL CA-360; add fresh: 5 mM DTT, Protease-inhibitor cocktail) and twice with
769 wash buffer 3 (20 mM Tris-HCl pH 7.5; 200 mM LiCl; 1 mM EDTA pH 8.0; 0.02%
770 IGEPAL CA-360; add fresh: 5 mM DTT, Protease-inhibitor cocktail) using the magnetic rack
771 and in the final washing step, tubes were spun down in the centrifuge at 2,000 g for 10
772 minutes at 4°C. Wash buffer 3 was then removed completely and beads were resuspended in
773 220µl nuclease-free water. An aliquot of 20 µl was taken to elute RNA and normalize the
774 samples. RNA was eluted in heat elution buffer. To this end, beads in the 20 µl aliquot were
775 collected and supernatant removed. Beads were then resuspended in 15 µl heat elution buffer
776 (20mM Tris-HCl (pH 7.5), 1mM EDTA in nuclease-free water) and incubated at 700 rpm at
777 95°C for 5 minutes and instantly placed in a magnetic rack. Supernatant was collected
778 immediately and RNA content was measured using NanoDrop (Thermo Fisher Scientific).
779 The volume of beads used for protein elution was then normalised to the RNA content. To
780 elute crosslinked proteins, beads were collected on the magnetic rack and supernatant was
781 removed. Resuspension in 90 µl of protein elution buffer (RNase A (100 U), 5mM DTT in
782 nuclease-free water) and subsequent incubation at 700 rpm at 37°C for 30 minutes was done
783 to release crosslinked protein from beads. 4x LDS sample buffer was added to a final volume

784 of 120 μ l and samples were boiled at 95°C for 10 minutes and analysed by SDS-PAGE and
785 Western Blot.

786

787 **Quantitative proteomics of XRNAX and poly-A pulldown samples**

788 After RNA digestion, samples were dried in a speed vacuum centrifuge and diluted in 15 μ l
789 8 M Urea/0.4 M NH_4HCO_3 . Proteins were reduced using dithioerythritol (final concentration:
790 5 mM) for 30 minutes at 37°C. Subsequently, alkylation of cysteines was done with
791 iodoacetamide (final concentration: 15 mM) for 30 minutes and quenched with 15 mM
792 dithioerythritol for 15 minutes at room temperature in the dark. The first digestion step was
793 performed using Lys-C (1:100, enzyme:protein ratio, Wako) at 37°C for 4 h. Prior to tryptic
794 digestion, samples were diluted with H_2O to give 1 M Urea. Tryptic digestion was performed
795 (1:50, enzyme:protein ratio, Promega) at 37°C for 16 h. For LC-MS/MS analysis each sample
796 was injected in an Ultimate 3000 nano-chromatography system (Thermo Fisher Scientific)
797 and transferred to a trap column (Acclaim PepMap 100 $\mu\text{m} \times 2\text{cm}$, 5 μm particles, 100Å,
798 ThermoFisher Scientific). Separation was performed at 250 nl/minute using a 50 cm
799 reversed-phase separation column (PepMap RSLC C18 2 μm 100 Å 75 $\mu\text{m} \times 50\text{cm}$, Thermo
800 Fisher Scientific). Solvent A consisted of 0.1 % formic acid in water and solvent B consisted
801 of 0.1 % formic acid in acetonitrile. For separation, two consecutive gradients from 3% to
802 25% solvent B in 40 minutes and 25% to 40 % solvent B in 5 minutes were applied. Eluting
803 peptides were analysed on a QExactive HF-X mass spectrometer (Thermo Fisher Scientific)
804 with a top 15 data-dependent acquisition method. Data processing, peptide search and
805 quantification was done with MaxQuant (v.1.6.7.0)⁹ and the human subset of the UniProt
806 database

807

808 **Statistical analysis of MS data**

809 Statistical analysis of MS data was performed in R (version 4.1.2). For XRNAX analysis
810 (Fig. 1f), LFQ intensity values were log₂ transformed and filtered for proteins identified in
811 all three replicates of either formaldehyde or 4-SU+UVA treated samples. Additionally,
812 proteins were discarded if they were identified more than once in the untreated control.

813 For phosphoproteome analysis (Fig. 2a, b and Extended Data Fig. 2a), only peptides
814 with a localization probability ≥ 0.75 and no missing values were considered. TMT-reporter
815 intensities were log₂ transformed and quantile normalised between the replicates using the R
816 package preprocessCore (version 1.56.0). Significantly regulated phosphorylation sites were
817 identified by employing a moderated T test using limma with Benjamini-Hochberg FDR
818 correction. Only sites with a log₂-fold change > 1 and an FDR-adjusted p value ≤ 0.01 were
819 considered significant. Phosphosite annotation and kinase-substrate relations were obtained
820 from the PhosphoSitePlus database. For phosphosite identification the flanking sequence (+/-
821 7 aa) was used. Kinase activity was estimated using the KSEA App web application with a p
822 value ≤ 0.01 and a minimum NetworKIN score cut-off of 2^{10} .

823 For poly-A pulldown MS analysis, LFQ intensities were log₂ transformed and filtered
824 for proteins detected in at least 50% of all 4-SU+UVA treated replicates. Additionally, for
825 experiments shown in Fig. 5a, b, d, e, g, h only proteins detected in at least three out of four
826 replicates were kept. Quantile normalization was employed between the replicates and missing
827 values were imputed based on a mixed imputation strategy using the MSnbase package
828 (version 2.20.1). In detail, proteins with a higher mean intensity than the top five most abundant
829 proteins with $33\% \leq$ (10% for Fig. 5a, b, d, e, g, h missing values) were considered missing at
830 random and imputed using the k-nearest neighbours algorithm. Proteins below that threshold
831 were imputed using the MinDet method. To test for differential protein abundance a moderated
832 T test using limma with Benjamini-Hochberg FDR correction was employed. For figure 4d
833 proteins with a log₂ fold change ≥ 1 or ≤ -1 and an adjusted p value ≤ 0.05 were considered

834 significant. For figures 5a, b, d, e, g, h proteins with a log₂ fold change ≥ 0.5 or ≤ -0.5 and an
835 adjusted *p* value ≤ 0.01 were considered significant.

836

837 **Data availability statement**

838 The mass spectrometry data reported in this manuscript were deposited to the
839 ProteomeXchange Consortium (www.proteomexchange.org,) via the Proteomics Identification
840 Database (PRIDE) partner repository. Data shown in Fig. 1f-g, Fig. 4b, d, Fig. 5a, b, d, e, g, h
841 and Extended Data Fig. 6a, c, e were deposited with the dataset identifiers PXD038332 for all
842 data sets; Data shown in Fig. 2a-b reported in this manuscript were deposited with the dataset
843 identifier PXD038398. RNA-seq data (Fig. 3c-e, g, Extended Data Fig. 4b, c) have been
844 deposited in the GEO under accession code GSE219055.

845

846 **Code availability statement**

847 Custom python scripts used in analysing the ribosome profiling data are freely available at
848 https://github.com/greenlabjhmi/rna_protein_crosslinks

849

850 **Methods references**

851

- 852 1 Hewitt, G. *et al.* Defective ALC1 nucleosome remodeling confers PARPi sensitization and synthetic
853 lethality with HRD. *Mol Cell* **81**, 767-783 e711, doi:10.1016/j.molcel.2020.12.006 (2021).
- 854 2 Borisova, M. E., Wagner, S. A. & Beli, P. Mass Spectrometry-Based Proteomics for Quantifying DNA
855 Damage-Induced Phosphorylation. *Methods Mol Biol* **1599**, 215-227, doi:10.1007/978-1-4939-6955-
856 5_16 (2017).
- 857 3 Michalski, A. *et al.* Mass spectrometry-based proteomics using Q Exactive, a high-performance
858 benchtop quadrupole Orbitrap mass spectrometer. *Mol Cell Proteomics* **10**, M111 011015,
859 doi:10.1074/mcp.M111.011015 (2011).
- 860 4 Kelstrup, C. D., Young, C., Lavalley, R., Nielsen, M. L. & Olsen, J. V. Optimized fast and sensitive
861 acquisition methods for shotgun proteomics on a quadrupole orbitrap mass spectrometer. *J Proteome*
862 *Res* **11**, 3487-3497, doi:10.1021/pr3000249 (2012).
- 863 5 Olsen, J. V. *et al.* Higher-energy C-trap dissociation for peptide modification analysis. *Nat Methods* **4**,
864 709-712, doi:10.1038/nmeth1060 (2007).
- 865 6 Sanjana, N. E., Shalem, O. & Zhang, F. Improved vectors and genome-wide libraries for CRISPR
866 screening. *Nat Methods* **11**, 783-784, doi:10.1038/nmeth.3047 (2014).
- 867 7 Veltri, A. J. *et al.* Distinct elongation stalls during translation are linked with distinct pathways for
868 mRNA degradation. *Elife* **11**, doi:10.7554/eLife.76038 (2022).

- 869 8 Dobin, A. *et al.* STAR: ultrafast universal RNA-seq aligner. *Bioinformatics* **29**, 15-21,
870 doi:10.1093/bioinformatics/bts635 (2013).
871 9 Cox, J. & Mann, M. MaxQuant enables high peptide identification rates, individualized p.p.b.-range
872 mass accuracies and proteome-wide protein quantification. *Nat Biotechnol* **26**, 1367-1372,
873 doi:10.1038/nbt.1511 (2008).
874 10 Wiredja, D. D., Koyuturk, M. & Chance, M. R. The KSEA App: a web-based tool for kinase activity
875 inference from quantitative phosphoproteomics. *Bioinformatics* **33**, 3489-3491,
876 doi:10.1093/bioinformatics/btx415 (2017).
877

878

879 **Acknowledgements**

880 We thank D. Nedialkova for comments on the manuscript and F. Schleich for preliminary
881 work on this study. We also thank the Core Facility Flow Cytometry at Biomedical Center,
882 LMU Munich and Proteomics Core Facility at Institute Molecular Biology, Mainz for
883 experimental support. J.C. and P.W., are supported by the International Max-Planck Research
884 School for Molecular Life Sciences and S.Z. by the LMU – China Scholarship Council
885 Program. J.S. is supported by the European Research Council (ERC Starting Grant 801750
886 DNAProteinCrosslinks), by the Alfred Krupp Prize for Young University Teachers awarded
887 by the Alfred-Krupp von Bohlen und Halbach-Stiftung, the European Molecular Biology
888 Organization (YIP4644), and a Vallee Scholarship. G.H. is supported by the Radiation
889 Research Unit at the Cancer Research UK City of London Centre Award (C7893/A28990).
890 A.R.B. is supported by National Institutes of Health (Grant GM136960), R.G. is supported by
891 Howard Hughes Medical Institute.

892

893 **Author contributions**

894 S.Z., J.C., and J.S. conceived the project. S.Z. and J.C performed the majority of experiments.
895 K.C. performed label-free MS measurements. M.J.G analysed all mass spectrometry data.
896 T.M.-K. conducted polysome profiling experiments. A. J. V. and N. K. S. performed
897 ribosome profiling experiments, analysed by A.R.B. P.W. generated expression constructs.

898 G.H. generated inducible KO cell lines. T.F, R.B., R.G, and J.S supervised the work. S.Z.,
899 J.C., and J.S. wrote the manuscript with input from all authors.

900

901 **Competing interest declaration**

902 The authors declare no competing interests.

903

904 Correspondence and requests for materials should be addressed to

905 stingele@genzentrum.lmu.de.

906

907 Supplementary Information is available for this paper.

908

909

910

911 **Extended Data Figure Legends**

912

913

914 **Extended Data Figure 1. Photoactivatable-ribonucleoside-enhanced crosslinking and**
915 **formaldehyde trigger toxic RNA-protein crosslink formation.**

916 **a-b:** Colony formation assay (a) and cell viability measurement (b) of HeLa T-REx Flp-In
917 cells after treatment with indicated doses of 4-SU (16 h) and UVA. Values in (b) represent
918 the mean \pm SD of three biological replicates normalised to the mean of corresponding control
919 of each replicate.

920 **c-d:** Colony formation assay (c) and cell viability measurement (d) of HCT116 cells after
921 treatment with indicated doses of 4-SU (16 h) and UVA. Values in (d) represent the mean \pm
922 SD of three biological replicates normalised to the mean of corresponding control of each
923 replicate.

924 **e:** HAP1 cells treated with indicated formaldehyde (FA) concentrations for 1 h. Cell viability
925 was measured by AlamarBlue assay 24 h after formaldehyde treatment. Values represent the
926 mean \pm SD of four biological replicates normalised to the mean of corresponding control of
927 each replicate.

928 **f:** DNA-protein crosslinks quantified by KCl-SDS precipitation assay in HeLa T-REx Flp-In
929 cells following treatment as in (Fig. 1d). Crosslinked DNA was determined using Qubit DNA
930 HS assay. Values represent the mean \pm SD of the fold change of crosslinked DNA of three
931 technical replicates normalised to the mean of untreated controls.

932 **g:** Gene ontology (biological function, panther) enrichment analysis of proteins purified by
933 XRNAX assay (Fig. 1 f-g), upon formaldehyde (FA) and PAR-CL (4-SU+UVA) treatment
934 using all genes in the reference list as a background. The 20 most enriched terms with an
935 FDR \leq 0.01 and a reference list size \geq 10 are displayed.

936

937

938 **Extended Data Figure 2. PAR-CL induces ZAK α - and GCN2-dependent stress**
939 **responses.**

940 **a:** Kinase-substrate enrichment analysis (KSEA) showing kinase Z-scores (4-SU (5 μ M, 16
941 h) +UVA (6 kJ/m²) vs control) based on significantly altered phospho-sites shown in (Fig.
942 2a).

943 **b-c:** Representative western blot analysis of clonal HeLa T-REx Flp-In (b) and HCT116 (c)
944 ZAK KO cells complemented with constructs expressing GFP, ZAK α ^{WT} or ZAK α ^{K45R}, and
945 matched AAVS1 control cells treated with 4-SU (5 μ M, 16 h), UVA (6 kJ/m²), or ANS (1
946 μ M, 0.5 h), as indicated. Asterisk indicates unspecific band.

947 **d-e:** Representative western blot analysis of clonal HeLa T-REx Flp-In (d) and HCT116 (e)
948 GCN2 KO cells complemented with constructs expressing GFP, GCN2^{WT} or GCN2^{D848N} and
949 matched AAVS1 control cells treated with 4-SU (5 μ M, 16 h), UVA (6 kJ/m²), or ANS (1
950 μ M), as indicated.

951 **f-g:** Representative western blot analysis of eHAP cells expressing doxycycline-inducible
952 Cas9 and AAVS1 or ZAK gRNAs (f) or GCN2 gRNAs (g) incubated with doxycycline (1
953 μ g/ml, 48 h) followed by the treatment of 4-SU (5 μ M, 16 h) and UVA irradiation (6 kJ/m²)

954 or the treatment of anisomycin (ANS, 1 μ M, 0.5 h), as indicated. Asterisk indicates
955 unspecific band.

956 **h-i:** Representative western blot analysis of HeLa T-REx Flp-In cells treated with 4-SU (5
957 μ M, 16 h) followed by HAR (2 μ g/ml, 0.5 h) pre-treatment prior to irradiation with UVA (6
958 kJ/m^2) and anisomycin (ANS, 1 μ M, 0.5 h) (h) or anisomycin pre-treatment (ANS, 375 μ M,
959 0.5 h) prior to irradiation with UVA (6 kJ/m^2) (i), as indicated. Asterisk indicates unspecific
960 band.

961

962

963 **Extended Data Figure 3. Formaldehyde induces ZAK α - and GCN2-dependent stress**
964 **responses.**

965 **a-b:** Representative western blot analysis of clonal HeLa T-REx Flp-In ZAK KO (a) and
966 GCN2 KO (b) cells and matched AAVS1 control cells treated with increasing doses of 4-SU
967 (0.04, 0.2, 1 and 5 μ M, 16 h), followed by UVA irradiation (6 kJ/m^2) or increasing doses of
968 formaldehyde (FA, 100, 200, 500, 1000 μ M, 1 h).

969 **c-d:** Representative western blot analysis of HAP1 (c) and HeLa T-REx Flp-In (d) cells
970 treated with 4-SU (5 μ M, 16 h) followed by harringtonine (HAR, 2 μ g/ml, 0.5 h) pre-
971 treatment prior to irradiation with UVA (6 kJ/m^2) or the treatment of increasing doses of
972 formaldehyde (FA, 100, 200, 500, 1000 μ M, 1 h), as indicated. Asterisk indicates unspecific
973 band.

974

975

976 **Extended Data Figure 4. PAR-CL induces translation stress and ribosome collisions.**

977 **a:** Relative levels of O-propargyl-puromycin (OPP) incorporation measured by flow
978 cytometry to determine protein synthesis rate in HeLa T-REx Flp-In cells following treatment
979 with indicated doses of 4-SU (16 h) followed by UVA irradiation (6 kJ/m^2). Values represent
980 fluorescence intensities of live, single cells normalised to the mean of untreated controls.

981 **b:** Frequency of C-T conversion in 30-mer ribosome footprints isolated from HAP1 cells
982 treated with 4-SU (5 μ M, 18 h) and UVA (6 kJ/m^2), as indicated compared to controls.
983 Values represent the mean \pm SD of three replicates.

984 **c:** Representative size distribution of ribosome footprints from HAP1 cells treated with 4-SU
985 (5 μ M, 18 h) and UVA (6 kJ/m^2) compared to controls.

986 **d:** Polysome profiles of RNase-digested lysates of HAP1 cells treated with 4-SU alone (5
987 μ M, 18 h) or 4-SU+UVA (6 kJ/m^2), as indicated and harvested 0.5 h after irradiation.
988 Following lysis and RNase A digestion, lysates were fractionated over 10-35% sucrose
989 gradients followed by UV(A₂₆₀) absorbance measurement

990 **e-f:** Representative western blot analysis of clonal HeLa T-REx Flp-In (e) and HCT116 (f)
991 ZNF598 KO cells complemented with constructs expressing GFP, ZNF598^{WT} or ZNF598^{C29A}
992 and matched AAVS1 control cells treated with 4-SU (5 μ M, 16 h), UVA (6 kJ/m^2), or
993 anisomycin (ANS, 1 μ M, 0.5 h), as indicated.

994 **g-i:** Representative western blot analysis of clonal HAP1(g), HeLa T-REx Flp-In (h) and
995 HCT116 (i) ZAK or GCN2 KO cells and matched AAVS1 control cells treated with 4-SU (5
996 μ M, 16 h), UVA (6 kJ/m^2) or anisomycin (ANS, 1 μ M, 0.5 h), as indicated.

997 **j-l:** Representative western blot analysis of clonal HAP1(j), HeLa T-REx Flp-In (k) and
998 HCT116 (l) *ZNF598* KO cells and matched *AAVS1* control cells treated with 4-SU (5 μ M, 16
999 h), UVA (6 kJ/m²) or anisomycin (ANS, 1 μ M, 0.5 h), as indicated. Asterisk indicates
1000 unspecific band.

1001
1002

1003 **Extended Data Figure 5. RQC is not essential for resolution of PAR-CL-induced**
1004 **translational stress.**

1005 **a:** Representative western blot analysis of eHAP cells expressing doxycycline-inducible *Cas9*
1006 and *AAVS1* or *ZNF598* gRNAs were incubated with doxycycline (Dox, 1 μ g/ml, 48 h)
1007 followed by treatment with 4-SU (5 μ M, 16 h) and UVA irradiation (6 kJ/m²) or anisomycin
1008 (ANS, 1 μ M, 0.5 h), as indicated.

1009 **b:** eHAP cells expressing doxycycline-inducible *Cas9* and *AAVS1* or *ZNF598* gRNAs were
1010 incubated with doxycycline (Dox, 1 μ g/ml, 48 h) followed by treating with indicated doses of
1011 4-SU (16 h) and UVA irradiation (6 kJ/m²) or indicated doses of formaldehyde. After 24 h,
1012 viability was determined using AlamarBlue assay. Values represent the mean \pm SD of three
1013 (PAR-CL, 4-SU+UVA) or four (FA) biological replicates normalised to the mean of
1014 corresponding controls of each replicate.

1015 **c:** O-propargyl-puromycin (OPP) incorporation analysed by flow cytometry in HeLa T-REx
1016 Flp-In cells treated with 4-SU (5 μ M, 16 h) and UVA (6 kJ/m²) at different timepoints after
1017 irradiation. Values represent fluorescence intensities of live, single cells normalised to the
1018 mean of controls.

1019
1020

1021 **Extended Data Figure 6. Resolution of mRNA-protein crosslinks is independent of**
1022 **autophagy, ZAK, GCN2, or ZNF598.**

1023 **a:** Bar graphs depicting normalised label free quantification (LFQ) intensities of YBX3-
1024 mRPCs isolated by poly-A pulldown from HAP1 cells treated with 4-SU (2.5 μ M, 16 h) and
1025 ubiquitin E1 inhibitor (Ub-E1i, TAK-243, 1 μ M, 1 h), as indicated, prior to irradiation with
1026 UVA (6 kJ/m²) at indicated timepoints. Bar graphs depict mean \pm SD of four biological
1027 replicates

1028 **b:** Representative western blot showing indicated timepoints of recovery of mRPCs isolated
1029 by poly-A pulldown from HAP1 cells treated with 4-SU (2.5 μ M, 16 h) and treated with
1030 autophagy inhibitor (Bafilomycin A1, BAF, 50 nM, 1 h) prior to irradiation with UVA (6
1031 kJ/m²).

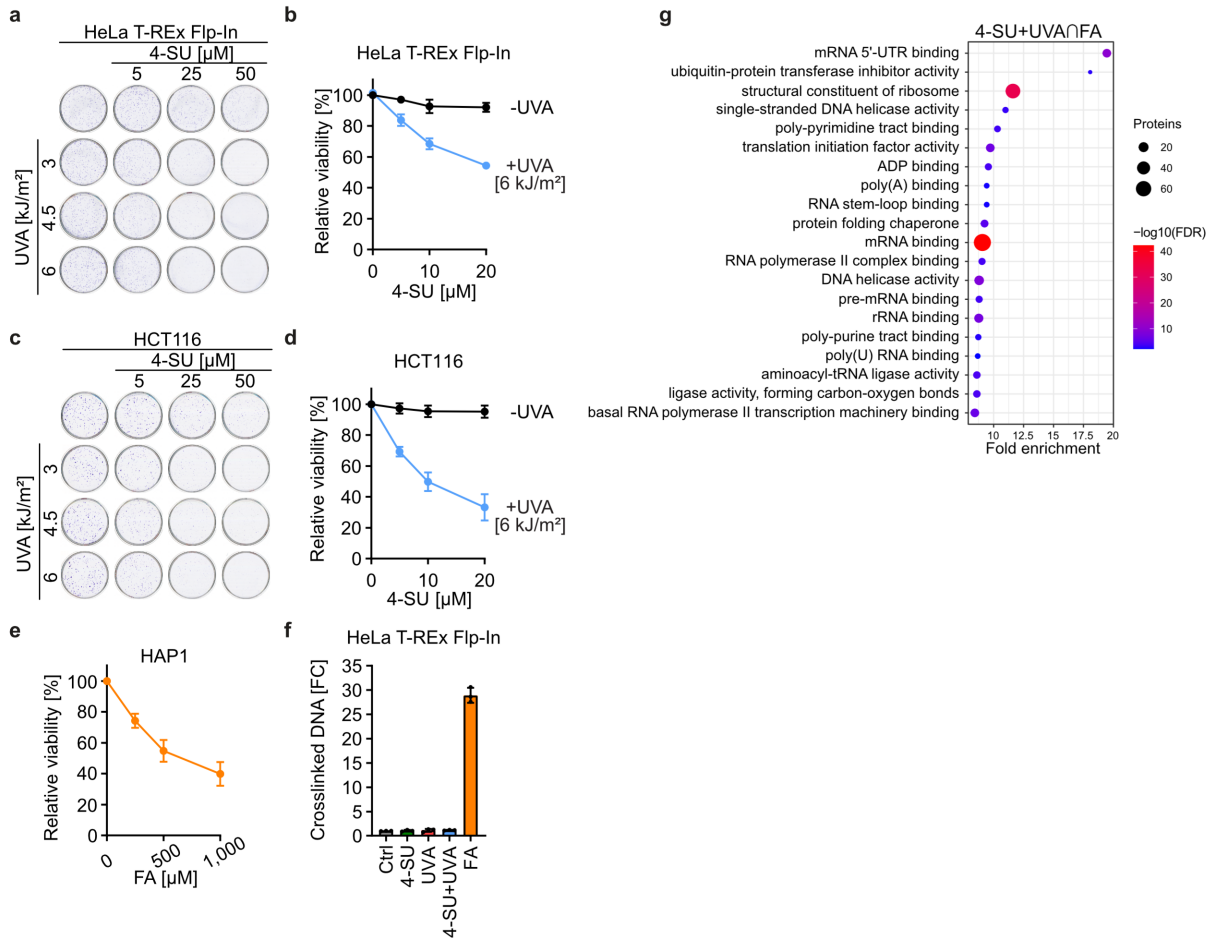
1032 **c:** Bar graphs depicting normalised label free quantification (LFQ) intensities of YBX3-
1033 mRPCs isolated by poly-A pulldown from HAP1 cells treated with 4-SU (2.5 μ M, 16 h) and
1034 proteasome inhibitor (MG132, 5 μ M, 1 h), as indicated, prior to irradiation with UVA (6
1035 kJ/m²) at indicated timepoints. Bar graphs depict mean \pm SD of four biological replicates

1036 **d:** Representative western blot showing indicated timepoints of recovery of mRPCs isolated
1037 by poly-A pulldown from clonal HAP1 *ZAK*, *GCN2* or *ZNF598* KO cells and matched
1038 *AAVS1* control cells treated with 4-SU (2.5 μ M, 16 h) and UVA (6 kJ/m²).

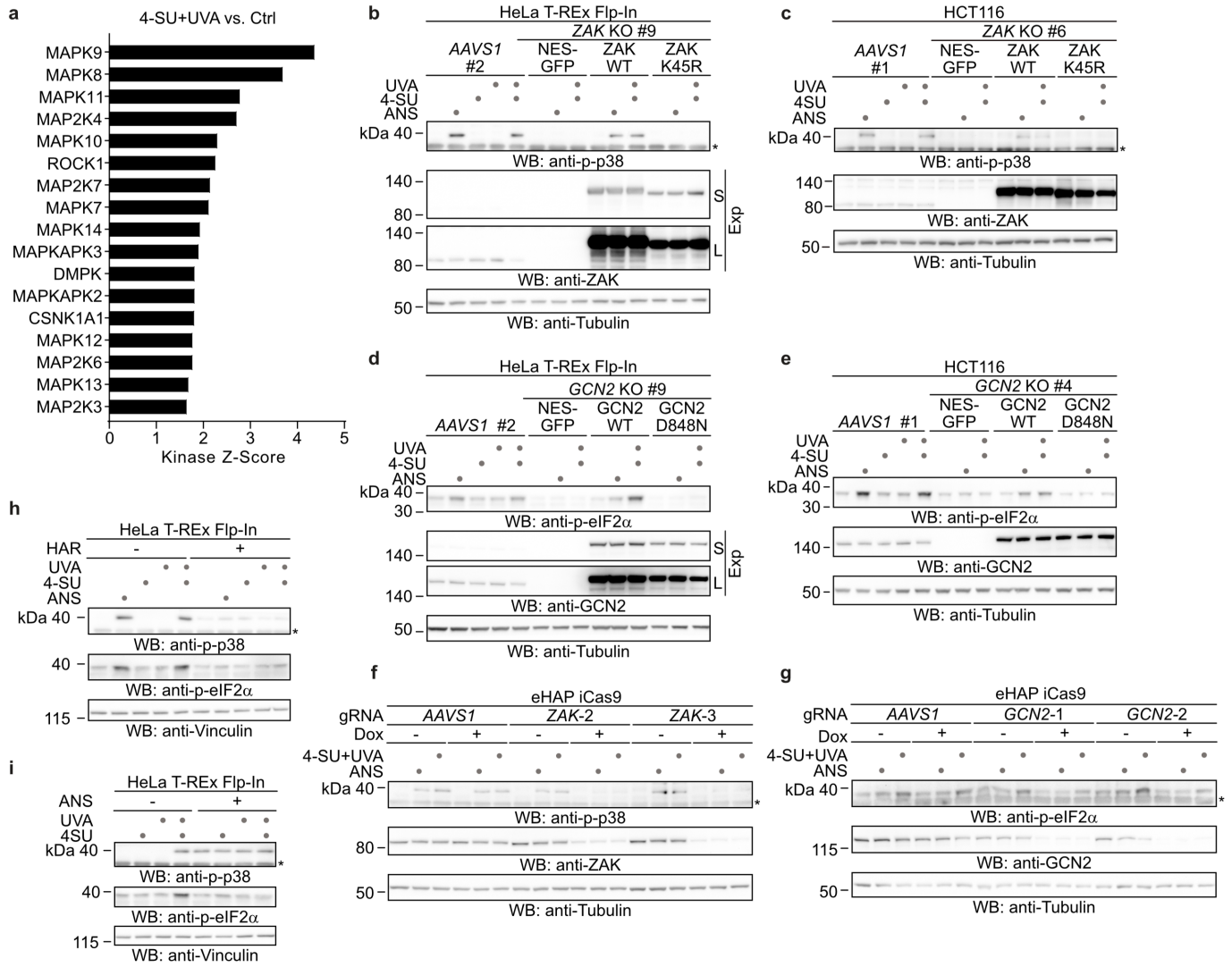
1039 **e:** Bar graphs depicting normalised label free quantification (LFQ) intensities of YBX3-
1040 mRPCs isolated by poly-A pulldown from HAP1 cells treated with 4-SU (2.5 μ M, 16 h) and

1041 translation inhibitor anisomycin (ANS, 375 μ M, 1 h), as indicated, prior to irradiation with
1042 UVA (6 kJ/m²) at indicated timepoints. Bar graphs depict mean \pm SD of four biological
1043 replicates
1044 **f:** Representative western blot analysis of HAP1 cells treated with ubiquitin E1 inhibitor (Ub-
1045 E1i, TAK-243, 1 μ M, 1 h) and translation inhibitor anisomycin (375 μ M ANS, 1 h), followed
1046 by UVC (50 J/m²) irradiation.
1047
1048

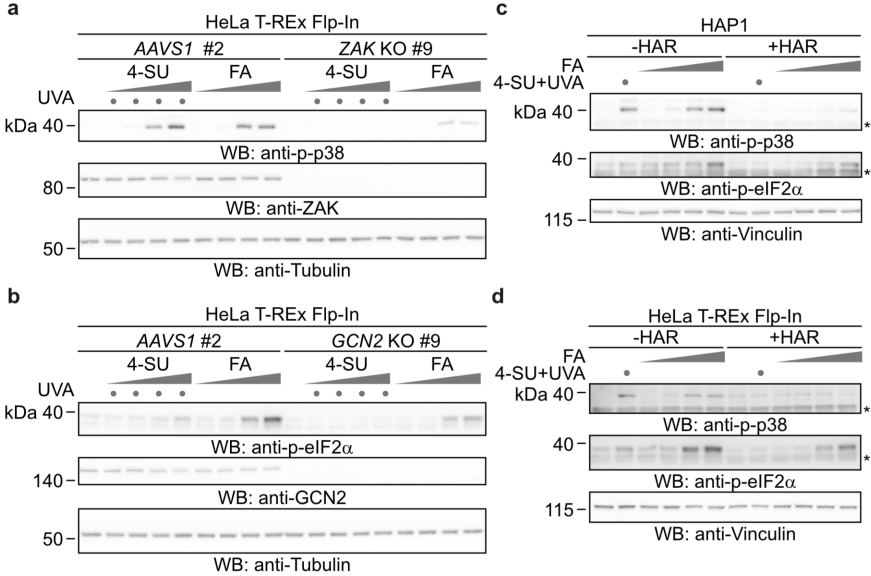
Extended Data Figure 1



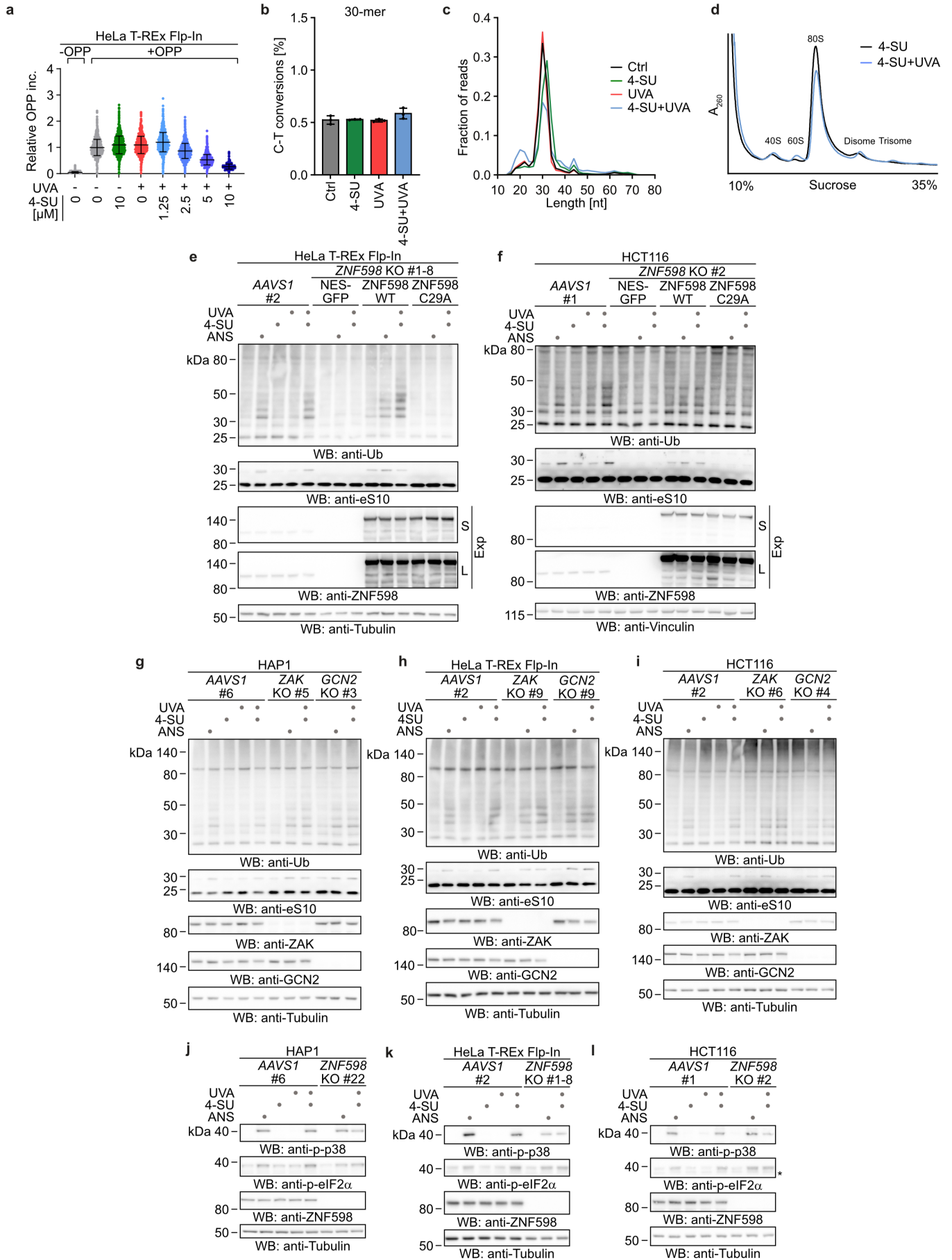
Extended Data Figure 2



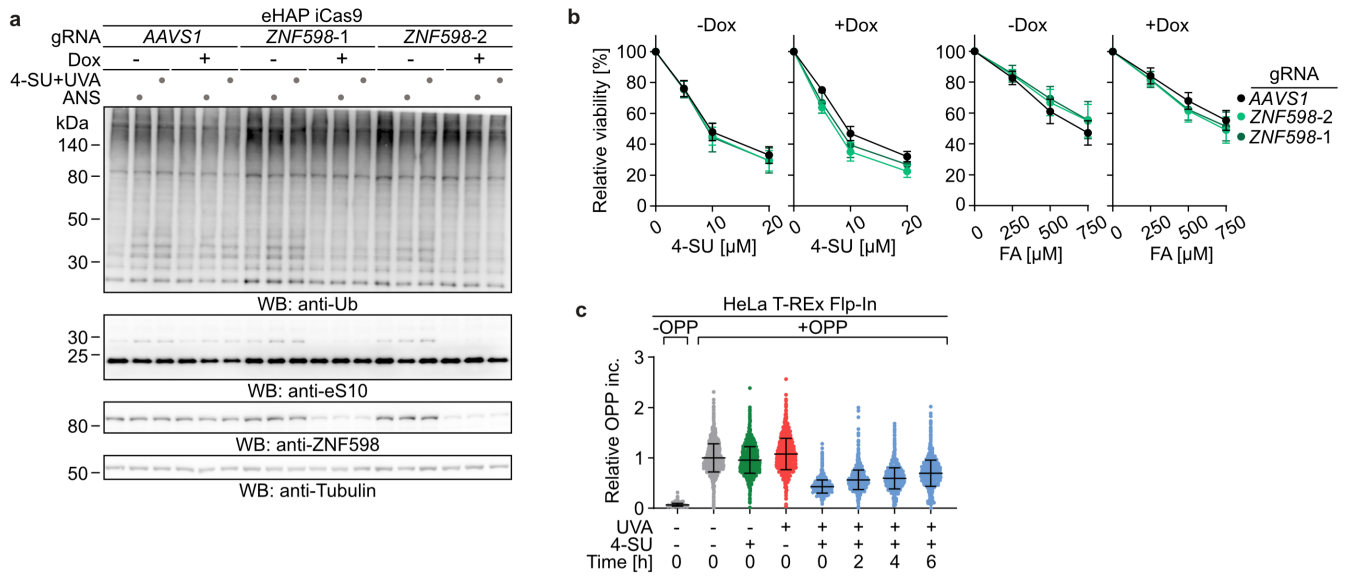
Extended Data Figure 3



Extended Data Figure 4



Extended Data Figure 5



Extended Data Figure 6

